

Molecular Basis of the Multivalent Glycine and  
 $\gamma$ -Aminobutyric Acid Type A Receptor Anchoring

Molekulare Basis der Multivalenten Verankerung der  
Glycin und  $\gamma$ -Aminobuttersäure Typ A Rezeptoren



Doctoral thesis for a doctoral degree  
at the Graduate School of Life Sciences,  
Julius-Maximilians-Universität Würzburg  
Section Biomedicine

submitted by  
Hans-Michael Maric  
from  
Stuttgart

Würzburg, August 2012

Submitted on: .....

Office stamp

Members of the Promotionskomitee:

Chairperson: Thomas Dandekar

Primary Supervisor: Hermann Schindelin

Supervisor (Second): Matthias Kneussel

Supervisor (Third): Utz Fischer

Date of Public Defense: .....

Date of Receipt of Certificates: .....

## A Table of Contents

A Table of Contents .....	1
B Summary - English .....	6
C Zusammenfassung - Deutsch .....	8
<b>1 Introduction .....</b>	<b>11</b>
1.1 Synaptic Transmission .....	11
1.2 $\gamma$ -Aminobutyric Acid Type A and Glycine Receptors .....	11
1.2.1 Receptor Architecture .....	12
1.2.2 Receptor Subunit Composition.....	13
1.2.3 Cellular and Subcellular Receptor Localization .....	13
1.3 Gephyrin .....	14
1.3.1 Self-Association of Gephyrin.....	16
1.3.2 Gephyrin-Mediated GlyR Clustering.....	17
1.3.3 Gephyrin-Mediated GABA <sub>A</sub> R Clustering.....	18
1.4 Collybistin .....	20
1.4.1 Collybistin`s Role in GABA <sub>A</sub> R Clustering.....	21
1.4.2 Collybistin`s Role in Gephyrin Clustering.....	22
1.5 Radixin .....	23
1.5.1 Function of the FERM Domain of Radixin .....	24
1.5.2 Radixin-Mediated GABA <sub>A</sub> R Clustering.....	26

<b>2 Materials and Methods</b> .....	<b>28</b>
<b>2.1 Biochemicals</b> .....	<b>28</b>
2.1.1 Bacterial Strains.....	28
2.1.2 Crosslinkers .....	28
2.1.3 Enzymes.....	29
2.1.4 Peptides.....	29
2.1.5 Plasmids.....	30
<b>2.2 Chemicals</b> .....	<b>32</b>
2.2.1 Crystallization Screens.....	32
2.2.2 Low Molecular Weight Chemicals .....	32
2.2.3 Solutions.....	33
<b>2.3 Equipment</b> .....	<b>35</b>
2.3.1 Instruments .....	35
2.3.2 Consumables .....	36
2.3.3 Kits.....	36
2.3.4 Software and Databases.....	36
<b>2.4 DNA Analysis and Manipulation</b> .....	<b>37</b>
2.4.1 DNA Gel Electrophoresis .....	37
2.4.2 DNA Gel Extraction .....	37
2.4.3 DNA Digestion and Ligation.....	37
2.4.4 Site-Directed Mutagenesis .....	37
2.4.5 Plasmid Isolation .....	38
2.4.6 DNA Sequencing.....	38
<b>2.5 Cell Culture and Protein Expression</b> .....	<b>39</b>
2.5.1 Cell Cultivation and Storage .....	39
2.5.2 Preparation of Competent Cells .....	39
2.5.3 Transformation.....	39
2.5.4 Protein Expression.....	39
2.5.5 Cell Lysis .....	39

<b>2.6 Protein Purification.....</b>	<b>40</b>
2.6.1 Affinity Chromatography .....	40
2.6.2 Size Exclusion Chromatography.....	40
<b>2.7 Protein Characterization.....</b>	<b>41</b>
2.7.1 Protein Electrophoresis .....	41
2.7.2 UV/Vis Spectrophotometry .....	41
2.7.3 Thermofluor .....	41
<b>2.8 Analysis of Protein Complexes .....</b>	<b>43</b>
2.8.1 Analytical Size Exclusion Chromatography .....	43
2.8.2 Analytical Ultracentrifugation .....	43
2.8.3 Differential Scanning Calorimetry.....	43
2.8.4 Dynamic Light Scattering .....	44
2.8.5 Isothermal Titration Calorimetry .....	45
2.8.6 Native Agarose Gel Electrophoresis.....	45
2.8.7 Pulldown Assay.....	45
<b>2.9 X-Ray Crystallography.....</b>	<b>46</b>
2.9.1 Protein Crystallization .....	46
2.9.2 Data Collection .....	46
2.9.3 Data Processing and Molecular Replacement .....	47
2.9.4 Model Refinement.....	48

<b>3 Results and Discussion .....</b>	<b>50</b>
<b>3.1 Radixin-Mediated GABA<sub>A</sub>R α5 Clustering.....</b>	<b>50</b>
3.1.1 GABA <sub>A</sub> R α5 and Radixin FERM Purification .....	50
3.1.2 Characterization of the FERM Domain α5-Loop Complex .....	52
3.1.3 Fine-Mapping of the FERM-α5 Binding Site.....	54
3.1.4 Structural Basis of FERM Domain Self-Masking.....	56
3.1.5 FERM Mediates GABA <sub>A</sub> R-Clustering via a Universal Ligand Binding Site .....	58
<b>3.2 Gephyrin-Mediated GABA<sub>A</sub>R and GlyR Clustering.....</b>	<b>62</b>
3.2.1 Mapping the GABA <sub>A</sub> R Gephyrin Interaction .....	63
3.2.2 Deciphering Gephyrin`s Receptor Subunit Preference .....	64
3.2.3 Gephyrin Binds Different Receptors in a Mutually Exclusive Fashion.....	66
3.2.4 Molecular Basis of Gephyrin-Mediated GlyR and GABA <sub>A</sub> R Clustering .....	67
3.2.5 Regulation of Gephyrin-Mediated GABA <sub>A</sub> R Clustering .....	75
<b>3.3 Development of Bivalent Receptor Peptides that Specifically Target Gephyrin`s Receptor-Binding Capacities .....</b>	<b>77</b>
3.3.1 Identification of a Gephyrin-Binding Minimum Sequence with Maximized Affinity.....	78
3.3.2 Peptide Dimerization.....	83
3.3.3 Bivalent Peptides Target Gephyrin`s Receptor Binding Site with an Unmatched Affinity ...	86
3.3.4 Analysis of a Low Affinity Gephyrin Ligand after Dimerization .....	90
3.3.5 Bivalent Peptides Reveal Different Modes of Gephyrin`s Domain Architecture.....	92
<b>3.4 Characterization of the Collybistin SH3 GABA<sub>A</sub>R Complex.....</b>	<b>94</b>
3.4.1 Purification of Collybistin`s SH3 Domain .....	94
3.4.2 Divalent Cations Induce Structural Rearrangements within the SH3 Domain .....	95
3.4.3 Characterization of the Subunit Specific GABA <sub>A</sub> R-SH3 Domain Interaction.....	100
3.4.4 The SH3 Domain and Gephyrin Share a Reciprocal GABA <sub>A</sub> R Subunit Preference .....	104
3.4.5 GephE and the SH3 Domain Compete for the GABA <sub>A</sub> R α2 Subunit .....	106
3.4.6 The GABA <sub>A</sub> R α2 Subunit Activates Collybistin for Gephyrin Binding.....	107

4 Concluding Discussion .....	108
4.1 Radixin-Mediated GABA <sub>A</sub> R Clustering .....	109
4.2 Gephyrin-Mediated GABA <sub>A</sub> R Clustering .....	110
4.3 Collybistin`s Role in GABA <sub>A</sub> R Clustering .....	112
4.4 Targeting Receptor-Scaffold Interactions .....	113
4.4.1 Receptor-Scaffold Interaction Share Common Features .....	113
4.4.2 Receptor-Scaffold Interactions Are Promising Drug Targets .....	114
4.4.3 Architecture of a Hypothetical Gephyrin Inhibitor .....	115
4.4.4 Theory of Avidity-Enhanced Binding.....	116
4.4.5 Gephyrin-Mediated GlyR and GABA <sub>A</sub> R binding Is a Multivalent Process .....	118
5 Tables .....	120
5.1 Abbreviations.....	120
5.2 Aminoacids .....	121
5.3 Figures .....	122
5.4 Tables.....	124
5.5 Protein Data Bank References.....	126
5.6 Literature References .....	127
D Acknowledgements.....	138
E Own Publications and Congress Contributions .....	140
F Curriculum Vitae .....	142
G Affidavit.....	143

## B Summary - English

$\gamma$ -Aminobutyric acid type A receptors (GABA<sub>A</sub>Rs) and glycine receptors (GlyRs) are the major mediators of fast synaptic inhibition in the central nervous system. For proper synaptic function their precise localization and exact concentration within the neuronal surface membrane is essential. These properties are mediated by scaffolding proteins which directly contact the large intracellular loops of the receptors and tether them to cytoskeletal elements of the neuronal cells. In my thesis I deciphered the molecular details of several underlying protein-protein interactions, namely the interaction of a subset of GABA<sub>A</sub>R and GlyR subunits with the scaffolding proteins gephyrin, radixin and collybistin. I determined short linear motifs within the large intracellular loops of the receptors that directly engage in subunit specific scaffold protein interactions. My quantitative binding studies revealed that gephyrin's E domain primarily recognizes the GABA<sub>A</sub>R  $\alpha$ 1 ( $K_d = 17 \mu\text{M}$ ) and  $\alpha$ 3 ( $K_d = 5 \mu\text{M}$ ) subunits, in contrast, the SH3 domain of collybistin mainly interacts with the GABA<sub>A</sub>R  $\alpha$ 2 subunit ( $K_d = 1 \mu\text{M}$ ), while the FERM domain of radixin tightly binds to the GABA<sub>A</sub>R  $\alpha$ 5 subunit ( $K_d = 8 \mu\text{M}$ ). My work additionally demonstrated that this simple relationship is complicated by (i) missing or (ii) overlapping binding specificities between the scaffold proteins and the receptor subunits. Moreover, this thesis addressed the possibility of (iii) posttranslational negative regulation as well as amplification generated by (iv) avidity effects as summarized below.

(i) First, using biochemical methods I mapped the radixin-GABA<sub>A</sub>R  $\alpha$ 5 interaction in detail. My structural analysis and competition assays suggest that radixin mediates the receptor subunit binding via a universal binding site within the F3 subdomain of its FERM domain. This binding site is formed by an  $\alpha$ -helix that offers a large hydrophobic pocket, which accepts a variety of different hydrophobic residues adopting different conformations, and a  $\beta$ -strand that readily engages in peptide backbone interactions. Not surprisingly, this binding site has been implicated in a wide variety of different scaffold interactions, thus emphasizing the importance of the essential FERM activation mechanism described earlier and suggesting additional pathways to allow tight regulation of this interaction.

(ii) Next, I analyzed in detail the process of gephyrin-mediated GABA<sub>A</sub>R clustering. My X-ray crystallographic studies and binding assays revealed that gephyrin mediates binding of the GABA<sub>A</sub>R  $\alpha$ 1,  $\alpha$ 2 and  $\alpha$ 3 subunit via a universal binding site that also mediates the interactions with the GlyR  $\beta$  subunit. Using structure-guided mutagenesis I identified key residues within gephyrin and the receptor subunits that act as major contributors to the overall binding strength. Namely, two conserved aromatic residues within the N-terminal half of the receptor binding region engage in crucial hydrophobic interactions with gephyrin. Accordingly, J. Mukherjee from the group of our collaborator Steven J. Moss verified a substantial decrease in GABA<sub>A</sub>R cluster number and size in primary hippocampal neurons upon exchange of these residues within the GABA<sub>A</sub>R  $\alpha$ 2 subunit. Extension of my studies to collybistin (CB) revealed an overlapping but reciprocal subunit preference for this protein in comparison to gephyrin. The GABA<sub>A</sub>R  $\alpha$ 3 subunit exclusively binds gephyrin, in contrast the GABA<sub>A</sub>R  $\alpha$ 1 subunit mainly targets gephyrin ( $K_d = 17 \mu\text{M}$ ) but additionally displays a moderate affinity ( $K_d \approx 400 \mu\text{M}$ ) towards the SH3 domain of CB. The GABA<sub>A</sub>R  $\alpha$ 2 subunit binds tightly to the SH3 domain of CB ( $K_d = 1 \mu\text{M}$ ) and additionally displays a weak gephyrin affinity ( $K_d \approx 500 \mu\text{M}$ ). Notably, I could exclude the possibility of synergistic effects between gephyrin's E domain, the SH3 domain of CB and the GABA<sub>A</sub>R  $\alpha$ 2 subunit. Instead, I found that the GABA<sub>A</sub>R  $\alpha$ 2 subunit binds gephyrin and CB in a mutually exclusive manner. These results suggest that CB's role in receptor clustering is solely determined by competing binding events of its constituting domains. Namely, the



intra-molecular association between the PH/DH domain and the SH3 domain within CB competes with different inter-molecular interactions of CB: GABA<sub>A</sub>R  $\alpha$ 2 binding to the SH3 domain, PIP<sub>2</sub> binding to the PH domain and gephyrin presumably binding to the PH and DH domain of CB.

(iii) Interestingly, the receptor motifs, which have been mapped in my thesis to directly interact with the scaffold proteins, were shown in earlier studies to be posttranslationally modified *in vivo*. In particular, the GABA<sub>A</sub>R  $\alpha$ 1 and GlyR  $\beta$  subunits have been implicated as targets of the ERK/MAPK and PKC phosphorylation-pathways, respectively, while the GABA<sub>A</sub>R  $\alpha$ 5 subunit motif was shown to be ubiquitinated. In this dissertation, I analyzed Thr348, a possible ERK phosphorylation site within GABA<sub>A</sub>R  $\alpha$ 1. My binding assays verified a severe reduction of the direct gephyrin binding strength upon introduction of the respective phosphomimetic residue. The relevance of this *in vitro* result was highlighted by J. Mukherjee who confirmed a significant reduction in GABA<sub>A</sub>R cluster number and size upon introduction of the same mutation. The ERK/MAPK pathway is therefore a promising candidate for regulation of GABAergic transmission.

(iv) *In vivo*, gephyrin presumably forms a multivalent scaffold, which is based on the self-association of its G (GephG) and E domains (GephE). Given the multimeric nature of gephyrin and the pentameric receptor architecture, I tested the possibility of avidity in the clustering of inhibitory neurotransmitter receptors. Cocrystallization of selected minimum peptides with GephE and their crystal structure analyses enabled me to define a receptor-derived peptide that offers a maximized gephyrin affinity. The structure of the GephE-GlyR  $\beta$  receptor complex reveals two receptor-binding sites in close spatial vicinity (15 Å). I therefore designed bivalent peptides that enable to target both GephE sites at the same time and, as expected, a variety of biophysical methods verified an avidity-potentiated and unmatched high gephyrin affinity for these bidentate compounds. Notably, I could extend the dimerization approach to low affinity gephyrin ligands, namely short GABA<sub>A</sub>R-derived peptides that could not be studied using conventional monomeric ligands. Additionally, I verified that this compound specifically targets GephE's receptor binding site, and that it thereby inhibits its receptor binding activity. Further development of this molecule may offer the possibility to specifically analyze the effect of uncoupling the gephyrin-receptor interaction in cell culture-based assays, without altering protein function or expression level that accompanies conventional methods such as protein knock-out, RNA interference or the usage of antibodies.

## C Zusammenfassung - Deutsch

$\gamma$ -Aminobuttersäure-Rezeptoren vom Typ A (GABA<sub>A</sub>Rs) und Glyzin-Rezeptoren (GlyRs) sind die wichtigsten Vermittler der schnellen synaptischen Inhibition im zentralen Nervensystem. Von wesentlicher Bedeutung für ihre ordnungsgemäße Funktion in der inhibitorischen Signalübertragung ist ihre präzise Lokalisation und Konzentration innerhalb der neuronalen Oberflächenmembran. Diese Eigenschaften werden durch Gerüstproteine vermittelt, welche direkt an die großen intrazellulären Schleifen der Rezeptoren, sowie an Bausteine des neuronalen Zytoskeletts binden. In meiner Dissertation habe ich die molekularen Details mehrerer zugrunde liegenden Protein-Protein Wechselwirkungen untersucht. Im Speziellen habe ich die Interaktion ausgewählter GABA<sub>A</sub>R und GlyR Untereinheiten mit den Gerüstproteinen Gephyrin, Radixin und Collybistin analysiert. Ich habe kurze lineare Aminosäuren-Motive innerhalb der großen intrazellulären Schleifen der Rezeptoren identifiziert, welche die direkten und Untereinheit-spezifischen Interaktionen vermitteln. Die Quantifizierung der jeweiligen Bindungsstärke ergab, dass Gephyrins E-Domäne vor allem an die GABA<sub>A</sub>R  $\alpha$ 1 ( $K_d = 17 \mu\text{M}$ ) und  $\alpha$ 3 ( $K_d = 5 \mu\text{M}$ ) -Untereinheiten bindet, wohingegen die SH3-Domäne von Collybistin hauptsächlich mit der GABA<sub>A</sub>R  $\alpha$ 2-Untereinheit interagiert ( $K_d = 1 \mu\text{M}$ ). Demgegenüber bindet die FERM-Domäne von Radixin fest an die  $\alpha$ 5-Untereinheit des GABA<sub>A</sub>R ( $K_d = 8 \mu\text{M}$ ). Weiterhin zeigt meine Arbeit, dass diese einfache Beziehung durch (i) fehlende oder (ii) überlappende Bindungsspezifitäten zwischen den Gerüstproteinen und den Rezeptor-Untereinheiten komplex reguliert wird. Ferner beschreibe ich hier, wie im Folgenden ausgeführt, die Möglichkeit einer (iii) negativen Modulation mittels posttranslationaler Modifikation, sowie einer Verstärkung der Bindung durch (iv) Aviditäts-Effekte.

(i) Als erstes habe ich mit Hilfe biochemischer Methoden die Radixin-GABA<sub>A</sub>R  $\alpha$ 5 Interaktion im Detail untersucht. Meine Strukturanalyse und Kompetitionsstudien legen den Schluss nahe, dass Radixin die betreffende Rezeptor-Untereinheit mittels einer universellen Bindungstasche in der F3 Subdomäne innerhalb seiner FERM Domäne bindet. Diese Bindungsstelle wird durch zwei markante Strukturelemente gebildet: Einer  $\alpha$ -Helix, die eine große hydrophobe Tasche bildet, welche eine Vielzahl unterschiedlicher hydrophober Reste in verschiedenen Konformationen akzeptiert, sowie ein  $\beta$ -Strang, der Peptidrückgrat-Interaktionen eingehen kann. Es überrascht nicht, dass eine Vielzahl an Studien die Beteiligung dieser Bindungsseite mit unterschiedlichen Liganden beschrieben hat. Diese Promiskuität unterstreicht die Bedeutung des Aktivierungsmechanismus der zuvor für die Radixin FERM GABA<sub>A</sub>R  $\alpha$ 5-Untereinheit beschrieben wurde und impliziert weitere Regulationsmechanismen, die eine koordinierte Interaktion *in vivo* ermöglichen.

(ii) Weiterhin habe ich mich ausführlich der Analyse der Gephyrin-vermittelten GABA<sub>A</sub>R Clusterbildung gewidmet. Meine röntgenkristallographischen Studien und Bindungsstudien zeigen, dass Gephyrin mit den GABA<sub>A</sub>R  $\alpha$ 1,  $\alpha$ 2 und  $\alpha$ 3 Untereinheiten über eine universelle Bindungsstelle interagiert, welche auch die Wechselwirkungen mit der  $\beta$ -Untereinheit des GlyR vermittelt. Mittels Struktur-basierter Mutagenesestudien konnte ich die Schlüsselreste innerhalb von Gephyrin und der Rezeptor-Untereinheiten identifizieren, die einen entscheidenden Beitrag zur Gesamt-Bindungsstärke liefern. Insbesondere zwei konservierte aromatische Reste in der N-terminalen Hälfte der Rezeptorbindungsregion gehen entscheidende hydrophobe Wechselwirkungen mit Gephyrin ein. Dementsprechend konnte J. Mukherjee, ein Mitarbeiter in der Gruppe unseres Kooperationspartners Steven J. Moss, zeigen, dass der Austausch dieser Reste innerhalb der  $\alpha$ 2-Untereinheit des GABA<sub>A</sub>R ausreicht, um einen deutlichen Rückgang der Rezeptor Cluster-Anzahl und ihrer Größe in primären

hippokampalen Neuronen zu verursachen. Die Ausweitung meiner Rezeptor-Interaktions-Studien auf Collybistin (CB) ergab, dass dieses Protein im Vergleich zu Gephyrin eine umgekehrte, aber dennoch überlappende Rezeptor-Untereinheiten-Präferenz aufweist. Die GABA<sub>A</sub>R  $\alpha$ 3-Untereinheit bindet ausschließlich an Gephyrin ( $K_d = 5 \mu\text{M}$ ), während die GABA<sub>A</sub>R  $\alpha$ 1-Untereinheit zwar vor allem Gephyrin bindet ( $K_d = 17 \mu\text{M}$ ), zusätzlich jedoch eine schwache Affinität ( $K_d \approx 400 \mu\text{M}$ ) für die SH3-Domäne von CB aufweist. Im Gegensatz dazu bindet die GABA<sub>A</sub>R  $\alpha$ 2-Untereinheit hochaffin an die SH3-Domäne von CB ( $K_d = 1 \mu\text{M}$ ) und zeigt zusätzlich eine schwache Gephyrin Affinität ( $K_d \approx 500 \mu\text{M}$ ). Interessanterweise konnte ich Synergieeffekte zwischen der GABA<sub>A</sub>R  $\alpha$ 2-Untereinheit, Gephyrins E-Domäne und CBs SH3-Domäne ausschließen und statt dessen zeigen, dass diese Rezeptor-Untereinheit exklusiv entweder Gephyrin oder CB bindet. Diese Ergebnisse lassen vermuten, dass die Rolle von CB in der Rezeptor-Anhäufung allein durch die konkurrierenden Bindungs-Ereignisse seiner konstituierenden Domänen bestimmt wird. Die intramolekulare Assoziation zwischen der PH und der DH-Domäne mit der SH3-Domäne von CB konkurriert mit unterschiedlichen intermolekularen Wechselwirkungen von CB. Und zwar mit der GABA<sub>A</sub>R  $\alpha$ 2-Untereinheit-Bindung an die SH3-Domäne, mit der PIP<sub>2</sub>-Bindung an die PH-Domäne, sowie mit der Gephyrin-Bindung, welche vermutlich von der PH und DH-Domäne von CB vermittelt wird.

(iii) Interessanterweise bestätigen frühere Studien, dass die Rezeptor-Motive, die ich hier identifiziert habe und welche direkt mit den Gerüst-Proteinen wechselwirken, *in vivo* posttranslational modifiziert vorliegen. Insbesondere wurde gezeigt, dass die Gephyrin-Bindemotive der GABA<sub>A</sub>R  $\alpha$ 1-Untereinheit und GlyR  $\beta$ -Untereinheiten Ziele des ERK/MAPK und PKC-Phosphorylierungs-Weges sind, während das Radixin-Bindungs-Motiv innerhalb der GABA<sub>A</sub>R  $\alpha$ 5-Untereinheit ubiquitiniert vorliegt. In dieser Dissertation habe ich im Besonderen die ERK-Phosphorylierung von Thr348 in der GABA<sub>A</sub>R  $\alpha$ 1-Untereinheit untersucht. Tatsächlich konnten meine Bindungs-Assays eine starke Reduktion der direkten Gephyrin Bindungsstärke beim Einbringen eines phosphomimetischen Restes bestätigen. Darüber hinaus konnte J. Mukherjee eine signifikante Reduktion der Cluster-Anzahl und Größe beim Einführen der gleichen Mutation in die  $\alpha$ 1-Untereinheit beinhaltenden GABA<sub>A</sub>Rs in hippocampalen Neuronen beobachten. Der ERK/MAPK-Regulation-Weg ist daher ein aussichtsreicher Kandidat für die Regulation der GABAergen-Signalübertragung.

(iv) *In vivo* bildet Gephyrin vermutlich durch Selbstorganisation seiner G (GephG) und E-Domänen (GephE) ein multivalentes Gerüst. Angesichts der multimeren Natur Gephyrins und der pentameren Rezeptorarchitektur habe ich die Möglichkeit von Aviditäts-Effekten im Prozess der synaptischen Neurotransmitter-Rezeptor-Anhäufung untersucht. Die Kristallstrukturen von GephE im Komplex mit ausgewählten Peptiden zeigen zwei Rezeptor-Bindungsstellen in räumlicher Nähe (15 Å). Auf der Basis dieser Information habe ich bivalente Peptide entworfen, welche beide Rezeptor-Bindungsstellen in Gephyrin simultan besetzen können und, wie erwartet, konnte ich mit Hilfe verschiedener biophysikalischen Methoden eine unübertroffen hohe, durch Avidität potenzierte, Gephyrin-Affinität nachweisen. Mir gelang es diesen Aviditäts-Effekt für einen schwachen Gephyrin Liganden, ein GABA<sub>A</sub>R-abgeleitetes Peptid, welcher nicht mit herkömmlichen monomeren Liganden untersucht werden konnte, nutzbar zu machen. Darüber hinaus konnte ich zeigen, dass diese Verbindung gezielt die Rezeptor-Bindungsstelle in GephE besetzt und auf diese Weise hemmend auf Gephyrins Rezeptorbindungsaktivität wirkt. Eine weitere Entwicklung dieser Verbindung könnte die Möglichkeit eröffnen, spezifisch die Wirkung der Entkopplung der Gephyrin Rezeptor-Interaktion in der Zellkultur-Experimenten zu analysieren ohne dabei die Anzahl oder die Funktion der Proteine zu

beeinträchtigen, was einen Nebeneffekt von konventionellen Methoden wie Gen „knock-out“, RNA-Interferenz oder den Einsatz von Antikörpern darstellt.

# 1 Introduction

The nervous system is a network of cells that are specialized to process and transmit information. In vertebrates and most invertebrates the brain forms its center which, based on sensory input, allows for fast reactions to the environment by controlling, among other processes, muscle activity and hormone secretion. An adult male human brain weighs 1.5 kg on average and contains 86 billion neuronal cells together with 85 billion non-neuronal cells [1]. The neuronal cells are linked by trillions of specific connections which are referred to as synapses. The integration of information in the central nervous system is achieved by modulating the chemical signaling across the synaptic contacts. To understand neuronal function it is necessary to decipher the design and regulatory mechanisms of these synapses. Therefore, the aim of my work was to gain new insights into the architecture of inhibitory synapses by analyzing underlying protein-protein interactions at the molecular level.

## 1.1 Synaptic Transmission

The majority of all synapses are chemical synapses, where the plasma membrane of the signal-originating neuron is in close apposition to the membrane of the signal-receiving cell at distances ranging from 15 to 25 nm [2, 3]. Both, the pre- and postsynaptic site, contain a complex array of proteins that not only link together both membranes and the machinery on either side to the cytoskeletal matrix but also carry out the signaling events and regulate the strength of the synaptic transmission. Upon electrical triggering, the presynaptic neuron releases small molecules, which are referred to as neurotransmitters and these bind to receptors located in the postsynaptic membrane. The ligand-binding event is translated via structural rearrangements into an opening of the respective cognate receptor, which then functions as an ion-selective pore. Excitatory receptors allow for the influx of positively charged ions, which depolarize the neuronal membrane, increasing the possibility that the neuron will initiate electrical responses itself. In contrast, inhibitory receptors, allow the influx of negatively charged ions, which reduce the activity of the target neuron by stabilizing or hyperpolarizing the resting membrane potential, which in turn makes it more difficult to depolarize the neuron and generate an action potential. Fast synaptic inhibition in the human brain is mainly mediated by the two receptor classes discussed in the next section.

## 1.2 $\gamma$ -Aminobutyric Acid Type A and Glycine Receptors

$\gamma$ -Aminobutyric acid (GABA) and glycine are the major neurotransmitters mediating synaptic inhibition in the central nervous system. Their inhibitory action is mainly mediated by GABA receptors of the A subclass (GABA<sub>A</sub>Rs) and glycine receptors (GlyRs) which both belong to the superfamily of Cys-loop pentameric ligand-gated ion channels (pLGICs). This family additionally comprises the nicotinic acetylcholine receptor (nAChR), the serotonin receptor (5-HT) and the zinc-activated receptor [4]. The 44 known subunit members exhibit a minimal sequence identity of around 30% between subunit classes of different receptors, whereas subunits within the same class for a given receptor display around 70% identity [5]. Despite the low overall identity there is a great similarity at the level of the secondary, tertiary and quaternary structure, which will be described in detail in the next section.

### 1.2.1 Receptor Architecture

Cys-loop pLGICs are transmembrane proteins, composed of five symmetrically arranged subunits, in which similar domains establish the membrane topology (Figure 1). The N terminal extracellular region with the conserved Cys-loop motif is followed by four transmembrane (TM)  $\alpha$ -helices. The large intracellular loop of high sequence divergence is located between TM3 and TM4, while TM2 lines the ion-conducting pore. The end is formed by a relatively short extracellular C-terminal region.

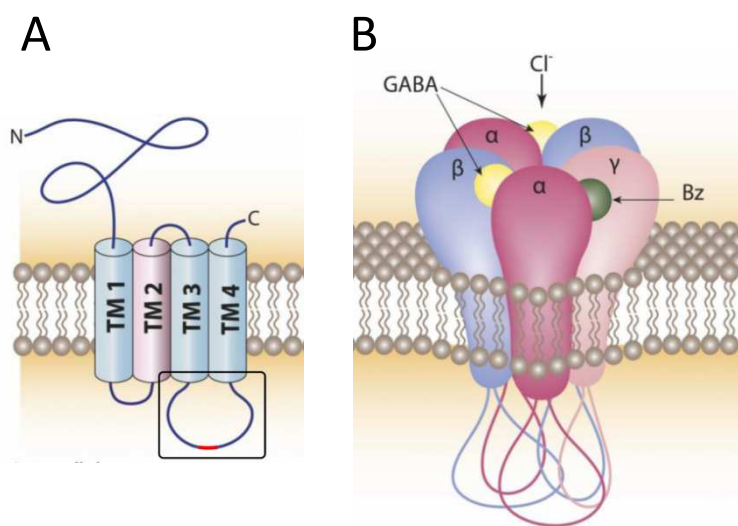


**Figure 1. Architecture of Cys-loop pLGICs.** A, Cys-loop pLGIC subunit architecture. A single subunit contains four hydrophobic transmembrane (TM) helices. The large N terminal domain is located extracellularly and contains the neurotransmitter binding site as well as binding sites for modulators. The intracellular domain between TM3 and TM4 (black box) is the most divergent part of individual receptor subunits and contains consensus sites for protein kinases and intracellular interactors. B, Pentameric assembly of the GABA<sub>A</sub>R. Most commonly GABA<sub>A</sub>Rs are composed of two  $\alpha$ , two  $\beta$  and one  $\gamma$  subunit. Abbreviations: Bz: Benzodiazepine, Cl<sup>-</sup>: Chloride-Ion, GABA:  $\gamma$ -amino butyric acid). © 2012 V Tretter, M Mukherjee, HM Maric, H Schindelin, W Sieghart and SJ Moss

While atomic resolution structures of integral mammalian pLGICs are still missing, several homologous or truncated proteins could be analyzed. Among them the molluscan acetylcholine-binding protein (AChBP), a homologue of the amino-terminal ligand-binding domain of an nAChR which was refined to 2.2 Å [6], the prokaryotic pLGIC homologue ELIC from the plant pathogen *Erwinia chrysanthemi* refined to 3.3 Å [7, 8] and GLIC from the cyanobacterium *Gloeobacter violaceus* refined to 2.9 Å [9].

For both, GABA<sub>A</sub>Rs and GlyRs, several subunits are available for receptor assembly. The resulting receptor composition determines key properties like pharmacological interactions, gating properties, expression pattern and finally accumulation at different neuronal surfaces, which is central to my work and therefore will be discussed extensively in the following three sections.

## 1.2.2 Receptor Subunit Composition

Until now one GlyR  $\beta$  subunit gene and four  $\alpha$  subunit encoding genes have been identified [10-12] and alternative exon splicing results in two additional isoforms for the GlyR  $\alpha$ 1-3 subunits [13]. GlyRs are thought to be most commonly assembled from two  $\alpha$  and three  $\beta$  subunits [14], with the resulting  $\alpha$ - $\beta$  subunit interfaces forming the ligand binding sites.

GABA<sub>A</sub>R subunits are encoded by at least 19 different genes, grouped by homology into eight subclasses ( $\alpha$ 1-6,  $\beta$ 1-3,  $\gamma$ 1-3,  $\delta$ ,  $\epsilon$ ,  $\theta$ ,  $\pi$ ,  $\rho$ 1-3) [15]. Within a subunit class the sequence identity is about 70% and between classes it is around 30% [5]. The  $\gamma$ 2 [16] and  $\beta$ 2 [17] subunits exist as splice variants differing in eight and 38 amino acids, respectively. In theory, all possible subunit combinations would allow millions ( $19^5$ ) of structurally distinct GABA<sub>A</sub>Rs, however, only eleven receptor subunit combinations of two  $\alpha$ , two  $\beta$  and single  $\gamma$ 2 or  $\delta$  subunit are thought to be reasonably abundant *in vivo* [18] and another fifteen receptor subunit combinations are proposed to exist with a limited distribution [18]. The next paragraph will summarize how the subunit composition determines receptor localization.

## 1.2.3 Cellular and Subcellular Receptor Localization

The large intracellular loop between TM3 and TM4 is thought to be the major determinant for the anchoring and accumulation of all pLGICs at postsynaptic and extrasynaptic sites. Due to their pentameric assembly GlyRs and GABA<sub>A</sub>Rs offer up to five intracellular loops per single receptor to interact with proteins beneath the neuronal surface membrane.

In GlyRs, the  $\beta$  subunit was identified early as the determinant of receptor anchoring and clustering at postsynaptic sites [19-21]. In contrast the molecular basis of GABA<sub>A</sub>R accumulation and the participating proteins remained elusive until recently. Similar to GlyRs subcellular targeting of GABA<sub>A</sub>Rs depends on their receptor subunit composition. The aim of my work was therefore to analyze recently proposed subunit-specific scaffold interactions. Verification and quantification as well as the identification of key residues would greatly enhance our understanding of the architecture and function of the inhibitory synapse.

Synaptic GABA<sub>A</sub>Rs are thought to be subunit combinations of two  $\alpha$ 1-3 subunits, two  $\beta$ 2-3 and one  $\gamma$ 2 subunit (Figure 2) [22]. In contrast, extrasynaptic receptors were shown to contain  $\delta$  instead of  $\gamma$  subunits or  $\alpha$ 4-6 subunits instead of  $\alpha$ 1-3 subunits (Figure 2) [23-26]. In line with these findings Tretter et al. identified for the first time a direct interaction of GABA<sub>A</sub>Rs with gephyrin [27]. My thesis, presented here, provides a detailed analysis of this and additional GABA<sub>A</sub>R-gephyrin interactions and therefore the next section will summarize key findings concerning gephyrin's role in the architecture of inhibitory synapses.

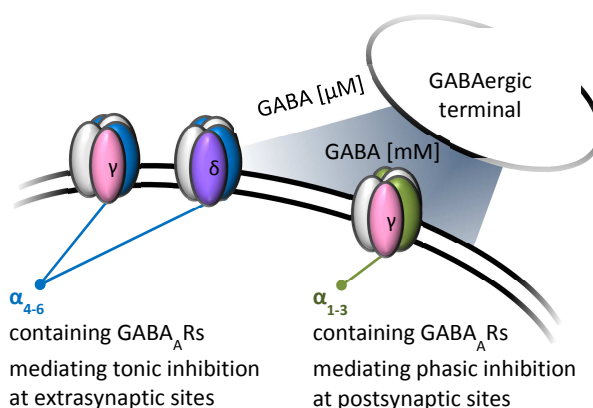


Figure 2. **Subcellular localization of GABA<sub>A</sub>Rs is determined by their subunit composition.** GABA<sub>A</sub>Rs containing  $\alpha$ 1-3 or the  $\gamma$  subunit are mainly localized at postsynaptic sites. In contrast, receptors containing the  $\alpha$ 4-6 or  $\delta$  subunit are commonly found at extrasynaptic sites. © 2012 HM Maric

## 1.3 Gephyrin

Gephyrin (after the Greek word bridge (γέφυρα)) was first identified as a 93 kDa protein that copurified with GlyRs [28]. Gephyrin is broadly expressed and essential for postsynaptic receptor clustering [19, 21, 29-31] and molybdenum cofactor (Moco) biosynthesis [32]. Gephyrin knock-out mice appear superficially normal at birth but because of respiratory and nutritional defects they die within hours after birth [33]. They display a progressive startle reflex in response to tactile stimuli, similar but more severe than mice carrying mutations in the genes encoding the GlyR  $\alpha$ 1 or  $\beta$  subunit that cause Startle disease [34], which is also referred to as hyperekplexia. Until now more than ten different gephyrin splice variants have been reported [30, 35, 36], however, their distinct functions remain to be elucidated.

A large variety of proteins were shown to directly interact with gephyrin. In particular, several proteins were demonstrated to be critical for gephyrin's function in mediating receptor clustering at postsynaptic sites (Figure 3):

(A) Microtubules [37] and cytoskeleton-associated proteins such as the small actin-binding protein profilin [38] or Mena/VASP [39].

(B) The peptidyl-prolyl-cis-trans-isomerase NIMA interacting 1 protein (PIN1) that was proposed to promote a conformational change in gephyrin, which would alter its GlyR affinity [40].

(C) The cell adhesion molecules neuroligin 2 (NL2) [41] and neuroligin 4 (NL4) [42], which, together with the Cdc42-specific guanine nucleotide exchange factor collybistin (CB) [43], are thought to induce gephyrin clustering.

(D) Proteins involved in microtubule-based anterograde and retrograde transport such as kinesin [44] and the dynein light chain [45].

(E) GABA<sub>A</sub>R associated protein (GABARAP) which interacts with the GABA<sub>A</sub>R  $\gamma$ 2 subunit as well as with gephyrin [46, 47]. GABARAP was discussed as the possible missing link, explaining coclustering of gephyrin and certain GABA<sub>A</sub>Rs, however, GABARAP knockout mice were shown to be viable and neuronal cultures from these mice still exhibited a strong postsynaptic coclustering of gephyrin and GABA<sub>A</sub>Rs [48]. Instead, the major role of GABARAP may be receptor insertion into the cell surface membrane during synaptic delivery [49, 50].



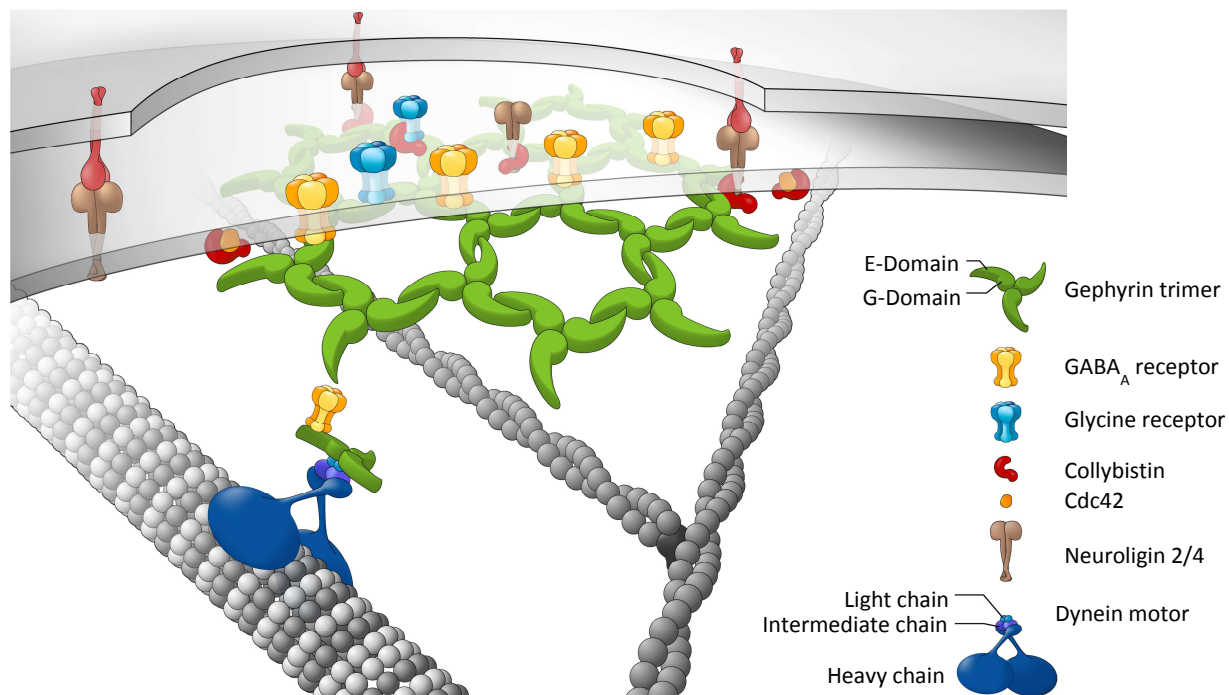


Figure 3. **Minimum-scheme of receptor clustering at the postsynaptic membrane.** Neuroligins are thought to link the pre- and postsynaptic membrane and induce the formation of postsynaptic specializations. Recent investigations suggest that collybistin (red), a Cdc42 (orange) guanine nucleotide exchange factor, induces clustering of gephyrin (green). Gephyrin is thought to form a hexagonal lattice (green) beneath the postsynaptic neuronal membrane which interacts directly with microtubules (grey, thick helical arrangements) and indirectly with F-actin (grey, thin helical arrangement). GlyR number at the neuronal surface membrane depends on transport processes mediated by the dynein motor (blue). Direct interactions of the GlyR (blue) and possibly also GABA<sub>A</sub>R (yellow) with the gephyrin scaffold are thought to be main determinants of the receptor residence time at postsynaptic sites, thereby regulating fast inhibitory synaptic transmission. © 2012 C Delto

The described interactions of gephyrin with key proteins of the synapse additionally depend on gephyrin's regulated self-association and the resulting higher order architecture which will be presented in detail in the next chapter.

### 1.3.1 Self-Association of Gephyrin

Gephyrin is a modular protein composed of an N-terminal G domain and a C-terminal E domain. Based on the crystal structures of the bacterial MogA [51] and MoeA [52] proteins, which are homologous to the G and E domain, respectively, it was hypothesized that gephyrin forms a two-dimensional hexagonal lattice [53] beneath the neuronal surface membrane (Figure 4) at postsynaptic sites. Crystallographic analyses revealed that the E domain forms a dimer [52, 54, 55] and that the G domain trimerizes [51, 56, 57] (Figure 4), however, bacterially expressed full-length protein only forms a trimer in solution [58]. Subsequently, *in vitro*, trimeric, hexameric and higher order structures have been observed, depending in part on whether the E-domain is in a dimeric or monomeric conformation [59, 60].

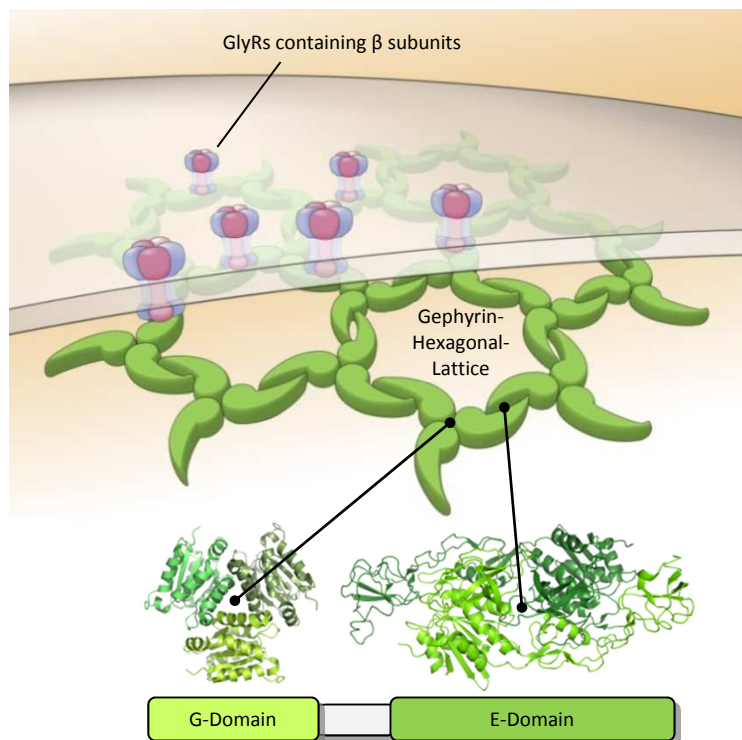


Figure 4. **Architecture of gephyrin.** Gephyrin is composed of an N-terminal G domain and a C-terminal E domain, which are connected by a presumably unstructured linker. Based on X-ray crystallographic structures, which revealed the E domain to form a dimer and the G domain to trimerize, it was hypothesized that gephyrin forms a hexagonal lattice beneath the neuronal membrane at postsynaptic sites. © 2012 V Tretter, M Mukherjee, HM Maric, H Schindelin, W Sieghart and SJ Moss

While the molecular mechanisms responsible for gephyrin cluster assembly and disassembly still remain to be elucidated, it was demonstrated that oligomerization is essential for postsynaptic clustering [60] and that it differs between the splice variants [59, 61]. Interestingly, alternative splicing additionally alters gephyrin's folding, phosphorylation status and even GlyR binding [61], while its metabolic function was shown to be independent of splicing effects [62]. How these differences in function correlate with the respective oligomerization state has not yet been elucidated at the molecular level. Possibly, gephyrin's oligomeric state allows for an avidity-based ligand selection. Until now, quantitative studies applied only monomeric intracellular receptor loops or parts of them and hence did not take into account the multivalency of the interaction presumably present *in vivo*. Nonetheless, the gephyrin receptor complex has to be considered as a multimeric assembly. Each GlyR contains up to three gephyrin-binding  $\beta$ -subunits [14] while gephyrin offers three binding sites in its soluble trimeric form [58], and most likely a high density of binding sites in its clustered form. Therefore it can be inferred that the actual interaction strength *in vivo* is potentiated by avidity effects depending on the number of gephyrin-binding subunits in the pentameric receptor assembly and the oligomeric state of gephyrin. Hence, the second goal of my work was the analysis of a multivalent scaffold receptor complex, as well as the quantification of the avidity-based potentiated binding affinity. This aim is based on the detailed crystallographic and biophysical characterization of the gephyrin-GlyR complex [55] which will be highlighted in the next paragraph.

### 1.3.2 Gephyrin-Mediated GlyR Clustering

It is well established that GlyRs are highly enriched at postsynaptic sites located opposite of glycinergic nerve endings via a direct interaction with gephyrin, and that this process relies on synaptic activity [19, 21, 29-31, 63, 64]. Accordingly, GlyR clustering is abolished in spinal cord cultures after depletion of gephyrin expression using antisense-oligonucleotides [31] as well as in gephyrin knock-out mice [33].

Colocalization of GlyRs and gephyrin depends on a 13 residue motif residing in the cytoplasmic TM3-TM4 loop of the  $\beta$ -subunit which was identified by biochemical techniques [19, 21] and subsequently described by X-ray crystallography [55] (Figure 5). On the other hand, gephyrin can interact with sub-synaptic microtubules [37], microfilaments [63], and their regulators such as profilin I and II [38], as outlined in Section 1.3 and Figures 3 and 4. Taken together, it was therefore concluded that gephyrin regulates the density of GlyRs at postsynaptic sites via direct interactions with the receptors and the cytoskeleton [63]. Following these results a more recent study [65] identified a protein kinase C (PKC) phosphorylation site within the structurally resolved part of the GlyR  $\beta$ -loop (residue Ser403, marked in red in figure 5) that causes a reduction of the binding affinity between the receptor and gephyrin. The same study identified accelerated receptor diffusion in the plasma membrane and that such GlyRs accumulate less strongly at synapses. It can therefore be concluded that the plasticity of inhibitory synapses can be regulated by kinases.

The insights on the structural basis of gephyrin-mediated GlyR clustering form the basis of my studies on the multivalency of the GlyR-gephyrin interaction and turned out to be of great importance for my investigations of gephyrin's role in GABA<sub>A</sub>R clustering. Indeed, gephyrin was proposed early to play a similar role in the accumulation of GABA<sub>A</sub>Rs at postsynaptic sites, and following this idea a pleiotropy of neurobiological studies, summarized in the following chapter, already addressed gephyrin's role in GABA<sub>A</sub>R clustering.

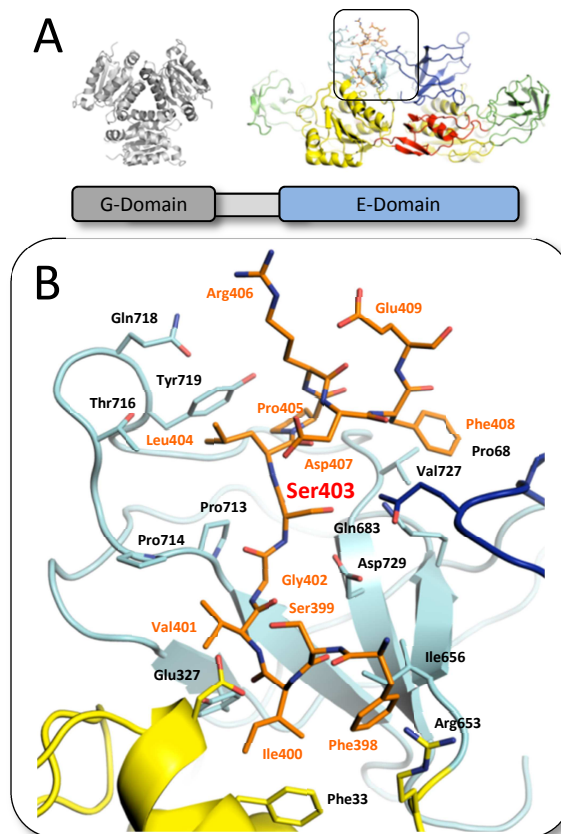


Figure 5. **Structural basis of gephyrin-mediated GlyR anchoring.** A, Overall architecture of the complex (PDB-ID: 2FTS). The GlyR  $\beta$ -loop is shown in stick representation whereas gephyrin's E domain and G domain are shown in cartoon representation. B, Close-up view into the binding pocket. The GlyR  $\beta$ -loop is tightly packed in the cleft formed by subdomains III and IV from one monomer, as well as subdomain IV from the other monomer. All residues in close proximity to the interface are highlighted as stick model and numbered. Phosphorylation of Ser403 (marked in red) by PKC results in a weakened gephyrin interaction strength. © 2012 HM Maric

### 1.3.3 Gephyrin-Mediated GABA<sub>A</sub>R Clustering

As described in the previous paragraph, gephyrin-mediated GlyR clustering was identified early, and could be analyzed at atomic resolution later, however, gephyrin's role in GABA<sub>A</sub>R-clustering remained elusive until recently. GlyRs and GABA<sub>A</sub>Rs share a close evolutionary relationship, as indicated by similarities in the respective gene structures [34]. Additionally, the neurotransmitters glycine and GABA share the same presynaptic transporter, the vesicular inhibitory amino acid transporter (VIAAT) [29, 66, 67]. Not surprisingly, in the spinal cord and several distinct brainstem areas, glycine and GABA can be coreleased from the same presynaptic terminal to activate postsynaptic GlyRs and GABA<sub>A</sub>Rs. Interestingly, gephyrin is indeed also involved in the aggregation and postsynaptic stabilization of GABA<sub>A</sub>Rs, and it is well established that glycinergic and GABAergic neurotransmission can be intermingled to provide inhibition of neuronal activity.

The early finding of colocalization of a subset of GABA<sub>A</sub>Rs and gephyrin in clusters on neuronal surfaces implied that these receptors are either directly associated with this scaffold protein, or interact via a linker protein [68-70]. Reducing the expression of gephyrin in cultured neurons or mice results in the selective loss of synaptic localization of GABA<sub>A</sub>Rs composed of  $\alpha 2\beta\gamma 2$  or  $\alpha 3\beta\gamma 2$  subunits [69, 71]. In contrast to this finding, a major subset of GABA<sub>A</sub>Rs comprised of either  $\alpha 1\beta\gamma 2$  or  $\alpha 5\beta\gamma 2$  subunits can accumulate and cluster at synapses independently of gephyrin [72, 73], indicating a receptor subunit-specific role of gephyrin. *Vice versa*, the picture is complicated by the finding that GABA<sub>A</sub>Rs are essential for postsynaptic clustering of gephyrin at all synapses, independently of the GABA<sub>A</sub>R subunits being present [69, 74-77].

The  $\gamma 2$  subunit has been consistently proposed as a candidate for mediating synaptic targeting of GABA<sub>A</sub>Rs [78, 79]. In line with this idea, knockout mice with a deletion of the  $\gamma 2$  subunit die soon after birth and lack GABA<sub>A</sub>R clusters [71]. Transfection of neuronal cultures from these mice with  $\gamma 2$  cDNA restored clustering [80], while transfection of cultured hippocampal neurons with shRNAi constructs against gephyrin reduced the number of  $\gamma 2$ -containing GABA<sub>A</sub>R clusters [81]. Despite this evidence, a direct interaction of the GABA<sub>A</sub>R  $\gamma 2$  subunit and gephyrin could not be demonstrated until now. Compared to  $\alpha 1-3$  containing GABA<sub>A</sub>Rs,  $\gamma 2$ -containing receptors show a stronger extrasynaptic localization as judged from stainings of hippocampal pyramidal neurons in culture and *in vivo* [82]. Indeed GABA<sub>A</sub>Rs of the  $\alpha 5\beta\gamma 2$  composition were found to be located mostly at extrasynaptic sites, despite containing a  $\gamma 2$  subunit, where they are associated with the sub-membraneously located protein radixin [25, 26, 83]. While a role in the synaptic anchoring of GABA<sub>A</sub>Rs cannot be ruled out, it can be assumed that  $\gamma 2$  subunits might not be the major single determinant for the synaptic targeting of GABA<sub>A</sub>Rs.

In 2008 Tretter et al. succeeded in demonstrating a specific interaction between gephyrin and the GABA<sub>A</sub>R  $\alpha$ 2 subunit. Detergent-free conditions allowed the definition of a minimal core-sequence which is sufficient for gephyrin-mediated receptor clustering (Figure 6) [27]. The lack of a detailed and quantitative *in vitro* characterization of this interaction may be attributed to the extensive hydrophobic nature of the identified GABA<sub>A</sub>R  $\alpha$ 2 gephyrin-binding motif. Interestingly, the

identified linear motif is unique among all 19 GABA<sub>A</sub>R subunits and in addition displays no obvious conservation with the GlyR  $\beta$  subunit motif. This possibly implies a different binding site on gephyrin and suggests a distinct regulation of this interaction. Recent yeast two-hybrid (Y2H) assays further suggested an interaction between gephyrin and the GABA<sub>A</sub>R  $\alpha$ 3 subunit [84] and, interestingly, propose unique binding sites on gephyrin for the GABA<sub>A</sub>R  $\alpha$ 2,  $\alpha$ 3 as well as GlyR  $\beta$  subunits [84]. Prompted by the findings described in section 1.3.2 and 1.3.3 we formulated five gephyrin-related goals, which were central to my thesis:

- Development of bivalent receptor derived minimum peptides to verify and quantify the multivalency of the receptor gephyrin interaction *in vitro*.
- Falsification or verification of the proposed [27, 84] direct gephyrin GABA<sub>A</sub>R  $\alpha$ 1-3 interactions, mapping of the binding sites as well as identification of key residues for complex formation.
- Deciphering gephyrin's receptor subunit preference and test for synergistic or competitive binding effects.
- If applicable, obtaining cocrystal structures of the different gephyrin-GABA<sub>A</sub>R subunit complexes.
- If possible identify possible phosphorylation sites within the identified motifs and demonstrate reduction of the direct gephyrin affinity upon introduction of phosphomimetic residues.

Interestingly recent Y2H experiments suggested a possible role of CB in the process of gephyrin-mediated receptor clustering [84]. In particular, a tripartite complex of gephyrin, CB and GABA<sub>A</sub>R  $\alpha$ 2 was proposed. Therefore my study was expanded to cover CB which will be introduced in the next chapter.

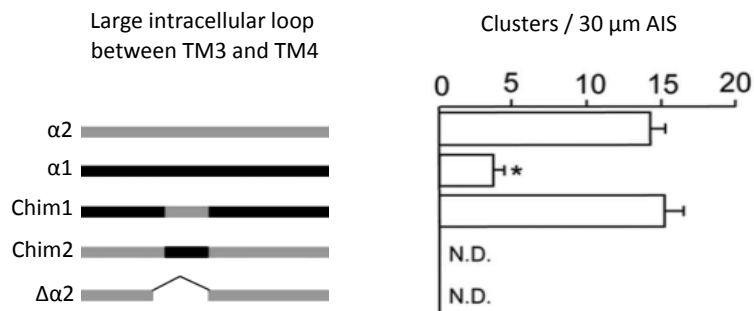


Figure 6. **Residues 360-375 mediate clustering of  $\alpha$ 2-containing GABA<sub>A</sub>Rs.** The structures of the chimeric variants are indicated in the line diagram with grey lines indicating the intracellular loop of  $\alpha$ 2 and black lines indicating the  $\alpha$ 1-loop.  $\alpha$ 2 containing receptors display a stronger clustering than  $\alpha$ 1 containing receptors. Specifically residues 360-375 in the  $\alpha$ 2 subunit determine the receptor subunit cluster number. The  $\alpha$ 1-loop in which  $\alpha$ 2 residues 360-375 are introduced instead of the corresponding  $\alpha$ 1 residues (Chim1) shows strong clustering. In contrast, absence of  $\alpha$ 2 residues 360-375, either by exchange or deletion, disrupts receptor clustering (Chim2 and  $\Delta\alpha$ 2). © 2008 V Tretter, TC Jacob, J Mukherjee, JM Fritschy, MN Pangalos, SJ Moss

## 1.4 Collybistin

Collybistin (CB) (from the Greek word to exchange (κολλυ-βιστομαι)) and its human homolog hPEM-2 (human homolog of posterior end mark-2) are members of the guanine nucleotide exchange factor (GEF) superfamily. The CB gene is highly expressed in the brain and is located on the human X-chromosome. GEFs catalyze GDP-GTP exchange on small GTPases and those that act on the Rho/Rac/Cdc42 GTPase family [85] and universally feature a Dbl homology (DH) domain (also called RhoGEF domain) followed by a pleckstrin homology (PH) domain. hPEM-2 appears to activate Cdc42 but not Rac or RhoA [86-88], which influences cell morphology by initiating actin cytoskeleton remodeling [89]. Accordingly, it has been proposed that, at inhibitory synapses, CB initiates local remodeling of the sub-synaptic cytoskeleton [90]. In contrast, analysis of Cdc42 knockout mice indicated that Cdc42 is dispensable for gephyrin and GABA<sub>A</sub>R clustering [91].

While there is only one CB isoform identified in humans, there exist at least six in rats and four in mice. CB splice variants differ either in their C termini or in the presence or absence of an N-terminal SH3 domain [43, 87, 92] (Figure 7). The highly conserved DH domain interacts directly with the GTPase while the PH domain binds with high affinity to membrane phosphoinositides and thereby recruits CB to the membrane [43, 91, 93].

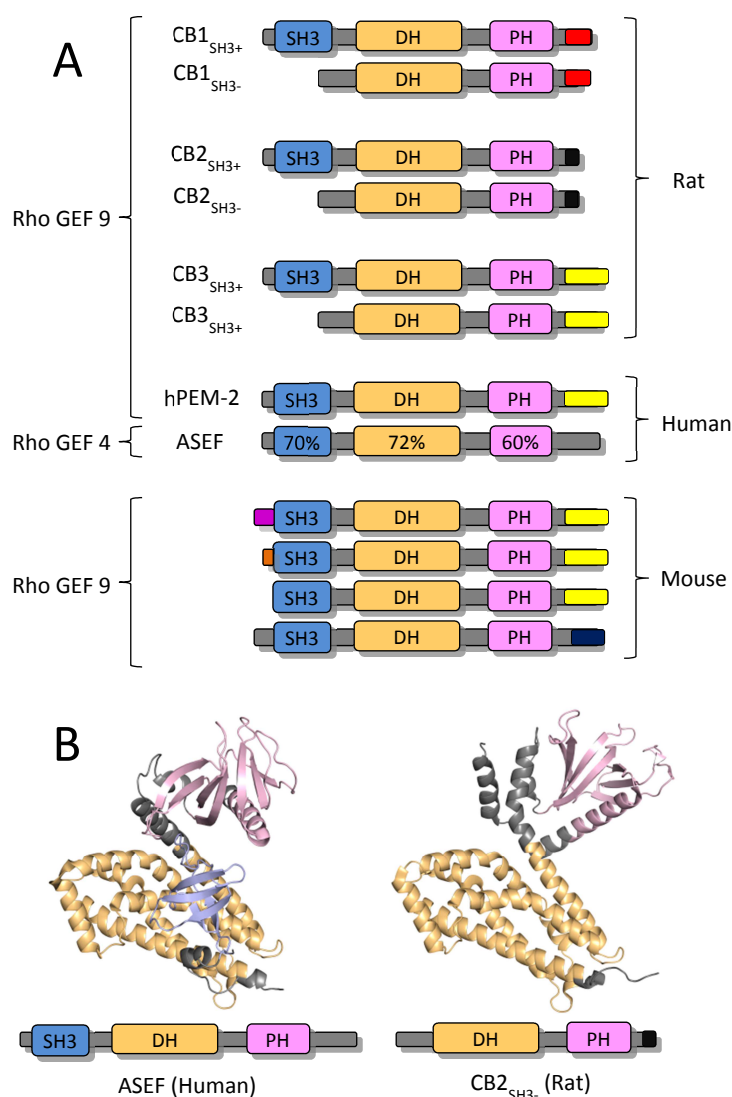


Figure 7. **Architecture and structure of Rho GEFs 4 and 9.** A, Schematic representation of the domain architecture of known Rho GEF 9 (CB) isoforms and Rho GEF 4 (ASEF). Different colors denote distinct sequences at the N or C termini. The C terminal region of CB3 is identical to hPEM-2, the only isoform described in humans. Human Rho GEF 9 and 4 domains share between 60% and 72% sequence identity. In mice, the CB1-CB3 nomenclature does not apply because the sequence closest to rat CB3 is encoded in three variants with different N-termini, whereas the sequence closest to either CB1 or CB2 has a unique C terminus. B, Rho GEF crystal structures. Structure of Rho GEF 4 (ASEF) PDB-ID: 2PZ1 and Rho GEF 9 (CB) PDB-ID: 2DFK. The high sequence identity is mirrored at the level of secondary structure. © 2012 HM Maric

### 1.4.1 Collybistin's Role in GABA<sub>A</sub>R Clustering

The SH3 domain of CB was proposed to act as an auto-inhibitory domain by binding intramolecularly to both the PH and DH domains. In line with this idea, the crystal structure of CB without the SH3 domain but in complex with Cdc42 describes CBs open active form, while the structure of the CB homologous protein ASEF which contains an SH3 domain describes a closed inactive conformation [94, 95] (Figure 8). In theory, either PH domain-binding phosphoinositides, or SH3 ligand-binding could trigger the disruption of the possibly inhibiting SH3-PH domain interaction.

Recent Y2H assays suggested GABA<sub>A</sub>R  $\alpha$ 2 [84] and NL-2 [41] as possible activators for CB by directly interacting with the SH3 domain and thereby releasing it from the PH and DH domains. Interestingly, mapping studies additionally proposed an overlapping binding site for gephyrin and CB on the large intracellular loop of the GABA<sub>A</sub>R  $\alpha$ 2 subunit and based on Y2H studies it was even suggested that a tripartite gephyrin-CB-GABA<sub>A</sub>R  $\alpha$ 2 complex may form in a synergistic binding event. In line with the GABA<sub>A</sub>R-dependent function of CB to initiate sub-membranous postsynaptic gephyrin-clustering, the missense mutation G55A within the SH3 domain of CB disrupts both the clustering of  $\alpha$ 2-containing GABA<sub>A</sub>Rs and of gephyrin in cultured neurons [84], as well as the direct receptor-CB interaction in Y2H assays. Interestingly, this naturally occurring mutation is associated with hyperekplexia, epilepsy, and mental retardation in patients [43, 96]. So far neither NL-2 nor GABA<sub>A</sub>R  $\alpha$ 2 binding could be verified with purified proteins [43, 87].

Based on these recent findings we added the following CB-related goals to the work presented here:

- Verification or falsification of possible direct interactions between CB SH3 and GABA<sub>A</sub>R  $\alpha$ 1-3 subunits using recombinant purified proteins.
- Determination of binding parameters and hence determination of SH3-mediated GABA<sub>A</sub>R subunit preference of CB.

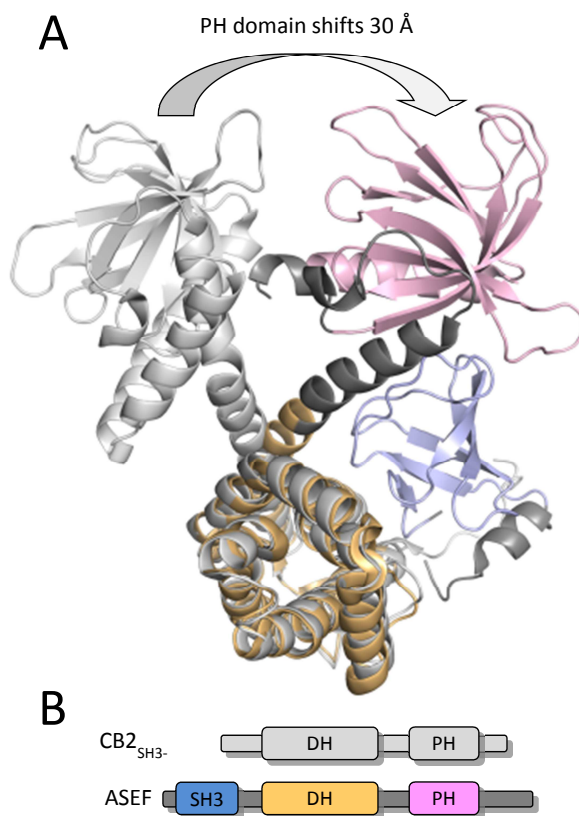


Figure 8. **Structural basis of SH3-mediated CB inhibition.** A, Superposition of CB<sub>2SH3</sub> (marked in grey) lacking the SH3 domain and its close homolog ASEF (colored in blue, orange and pink) with an N-terminal SH3 domain. (Rho GEF 4 (ASEF) PDB-ID: 2PZ1 and Rho GEF 9 (CB) PDB-ID: 2DFK). The DH and PH domains engage in direct intra-molecular interactions with the SH3 domain resulting in a 30 Å shift towards the SH3 domain, when compared to the domain arrangement in CB. Possible inter-molecular ligands may have to compete against this domain self-masking. It was therefore proposed that the CB structure lacking the SH3 domain displays a Rho GEF domain arrangement that resembles its activated form, while the ASEF structure would provide a view of an inactivated Rho GEF. B, Schematic domain architecture of CB<sub>2SH3</sub> and ASEF. © 2012 HM Maric

### 1.4.2 Collybistin's Role in Gephyrin Clustering

Interestingly, in addition to GABA<sub>A</sub>R clustering, CB has been consistently implicated in the postsynaptic clustering of gephyrin [97]. Mass spectrometry-based proteomic studies identified CB at inhibitory synapses [98] and video-microscopic analysis verified colocalization with gephyrin at inhibitory synapses [84]. Furthermore, coexpression of CB with gephyrin in heterologous cells, yields gephyrin aggregates that can be either found intracellularly or at the membrane, depending on whether CB contains an SH3 domain (intracellular) or lacks it (sub-membrane) [87].

Knockout (KO) studies with the collybistin gene [99] revealed a complex role of CB in gephyrin-mediated GABA<sub>A</sub>R clustering. CB KO mice show a loss of gephyrin and GABA<sub>A</sub>R clusters in the hippocampus and amygdala, while in the brainstem, neocortex and several other brain areas the clustering of gephyrin, GABA<sub>A</sub>Rs or GlyRs is unaffected. It was suggested that other GEFs might compensate for the loss of CB function in these brain areas. In line with the unaltered GlyR distribution, CB KO mice showed no signs of a motor neuron phenotype, which would be indicative of an impaired glycinergic inhibition [100]. However, in accordance with a region-specific loss of  $\gamma$ 2-subunit containing GABA<sub>A</sub>R clusters, the CB KO mice show an enhanced reaction to aversive stimuli, as demonstrated by anxiety-related test paradigms, like the open field and the elevated plus-maze [99]. Indeed, a similar anxiety phenotype has been observed in mice expressing only a single functional GABA<sub>A</sub>R  $\gamma$ 2-subunit allele [101] and therefore the anxiety-related responses were explained by the reduced synaptic GABA<sub>A</sub>R clusters in the CB KO mice in the septohippocampal and amygdala systems.

In contrast, the molecular basis of CB's role in gephyrin and GABA<sub>A</sub>R clustering still remains to be established. While gephyrin was identified early on as a potential direct binding partner in yeast two-hybrid assays [43], an interaction that could later be verified with purified proteins [94], the specific interaction sites and the overall binding strength of this interaction remain elusive. Based on the findings summarized in this chapter we expanded my CB-related aims:

- Comparison of gephyrin's and CB's GABA<sub>A</sub>R binding with purified proteins *in vitro*.
- Analysis of a possible gephyrin, CB SH3 and GABA<sub>A</sub>R tripartite interaction to reveal synergistic or competitive binding events among the different binding partners.

This work focused on GABA<sub>A</sub> and glycine receptor-related direct scaffold interactions and therefore the analysis of the interaction of full-length CB with gephyrin was not addressed. While gephyrin and CB were proposed to mediate GABA<sub>A</sub>R clustering at postsynaptic sites, radixin was shown to cluster these receptors at extrasynaptic sites. Radixin-mediated clustering was analyzed in this work and therefore will be discussed in the following final chapter of the introduction.



## 1.5 Radixin

Radixin (derived from the Latin word for root (radix)), was originally identified as an actin-binding protein [102]. A Radixin-knockout in mice leads to deafness [103] due to defective stereocilia in the inner and outer hair cells, which show a high radixin expression level [104]. In line with this finding, mutations in the human radixin gene also correlate with neurosensory hearing loss [105]. Additionally, radixin modulates the localization of the multidrug resistance-associated protein 2 (MRP2), an organic anion transporter, at the canalicular membrane in hepatocytes [106, 107].

Together, ezrin, radixin and moesin (ERM) share 70% identity and form the ERM protein family. The majority of ERM proteins were shown to act as linker proteins that couple extracellular proteins to the cytoskeleton. They are composed of three conserved domains (Figure 9):

(A) An N terminal FERM domain which functions as a universal protein-binding module. Its name derives from the first proteins that were shown to contain this domain (four-point-one (4.1), ezrin, radixin, moesin). This domain was demonstrated to directly interact with receptors, other transmembrane proteins, extracellular matrix molecules and adhesion proteins [26, 108-113].

(B) A central  $\alpha$ -helical domain, which either adopts an elongated conformation or folds back on the FERM domain, thus allowing the C terminal domain to mask FERM ligand binding sites.

(C) The high affinity auto-inhibitory module of the FERM domain which is therefore also referred to as ERM adhesion domain (ERMAD). The mechanisms of ERMAD-mediated FERM inhibition could be resolved structurally and will be discussed in the next paragraph.

(D) The C terminal domain, which was shown to directly bind to actin filaments [114].

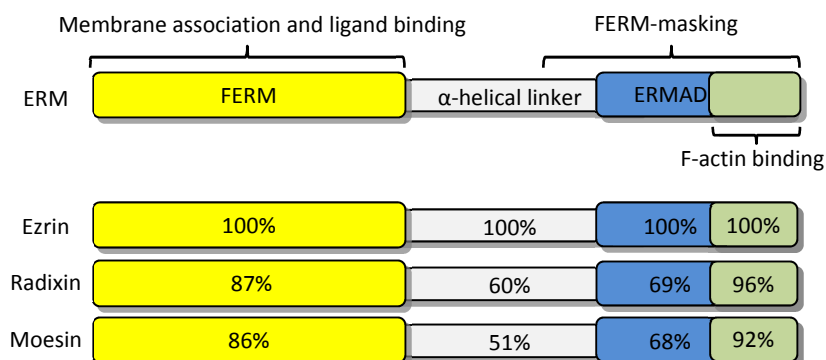


Figure 9. **Architecture of ERM protein family members.** Schematic representation of the domain architectures of ezrin, moesin and radixin. Sequence identities, are indicated for each domain. © 2012 HM Maric

Despite their close sequence and structural homology ERM protein family members display a unique expression pattern in various cell types and tissues, even within the CNS [115, 116]. In the brain, ERM proteins have been implicated in growth cone development [116-119], axonal outgrowth, morphological rearrangements, motility and signaling [120, 121]. Radixin has been detected in dorsal root ganglion neurons [122], embryonic hippocampal cells [117] and in adult hippocampal astrocytes [115].

Numerous studies demonstrate that the variety of functions displayed by ERM family members is mirrored by a variety of different modes of self-association, phosphorylation and ligand binding [123, 124]. The next section will specifically summarize the functional implications of FERM-ligand cocrystal structures.

### 1.5.1 Function of the FERM Domain of Radixin

Among the FERM domain structures of different proteins that have been solved independently using X-ray crystallography are:

- Ezrin [125], radixin [126] and moesin [127], which together form the ERM-protein family described in the previous section.
- Talin [128], a protein concentrated at regions of cell-substratum contact in lymphocytes and at cell–cell contacts.
- Merlin [129] [130] and DAL-1 (differentially expressed in adenocarcinoma of the lung protein, also known as 4.1B) [131], which are important tumor suppressor proteins.
- Myosin-x [132], an unconventional myosin motor protein.
- Focal adhesion kinase (FAK) [133], a tyrosine kinase involved in signaling through integrins.
- 4.1R [134] (part of the 4.1 gene family consisting of 4.1B, 4.1R, 4.1G and 4.1N), which plays a key role in regulating physical properties of the erythrocyte membrane skeleton by stabilizing the spectrin-actin interaction and due to its importance to the red blood cell designated 4.1R

The FERM domain can be subdivided into three subdomains (F1, F2 and F3) which are arranged in a shape resembling a clover leaf (Figure 10A). A single exception to this arrangement is talin's FERM domain which instead adopts a linear subdomain arrangement, despite sharing 26% sequence identity with radixin's FERM domain (Figure 10B). The three subdomains display significant structural homology to protein folds associated with specific functions. Specifically, F1 folds similar to ubiquitin, F2 shows a secondary structure comparable to the acyl coenzyme A binding protein while F3 adopts a fold similar to the phosphotyrosine binding (pTB) domain. Interestingly, pTB domains adopt a similar fold as PH domains and, in case of CB and FERM, they both mediate membrane targeting by binding membrane-bound phosphoinositols.

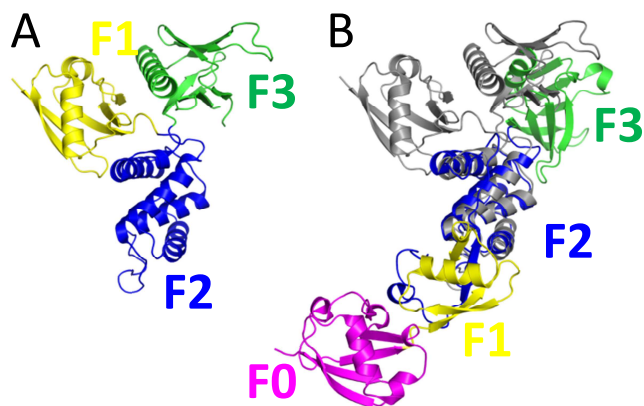


Figure 10. **Comparison of different FERM domain crystal structures.** A, Most commonly FERM domains adopt a typical clover-like architecture (PDB-ID: 1GC7) formed by their three subdomains F1, F2 and F3. B, The Talin FERM domain (PDB-ID: 3IVF) instead adopts a linear conformation (colored according to the subdomain architecture), which is superimposed onto a clover-like FERM domain in grey. © 2012 HM Maric

Crystal structures of the isolated FERM domains provide a view of its active form since the inhibitory ERMAD is absent. Various crystal structures of FERM domain-ligand complexes define different modes of binding which rely on distinct consensus motifs (Figure 11). The pocket between F2 and F3 can be occupied by inositol triphosphate (IP<sub>3</sub>), the soluble head group of phosphatidylinositol 4,5-bisphosphate (PIP<sub>2</sub>) (Figure 11A). The cytoplasmic tails of the intercellular adhesion molecule 2 (ICAM2), cluster of differentiation (CD) proteins 43 and 44, p-selectin glycoprotein ligand 1 (pSGl1), neutral endopeptidase (NEP) and tumor suppressor in lung cancer 1 (TSLC1) bind into the large groove bordered by a  $\beta$ -strand and an  $\alpha$ -helix of subdomain F3 (Figure 11B), although they are only moderately conserved. This interaction involves a peptide backbone interaction with a FERM  $\beta$ -strand (Figure 11B) and is similar to the binding of the phosphorylated peptide of insulin receptor substrate 1 (IRS1) to the pTB domain of the insulin receptor [135, 136]. In contrast, peptides, which are derived from either NHERF-1 or EBp50 (Figure 11C), display no sequence homology to the aforementioned FERM ligands and bind through a different surface on subdomain F3 [137].

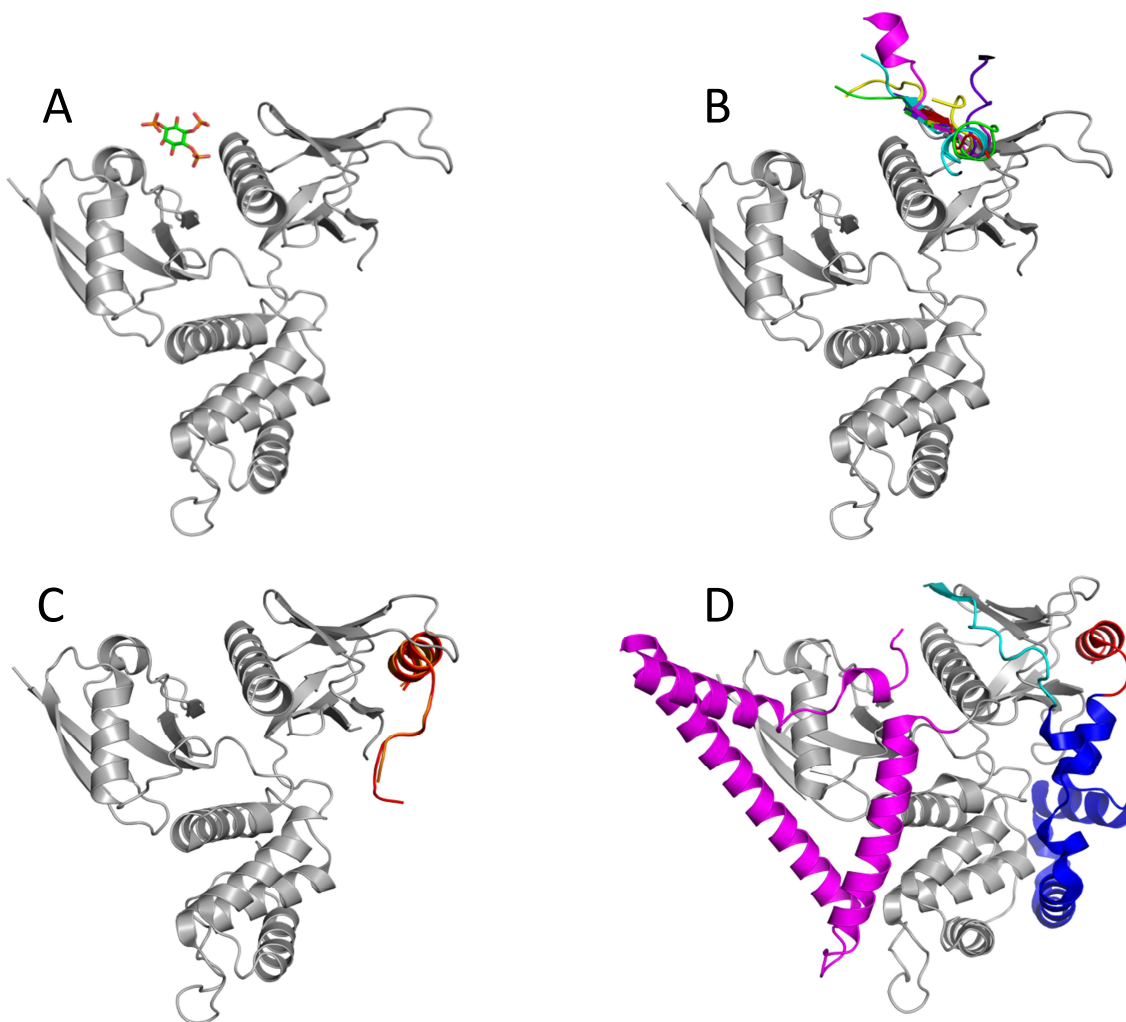


Figure 11. **Structural basis of the multiple ligand-binding modes of FERM.** A, FERM-IP<sub>3</sub>-complex (PDB-ID: 1GC6). B, FERM in complex with ICAM1 (cyan, PDB-ID: 1J19), NEP (violet, PDB ID: 2YVC), CD-43 (green, PDB-ID: 2EMS), FERM (pink, PDB-ID: 2D2Q), TSLC1 (red, PDB-ID: 3BIN) and PSGL1 (yellow, PDB-ID: 2EMT). C, FERM in complex with NHERF-1 (red, PDB-ID: 2D11), EBp50 (orange, PDB-ID: 1SGH). D, Structure of full-length moesin. Moesin's ERMAD and helical linker region occupy all known ligand binding sites of FERM. The linker interferes with IP<sub>3</sub> binding (magenta), ERMAD interferes with ICAM1, NEP, CD-43, TSLC1, PSGL1 binding (cyan), as well as EBp50 and NHERF-1 binding (red) and additionally occupies large parts of the FERM domain surface (blue). © 2012 HM Maric

Interestingly, Ebp50 reduces the affinity of the FERM domain for the ligands discussed above, despite binding to a different binding site [138]. The crystal structure of the moesin FERM domain in complex with its ERMAD defined the molecular basis of ERMAD-based FERM inactivation [139] (Figure 11D). Specifically, a  $\beta$ -strand and four  $\alpha$ -helices mask a large surface on the F2 and F3 subdomains [140]. ERMAD occupies both, the ICAM2 and the Ebp50 binding sites. The independent binding of ERMAD helices to FERM [141] is thought to result in an avidity-based potentiation of the FERM-ERMAD binding affinity. Therefore, this masking mechanism most likely explains earlier findings of inactive full-length ERMs [142]. ERM protein oligomerization was shown early [143, 144] and functional implications have been proposed. Indeed, a second masking mechanism was identified, which relies on a FERM domain head to tail dimerization [145].

Activation of ERM proteins is a multistep process [146], which requires several conformational changes [114]. The intra-molecular FERM-ERMAD association is thought to mask the F-actin [147, 148] as well as the ligand binding sites. PIP<sub>2</sub> binding of FERM [149] induces a conformational change which renders a conserved threonine residue more accessible to phosphorylation [146]. In line with this idea, simultaneous mutation of four lysine residues in the ezrin FERM domain (analogous to the mutant radixin-GFP K(253,254,262,263)N blocks PIP<sub>2</sub> binding and therefore membrane association [150]. PIP<sub>2</sub> binding together with the phosphorylation opens the intra-molecular FERM-ERMAD association, thereby exposing the C terminal F-actin and N terminal ligand binding sites [147].

### 1.5.2 Radixin-Mediated GABA<sub>A</sub>R Clustering

The group of Matthias Kneussel (ZMNH Hamburg) identified radixin as an essential clustering factor for  $\alpha$ 5-containing GABA<sub>A</sub>Rs [26].

Making use of the Y2H system the binding sites on both proteins were mapped (Figure 12) and direct binding was verified using recombinant proteins in pull-down-assays of brain lysates. The same study furthermore revealed that both, radixin's phosphorylation-dependent activation as well as its binding to actin, are crucial prerequisites for receptor clustering. Additionally, the study ruled out that radixin is involved in receptor trafficking and

verified that the direct interaction with the receptor is specific to radixin and does not occur with either one of its close homologs moesin or ezrin. Finally, radixin and gephyrin were shown to neither colocalize nor bind to each other and hence most likely represent separate receptor-anchoring systems.

Previous studies showed that GABA<sub>A</sub>Rs with an  $\alpha_5\beta_x\gamma_2$  composition are mainly localized extrasynaptically despite the presence of a  $\gamma_2$  subunit, [79, 151]. Extrasynaptic inhibitory receptors mediate tonic inhibition, which reduces the overall probability for action potential generation. Interestingly, upon loss of extrasynaptic GABA<sub>A</sub>R  $\alpha_5$  clusters, bicuculline-sensitive tonic currents are still present, indicating that un-clustered receptors remain functional in the neuronal surface [26]. Therefore, the reason why extrasynaptic GABA<sub>A</sub>R containing  $\alpha_5$  subunits assemble into clusters [151,

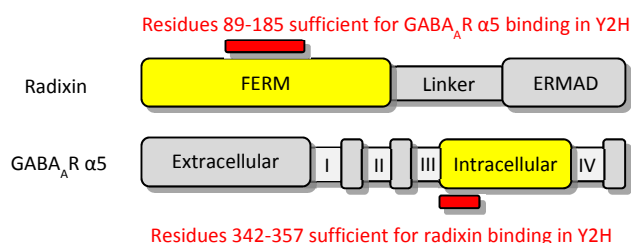


Figure 12. **Mapping of the direct FERM GABA<sub>A</sub>R  $\alpha_5$  subunit interaction.** In Y2H studies residues 89-185 of radixin are sufficient to yield a positive signal for GABA<sub>A</sub>R  $\alpha_5$  binding and *vice versa*  $\alpha_5$  residues 342-357 are sufficient for radixin binding. © 2012 HM Maric

152] remains unclear, nevertheless, different possible functions of the clustering have been proposed [26]:

(A) Glial cells were shown earlier be able to release neurotransmitters including GABA [153, 154], therefore extrasynaptic GABA<sub>A</sub>R  $\alpha$ 5 clusters might represent neuron–glia contact membrane specializations.

(B) Extrasynaptic GABA<sub>A</sub>R clusters might be involved in signaling cascades similar to those proposed for extrasynaptic glutamate receptors. Here, activation of extrasynaptic NMDARs, unlike synaptic receptors, would cause cAMP-response element binding protein (CREB) dephosphorylation eventually resulting in mitochondrial dysfunction and cell death [155].

(C) Clusters at extrasynaptic sites may function as a reserve pool for the rapid recruitment into synapses. Although the majority of radixin-associated GABA<sub>A</sub>R  $\alpha$ 5 subunit clusters are located at extrasynaptic sites, both proteins indeed occasionally localize to inhibitory synapses [26, 79].

To decipher the molecular basis of radixin-mediated extrasynaptic GABA<sub>A</sub>R clustering my experiments addressed the following issues:

- Verification or falsification of the direct FERM  $\alpha$ 5-loop interaction with purified proteins and determination of the respective binding affinity.
- Fine-mapping of the involved binding regions and comparison to known FERM ligand-binding sites.
- If possible, obtaining a high resolution cocrystal structure of the FERM  $\alpha$ 5-loop complex.
- Identification of possible posttranslational modifications within the fine-mapped binding sites proposing a regulation mechanism.

## 2 Materials and Methods

### 2.1 Biochemicals

#### 2.1.1 Bacterial Strains

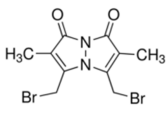
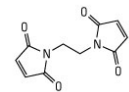
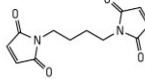
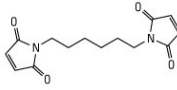
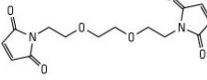
Table 1. Bacterial strains.

Name	Genotype	Source
BL21-CodonPlus(DE3)-RIL	<i>E. coli</i> B F- <i>ompT hsdS</i> (r <sub>B</sub> -m <sub>B</sub> -) <i>dcm</i> <sup>+</sup> Tet <sup>r</sup> <i>gal</i> I (DE3) <i>endA</i> Hte [ <i>argU ileY leuW Cam</i> <sup>r</sup> ]	Stratagene
DH5α	F- φ80/ <i>lacZ</i> ΔM15 Δ( <i>lacZYAargF</i> ) U169 <i>deoR recA1 endA1 hsdR17</i> (rk-, mk+) <i>phoA supE44thi-1 gyrA96 relA1</i> λ-	Invitrogen

#### 2.1.2 Crosslinkers

Maleimide crosslinkers were purchased from Pierce Thermo Scientific (Rockford, USA) and haloalkyl crosslinkers from Invitrogen (Carlsbad, USA).

Table 2. Crosslinker.

Crosslinker	Sulfhydryl reactive group	Linker and Length (Å)	Molecular Weight (g/mol)	Structure
Bromomethyl-2,6-dimethyl-pyrazolo 1,2a-pyrazole-1,7-dione (Dibromobimane) (bbBr)	Haloalkyl	Pyrazolopyrazole (6)	350.10	
1,2-Bismaleidoethane (BMOE)	Maleimide	Ethyl (8)	220.18	
1,4-Bismaleidobutane (BMB)	Maleimide	Butyl (11)	248.23	
1,6-Bismaleidohexane (BMH)	Maleimide	Hexyl (13)	276.23	
1,8-Bismaleidodiethylenglycol (BM(PEG) <sub>2</sub> )	Maleimide	Diethyleneglycol (15)	308.29	

## 2.1.3 Enzymes

Table 3. **Enzymes.**

Enzyme	Source
Chymotrypsin	Sigma-Aldrich
Desoxyribonuclease I	Invitrogen
DpnI	New England Biolabs
Factor Xa	Calbiochem
Papain	Roth
Phusion DNA Polymerase	Finnzymes
Thrombin	GE Healthcare
Trypsin	Sigma-Aldrich

## 2.1.4 Peptides

Table 4. **Peptides.**

Peptides were purchased from Genscript USA Inc. (Piscataway, New Jersey, USA) and PANATecs (Tübingen, Germany) at a minimal purity of 90%.

Source Protein	Sequence	Modification	Solubility (1 mM)	Binding Assays / Dimerization / Crystallization
GABA <sub>A</sub> R α1 336-350	KNNTYAPTATSYTPN	-	pH 6-8	Y / N / N
GABA <sub>A</sub> R α1 336-350	KNNTYAPTATSYTPN	N-Biotin	pH 6-8	Y / N / N
GABA <sub>A</sub> R α1 + Cys	TYAPTATSYTPNLARGDC	-	pH 6-8	Y / Y / N
GABA <sub>A</sub> R α1 / GlyR β	TYAPTATLPRDFELSNYDCY	-	pH 6-8	Y / Y / N
GABA <sub>A</sub> R α2 335-359	QNNAYAVAVANYAPN	-	20% DMSO	Y / N / N
GABA <sub>A</sub> R α2 335-359	QNNAYAVAVANYAPN	N-Biotin	20% DMSO	Y / N / N
GABA <sub>A</sub> R α2 + Cys	AYAVAVANYAPNLSKDC	-	20% DMSO	Y / Y / N
GABA <sub>A</sub> R α3 366-380	KNTTFNIVGTTYPIN	-	10% DMSO	Y / N / N
GABA <sub>A</sub> R α3 366-380	KNTTFNIVGTTYPIN	N-Biotin	10% DMSO	Y / N / N
GABA <sub>A</sub> R α3 + Cys	TFNIVGTTYPINLAKDTEC	-	10% DMSO	Y / Y / N
GABA <sub>A</sub> R α5 342-357	NYFTKRGWAWDGKKAL	N-Biotin	pH 6-8	Y / N / N
GABA <sub>A</sub> R α5 342-364	NYFTKRGWAWDGKKALEAAKIKK	N-Biotin	pH 6-8	Y / N / N
GABA <sub>A</sub> R α5 346-365	KRGWAWDGKKALEAAKIKK	-	pH 6-8	Y / N / N
GABA <sub>A</sub> R β2+Cys	DFSLYTMPHENILLSTC	-	pH 6-8	Y / Y / N
GABA <sub>A</sub> R γ2+Cys	MFSFKAPTIDIRPRSATIC	-	pH 6-8	Y / Y / N
GlyR β 398-411	FSIVGSLPRDFELS	-	pH 6-8	Y / N / Y
GlyR β 398-411	FSIVGSLPRDFELS	N-Biotin	pH 6-8	Y / N / N
GlyR β 397-416	DFSIVGSLPRDFELSNYDCY	-	pH 6-8	Y / Y / Y
GlyR β / GABA <sub>A</sub> R α1	DFSIVGSSYTPNLARGDPGL	-	pH 6-8	Y / N / N
GlyR β / GABA <sub>A</sub> R α3	DFSIVGSTYPINLAKDTEFS	-	pH 6-8	Y / N / N

## 2.1.5 Plasmids

Table 5. Plasmids.

Insert	Tag / Vector / Cleavage	Purification / Crystallization	Source
Collybistin I 4-72 (SH3)			
SH3 WT	N-GST / PGEX-4T2 / Thrombin	Y / N	Brose N.
SH3 D33N	N-GST / PGEX-4T2 / Thrombin	-	Amato M.
SH3 D33N,D51N	N-GST / PGEX-4T2 / Thrombin	Y / N	Amato M.
SH3 W45A	N-GST / PGEX-4T2 / Thrombin	-	Amato M.
GABA <sub>A</sub> R α1 (α1)			
α1 full-length WT	pEGFP-N2	-	Kneussel M.
α1 (307-393) WT	N-GST / PGEX-5x-1 / FactorXa	-	Kneussel M.
α1 (307-393) WT	N-His <sub>6</sub> / pET M-11 / TEV	Y / N	Maric H.M.
α1 (307-393) Y340A	N-His <sub>6</sub> / pET M-11 / TEV	Y / N	Maric H.M.
α1 (307-393) Y347A	N-His <sub>6</sub> / pET M-11 / TEV	Y / N	Maric H.M.
α1 (307-393) A341S, P342I	N-His <sub>6</sub> / pET M-11 / TEV	Y / N	Maric H.M.
α1 (307-393) A341S	N-His <sub>6</sub> / pET M-11 / TEV	Y / N	Maric H.M.
α1 (307-393) P342I	N-His <sub>6</sub> / pET M-11 / TEV	Y / N	Maric H.M.
α1 (307-393) T348A	N-His <sub>6</sub> / pET M-11 / TEV	Y / N	Maric H.M.
α1 (307-393) T348E	N-His <sub>6</sub> / pET M-11 / TEV	Y / N	Maric H.M.
α1 (307-393) T348D	N-His <sub>6</sub> / pET M-11 / TEV	Y / N	Maric H.M.
α1 (307-393) Δ357–368	N-His <sub>6</sub> / pET M-11 / TEV	Y / N	Maric H.M.
α1 (307-393) Δ333–348	N-His <sub>6</sub> / pET M-11 / TEV	Y / N	Maric H.M.
α1 (307-393) α6 (333–348)	N-His <sub>6</sub> / pET M-11 / TEV	Y / N	Maric H.M.
GABA <sub>A</sub> R α2 (α2)			
α2 (307-391) WT	N-His <sub>6</sub> / pET M-11 / TEV	Y / N	Tretter V.
α2 (307-391) V343G	N-His <sub>6</sub> / pET M-11 / TEV	Y / N	Maric H.M.
α2 (307-334) (Q335stop)	N-His <sub>6</sub> / pET M-11 / TEV	-	Amato M.
α2 (307-350) (S351stop)	N-His <sub>6</sub> / pET M-11 / TEV	-	Amato M.
GABA <sub>A</sub> R α3 (α3)			
α3 (332-429) WT	N-His <sub>6</sub> / pET M-11 / TEV	Y / N	Tretter V.
α3 (332-429) F369A	N-His <sub>6</sub> / pET M-11 / TEV	Y / N	Maric H.M.
α3 (332-429) I371A	N-His <sub>6</sub> / pET M-11 / TEV	Y / N	Maric H.M.
α3 (332-429) G373V	N-His <sub>6</sub> / pET M-11 / TEV	Y / N	Maric H.M.
α3 (332-429) Y376A	N-His <sub>6</sub> / pET M-11 / TEV	Y / N	Maric H.M.
α3 (332-429) Δ369–378	N-His <sub>6</sub> / pET M-11 / TEV	Y / N	Tretter V.
α3 (332-429) Δ362-378	N-His <sub>6</sub> / pET M-11 / TEV	Y / N	Tretter V.
α3 (332-429) Δ362-368	N-His <sub>6</sub> / pET M-11 / TEV	Y / N	Tretter V.
α3 (332-429) Δ362-378	N-His <sub>6</sub> / pET M-11 / TEV	Y / N	Tretter V.
GABA <sub>A</sub> R α5 (α5)			
α5 (342-429) WT	N-His <sub>6</sub> / pET M-11 / TEV	Y / N	Maric H.M.
α5 (348-429) WT	N-His <sub>6</sub> / pET M -11 / TEV	Y / N	Maric H.M.
α5 (352-429) Wt	N-His <sub>6</sub> / pET M -11 / TEV	Y / N	Maric H.M.
α5 (357-429) WT	N-His <sub>6</sub> / pET M -11 / TEV	Y / N	Maric H.M.
α5 (342-429) K354A/K355A	N-His <sub>6</sub> / pET M -11 / TEV	-	Maric H.M.
α5 (342-429) W349A/W351A	N-His <sub>6</sub> / pET M -11 / TEV	-	Maric H.M.
α5 (342-429) L350A	N-His <sub>6</sub> / pET M -11 / TEV	Y / N	Maric H.M.
α5 (342-429) WT	N- GST / pET M -30 / TEV	Y / N	Maric H.M.
α5 (342-429) WT	N-NusA / pET M-60 / TEV	Y / N	Maric H.M.
α5 full-length WT	Myc / pBK-CMV / -	-	Kneussel M.
α5 full-length WT	HA / pBK-CMV / -	-	Kneussel M.
α5 (342-429) WT	N-GST / PGEX-5x-1 / FactorXa	Y / N	Kneussel M.
GABA <sub>A</sub> R β2 (β2)			
β2 (302-464) WT	N-GST / PGEX-5x-1 / FactorXa	-	Moss S.J.



GABA <sub>A</sub> R $\gamma$ 2 ( $\gamma$ 2)				
$\gamma$ 2 (317-403) WT	N-GST / PGEX-5x-1 / FactorXa	-		Moss S.J.
Gephyrin (Geph)				
GephGL WT (1-310)	N-His <sub>6</sub> / pQE-30 / Thrombin	Y / N		Kim E.Y.
GephG WT (1-188)	N-His <sub>6</sub> / pQE-30 / Thrombin	Y / Y		Kim E.Y.
Full-length Geph P2 (1-736) WT	N-His <sub>6</sub> / pQE-30 / Thrombin	Y / N		Kim E.Y.
GephE (318-736) WT	N-Intein / pTWIN / pH-Shift	Y / Y		Kim E.Y.
GephE (318-736) F330A	N-Intein / pTWIN / pH-Shift	Y / N		Kim E.Y.
GephE (318-736) P713E	N-Intein / pTWIN / pH-Shift	Y / N		Kim E.Y.
GephE (318-736) P713E, P714E	N-Intein / pTWIN / pH-Shift	Y / N		Kim E.Y.
Full-length Geph P2 (1-736) WT	N-Intein / pTWIN / pH-Shift	Y / N		Kim E.Y.
Full-length Geph P2 (1-736) F330A	N-Intein / pTWIN / pH-Shift	Y / N		Kim E.Y.
Full-length Geph P2 (1-736) P713E	N-Intein / pTWIN / pH-Shift	Y / N		Kim E.Y.
Full-length Geph P2 (1-736)P713E, P714E	N-Intein / pTWIN / pH-Shift	Y / N		Kim E.Y.
GlycR $\beta$ ( $\beta$ )				
$\beta$ (378-426) WT	C-Intein / pTYB-2 / Thiolat	Y / Y		Kim E.Y.
$\beta$ (378-426) F398A	C-Intein / pTYB-2 / Thiolat	Y / N		Kim E.Y.
$\beta$ (378-426) S399A	C-Intein / pTYB-2 / Thiolat	Y / N		Kim E.Y.
$\beta$ (378-426) I400A	C-Intein / pTYB-2 / Thiolat	Y / N		Kim E.Y.
$\beta$ (378-426) S403A	C-Intein / pTYB-2 / Thiolat	Y / N		Kim E.Y.
$\beta$ (378-426) F408A	C-Intein / pTYB-2 / Thiolat	Y / N		Kim E.Y.
$\beta$ (378-426) F398A, I400A	C-Intein / pTYB-2 / Thiolat	Y / N		Kim E.Y.
$\beta$ (378-426) F398A, I400A, F408A	C-Intein / pTYB-2 / Thiolat	Y / N		Kim E.Y.
Radixin (Rdx)				
Rdx FERM (1-310) WT	N-GST / pET M-30 / TEV	Y / N		Maric H.M.
Rdx FERM (1-310) WT	N-NusA / pET M-60 / TEV	Y / N		Maric H.M.
Rdx FERM (1-310) WT	N-His <sub>6</sub> / pET M-11 / TEV	Y / Y		Maric H.M.
Rdx FERM (1-295) WT	N-His <sub>6</sub> / pET M-11 / TEV	Y / Y		Maric H.M.
Rdx full-length (1-583) WT	N-GST / pGEX-5x-1 / FactorXa	Y / N		Maric H.M.
Rdx full-length (1-583) T564A	N-GFP / pEGFP-N2 / -	-		Kneussel M.
Rdx full-length (1-583) T564D	N-GFP / pEGFP-N2 / -	-		Kneussel M.
Rdx (1-468) WT	N-GFP / pEGFP-N2 / -	-		Kneussel M.
Rdx (1-468) WT	myc / pBK-CMV / -	-		Kneussel M.
Rdx (1-468) K(253/254/262/263)N	myc / pBK-CMV / -	-		Kneussel M.

Abbreviations: Y: Yes; N: No.

## 2.2 Chemicals

### 2.2.1 Crystallization Screens

Screen formulations were based on commercial available screens given in table 6 and pipeted in-house using the Lissy liquid handling robot and the appropriate stock solutions.

Table 6. **Crystallization screens.**

Name	Source
Additive Screen	Hampton Research
Crystal Screen I + II	Hampton Research
Index Screen HT	Hampton Research
Nextal PEG Suite	Qiagen
Nucleix Suite	Qiagen
Optimix 1 – 5	Topaz
Protein Complex Screen	Qiagen
Wizard Screen 1	Emerald BioSystems
Wizard Screen 2	Emerald BioSystems

### 2.2.2 Low Molecular Weight Chemicals

Chemicals were purchased at analytical grade or better from Applichem (Darmstadt), Carl Roth (Karlsruhe), Fluka (Neu-Ulm), Hampton Research (Laguna Hills, USA) or Sigma Aldrich (Seelze).

Table 7. **Low molecular weight chemicals.**

Chemical	Catalogue ID	Supplier
2-Propanol (Isopropanol)	6752.4	Roth
Acetic acid (glacial)	7332.2	Roth
Acetonitrile	AE70.2	Roth
Ammonia	CP17.1	Roth
Ammonium carbonate	09832	Fluka
Ammonium peroxodisulfate	09913	Fluka
Ammonium sulfate	9318.1	Roth
Ampicillin (sodium salt)	K029.2	Roth
Calcium chloride	HN04.3	Roth
Chelex-100 Sodium	790150	Sigma-Aldrich
Chloramphenicol	3886.3	Roth
Coomassie Brilliant Blue R25	3862.2	Roth
Dimethylformamide	T921.1	Roth
Dimethylsulfoxide	A994.2	Roth
Dithiothreitol	6908.4	Roth
Ethanol (absolute)	9065.2	Roth
Ethanol (denatured)	K928.4	Roth
Formic acid	399388	Sigma-Aldrich
Glycerol	A3552	AppliChem
Guanidinium chloride	0037.1	Roth
Hydrochloric acid	4623.2	Roth

Imidazole	3899.4	Roth
L-Glutathione (reduced)	A2084	AppliChem
Magnesium chloride	HN03.3	Roth
MES	69892	Sigma-Aldrich
Methanol	4627.5	Roth
Nickel sulfate	T111.1	Roth
Phenylmethylsulfonyl fluoride	6367.2	Roth
Polyethylene glycol 10,000	81280	Fluka
Polyethylene glycol 3,000	81227	Fluka
Polyethylene glycol 400	81350	Fluka
Polyethylene glycol 5,000 monomethyl ether	81323	Sigma-Aldrich
Potassium chloride	HN02.3	Roth
Potassium hydroxide	6751	Roth
Potassium phosphate dibasic	P749.3	Roth
Potassium phosphate monobasic	P9791	Sigma-Aldrich
Potassium phosphate tribasic	60494	Fluka
Sodium acetate	3580.1	Roth
Sodium azide	K305.1	Roth
Sodium chloride	3957.2	Roth
Sodium dodecylsulfate	2326.2	Roth
Sodium hydroxide	6771.1	Roth
Trichloroacetic acid	91228	Fluka
Trifluoroacetic acid	302031	Sigma-Aldrich
TRIS (2-Amino-2-hydroxymethyl-propane-1,3-diol)	4855.3	Roth
Tris(2-carboxyethyl)phosphine	HN95.2	Roth
Urea	2317.2	Roth

### 2.2.3 Solutions

Buffers were adjusted to the respective pH values by adding either 32% (w/v) sodium hydroxide or 37% (v/v) hydrochloric acid.

Table 8. **Media for bacterial culture.**

	Composition	Plasmid dependent additives
LB-Medium	10 g/l Tryptone	Ampicillin (100 µg/ml)
	10 g/l NaCl	Kanamycin ( 50 µg/ml)
	5 g/l Yeast Extract	Chloramphenicol (34 µg/ml) IPTG (1 mM)

Abbreviations: LB: Lysogeny broth, IPTG: Isopropyl-β-1-thiogalactopyranoside

Table 9. **Buffers for bacterial lysis and transformation.**

<b>Bacterial lysis</b>	<b>Competent Cells - 1 (Comp1)</b>	<b>Competent Cells - 2 (Comp2)</b>
50 mM Hepes pH 7	30 mM Potassium Acetate pH 5.0	10 mM MOPS pH 6.8
500 mM NaCl	10 mM CaCl <sub>2</sub>	75 mM CaCl <sub>2</sub>
	15% Glycerol	15% Glycerol

Abbreviations: Hepes: 4-2-hydroxyethyl-1-piperazineethanesulfonic acid; MOPS: 3-N-morpholinopropanesulfonic acid.

Table 10. **Protein purification buffers.**

<b>Ni<sup>2+</sup>-Affinity</b>	<b>Ion exchange</b>	<b>Size exclusion</b>
10 mM Tris pH 8	10 mM Tris pH 8	10 mM Tris pH 8
500 mM NaCl	50-500 mM NaCl	250 mM NaCl
5-300 mM Imidazole pH 8	1 mM BME	1 mM BME

Abbreviations: Tris: Trishydroxymethylaminoethane; BME: β-mercapthoethanol

Table 11. **Protein interaction buffers.**

<b>SEC, ITC, DSC, Octet and pull-down experiments</b>	<b>Native gel buffer</b>
10 mM Tris pH 8	25 mM Tris pH 8
250 mM NaCl	192 mM Glycine pH 8
1 mM BME	

Abbreviations: Tris: Trishydroxymethylaminoethane; BME: β-mercapthoethanol; SEC: Size-exclusion chromatography, ITC: Isothermal titration calorimetry; DSC: Differential scanning calorimetry.

Table 12. **Protein-Gel Solutions.**

<b>PAGE Staining</b>	<b>PAGE Destaining</b>	<b>PAGE Running Buffer (1x)</b>
50% Ethanol	1% Acetic acid	192 mM Glycine
10% Acetic acid		0.1% SDS
0.1% Coomassie brilliant blue		25 mM Tris
<b>PAGE Loading Buffer</b>	<b>PAGE 10-25% Resolving Gel</b>	<b>PAGE 5-10% Stacking Gel</b>
50 mM Tris pH 6.8	10-25% AA / BAA (30:1)	5-10% AA/ BAA (30:1)
100 mM DTT	375 mM Tris pH 8.8	125 mM Tris pH 6.8
2% SDS	0.1% SDS	0.1% SDS
0.1% Bromphenol Blue	0.25% APS	0.25% APS
	0.05% TEMED	0.15% TEMED
<b>1x DNA Gel Buffer</b>	<b>5% Native Gel</b>	<b>1x Native Gel Running Buffer</b>
10 mM Tris pH 8	5% AA/ BAA (30:1 to 100:1)	25 mM Tris
1 mM EDTA	0.5x Tris-Glycine pH 8	192 mM Glycine
	0.2% APS	
	0.1% TEMED	

Abbreviations: PAGE: Polyacrylamide gel electrophoresis; AA: Acrylamide, BAA, Bisacrylamide, APS: Ammoniumpersulfate, TEMED: Tetramethylethylenediamine; DTT: Dithiothreitol; SDS: Sodiumdodecylsulfate.

## 2.3 Equipment

### 2.3.1 Instruments

Table 12. Instruments.

Type	Model	Supplier
Autoclave	Systec V-150	Systec
Balance 0.5-500 g	XS 6002S Dual Range	Mettler Toledo
Balance 0-1 g	XS 105 Dual Range	Mettler Toledo
CD-Spectropolarimeter	J-810	Jasco
Cell disruptors	M-110P	Microfluidics
	E615	Constant Cell Disruption Systems LTD
Centrifuge 0-1000 mL	Avanti J-26 XP	Beckmann Coulter
Centrifuge 0-2 mL	5417 R	Eppendorf
Centrifuge 0-50mL:	5810 R	Eppendorf
Column body (FPLC)	XK 16	GE Healthcare
Column body (gravity flow)	Econo-Column 1,5 x 15 cm	Biorad
	Econo-Column 2,5 x 20 cm	
Crystal mounting	CryoLoop	Hampton Research
Crystallization robot	HoneyBee 963	Zinsser Analytik
Dish washer	Professional G7883 CD	Miele
Fluorescence spectrometer	Fluoromax4	Horiba Jobin Yvon
FPLC system	Äkta purifier	GE Healthcare
FPLC: Anion exchange column	MonoQ 10/100 GL	GE Healthcare
FPLC: Size exclusion chromatography columns s	Superdex 200 HiLoad 26/60	
	Superdex 200 GL 10/300	GE Healthcare
	Superdex 75 GL 10/300	
FPLC: Nickel affinity column	Ni-MAC Cartridge 5 mL	Merck (Novagen)
Gelelectrophoresis chamber	Mini-Protean 3-cell	Biorad
Ice machine	Eismaschine 94774	Ziegra Eismaschinen
Illumination table	P265.1	Roth
Incubator	Type B15	Thermo Electron Corp.
Liquid culture incubators	ISF-1-W	Kühner
	ISF-1-X	
	VP-ITC	
Isothermal titration calorimetry	ITC <sub>200</sub>	Microcal, GE Healthcare
Liquid handling robot	Lissy	Zinsser Analytik
Magnetic stirrer	MR 3002	Heidolph
Microscope	SteREO Discovery.V12	Zeiss
Microscope: Camera	AxioCam MRC	Zeiss
Microscope: Light source	KL 2500 LCD	Zeiss
PCR Cycler	Mastercycler EPgradient S	Eppendorf
pH-Electrode	BlueLine 14pH	Schott
Pipettes	Pipet lite	Rainin
Pipetboy	Pipetus	Hirschmann Laborgeraete
Power supply	PowerPac Basic	Biorad
Scanner	Scanjet G2710	Hewlett-Packard
Spectrophotometer	Bio-Photometer	Eppendorf
Spectrophotometer	Nanodrop ND 1000	Peqlab
Thermoblock	Rotilabo-Block Heater 250	Roth
Thermomixer	Comfort	Eppendorf
X-ray cryosystem	X-Stream 2000	Rigaku
X-ray detector	R-AXIS HTC	Rigaku
X-ray generator	MicroMax-007HF	Rigaku
X-ray optics	VariMax HF	Osmic Inc.

## 2.3.2 Consumables

Table 13. **Consumables.**

Type	Model	Supplier
24-well plate	SuperClear	Crystalgen
96-well plate	ClearPlate Halfarea MB	Greiner
Chitin Beads	S6651L	New England Biolabs
Concentrator, MWO 3-60 kDa 0.5-20 mL	Vivaspin 0.5-20	Sartorius stedim Biotech
Cover slides	Circular (22 mm diameter)	Jena Bioscience
Disposable cuvettes	UVette	Eppendorf
DEAE Sepharose	DFF100	Sigma-Aldrich
Dialysis cassettes	Slide-A-Lyzer	Pierce Biotechnology
Dialysis tubing	Spectra/Por	SpectrumLabs.Com
Filter	0.22 µm	Roth
Micro reaction tubes	Safe-ock 1.5 mL / 2 mL	Eppendorf
Pipette tips	10 µl, 200 µl, 1000 µl, 5000 µl	Rainin
Reaction tubes	Greiner tube 15 ml / 50 ml	Greiner
Reaction tubes	Reaction tube 0.2, 0.5, 1.5, 2.0 ml	Eppendorf

## 2.3.3 Kits

Table 13. **Kits.**

Kit	Purpose	Supplier
Quick Ligation Kit	DNA Ligation	New England Biolabs
Site-Directed Mutagenesis Kit	Site-Directed Mutagenesis	Stratagene
NucleoSpin Extract Kit	Plasmid isolation from gels	Macherey-Nagel
NucleoBond Plasmid Kit	Plasmid isolation from solutions	Macherey-Nagel

## 2.3.4 Software and Databases

Table 14. **Software and databases.**

Software	Author/Reference
CCP4 program suite	[156]
ClustalW2	EMBL-EBI
Coot	[157]
Crystal Clear	Rigaku
Excel Script for thermofluor analysis	Structural Genomics Consortium, Oxford
EXPASY	<a href="http://www.expasy.ch/">http://www.expasy.ch/</a>
Mosflm	[158]
MolProbity Server	[159]
Origin 7 ITC	Microcal
OriginPro 8.5	Origin Lab Corporation
PDB	<a href="http://www.pdb.org">www.pdb.org</a>
Phaser	[160]
Phenix	[161]
Pubmed	NCBI
Pymol	DeLano 2002
Quantity One (Molecular Imager)	Biorad
Refmac	[162]
Scala	[163]
XDS	[164]

## 2.4 DNA Analysis and Manipulation

This section describes methods to isolate, analyze and manipulate DNA.

### 2.4.1 DNA Gel Electrophoresis

Deoxyribonucleic acid (DNA) fragments were separated by size via electrophoresis in agarose gels containing 1% (w/v) NEE0 ultra quality agarose (Carl Roth), 1x TE buffer and 0.5 µg ethidium bromide per ml gel. Prior to electrophoresis at 100 V for 30 min, DNA-containing samples were mixed with DNA sample buffer and the gel was immersed into TE buffer. Ethidium bromide intercalates into the DNA double helix and allows for fluorescence-based DNA detection.

### 2.4.2 DNA Gel Extraction

DNA was recovered from agarose gels using the NucleoSpin extract kit (Macherey-Nagel) according to the manual of the manufacturer. Bands of interest were excised under low intensity UV light, the gel was dissolved and the DNA bound to an anion exchange column. After washing with ethanol the DNA was eluted with buffer from the extraction kit.

### 2.4.3 DNA Digestion and Ligation

Plasmids were specifically linearized using restriction enzymes and buffers (New England Biolabs) according to the instructions of the supplier. Inserts and linearized plasmids were ligated using the Quick Ligation Kit (New England Biolabs) according to the manual of the manufacturer.

### 2.4.4 Site-Directed Mutagenesis

Mutants were generated using the QuickChange Site-Directed Mutagenesis kit (Stratagene) according to the manufacturer's instructions. In short, two complementary primers were designed carrying the mutated sequence. Making use of a two-stage protocol [165] with one PCR cycle containing just a single forward or reverse primer the formation of primer dimers was avoided. The single reactions were combined and subjected to 25 additional PCR cycles. The PCR reaction mix and the PCR program were adapted to the Phusion High Fidelity polymerase (Fermentas) according to the manual.

Table 15. QuickChange PCR reaction mix.

Additive	Stock concentration	Final concentration	Amounts for 20 µl reaction
Reaction buffer	5 x	1 x	4 µl
Template	10 ng/ µl	10 ng	1 µl
Primer	10 µM	500 nM	1 µl
DNTPs	10 mM	500 µM	1 µl
Phusion Polymerase	2 U/µl	0.1 U	1 µl
ddH <sub>2</sub> O			12 µl

Table 16. QuickChange PCR program.

Step	Temperature	Time	Cycles
Initial Denaturation	98 °C	30 sec	
Denaturation	98 °C	10 sec	1 Cycle each Primer
Annealing	65 °C	30 sec	+
Extension	72 °C	90 sec	25 Cycles Fwd and Rev Primers combined
Final Extension	72 °C	5 min	
Cooling	4 °C		

Next 10 U of *DpnI* were added to each reaction followed by overnight incubation at room temperature. 3 µl of the digested DNA were transformed into DH5α competent cells, plated on ampicillin LB agar plates and incubated overnight at 37 °C.

DNA extraction from single colonies was accomplished using the NucleoBond Plasmid Kit. Introduced mutations were verified using DNA sequence analysis (Seqlab, Göttingen).

### 2.4.5 Plasmid Isolation

Single colonies grown on a LB-agar plate were transferred to LB-medium containing the appropriate antibiotics. After incubation at 37 °C and shaking at 200 rpm overnight the suspensions were centrifuged at 4,000 x g for 10 min. The DNA was extracted from the resulting cell pellets using the NucleoBond Plasmid Kit (Macherey-Nagel) according to the manufacturer's instructions.

### 2.4.6 DNA Sequencing

All cloned and mutated plasmids were sequenced by SeqLab (Goettingen, Germany) using the Prepaid-AdvantageRead 900 offer using 10 µl of Plasmid (20-100 ng/µl) and T7 Primers (pETM-Vectors) or appropriate Primers (pGEX-Vectors).



## 2.5 Cell Culture and Protein Expression

This section describes methods employed to culture, transform, induce and lyse *E. coli* cells.

### 2.5.1 Cell Cultivation and Storage

For general usage the respective *E. coli* strain was grown in LB-Medium under permanent selection with the appropriate antibiotic(s). For long-term storage, 500 µl of an *E. coli* overnight culture were mixed with 1 ml of 20% (v/v) autoclaved glycerol, shock frozen in liquid nitrogen and stored at -80 °C.

### 2.5.2 Preparation of Competent Cells

*E. coli* cells were grown into early log phase ( $OD_{600} = 0.4$ ) and harvested by centrifugation (Eppendorf Centrifuge, 4000 x g, 10 minutes, 4 °C). The cell pellet was re-suspended in 15 ml of ice cold sterile-filtered Comp1-Buffer and incubated on ice for 90 minutes. The cells were then harvested by another centrifugation step (Eppendorf Centrifuge, 2000 x g, 20 minutes, 4 °C) and re-suspended in 2 mL of ice cold sterile-filtered Comp2-Buffer and aliquoted into 50 µl aliquots, which were flash frozen in liquid nitrogen and stored at -80 °C.

### 2.5.3 Transformation

1-10 ng DNA was added to an aliquot (50-100 µl) of chemo-competent *E. coli* cells (Stratagene). The cells were incubated on ice for 10 minutes and subsequently heat-shocked at 42 °C for 90 sec. After incubation on ice for 1 min 800 µl LB-medium was added and the cells were incubated at 37° C for 1 h at 200 rpm in a Thermomixer (Eppendorf). Afterwards the cells were plated on an LB-agar plate with the appropriate antibiotics and incubated overnight at 37 °C.

### 2.5.4 Protein Expression

50-200 mL LB-medium with the appropriate antibiotics were inoculated with one colony of freshly transformed cells and incubated overnight at 37 °C and 200 rpm (Kühner Shaker ISF1-X). 2.5 L LB-medium containing Erlenmeyer flasks with the appropriate antibiotics (Amp/Cam) were inoculated with 10 mL of the overnight-culture. After incubation at 37 °C and 200 rpm (Shaker ISF-1-W, Kühner) until an  $OD_{600}$  of 0.5 - 0.7 had been reached the expression was induced with 0.1 mM isopropyl-β-thiogalactoside (IPTG). Upon induction the temperature was decreased to 25 °C and after 18 h the cells were harvested by a 20 min centrifugation at 4000 x g and 4 °C (Beckmann Coulter Avanti Centrifuge J-26 XP) and either stored at -80 °C or lysed immediately for subsequent purification.

### 2.5.5 Cell Lysis

Cells were re-suspended in Lysis-buffer and passed twice through a cell disruptor (e616, Constant Cell Disruption Systems LTD or an M-110P microfluidizer, Microfluidics) at a pressure setting of 1.8 kbar. The resulting cell lysate was centrifuged at 34000 x g and 4 °C for 1 h to separate soluble proteins from insoluble proteins and cell debris (Rotor JA 25.50, Beckmann Coulter Avanti Centrifuge J-26 XP). The resulting supernatant was used for further protein purification steps.

## 2.6 Protein Purification

### 2.6.1 Affinity Chromatography

All purified proteins were subjected to affinity chromatography as the first purification step. Depending on the respective vector different affinity tags were introduced either N or C terminal of the target protein. In short, lysates of glutathione *S*-transferase (GST) -tagged (pGex-Vectors) and His-tagged (pETM and pET Vectors) proteins were incubated with the corresponding affinity resin and, after rigorous washing with the appropriate buffer, the respective competing ligand was applied to elute the tagged proteins. GST- and His-Tags were removed by the appropriate proteases recognizing specific cleave-sites between the tag and protein; thrombin and Factor Xa in case of the pGEX-vectors and TEV in case of pET and pETM-vectors. Intein-tagged proteins were cleaved and eluted in a single reaction step which was either based on a pH-shift (pTwin-Vector) or a nucleophilic attack of thiolates (pTYB-vectors). Incubation times and buffer compositions were based on the instructions of the manufacturer of the respective affinity resin (Table 17).

Table 17. Affinity chromatography.

Protein-Tag	Vector	Resin	Incubation and wash buffer	Elution buffer
GST	pGex (GE Healthcare)	Agarose GST-Beads (Novagen)	50 mM Tris pH 8 500 mM NaCl 5 mM BME	10 mM Tris pH 8 250 mM NaCl 20 mM red. glutathione
His <sub>6</sub>	pETM-11 (EMBL), pET-28a (Novagen)	Ni Sepharose 6 Fast Flow (GE Healthcare), Ni- NTA (Quiagen), Ni-TED (Protino)	50 mM Hepes pH 7 500 mM NaCl 5 mM Imidazole pH 7	10 mM Hepes pH 7 250 mM NaCl 5-500 mM Imidazole pH 7
Intein	IMPACT- pTYB (NEB)	Chitin Beads (NEB)	50 mM Tris pH 8 500 mM NaCl	50 mM Tris pH 8 100 mM NaCl 50 mM DTT
Intein	IMPACT- pTWIN (NEB)	Chitin Beads (NEB)	50 mM Tris pH 8 500 mM NaCl 10 mM BME	50 mM Hepes pH 7 100 mM NaCl 1 mM BME

Abbreviations: GST: Glutathione S-transferase; His<sub>6</sub>: Hexa-Histidine; DTT: Dithiothreitol; BME:  $\beta$ -Mercaptoethanol; Tris:Trishydroxymethylaminoethane; Hepes: 4-2-hydroxyethyl-1-piperazineethanesulfonic acid.

### 2.6.2 Size Exclusion Chromatography

Size exclusion chromatography (SEC) separates proteins by size and form and was used as final purification step in all protein purifications. In all cases a Superdex 200 26/60 column was used which consists of dextran covalently linked to a highly cross-linked agarose-matrix. The column volume of the Superdex 200 26/60 is ~330 ml and proteins between 10 kDa and 600 kDa can be separated. In contrast to small proteins large proteins cannot enter the particles and therefore elute earlier. Proteins were applied at a flow of 1 ml/min for 1.2 CV with sample loops of 1 to 10 ml size to the column which had been equilibrated with SEC buffer (10 mM Tris pH 8, 250 mM NaCl, 1 mM BME). The UV-detector was adjusted to wavelengths according to the nature of the sample, most commonly 270 nm (tyrosine) and 280 nm (tryptophan).

## 2.7 Protein Characterization

### 2.7.1 Protein Electrophoresis

The sodium dodecyl sulfate poly-acrylamide gel electrophoresis (SDS PAGE) [166] separates proteins according to their molecular weight under denaturing conditions. Optionally, reducing agents are used to disrupt possible disulfide bonds. SDS is an anionic detergent that binds the peptide-backbone of proteins yielding SDS-protein complexes which are charged proportional to their molecular weight. The resulting complexes can subsequently be separated by gel electrophoresis according to their size, independently of their native charge and conformation.

In short, samples were incubated with 5x protein sample buffer and heated for 30 sec. at 90° C. The protein-SDS-samples and a molecular weight marker (PageRuler protein ladder, Fermentas) were loaded on 0.75 cm thin gels and the electrophoresis was performed for 30 min at 200 V. Subsequently the gels were stained in Coomassie staining solution and, after removing excess dye by heating in water, the gels were digitized using a Scanjet G2710 (HP, USA) scanner.

### 2.7.2 UV/Vis Spectrophotometry

Protein concentrations were determined via absorption measurements with a nanodrop UV/Vis spectrophotometer (Pecolab). Concentrations were calculated using the protein specific extinction coefficient  $\epsilon$  at the measured absorbance, the thickness of the cuvette  $d$  and the relative absorbance compared to the buffer background using the Lambert-Beer law [167]:

$$c = \frac{A}{\epsilon \cdot d}$$

Extinction coefficients were estimated by addition of the tryptophan-, tyrosine- and cysteine-residue absorption of the respective protein:

$$\epsilon_{280} = (n_{\text{Trp}} \cdot 5690 + n_{\text{Tyr}} \cdot 1280 + n_{\text{Cys}} \cdot 120)$$

### 2.7.3 Thermofluor

The thermofluor method was used to monitor the thermal unfolding of proteins by making use of a fluorescent dye that interacts specifically with denatured proteins. SYPRO Orange (Sigma-Aldrich) binds in aqueous solution to hydrophobic regions exposed by unfolding. The resulting environmental change increases the absorption at 492 nm and emission at 610 nm and hence can be used to estimate the relative amount of unfolded protein in the solution [168].

Table 18. Thermofluor reaction mix.

Additive	Stock concentration	Final concentration	Amounts for 10 $\mu$ l reaction
Protein	1 mg/ml	0.1 mg/ml	1 $\mu$ l
SYPRO Orange dye	x10	x1	1 $\mu$ l
Buffer	x1	x1	9 $\mu$ l

Prior to the thermal unfolding assay samples were prepared with the appropriate buffer and the SYPRO Orange dye (Sigma-Aldrich) as described in Table 18 in a 96 PP-PCR-plate (Greiner Bio-One International AG). The experiment was performed in a Real-Time PCR system (Stratagene Mx3005P) and consisted of a step-wise temperature increase followed by an absorption measurement. Starting at 25 °C 70 steps were conducted with each step increasing the temperature by 1 °C, thus the experiment ended at 95 °C. The resulting data were analyzed with an Excel sheet provided by the Structural Genomics Consortium (SGC) in Oxford.

## 2.8 Analysis of Protein Complexes

### 2.8.1 Analytical Size Exclusion Chromatography

Analytical size exclusion chromatography (SEC) of protein complexes can be used to visualize changes in protein conformation as well as complex stoichiometry and stability. Depending on protein size analytical Superdex 200 10/300 (24 ml volume, separation range 70-600 kDa) or Superdex 75 10/300 (24 ml volume, separation range 3-70 kDa) columns were used. The sensitivity of this method is restricted to  $K_d$  values of approx. 1/10th of the injection concentration due to dilution on the column. Additionally complexes with small dissociation rate constants ( $k_{off}$ ) cannot be analyzed, while large association rate constants ( $k_{on}$ ) can be compensated for by complex incubation prior to the experiment.

In short, equilibrated protein complex solutions were applied with a sample loop of 100  $\mu$ l to the respective column equilibrated with SEC buffer (10 mM Tris pH 8, 250 mM NaCl, 1 mM BME) with a flow of 0.5 ml/min for 1.2 CV. The UV-detector was adjusted to wavelengths of 270 nm (tyrosine) and 280 nm (tryptophan) according to the nature of the sample.

### 2.8.2 Analytical Ultracentrifugation

Analytical ultracentrifugation (AUC) allows examination of the hydrodynamic shape of proteins as well as estimation of their oligomeric state by measuring sedimentation velocity (SV) in a centrifugal field. Proteins subjected to this method are used in solution under native conditions.

Protein samples adjusted to concentrations yielding a molar extinction coefficient of 0.1 at 280 nm were dialyzed with AUC-buffer (10 mM Tris-HCl pH 8.0, 250 mM NaCl, 1 mM BME) and subjected to a centrifugal field (40.000 rpm) using a Beckman-Coulter XL-I centrifuge. The ORIGIN data analysis software (OriginLab Corporation) allowed the calculation of sedimentation coefficients, molecular weights and frictional ratios based on the measured sedimentation velocity.

### 2.8.3 Differential Scanning Calorimetry

Differential scanning calorimetry (DSC) was used to monitor protein unfolding by measuring the change in heat capacity upon thermal denaturation. Folding and stability of native proteins is determined by the magnitude of hydrophobic interactions, hydrogen bonds, conformational entropy and the physical environment such as pH and ionic strength. A biomolecule in aqueous solution is in equilibrium between its native and its denatured conformation which can be described by the Gibbs free energy equation.

$$\text{Gibbs free energy of the binding event: } \Delta G = \Delta H - T\Delta S$$

Upon heating the conformational entropy eventually overcomes stabilizing forces, thus allowing the protein to unfold. DSC measures the enthalpy of unfolding ( $\Delta H$ ) due to heat denaturation. The transition midpoint  $T_m$  is the temperature where 50% of the protein is in its native conformation and the other 50% is denatured. During the same experiment DSC also measures the change in heat capacity ( $\Delta C_p$ ) for denaturation. Heat capacity changes associated with protein unfolding are

primarily due to changes in the hydration of side chains that are buried in the native state, but become solvent exposed in the denatured state.

In DSC the amount of heat required to increase the temperature of a sample and reference is measured as a function of temperature. Both the sample and reference are maintained at nearly the same temperature throughout the experiment. In a DSC analysis the sample temperature increases linearly as a function of time. The result of a DSC experiment is a curve of heat flux versus temperature. This curve can be used to calculate enthalpies of transitions. This is done by integrating the peak corresponding to a given transition.

$$\text{Enthalpy of transition: } \Delta H = K A$$

where  $\Delta H$  is the enthalpy of the transition,  $K$  the calorimetric constant and  $A$  the area under the curve. The calorimetric constant will vary from instrument to instrument, and can be determined by analyzing a well-characterized sample with known enthalpies of transition.

Prior to all DSC experiments, protein samples were extensively dialyzed against DSC-Buffer (10 mM Tris-HCl pH 8.0, 250 mM NaCl, 1 mM BME) at 4°C overnight, followed by filtration and degassing. All experiments were performed using a VP-DSC instrument (MicroCal, Northampton, MA, USA). The Buffer was measured simultaneously so that aqueous buffer effects could be subtracted from the sample measurement. The enthalpy of the transition was directly measured, while the  $T_m$  and van t' Hoff enthalpy was obtained by data analysis using the ORIGIN software.

## 2.8.4 Dynamic Light Scattering

Dynamic light scattering (DLS) is a spectroscopic method to determine the size distribution of particles in solution. First, particle movement speed profiles are calculated based on the scattering of monochromatic light. Next, molecular weights can be estimated under the assumption that each particle has a spherical shape.

In short, a quartz cuvette is filled with freshly filtered and centrifuged protein sample (80  $\mu$ l, 0.5 mg/ml) and measured several times using the DynaPro Titan DLS photometer (Wyatt Technology). A single experiment consists of a series of measurements with the following parameters:

Table 19. DLS parameters.

Parameter	Setting	Parameter	Setting
Acquisition time	10 sec	Solvent Model	PBS
Number of Acquisitions	20	Refraction Index*	1.333
Laser Power	100%	Viscosity*	1.019 cp
Temperature	10 °C	Cauchy Coefficient*	3119 nm <sup>2</sup>

\* Solvent model 'PBS'

The data is automatically evaluated by the Dynamics V6 software supplied with the equipment and presented as a distribution of molecular radii and molecular weights.

### 2.8.5 Isothermal Titration Calorimetry

Isothermal titration calorimetry (ITC) provides a complete thermodynamic profile of a bimolecular interaction in a single experiment. While it directly measures the change in enthalpy ( $\Delta H$ ) during a binding event, it additionally allows the accurate determination of binding constants ( $K_B$ ), reaction stoichiometry ( $N$ ), and entropy ( $\Delta S$ ) as given by:

$$\text{Gibbs free energy of the binding event: } \Delta G = \Delta H - T\Delta S$$

Additionally ITC assays can be modified to reveal synergistic, competitive or sequential binding events. ITC-measurements are usually conducted at a  $c$ -value of 5 or higher:

$$c\text{-value: } c = \frac{K_d}{[M]} > 5$$

with  $K_d$  describing the affinity of the interaction to be analyzed and  $[M]$  the concentration of the macromolecule in the cell. Measurements at  $c$ -values below 5 are so-called “low  $c$ ” measurements, which yield good estimates of the  $K_d$ , but due to the incomplete complex formation they only poorly describe the enthalpy and stoichiometry.

Prior to all ITC experiments, protein samples were extensively dialyzed against ITC-Buffer (10 mM Tris-HCl pH 8.0, 250 mM NaCl, 1 mM BME) at 4°C overnight, followed by filtration and degassing. Experiments were performed at 25°C using either the VP-ITC or ITC<sub>200</sub> Instrument (MicroCal, Northampton, MA, USA). Buffer-to-buffer titrations were carried out, so that the heat produced by injection, mixing and dilution could be subtracted prior to curve fitting. The binding enthalpy was directly measured, while the dissociation constant ( $K_d$ ) and stoichiometry ( $N$ ) were obtained by data analysis using the ORIGIN software. Measurements were conducted several times and are given as mean values with the resulting standard derivation.

### 2.8.6 Native Agarose Gel Electrophoresis

Prior to native agarose gel electrophoresis (NAGE) protein samples were mixed with OrangeG dye (Carl Roth) and 10% glycerol. 5  $\mu$ l samples containing 5-100  $\mu$ M of the respective protein were applied to 0.8% NEE0 ultra quality agarose (Carl Roth) gels containing 50 mM Tris/glycine pH 8.4 buffer. Electrophoresis was conducted at 4 °C and a current of 10 mA and terminated when the dye front was leaving the gel. Gels were stained for 10 minutes in 5% acetic acid, 10% ethanol and 0.005% Coomassie Brilliant Blue R250 (Carl Roth), and de-stained at least one day in 5% acetic acid and 10% ethanol at room temperature.

### 2.8.7 Pulldown Assay

N-terminally biotinylated peptides (Table 4) were coupled to streptavidin beads and incubated with protein in pulldown-buffer (10 mM Tris pH 8.0, 250 mM NaCl, and 1 mM BME) for 1 h. After three washing steps with the same buffer the beads were boiled with Laemmli buffer containing 10% SDS and the supernatant was applied to an SDS-PAGE.

## 2.9 X-Ray Crystallography

Until now, 88% of the approx. 83.000 protein and protein-ligand structures archived in the protein data bank (PDB) have been solved using X-ray crystallography (<http://www.rcsb.org/pdb/statistics/holdings.do>), underscoring the wide applicability of this method. Here I describe how I obtained crystal structures of either FERM-ligand complexes or gephyrin-ligand complexes which will be discussed in the results and discussion section.

### 2.9.1 Protein Crystallization

To determine the structure of a protein by X-ray diffraction, a well-ordered single protein crystal is required. In this work protein crystallization was achieved by vapor diffusion methods. First, proteins were mixed with precipitants and equilibrated against a larger reservoir of the precipitant solution with higher concentration. Diffusion slowly increases the precipitant and protein concentration in the protein drop until the nucleation barrier is reached and crystal nuclei can form. Ideally, crystal growth at the nuclei and solvent diffusion together allow the protein concentration to stabilize in a condition where protein crystallization can occur. This technique was performed either by placing the drop on a shelf that is surrounded by the reservoir solution (sitting drop) or by hanging the drop from a cover slide towards the reservoir solution (hanging drop).

The sitting drop method was used for initial screening for suitable conditions with the HoneyBee 963 crystallization robot (Genomic Solutions). The drop contained 0.3  $\mu$ L protein solution and 0.3  $\mu$ L crystallization solution and was equilibrated against 40  $\mu$ L reservoir solution in a 96-well crystallization plate (Greiner Bio-One International AG). Using the Lissy liquid handling robot (Zinsser Analytik) customized fine screens were generated. The hanging drop method was used for follow-up screens where drops of differing composition (1-3  $\mu$ L protein solution and 1-3  $\mu$ L crystallization solution) were equilibrated against 0.5-1 mL reservoir solution.

### 2.9.2 Data Collection

X-rays are scattered by the crystal lattice. The scattered radiation satisfies Bragg's law (Figure 13), thus yielding constructive interference which can be visualized using an X-ray sensitive detector system.

$$\text{Bragg's law: } n \lambda = 2 d \sin \theta$$

The intensity and the position of the reflections are collected together with the relative crystal position.

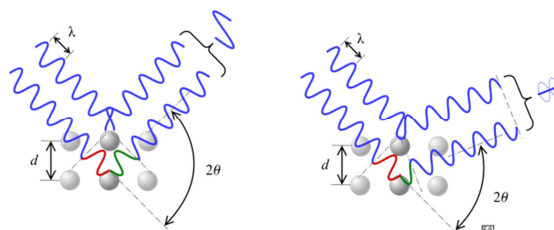


Figure 13. **Scheme of X-ray diffraction.** Following Bragg's law, X-rays scattered from adjacent planes combine constructively when the angle  $\theta$  between the plane and the X-ray results in a path-length difference that is an integer multiple  $n$  of the X-ray wavelength  $\lambda$ . © Public domain

For data collection, single crystals were transferred into cryo-protectand or, if possible, directly flash cooled in liquid nitrogen. Diffraction data were collected with a MicroMax-HF 007 generator (Rigaku) at a wavelength of 1.5418  $\text{\AA}$  and an R-AXIS HTC imaging plate detector. Using the crystal clear software (Rigaku) the following settings were used for an initial estimation of crystal quality:



Table 20. Parameters for in-house crystal diffraction evaluation.

Parameter	Setting
Detector distance	250 mm
Number of Images	2
φ angle	0.5°
Interval angle	90°
Exposure	5 min

Complete data sets were recorded using the European synchrotron beam lines BESSY (Berlin, Germany) and ESRF (Grenoble, France). Data collection statistics are summarized in the respective results sections.

### 2.9.3 Data Processing and Molecular Replacement

Diffraction images resulting from data collection were indexed and integrated, depending on the detector system, using either Mosflm [158] or XDS [164]. For scaling and all other subsequent steps the CCP4 software package was used [156]. Data processing was accomplished in five steps:

- **Indexing:** Selection of a preliminary space group and determination of unit cell parameters that describe the crystal lattice.
- **Integrating:** Correction for background and determination of spot intensities.
- **Merging:** Correction for relative strengths of the spots in different images (Scaling), as well as calculating a single averaged intensity for each structure factor.
- **Evaluation:**  $R_{\text{sym}}$  is calculated from the agreement between the separate observations of a reflection and its symmetry mates.
- **Calculation of the structure factor amplitudes** from the scaled and merged intensities. The electron density map is related to the diffracted waves as follows:

$$\rho(x, y, z) = \frac{1}{V} \sum_{hkl} F_{hkl} e^{-2\pi i(hx+ky+lz)}$$

The measured intensity  $I(hkl)$  of a reflection is proportional to the square of the structure factor amplitude  $|F(hkl)|$ :

$$I(hkl) \approx |F(hkl)|^2$$

To calculate the structure factor  $F(hkl)$  from the intensity, the phase  $\phi$  of the wave is needed:

$$F(hkl) = |F(hkl)| e^{i\phi(hkl)}$$

The phase information cannot be determined during data collection and is lost (phase problem of crystallography). To solve the phase problem molecular replacement (MR) was applied. MR uses an already available structure of high homology. Correct positioning in the unit cell of the unknown structure is achieved by calculating the phase independent Patterson function of the measured data and the search model:

$$\rho(x, y, z) = \sum_{hkl} |F_{hkl}|^2 e^{-2\pi i(hx+ky+lz)}$$

The number of molecules in the asymmetric unit can be estimated with the method of Matthews:

$$V_M = V_{EZ} / M_r \cdot z \cdot n$$

With  $M_r$  the molecular weight,  $V_{EZ}$  the volume of the unit cell,  $z$  the number of symmetry operators in the space group,  $n$  the number of molecules in the asymmetric unit,  $V_M$  the packing parameter describes the crystal volume per protein mass. The solvent content of the protein crystal is typically between 30% and 70%. After molecular replacement with the appropriate apo-structures (Protein Data Bank) the resulting initial model was refined as described in the next section.

### 2.9.4 Model Refinement

Structure models were built using Coot [157], which allows real space fitting of amino acids and ligand addition to the calculated electron density. Optimized models were refined with Refmac [162] or Phenix [161]. Alternating rounds of model building and automated refinement were carried out to successively improve the atomic model. The ratio of available data per model parameter can be optimized by introducing several restraints and constraints.

#### Restraints:

- Bond lengths and angles.
- Planarity of peptide bonds and aromatic groups.
- Atomic distances.
- Non-crystallographic symmetry (NCS) restraints. If more than one molecule is present in the asymmetric unit, they can be restrained to be similar
- Translation, rotation, screw-rotation (TLS) refinement, in which the protein is subdivided in a set of rigid bodies that are allowed to show displacement.

#### Constraints:

- Atom occupancy
- Hydrogen bond lengths and bond angles
- Non-crystallographic symmetry (NCS) constraints. If more than one molecule is present in the asymmetric unit, their conformation can be forced to be identical.

The success of refinement was evaluated by the R-factor and the  $R_{\text{free}}$ -factor. The R-factor is an indicator of the precision of the derived model in comparison to the measured data:

Calculation of the R-factor: 
$$R = \frac{\sum_{hkl} |F_o(hkl)| - |F_c(hkl)|}{\sum_{hkl} |F_o(hkl)|}$$

The R-factor is derived from data used during refinement and therefore biased towards the model. Therefore, additionally the free R-factor ( $R_{\text{free}}$ ) [169, 170] is calculated. Here, 5% of the data are randomly chosen and not used in the refinement process. After each refinement cycle, the  $R_{\text{free}}$  is calculated from these un-biased data.  $R_{\text{free}}$  reflects the accuracy of the model. Refinement was

considered as complete when difference density features could be explained by additional ligands and when the R-factors converged towards reasonable values.

To further evaluate the quality of the final model additional parameters are compared to average values of structures of similar resolution:

- Deviations of the bond lengths and angles from ideal values.
- Ramachandran plot. Here, the dihedral angles  $\phi$  and  $\psi$  of the amino acid residues in a protein structure are plotted against each other to identify amino acids which adopt unusual conformations.

## 3 Results and Discussion

### 3.1 Radixin-Mediated GABA<sub>A</sub>R $\alpha$ 5 Clustering

The lab of Matthias Kneussel (ZMNH, University of Hamburg) demonstrated that activated radixin is essential for anchoring and clustering of GABA<sub>A</sub>R<sub>s</sub> containing the  $\alpha$ 5 subunit at extrasynaptic sites [26]. In particular, residues 89-185 within the FERM domain of radixin were shown to interact with residues 342-357 at the N-terminal end of the TM 3-4 loop of the GABA<sub>A</sub>R<sub>s</sub>  $\alpha$ 5 subunit. Here, I describe the molecular details of this interaction, using biophysical and X-ray crystallographic methods and recombinantly purified FERM domain and the  $\alpha$ 5-loop.

#### 3.1.1 GABA<sub>A</sub>R $\alpha$ 5 and Radixin FERM Purification

Both, the radixin FERM domain (residues 1-310) and the intracellular loop of the GABA<sub>A</sub>R  $\alpha$ 5 subunit (residues 342-429) were expressed in *E. coli* using the pETM-11 (His-tag), pETM-30 (GST-tag), pETM-60 (NusA-tag) and pGEX (GST-tag) vector systems and purified by affinity and size exclusion chromatography (SEC) as described in the methods section.

Radixin FERM was purified using the fused His-tag (pETM-Vectors) or GST-tag (pGEX-Vector) resulting in similar yields. Incubation with TEV-protease (pETM-Vectors) or thrombin (pGEX-Vector) generated tag-free radixin FERM domain which displayed in each case a single peak corresponding to a molecular weight of 38 kDa, very close to the theoretical mass of 34 kDa for a single FERM monomer (Figure 14A and Table 20).

The intracellular loop of the GABA<sub>A</sub>R  $\alpha$ 5 subunit residues 342-429 ( $\alpha$ 5-loop) was handled similarly but precipitated after cleavage of the GST, NusA or His tag. Therefore, for all subsequent experiments the N-terminally His-tagged variant without cleavage was used, which could be purified to homogeneity (Figure 14B). In line with the idea that the  $\alpha$ 5-loop adopts an unstructured and hence elongated conformation, SEC over-estimates the molecular mass of this protein, and this effect is dependent on the ionic strength. Accordingly, its apparent mass in SEC varies between 16 kDa and 35 kDa depending on the NaCl concentration, while the theoretical mass of the monomeric peptide is 14 kDa (Table 21).

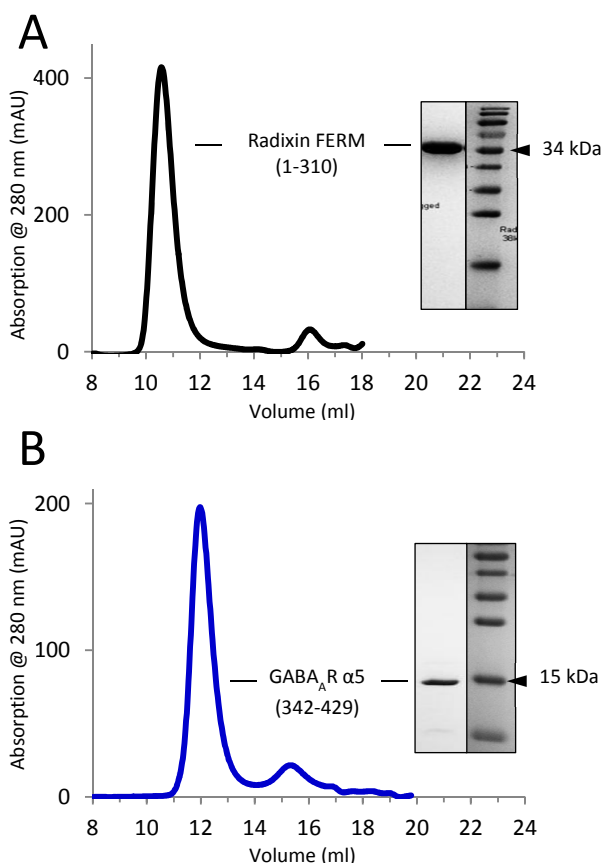


Figure 14. SEC and PAGE confirm the homogeneity of radixin FERM and the GABA<sub>A</sub>R  $\alpha$ 5 TM3-4. Representative elution profiles and SDS-PAGE of (A) radixin FERM (1-310) and (B) His-tagged GABA<sub>A</sub>R  $\alpha$ 5 (342-429). © 2012 HM Maric

Table 21. **Molecular weights of the radixin FERM domain and the GABA<sub>A</sub>R  $\alpha$ 5 loop.** Elution volumes determined in analytical SEC experiments and resulting calculated molecular weights. (SEC-buffer: 10 mM Tris pH 8; 1 mM BME; 0.15-2 M NaCl)

Protein	M <sub>w</sub> Sdx 200 26/60 (kDa)	M <sub>w</sub> Sdx 200 10/300 (kDa)	M <sub>w</sub> Sdx 75 10/300 (kDa)	M <sub>w</sub> ØSEC (kDa)	M <sub>w</sub> theoretical (kDa)
FERM (0.25 M NaCl)	36	37	42	38	34
$\alpha$ 5 (0.15 M NaCl)			35		
$\alpha$ 5 (0.25 M NaCl)	22	15	22	20	14
$\alpha$ 5 (0.5 M NaCl)			19		
$\alpha$ 5 (2 M NaCl)			16		

Next, buffer conditions were optimized using the thermofluor method. Here, the thermal unfolding was monitored in the presence or absence of critical additives, such as H<sup>+</sup> (pH) and sodium chloride (ionic strength) (Figure 15). In summary, the radixin FERM domain showed a maximal stability in buffers at pH values between 6 and 10 (Figure 15 A-D) and a preference for high sodium chloride concentrations (Figure 15E). In line with the elongated conformation in SEC, the purified receptor loop showed no melting curve in thermofluor (Figure 15F), and I therefore propose that the intracellular loop does not adopt any secondary structure in solution.

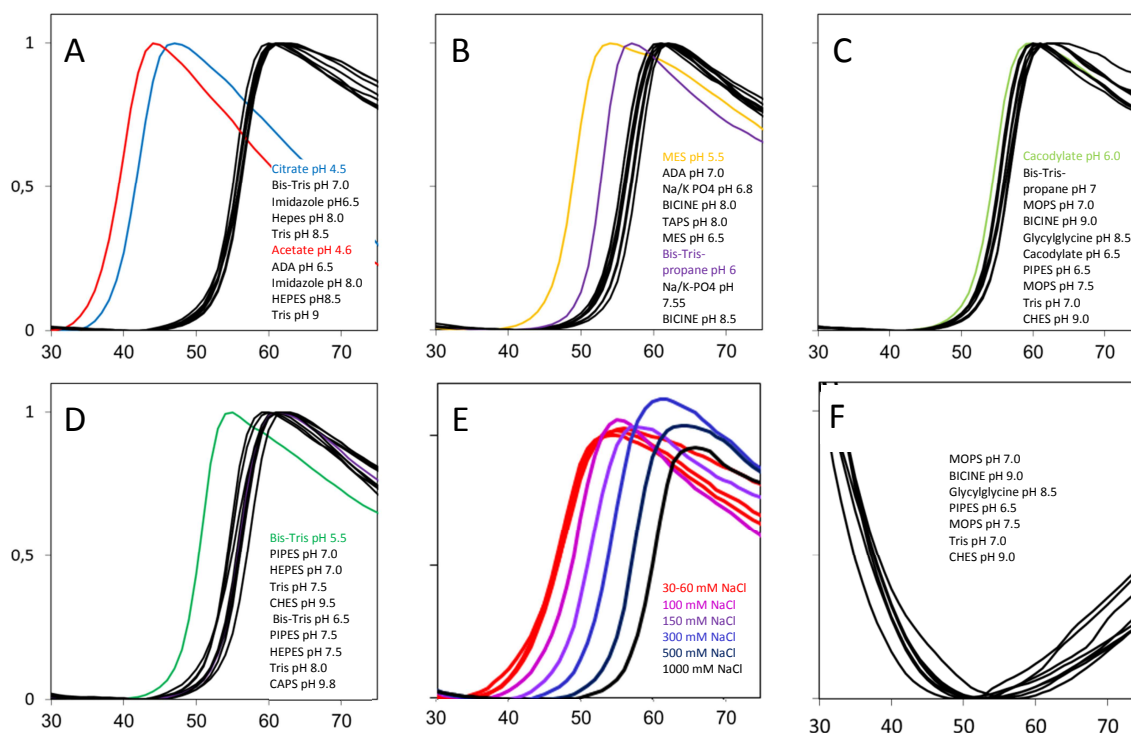


Figure 15. **Thermofluor defines the optimal pH and ionic strength of the radixin FERM domain.** A-D, Thermal unfolding of the FERM domain in different buffers. Buffers with pH values below 6 show a strong destabilizing effect and the corresponding unfolding curves are highlighted with colors. E, FERM domain unfolding as a function of ionic strength. Sodium chloride concentrations higher than 60 mM significantly increase the tolerance of the FERM domain towards thermal denaturation. F, No unfolding can be visualized in the thermofluor-analysis of the TM3-4 intracellular loop of the GABA<sub>A</sub>R  $\alpha$ 5 subunit, suggesting the absence of secondary structure. © 2012 HM Maric

Taken together, the chromatography and thermofluor results verify the suitability of the recombinant purification of radixin FERM and the  $\alpha$ 5-loop to yield soluble and homogenous protein samples. Furthermore, the thermofluor experiments suggest enhanced stability of the radixin FERM domain in buffers containing more than 100 mM sodium chloride at pH values between 6 and 10. In contrast, SEC and thermofluor suggest that the  $\alpha$ 5-loop adopts an elongated conformation without any secondary structure.

### 3.1.2 Characterization of the FERM Domain $\alpha$ 5-Loop Complex

After purification of the radixin FERM domain and the  $\alpha$ 5-loop I used the intrinsic fluorescence of tryptophan residues within the FERM domain and the  $\alpha$ 5-loop to verify the proposed complex formation *in vitro*. Upon titration of the FERM domain with the  $\alpha$ 5-loop the fluorescence emission spectrum indeed displays a strong red shift from 350 to 375 nm, which indicates complex formation of both proteins in solution and additionally suggest close proximity of the tryptophan residues to the binding site (Figure 16). Due to the addition of several tryptophan emission-spectra and the dilution of the FERM domain upon addition of the  $\alpha$ 5-loop a precise quantitative analysis was not possible, but based on the saturation of the emission shift at a 4-5 fold molar excess of the  $\alpha$ 5-loop the  $K_d$  of complex formation can be estimated to be in the low micromolar range. Due to the existence of several tryptophan residues in both proteins (six in the FERM domain and two in the  $\alpha$ 5-loop), the binding site could not be defined in this experiment.

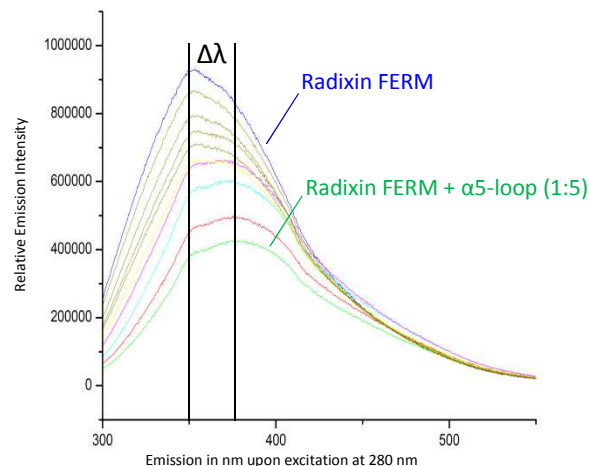


Figure 16. **Steady-state fluorescence analysis of the FERM domain  $\alpha$ 5-loop complex.** Superposition of ten independent experiments, in which increasing amounts of the  $\alpha$ 5-loop were added to the FERM domain and subsequently the intrinsic tryptophan fluorescence was measured. For clarity only the first spectrum (blue) and the last (green) is labeled. Upon addition of the  $\alpha$ 5-loop, a significant red-shift of the emission profile can be visualized, indicated as  $\Delta\lambda$ , suggesting a binding event in close proximity of tryptophan residues. © 2012 Maric HM.

Next, the stoichiometry of the FERM- $\alpha$ 5-loop complex was determined via analytical SEC. Equimolar amounts of the  $\alpha$ 5-loop and the FERM domain result in an elution profile which shows a significant shift towards higher masses. Excess of the  $\alpha$ 5-loop over FERM did not further reduce the elution volume indicating a stoichiometric binding event (Figure 17). In line with the fluorescence assay the full shift of FERM by applying a stoichiometric excess of the  $\alpha$ 5-loop (1:3) suggest a  $K_d$  in the low  $\mu$ M range. Finally, the elution volumes of the complex matches a 1:1 complex of one FERM domain binding specifically one  $\alpha$ 5-loop (Table 22). This ratio is also mirrored in the SDS-PAGE analysis of the corresponding fractions of the complex (Figure 17).

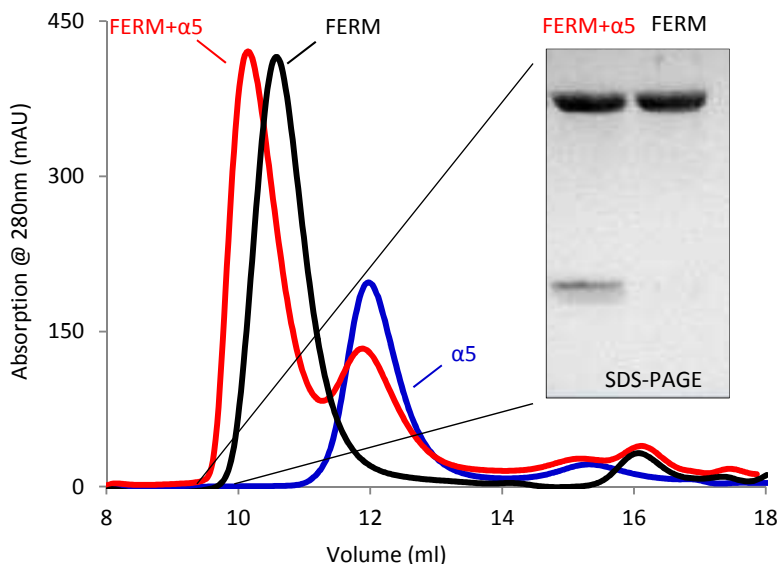


Figure 17. **Analytical SEC of the radixin FERM domain GABA<sub>A</sub>R  $\alpha$ 5 complex.** Comparison of three independent experiments conducted under identical conditions. The complex (red) elutes earlier than radixin FERM (black), while the receptor loop alone elutes the latest (blue). The complex elutes at volumes corresponding to a stoichiometric 1:1 complex. © 2012 HM Maric

Table 22. **Molecular weights of the FERM domain,  $\alpha 5$  loop and their complex.** Molecular weights determined by analytical SEC and DLS. (Buffer: 10 mM Tris pH 8, 250 mM NaCl, 1 mM BME.)

Protein	M <sub>w</sub> (Sdx 200 26/60) (kDa)	M <sub>w</sub> (Sdx 200 10/300) (kDa)	M <sub>w</sub> (Sdx 75 10/300) (kDa)	M <sub>w</sub> ∅ SEC (kDa)	M <sub>w</sub> ∅ DLS (kDa)	M <sub>w</sub> (calculated) (kDa)
Radixin FERM	36	37	42	38±3	67±9	34
GABA <sub>A</sub> R $\alpha 5$	22	15	22	20±4	58±1	14
FERM + $\alpha 5$	50	50	57	52±4	82±1	48

Taken together, the fluorescence measurements and the analytical SEC confirm the proposed direct interaction with recombinant proteins and additionally point towards a low micromolar affinity of both proteins in solution resulting in a soluble complex exhibiting a 1:1 stoichiometry. These results were further confirmed using the DLS method as summarized in table 22.

Encouraged by these results, my next target was the quantification of the FERM  $\alpha 5$ -loop binding event (Figure 18 and Table 23). ITC defined the binding stoichiometry to be roughly 1:1, thus verifying the results of the analytical SEC. Additionally, the thermally monitored titration reveals a binding affinity of 8  $\mu$ M and therefore again confirms the SEC and fluorescence experiments which suggested a low micromolar interaction strength. Finally, the thermal profile of the interaction together with the calculated affinity suggest a favourable enthalpic contribution that compensates an entropic penalty, thus indicating a large contribution of H-bridges and/or ionic interactions to the overall binding strength (Table 23).

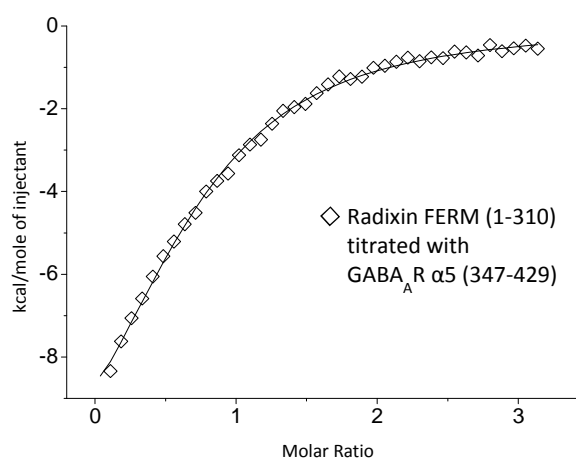


Figure 18. **ITC of the radixin FERM domain GABA<sub>A</sub>R  $\alpha 5$  complex.** Representative isothermal plot of the titration of the FERM domain with His-tagged- $\alpha 5$ -loop. Binding quantification was conducted in ITC-buffer (10 mM Tris pH 8.0, 250 mM NaCl, 1 mM BME) at 298K. © 2012 HM Maric

 Table 23. **Binding parameters of the radixin FERM domain  $\alpha 5$ -loop complex.** Binding parameters determined by ITC (Figure 18).

$\Delta H$ (kcal/mol)	$(-T\Delta S)$ (kcal/mol)	K <sub>d</sub> ( $\mu$ M)	Stoichiometry
-13.8 ± 0.4	+6.9	7.6 ± 0.3	0.75 ± 0.02

### 3.1.3 Fine-Mapping of the FERM- $\alpha$ 5 Binding Site

After biochemical and biophysical analysis of the FERM- $\alpha$ 5 interaction my major goal was the crystallization of the protein complex. To facilitate the crystallization process I further narrowed down the interaction site on the  $\alpha$ 5-loop deduced from earlier Y2H studies. The reduced molecular weight of the resulting minimum peptide would allow a higher molar ligand excess in FERM domain crystallisation conditions, which should facilitate the saturation of the FERM binding site.

Based on earlier Y2H studies [26] I used biotinylated peptides in pull-down assays (Figure 19) and truncated recombinant proteins in ITC to determine  $\alpha$ 5-loop residues critical for the FERM interaction. The results from both experiments are summarized in Table 23. Together they define 13 residues within the  $\alpha$ 5 loop as major contributors of the interaction. Notably, the first 16 residues of the  $\alpha$ 5-loop were sufficient for a positive signal in Y2H [26] but did not display full binding strength in my pull-down assays (Figure 19). As expected, the next larger fragment (23 residues) as well as the 33 residue fragment, displayed full binding strength towards the FERM domain (Figure 19). Additionally, deletion of the first 14 residues of the  $\alpha$ 5-loop did not abolish FERM binding but instead yielded only a moderate 5-fold reduction of binding strength, which again argues in favour of additional critical contributions of residues between positions 14 and 23 (Table 24).

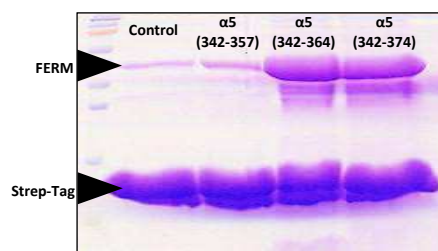


Figure 19. **FERM domain pull-down with GABA<sub>A</sub>R  $\alpha$ 5 derived peptides.** Strep-tag beads loaded with either no bait,  $\alpha$ 5-loop residues 342-357,  $\alpha$ 5-loop residues 342-364 or  $\alpha$ 5-loop residues 342-374 were incubated with the radixin FERM domain. After washing the bound proteins were eluted with SDS and subjected to SDS-PAGE. Only the elongated  $\alpha$ 5-loop fragments (342-364 and 342-374) were sufficient to bind significant amounts of the FERM domain. © 2012 HM Maric

Table 24. **Identification of the GABA<sub>A</sub>R  $\alpha$ 5 residues crucial for radixin FERM binding.**

GABA <sub>A</sub> R $\alpha$ 5 TM3-4 loop	Radixin FERM binding motif	K <sub>D</sub> ( $\mu$ M)
16 AA N-Term (342-357)	NYFTKRGWAWDGKKAL-----	n.d. in PD
23 AA N-Term (342-364)	NYFTKRGWAWDGKKALEAAKIKK-----	full binding in PD
33 AA N-Term (342-374)	NYFTKRGWAWDGKKALEAAKIKKKERELIL...	full binding in PD
WT (342-429)	NYFTKRGWAWDGKKALEAAKIKKKERELIL...	8 $\pm$ 0.3 in ITC
$\Delta$ 6 N-Term (348-429)	-----GWAWDGKKALEAAKIKKKERELIL...	12 $\pm$ 1 in ITC
$\Delta$ 10 N-Term (352-429)	-----DGKKALEAAKIKKKERELIL...	18 $\pm$ 2 in ITC
$\Delta$ 14 N-Term (356-429)	-----ALEAAKIKKKERELIL...	52 $\pm$ 6 in ITC
Minimum	-----DGKKALEAAKIKK-----	

Abbreviations: n.d.: binding could not be detected; PD: Pull-down assay; ITC: Isothermal titration calorimetry



Comparison of the corresponding sequences in all  $\alpha$  subunits of the GABA<sub>A</sub>Rs reveals only 4 unique residues within the identified minimum motif, two hydrophobic residues (Leu357 and Ile362) as well as two alanine residues (Ala256 and Ala 260) (Table 25 marked in red and boxed). Based on the exclusive binding of the  $\alpha$ 5-loop over the other subunits shown earlier [26] it can therefore be concluded that all of these residues or a subset are critical mediators of the FERM domain interaction.

Table 25. **Comparison of the N terminal TM3-4 sequences of GABA<sub>A</sub>R  $\alpha$ 1-6 subunits.** Residues marked in blue are unique to the respective subunit compared to  $\alpha$ 5. The minimum motif identified here is boxed and residues unique to  $\alpha$ 5 compared to  $\alpha$ 1-4 and  $\alpha$ 6 are marked in red.

GABA <sub>A</sub> R subunit TM3-4 loop	Radixin FERM binding motif
$\alpha$ 1	NYFTKRGYAWDGKSVVPEKPKKVKDPLI . . .
$\alpha$ 2	NYFTKRGWAWDGKSVVNDKKEKGSVMI . . .
$\alpha$ 3	NYFTKRSAWEGKKVPEALEMKKKTPAA . . .
$\alpha$ 4	NYFTNIQMOKAKKKISKPPPEVPAAPVL . . .
$\alpha$ 5	NYFTKRGWAWDGKKALEAAKIKKKEREL . . .
$\alpha$ 6	NYFTNLQSQKAERQAQTAA TPPVAKSKA . . .

### 3.1.4 Structural Basis of FERM Domain Self-Masking

For the cocrystallization of the FERM domain with the  $\alpha$ 5-loop I used both the full-length intracellular loop and an elongated minimum peptide compromising the first 26 residues of the  $\alpha$ 5 loop. Crystals could be obtained using 40 mg/ml FERM domain and the full length  $\alpha$ 5-loop at a 2-fold stoichiometric excess and a data set was acquired at our home source (Table 26). Molecular replacement with an *apo* FERM domain structure (PDB ID: 1GC7) allowed us to solve and refine the structure to 3.1 Å. While there was no electron density that could be attributed to the  $\alpha$ 5-loop, we found the FERM domain to engage in an inter-molecular FERM-FERM head to tail interaction. Interestingly, the FERM interaction interface specifically occupies a peptide-binding site in subdomain F3 identified earlier (Figure 20A), which was described in section 1.5.2 and Figure 11. To test the hypothesis that the FERM interaction interferes with  $\alpha$ 5-loop binding, I made use of an exposed trypsin cleavage site at the very C terminus of the FERM domain (Figure 20B), which is located directly N terminal to the possibly interfering C terminal motif.

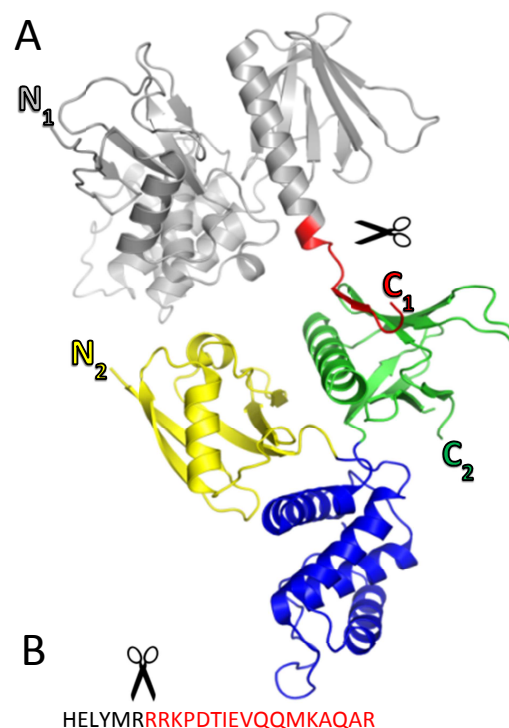


Figure 20. **Structural basis of FERM domain self-masking.** A, Cocrystallization of the FERM domain (1-310) and the  $\alpha$ 5-loop yielded the structure of a FERM head-to-tail oligomer. Specifically, residues 298-310 of one FERM domain engage in direct contacts with subdomain F3 of an adjacent FERM domain. The identical binding site is implicated in a pleiotropy of FERM ligand interactions and therefore the C terminus could possibly interfere with FERM ligand binding. B, By incident the exposed C terminal region, displays a trypsin cleavage site, which allows truncation of FERM by 17 residues marked red. © 2012 HM Maric

Table 26. **Radixin FERM (1-310) crystallization, X-ray data collection and refinement statistics.**

Data Collection statistics		Refinement statistics		Crystallization Condition
Wavelength (Å)	1.54178	Resolution (Å)	3.2-20.0	0.1 M Tris pH 7.5
Resolution (Å) <sup>a</sup>	3-50 (3.0-3.1)	No. of reflections	19929	15 % PEG 6000
Space group	P 3 <sub>1</sub> 2 1	R <sub>cryst</sub> (R <sub>free</sub> ) <sup>d</sup>	0.26 (0.35)	40 mg/ml radixin FERM
Cell dimensions		Root mean square deviations		
a=b, c (Å)	97.7, 79.7	Bond lengths (Å)	0.0124	
$\alpha=\beta, \gamma$ (°)	90, 120	Bond angles (°)	1.366	
Unique reflections	20602	Average B-factors (Å <sup>2</sup> )		
$\langle I/\sigma(I) \rangle$ <sup>a, b</sup>	5.0 (3.2)	Protein	71.8	
Completeness (%) <sup>a</sup>	99.9 (99.9)	Solvent	-	
Redundancy <sup>a, c</sup>	4.9 (3.4)			

<sup>a</sup> Numbers in parentheses refer to the respective highest resolution data shell in the data set.

<sup>b</sup> indicates the average of the intensity divided by its S.D. value.

<sup>c</sup>  $R_{sym} = \frac{\sum_{hkl} \sum_i |I_i - \langle I \rangle|}{\sum_{hkl} \sum_i \langle I \rangle}$ , where  $I_i$  is the  $i$ th measurement and  $\langle I \rangle$  is the weighted mean of all measurements of  $I$ .

<sup>d</sup>  $R_{cryst} = \frac{\sum ||F_o| - |F_c||}{\sum |F_o|}$ , where  $F_o$  and  $F_c$  are the observed and calculated structure factor amplitudes.  $R_{free}$ , same as  $R_{cryst}$  for 5% of the data randomly omitted from the refinement.

Incubation of a C-terminally His-tagged FERM domain in complex with the  $\alpha$ 5-loop with trypsin and subsequent SEC, SDS-PAGE and anti-His Western blot revealed that the C-terminal part of FERM is neither critical for protein stabilization nor complex formation with the  $\alpha$ 5-loop (Figure 21). The trypsin-mediated truncation by 17 residues could be verified by the slight shift in molecular size in SDS-PAGE (Figure 21) as well as by the abolishment of the His-tag signal in the Anti-His Western-Blot (Figure 21). Interestingly, the digested complex had a slightly lower elution volume despite its lower molecular weight, proposing either an enhanced complex stability in case of the C-terminally truncated FERM or a conformational change following trypsinization (Figure 21).

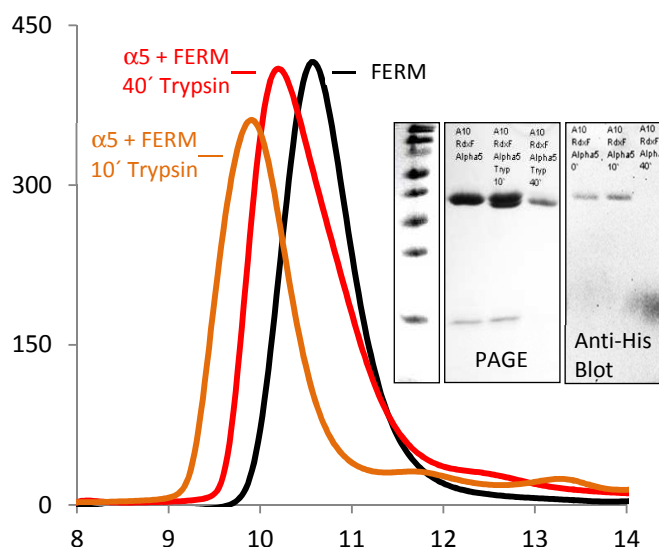


Figure 21. **SEC, SDS-PAGE and anti-His-blot of the trypsinized FERM- $\alpha$ 5-loop complex.** SEC of FERM- $\alpha$ 5-loop mixed with Trypsin (100:1) after 10' (orange) and 40' (red) as well as untreated FERM domain (black). The decreased elution volume as well as SDS PAGE verify complex formation for all trypsin incubation times. The slight shift in the molecular weight visualized by SDS PAGE result from the tryptic digestion of the very C-terminal part as verified by anti His-blotting: after 40 minutes the signal of the C-terminal His-tag is completely removed. © 2012 HM Maric

Taken together, both the derived crystal structure as well as the analysis of the trypsinized FERM- $\alpha$ 5-loop complex, suggest a possible interference of the C terminus of the FERM domain with  $\alpha$ 5 loop cocrystallization and furthermore verify the practicability of using a C terminally truncated FERM domain instead. Following this idea I cloned a C terminally truncated FERM domain and analyzed its respective  $\alpha$ 5-loop complex formation which is described in the next section.

3.1.5 FERM Mediates GABA<sub>A</sub>R-Clustering via a Universal Ligand Binding Site

Prompted by the finding of a possibly masked peptide-binding site I cloned a C-terminally truncated FERM domain (1-295). As expected from the trypsin cleavage experiments described in the previous section, expression and purification yielded a similarly pure and stable protein, as verified by SDS-PAGE (Figure 22A), which additionally visualizes the 15 residue truncation (Figure 22B). To test for a possible interference of the 15 C-terminal residues with the binding of the  $\alpha$ 5-loop, both the elongated and the truncated FERM domain were titrated with  $\alpha$ 5-loop under comparable conditions using ITC (Figure 22C). Surprisingly, both proteins displayed similar thermal signatures. Therefore it can be concluded that the FERM head-to-tail dimerization involves an unrelated binding site as compared to the GABA<sub>A</sub>R  $\alpha$ 5 subunit loop. Alternatively, the FERM-FERM association could have been induced by the crystallization condition, especially the high concentration in the mM range, or the crystallization process (e.g. preferable crystal contacts) and hence could not compete with the GABA<sub>A</sub>R  $\alpha$ 5 subunit binding under the conditions of the ITC experiment.

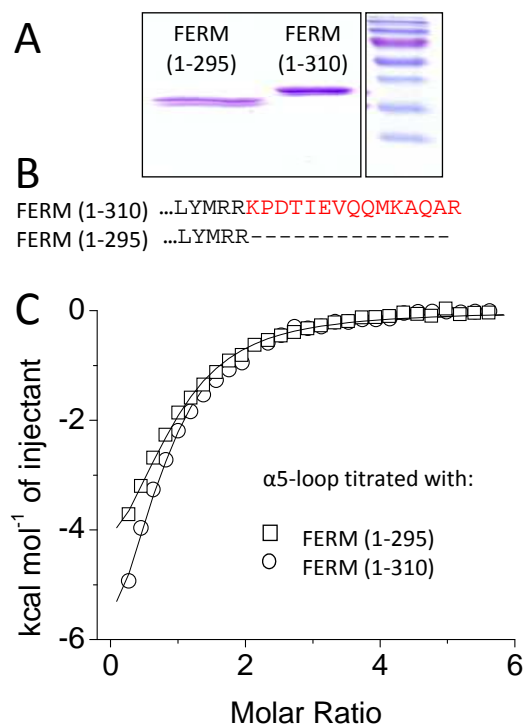


Figure 22. **Comparison of the  $\alpha$ 5-loop binding of radixin FERM (1-310) and FERM (1-295).** A, SDS PAGE of the FERM domain constructs 1-310 and 1-295 confirms the purity and size of both variants. B, Alignment of the C-terminal parts of both FERM variants. Residues critically interacting with a known peptide-binding site as observed in the initial crystal structure are marked in red and were deleted. C, ITC data of both FERM variants verify similar binding parameters towards the  $\alpha$ 5-loop. © 2012 HM Maric

Nonetheless, by making use of this construct I ruled out a possible interference of the FERM-FERM association upon crystallization. Following this idea, the truncated FERM domain was again subjected to crystallization trials, and crystals could be obtained with both the full-length  $\alpha$ 5-loop as well as with different minimum peptides. I solved the structure by molecular replacement using an *apo* radixin FERM domain (PDB-ID: 1GC7) and refined it to 2.1 Å resolution. Interestingly, the electron density map revealed additional density at the ligand binding site in subdomain F3 which was so far occupied by the C terminal peptide of the FERM domain in the structure described in the previous section. As expected, the electron density could not be attributed to the C terminus of FERM as found earlier. The resolution was high enough to allow unbiased modeling of the ligand residues which, very surprisingly, turned out to be a fragment of the purification process, namely the TEV cleaved His-tag of the FERM domain (Figure 23). Apparently, not only the C terminal FERM motif but also the TEV-cleavage site of the His-Tag could engage in specific interactions with the binding pocket on the F3 subdomain in the FERM domain. Comparison of my structures as well as earlier solved structures clearly point towards a highly promiscuous binding pocket recognizing a large variety of only moderately conserved substrates (Figure 23).

Table 27. Radixin FERM (1-295) crystallization, X-ray data collection and refinement statistics.

Data Collection statistics		Refinement statistics		Crystallization Conditions
Wavelength (Å)	0.84371	Resolution (Å)	2.3-20	0.1 M MES pH 6.5
Resolution (Å) <sup>a</sup>	2-36	No. of reflections	16131	15% PEG 550 MME
Space group	I 1 2 1	No. of protein/solvent atoms	2631/168	40 mg/ml radixin FERM
Cell dimensions		R <sub>cryst</sub> (R <sub>free</sub> ) <sup>d</sup>	0.21 (0.29)	
a, b, c (Å)	51.32, 51.55, 138.76	Root mean square deviations		
$\alpha=\gamma$ , $\beta$ (°)	90, 92.2	Bond lengths (Å)	0.009	
Unique reflections	25358	Bond angles (°)	1.176	
$\langle I/\sigma(I) \rangle$ <sup>a, b</sup>	11.0 (5.8)	Average B-factors (Å <sup>2</sup> )		
Completeness (%) <sup>a</sup>	98.8 (99.7)	Protein	24.0	
Redundancy <sup>a, c</sup>	3.1 (3.1)	Solvent	25.0	
R <sub>sym</sub> <sup>a</sup>	0.092 (0.40)	Ramachandran statistics (%) <sup>e</sup>		
		Favored	93.9	
		Allowed	4.2	
		Outliers	1.9	

<sup>a</sup> Numbers in parentheses refer to the respective highest resolution data shell in the data set.

<sup>b</sup> indicates the average of the intensity divided by its S.D. value.

<sup>c</sup>  $R_{sym} = \sum_{hkl} \sum_i |I_i - \langle I \rangle| / \sum_{hkl} \sum_i \langle I \rangle$ , where  $I_i$  is the  $i$ th measurement and  $\langle I \rangle$  is the weighted mean of all measurements of  $I$ .

<sup>d</sup>  $R_{cryst} = \sum ||F_o| - |F_c|| / \sum |F_o|$ , where  $F_o$  and  $F_c$  are the observed and calculated structure factor amplitudes. R<sub>free</sub>, same as R<sub>cryst</sub> for 5% of the data randomly omitted from the refinement.

<sup>e</sup> Ramachandran statistics indicate the fraction of residues in the favored (98%), allowed (>99.8%), and disallowed regions of the Ramachandran diagram, as defined by MolProbity [159].

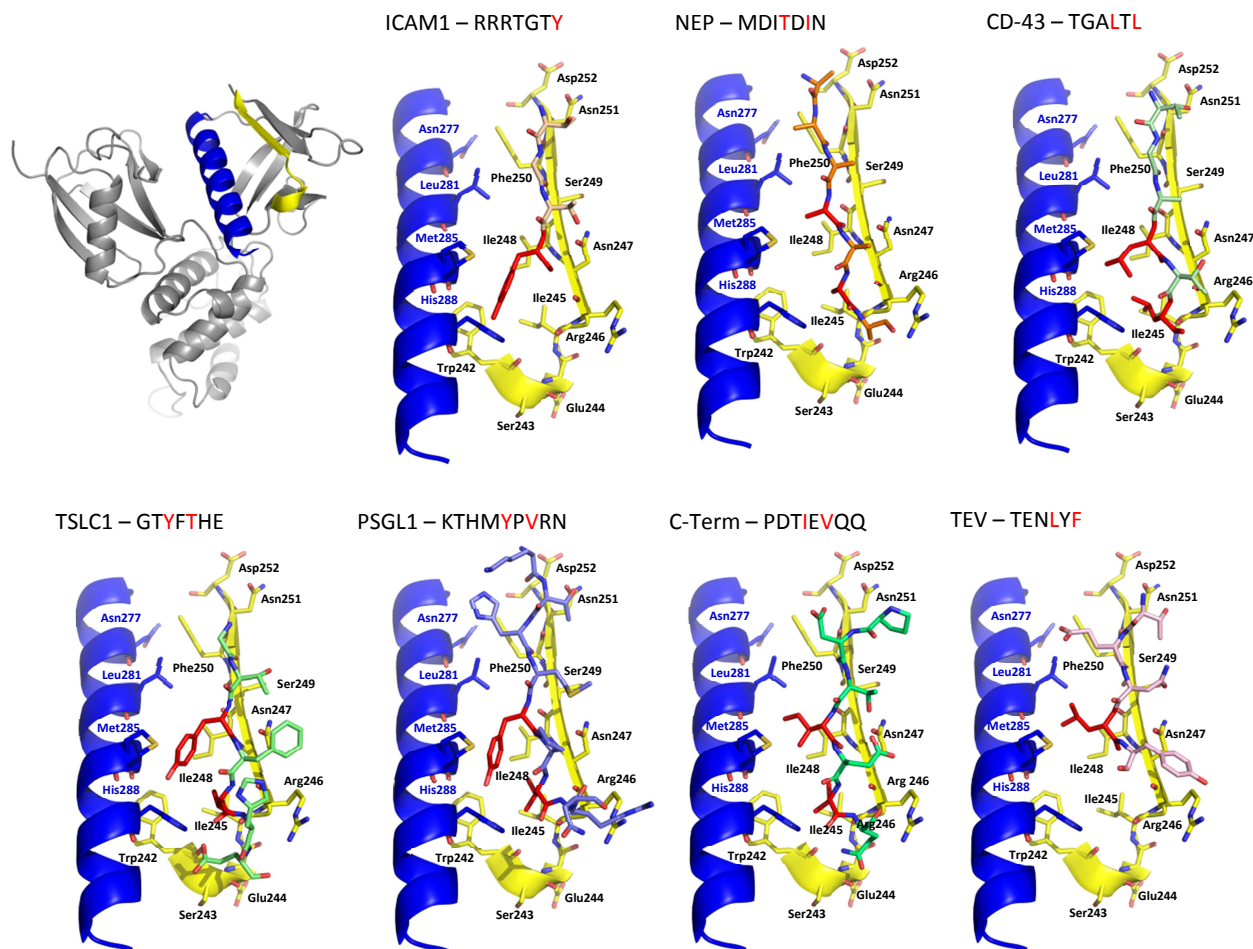


Figure 23. **Comparison of FERM domain cocrystal structures.** Different ligands engage in similar interactions with a promiscuous binding site in the F3 subdomain of the radixin FERM domain. ICAM1 (PDB ID: 1J19), NEP (PDB ID: 2YVC), CD-43 (PDB ID: 2EMS), TSLC1 (PDB ID: 3BIN), PSGL1 (PDB-ID: 2EMT), C-term (presented here) and TEV (presented here). FERM domain residues Leu281, Cys284, Met285, His288, Trp242, Ile245, Ile248 and Phe250, of the  $\alpha$ -helix marked in blue, together form a large hydrophobic pocket which accepts a variety of different hydrophobic ligand residues, marked in red, adopting different conformations. Additionally, FERM residues 246-252 form a  $\beta$ -strand, marked in yellow, that engages in peptide backbone interactions independent of the respective side chains of the ligand. © 2012 HM Maric

Prompted by this finding I compared ligand motifs that were shown to directly bind to this universal binding site on FERM subdomain F3. Strikingly, the  $\alpha$ 5-loop minimum FERM binding motif identified in this study fits very well to the ICAM2-binding motif (Table 28), and I therefore suggest that  $\alpha$ 5 occupies the same binding site. Interestingly, the conserved key residues of the FERM-ICAM1 complex are identical to the earlier described (Section 3.1.3)  $\alpha$ 5-subunit distinct residues (Table 25). Furthermore, this binding interaction would change the environment of Trp242 in the FERM domain as well as Trp349 and Trp351 of the  $\alpha$ 5-loop, thus explaining the red-shift in the intrinsic Trp-fluorescence upon complex formation described in section 3.1.2 and shown in figure 16. Additionally, the structurally resolved FERM beta-strand (residues 246-252) peptide backbone interaction would perfectly match the dominant contribution of enthalpy in the binding reaction as described by the ITC experiments presented in section 3.1.2. Finally, this hypothesis could explain the lack of bound  $\alpha$ 5-loop in the solved structures. Possibly, both the C-terminal FERM motif as well as the TEV-linker peptide were competing with the  $\alpha$ 5-loop for an identical binding site on the FERM domain. Earlier studies verified the  $\alpha$ 5-loop to be ubiquitinated *in vivo*. Comparison of the fine-mapped FERM binding region of the  $\alpha$ 5 subunit with the ICAM2-binding motif suggest that the ubiquitinated Lys355 engages in close spatial apposition to the FERM domain and hence suggests a severe negative

regulatory effect of this posttranslational modification on radixin-mediated GABA<sub>A</sub>R clustering (Table 28).

Table 28. **Comparison of ligand motifs binding to an identical binding site in the FERM domain.** Alignment of sequences that were found earlier to interact with the universal binding site of FERM on subdomain F3 and their respective binding affinities. Additionally, I aligned the peptides that occupied the respective FERM binding site in the derived crystal structures to the moderately conserved motifs. Compared to common binding partners the  $\alpha$ 5-loop has the lowest overall affinity. The  $\alpha$ 5-loop minimum motif (boxed), which is crucial for FERM binding, shows a high homology to the mICAM-polyA mutant. Conserved basic residues are marked in blue, conserved small residues in green and conserved hydrophobic residues in red. Remarkably, earlier studies verified that the identified  $\alpha$ 5-loop minimum motif forms a glycyl-lysine isopeptide interchain with C-terminal Gly of ubiquitin *in vivo* [171] at Lys355 (marked with "a"). Remarkably, this residue occupies a critical position within the FERM binding minimal motif of the  $\alpha$ 5-loop.

FERM binding	Binding motif	K <sub>d</sub> (nM)
His-link-TEV (X-ray)	T T E N L F Q G - - - -	-
FERM-C-term (X-ray)	K P D T I E V Q Q M K A	-
mICAM-2 (X-ray)	R T G T Y G V L A A W R	830
CD 43 (X-ray)	R T G A L T L S G G G K	104
GABA <sub>A</sub> R $\alpha$ 5	W <span style="border: 1px solid black; padding: 2px;">D G K K<sup>a</sup> A L E A A K I</span>	7000
mICAM (PolyA)	A T G A A G V L A A A R	830
PSGL 1 (X-ray)	K T H M Y P V R N Y S P	600
NEP (X-ray)	Q M D I T D I N A P K P	2300
CD 44	Q K K K L V I N G G N G	74
VCAM-1	M K G S Y S L V E A Q K	150
ICAM-3	R S G S Y H V R E E S T	760
SDC-1	D E G S Y S L E E P K Q	830
NRX-1	D E G S Y D L G K K P I	3800
NCAM-L1	K G G K Y S V K S K E D	61
TSLC 1 (X-ray)	H K G T Y F T H E A - -	1000

Based on the finding that the His-tag-peptide specifically interacts with a known universal binding site on FERM subdomain F3, I wanted to test whether the  $\alpha$ 5-loop also targets this binding site. Hence I performed ITC with both His-tagged and untagged FERM to control for a possible competition between the  $\alpha$ 5-loop and the His-tag. Indeed, the His-tagged FERM domain showed a strongly reduced  $\alpha$ 5-loop binding capacity in ITC, thus suggesting that despite the only moderate sequence homology the same or an overlapping binding site on the radixin FERM domain is directly involved in  $\alpha$ 5 binding (Figure 24). Therefore future crystallization trials, utilizing constructs that circumvent both unwanted binding events, may allow to determine the cocrystal structure of radixin in complex with the  $\alpha$ 5-loop.

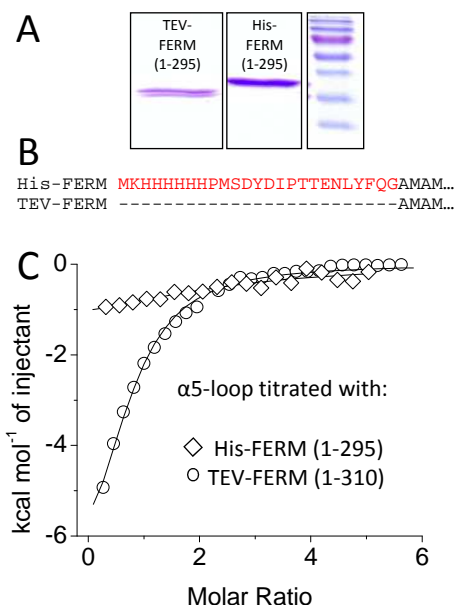


Figure 24. **Comparison of the  $\alpha$ 5-loop binding of His-tagged and untagged radixin FERM domain.** A, SDS-PAGE of the N-terminal His-tagged and the TEV-cleaved radixin FERM domain confirms their purity and expected size. B, Alignment of both variants. Residues removed by TEV cleavage and engaging in specific interactions with the F3 subdomain of the FERM domain are marked in red. C, ITC data of both FERM variants verify the interference of the His-tag with  $\alpha$ 5-loop binding. Both the overall heat release and the resulting binding affinity are significantly decreased, indicating that both the His-tag-peptide and the  $\alpha$ 5-loop compete for the identical binding site on the F3 subdomain of the FERM domain. © 2012 HM Maric

## 3.2 Gephyrin-Mediated GABA<sub>A</sub>R and GlyR Clustering

For around two decades gephyrin has been implicated in the clustering of GABA<sub>A</sub>Rs, however, the underlying direct interactions were only recently discovered [27]. In addition, these interactions have neither been quantified nor characterized at the molecular level. Following up on published and unpublished initial data of Dr. Jayhanta Mukherjee and Dr. Verena Tretter from the group of Steven J. Moss (Tufts University, Boston, USA) I studied different gephyrin receptor complexes with various biochemical and biophysical methods to provide the following insights into gephyrin-mediated GABA<sub>A</sub>R clustering, which are described in the next paragraphs:

- *In vitro* verification of a direct interaction.
- Mapping of the respective binding sites and determination of minimal receptor motifs.
- Deciphering gephyrin's subunit preference.
- Revealing possible competition or synergistic effects in receptor subunit binding.
- Crystallization of the GABA<sub>A</sub>R-gephyrin complex and comparison to the GlyR-gephyrin structure.
- Structure guided identification of key residues and estimation of their relative contribution to the overall binding strength of the interaction.
- Attenuation of receptor clustering in living neuron by the introduction of point mutations (Experiments conducted by Jayhanta Mukherjee).
- Regulation of receptor clustering by phosphorylation (in close collaboration with the Moss and Harvey (UCL, London, UK) groups).

The majority of these studies, described in section 3.2, are presented in a more condensed form compared to the remainder of the Results. They are described detailed in three recently published manuscripts:

1. Maric H.M., Mukherjee J., Tretter V., Moss S.J., Schindelin H.; *Gephyrin-mediated  $\gamma$ -aminobutyric acid type A and glycine receptor clustering relies on a common binding site.* J Biol Chem. 2011 Dec 9; 286(49): 42105-14. Epub 2011 Oct 17.
2. Tretter V., Kerschner B., Milenkovic I., Ramsden S.L., Ramerstorfer J., Saiepour L., Maric H.M., Moss S.J., Schindelin H., Harvey R.J., Sieghart W., Harvey K.; *Molecular basis of the  $\gamma$ -aminobutyric acid A receptor  $\alpha$ 3 subunit interaction with the clustering protein gephyrin.* J Biol Chem. 2011 Oct 28; 286(43): 37702-11. Epub 2011 Aug 31.
3. Mukherjee J., Kretschmannova K.\*, Gouzer G.\*, Maric H.M.\*, Ramsden S., Tretter V., Harvey K., Davies P.A., Triller A., Schindelin H., Moss S.J.; *The residence time of GABA(A)Rs at inhibitory synapses is determined by direct binding of the receptor  $\alpha$ 1 subunit to gephyrin.* J Neurosci. 2011 Oct 12;31(41):14677-87. \*Authors contributed equally.



### 3.2.1 Mapping the GABA<sub>A</sub>R Gephyrin Interaction

Following a proposed direct interaction of gephyrin with GABA<sub>A</sub>R  $\alpha$ 1 (J. Mukherjee, personal communication),  $\alpha$ 2 [27] and  $\alpha$ 3 (V. Tretter, personal communication), I cloned, expressed and purified the corresponding intracellular loops from *E. coli* and investigated their interaction with gephyrin by ITC.

For a first localization of the GABA<sub>A</sub>R binding site in gephyrin full-length gephyrin and the isolated E domain (GephE) were titrated with the  $\alpha$ 1-loop (Table 29A). These binding assays yielded similar parameters hence mapping the binding site to E domain, a result that is comparable to what we found earlier for the interaction between the GlyR  $\beta$  subunit and gephyrin [58]. Conversely, titration with GephG and the largest part of the linker region showed no detectable interaction, thus confirming that the GABA<sub>A</sub>R binding site resides in the E domain (Table 29A), which was therefore used for all subsequent experiments.

To determine the residues crucial for the interactions I cloned, based on initial biochemical assays of V. Tretter and J. Mukherjee, selected deletion and chimeric variants, purified them from *E. coli* and verified or falsified their GephE binding in ITC. Subsequently, I tested whether the identified minimum peptides are sufficient to specifically interact with GephE in pull-down assays by using the respective motifs as biotinylated variants. As a control, I employed the GlyR minimum motif identified earlier in a comparable manner for GephE binding in either the ITC or pull-down assays. The intracellular loops were purified and handled similarly as described in section 3.1.1 for the  $\alpha$ 5 subunit, with the exclusion that aggregated fractions of the  $\alpha$ 2 and  $\alpha$ 3 subunits were de-aggregated using guanidinium-chloride to optimize the overall yield. These experiments are summarized in Table 26 and together they define that  $\alpha$ 1 residues 361-375 (Table 29B) and  $\alpha$ 3 residues 392-406 (Table 29D) are necessary for GephE complex formation. In contrast, the  $\alpha$ 2-loop GephE affinity was too low to be measured in ITC under comparable conditions, and, due to the high hydrophobicity of this peptide, the experiments could not be scaled up to allow verification of a possible weak interaction. Therefore the interaction was verified using native agarose gel electrophoresis (NAGE) assays (Table 29C and Figure 25B and C).

Table 29. **GABA<sub>A</sub>R  $\alpha$ 1,  $\alpha$ 2,  $\alpha$ 3 and GlyR  $\beta$  loop gephyrin binding site mapping.** Summary of ITC, NAGE and pull-down assay data. (+++)  $K_D$  = 0.1-1  $\mu$ M; (++)  $K_D$  = 1-20  $\mu$ M; (+) no interaction detectable in ITC but verified via native PAGE or pull-down assays; (-) no interaction detectable via ITC, native PAGE or pull-down assays.

No.	Gephyrin	Receptor subunit	Affinity
A	1-734 (full-length gephyrin)	GABA <sub>A</sub> R $\alpha$ 1 334-420 (TM3-TM4)	(++)
	1-303 (GephG + Linker)	GABA <sub>A</sub> R $\alpha$ 1 334-420 (TM3-TM4)	(-)
	318-734 (GephE)	GABA <sub>A</sub> R $\alpha$ 1 334-420 (TM3-TM4)	(++)
B	GephE	GABA <sub>A</sub> R $\alpha$ 1 334-420 (TM3-TM4)	(++)
	GephE	GABA <sub>A</sub> R $\alpha$ 1 $\Delta$ 360-375	(-)
	GephE	GABA <sub>A</sub> R $\alpha$ 1 361-375	(+)
C	GephE	GABA <sub>A</sub> R $\alpha$ 2 335-419 (TM3-TM4)	(+)
D	GephE	GABA <sub>A</sub> R $\alpha$ 3 360-457 (TM3-TM4)	(++)
	GephE	GABA <sub>A</sub> R $\alpha$ 3 $\Delta$ 397-406	(-)
	GephE	GABA <sub>A</sub> R $\alpha$ 3 392-406	(+)
E	GephE	GlyR $\beta$ 398-411	(++)
	GephE	GlyR $\beta$ 387-426	(+++)/(++)

### 3.2.2 Deciphering Gephyrin's Receptor Subunit Preference

After verification of the respective receptor complexes my next aim was to elucidate gephyrin's subunit specific affinities. Hence, I determined the binding parameters for all analyzed receptor subunits under similar experimental conditions by ITC (Figure 25A), and, in case of the low affinity subunit  $\alpha 2$ , I used NAGE to estimate the relative binding strength (Figure 25 B and C).

As expected the GlyR  $\beta$  intracellular loop displayed the strongest GephE interaction with two binding sites displaying  $K_d$ -values of  $0.1 \mu\text{M}$  and  $8 \mu\text{M}$ , respectively, for the elongated 49 residue construct, while the corresponding GlyR  $\beta$  minimal peptide consisting of 12 residues showed a significant lower affinity of only  $4.3 \pm 0.4 \mu\text{M}$  (Figure 25A). The full-length GABA<sub>A</sub>R  $\alpha 3$ -loop displayed the strongest interaction among the analyzed GABA<sub>A</sub>R subunits with a  $K_d$  of  $5.3 \pm 1.5 \mu\text{M}$  (Figure 25A), followed by the full-length GABA<sub>A</sub>R  $\alpha 1$ -loop with a  $K_d$  of  $17 \pm 11 \mu\text{M}$  (Figure 25A). Under the same experimental conditions an interaction between the  $\alpha 2$  subunit of GABA<sub>A</sub>R and gephyrin could not be detected by ITC (Figure 25A), however, NAGE experiments verified that the GABA<sub>A</sub>R  $\alpha 2$  loop and gephyrin do form a complex, albeit with low affinity. Unlike the GABA<sub>A</sub>R  $\alpha 1$  and  $\alpha 3$  loops, which fully shifted GephE already at a molar ratio of 3 to 1 (Figure 25B), a 10-fold stoichiometric excess of GABA<sub>A</sub>R  $\alpha 2$  was required to complex all GephE under the experimental conditions (Figure 25C), thus suggesting a significantly lower affinity of  $\alpha 2$  for gephyrin compared to  $\alpha 1$  and  $\alpha 3$  while verifying at the same time a weak direct interaction.

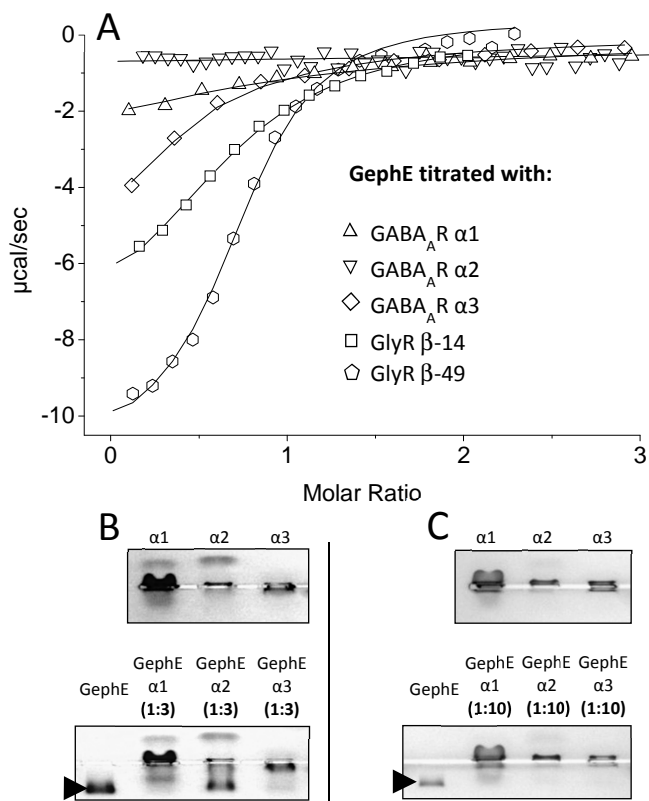


**Figure 25. ITC reveals gephyrin's receptor subunit preference.** A, ITC derived binding isotherms of GephE titrated with GABA<sub>A</sub>R  $\alpha 1$  334-420 (TM3-TM4), GABA<sub>A</sub>R  $\alpha 2$  335-419 (TM3-TM4), GABA<sub>A</sub>R  $\alpha 3$  360-457 (TM3-TM4), GlyR  $\beta$  398-411 and GlyR  $\beta$  387-426. Measured binding enthalpies are plotted as a function of the molar ratio of the respective receptor loop to gephyrin. Data of the titration of GABA<sub>A</sub>R  $\alpha 2$  to GephE could not be analyzed due to very weak binding. B, NAGE of GABA<sub>A</sub>R  $\alpha 1$ ,  $\alpha 2$  and  $\alpha 3$  subunits applied in a 3-fold stoichiometric excess over GephE. Whereas GABA<sub>A</sub>R  $\alpha 1$  and GABA<sub>A</sub>R  $\alpha 3$  retain GephE in the gel pocket, incomplete GephE GABA<sub>A</sub>R  $\alpha 2$  complex formation allows GephE (arrowhead) to enter the gel. C, NAGE of GABA<sub>A</sub>R  $\alpha 1$ -3 at a 10-fold stoichiometric excess over GephE. This molar ratio does not allow any GephE (arrowhead) to enter the gel and migrate towards the anode. © 2012 HM Maric

Interestingly, similar to the GlyR  $\beta$  loop, shortening of the GABA<sub>A</sub>R  $\alpha$ 1 and  $\alpha$ 3 loops lowered their affinity significantly, up to a level where the  $\alpha$ 1 and  $\alpha$ 3 derived minimum peptides could not be studied by ITC.

Instead, I performed pull-down experiments with the corresponding peptides coupled to streptavidin beads via covalently attached biotin (Figure 26). The pull-down data demonstrate that the residues contained within these peptides are sufficient to mediate a specific interaction with GephE with their relative binding strengths mirroring the full-length loops (Figure 26 and Table 29).

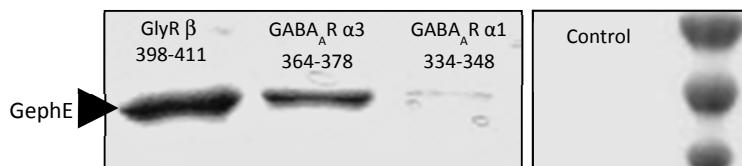


Figure 26. **Minimum peptides are sufficient to mediate a specific gephyrin pull-down.** Pull-down experiments of GephE with biotinylated GlyR  $\beta$  residues 398-411, GABA<sub>A</sub>R residues  $\alpha$ 3 392-406 and GABA<sub>A</sub>R  $\alpha$ 1 residues 361-375 coupled to streptavidin beads. Under the same experimental conditions GephE does not bind to the streptavidin beads alone (control). © 2012 HM Maric

### 3.2.3 Gephyrin Binds Different Receptors in a Mutually Exclusive Fashion

So far, I described the identification of the core motifs in the GABA<sub>A</sub>R  $\alpha$ 1-3 and GlyR  $\beta$  subunits and how gephyrin's E domain directly interacts with these motifs, albeit displaying a wide range of affinities. Alignment of the identified sequences (Table 30) reveals a moderate overall sequence homology and therefore may suggest distinct binding mechanisms. A notable exception to this finding are the N-terminal parts of the GABA<sub>A</sub>R  $\alpha$ 3 and GlyR  $\beta$  motifs (Table 30, marked in red), as well as the C terminal parts of the GABA<sub>A</sub>Rs (Table 30, marked in green) which share high levels of conservation, respectively. Prompted by these findings I investigated the possibility of a universal gephyrin binding site mediating all analyzed receptor interactions.

To address this issue I conducted ITC competition experiments between GABA<sub>A</sub>R  $\alpha$ 1 and GlyR  $\beta$  (Figure 27) which exhibit the lowest overall identity in their gephyrin-interacting region (Table 30). Should GABA<sub>A</sub>R  $\alpha$ 1,  $\alpha$ 2,  $\alpha$ 3 and GlyR  $\beta$  share a single binding site on gephyrin, I expected receptor binding to gephyrin to occur in a mutually exclusive fashion. Strikingly, my experiments revealed that pre-equilibration of gephyrin with a GlyR  $\beta$  derived peptide containing only the 15-residue core motif is sufficient to significantly weaken and ultimately abolish the GABA<sub>A</sub>R  $\alpha$ 1 gephyrin interaction depending on the molar ratio of both loops (Figure 27). Vice versa GABA<sub>A</sub>R  $\alpha$ 1 also interferes with GlyR  $\beta$  binding to GephE (data not shown), and taken together this indicates that GABA<sub>A</sub>R  $\alpha$ 1, and GlyR  $\beta$  compete for a single binding site located in gephyrin's E domain.

Table 30. **Comparison of the identified minimal peptides sufficient for gephyrin binding.** GABA<sub>A</sub>R  $\alpha$ 3 and GlyR  $\beta$  share a similar N-terminal region (boxed and residues marked in red), while GABA<sub>A</sub>Rs share high homology in their C terminal regions (boxed and residues marked in green). In contrast, GABA<sub>A</sub>R  $\alpha$ 1 and GlyR  $\beta$  display the lowest overall similarity.

Receptor	Gephyrin binding motif
GABA <sub>A</sub> R $\alpha$ 1	N T Y A P T A T <span style="border: 1px solid green; padding: 2px;">S Y T P N L</span>
GABA <sub>A</sub> R $\alpha$ 2	N A Y A V A V A <span style="border: 1px solid green; padding: 2px;">N Y A P N L</span>
GABA <sub>A</sub> R $\alpha$ 3	T T <span style="border: 1px solid red; padding: 2px;">F N I V G T</span> <span style="border: 1px solid green; padding: 2px;">T Y</span> P I <span style="border: 1px solid green; padding: 2px;">N L</span>
GlyR $\beta$	N D <span style="border: 1px solid red; padding: 2px;">F S I V G S</span> L P R D F E

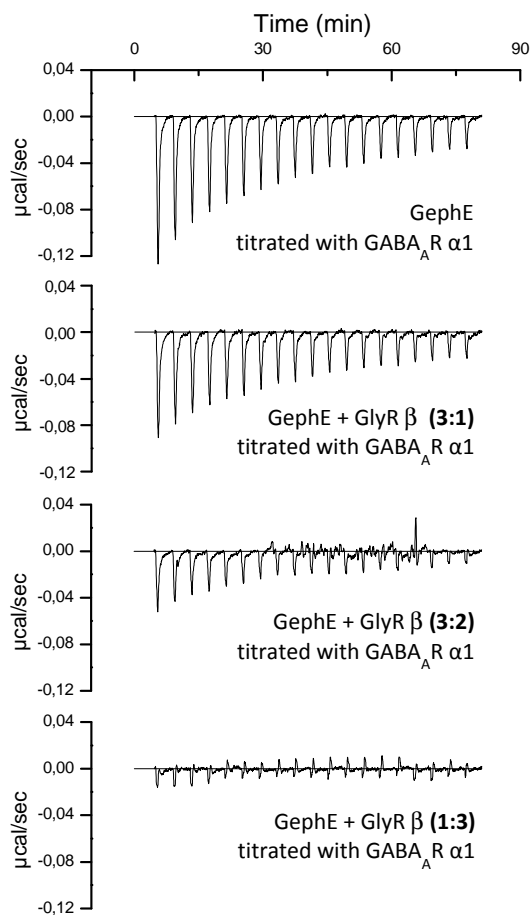


Figure 27. **ITC competition assays.** Heat signature of GephE [10  $\mu$ M] titrated with GABA<sub>A</sub>R  $\alpha$ 1 loop [200  $\mu$ M] A, in the absence, and in the presence of B, 3  $\mu$ M GlyR  $\beta$ , C, 6  $\mu$ M GlyR  $\beta$  and D, 30  $\mu$ M GlyR  $\beta$  peptide. Increasing amounts of GlyR  $\beta$  significantly reduce the heat being released which should still be measurable if GABA<sub>A</sub>R  $\alpha$ 1 binds to a different site in GephE. © 2012 HM Maric

3.2.4 Molecular Basis of Gephyrin-Mediated GlyR and GABA<sub>A</sub>R Clustering

Prompted by my biochemical findings I attempted to cocrystallize GephE with the GABA<sub>A</sub>R α1 and α3 loops by applying the identical gephyrin construct that was used for solving the GephE-GlyR β crystal structure earlier in our group. Employing a stoichiometric excess of the identified GABA<sub>A</sub>R α3 minimum motif over GephE I obtained crystals of the respective GephE complex and solved the corresponding crystal structure (Figure 28 and Table 31). The crystal contains an E domain dimer in the asymmetric unit, however, apparently caused by crystal contacts only a single binding site of the GephE-dimer was occupied with the GABA<sub>A</sub>R derived peptide. The structure of the GephE-GABA<sub>A</sub>R α3 complex indeed reveals that the GABA<sub>A</sub>R α3 residues occupy the same binding site as the respective GlyR β residues in the gephyrin GlyR β complex.

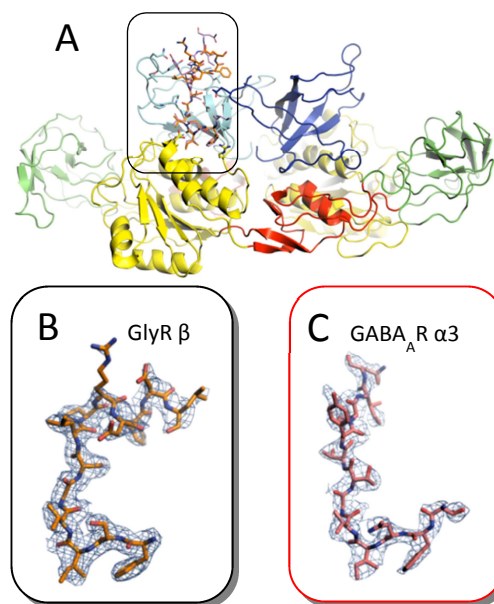


Figure 28. **Gephyrin binds different receptors with a universal binding site.** Superposition of the crystal structure of the GephE-GABA<sub>A</sub>R α3 loop solved in my thesis, and an earlier GlyR β complex structure. A, Ribbon diagram of GephE colored according to its subdomain architecture with the GABA<sub>A</sub>R α3 (solved here and marked in salmon) and GlyR β peptide (PDB-ID: 2FTS and marked in orange) as stick models. Both receptors occupy an overlapping binding site on gephyrin. Close up view of the additional electron density corresponding to the GlyR β peptide (B) in orange and the GABA<sub>A</sub>R α3 peptide (C) in salmon. © 2012 HM Maric

Table 31. X-ray data collection and refinement statistics of the GephE-GABA<sub>A</sub>R α3 complex.

Data Collection statistics		Refinement statistics		Crystallization Conditions
Wavelength (Å)	1.5418	Resolution (Å)	3.9-20	0.1 M Tris pH 8.5
Resolution (Å) <sup>a</sup>	3.9-40 (3.9-4.1)	No. of reflections	9958	30% PEG 400
Space group	P2 <sub>1</sub> 2 <sub>1</sub> 2	No. of protein/solvent atoms	6191/0	0.2 M MgCl <sub>2</sub>
Cell dimensions		R <sub>cryst</sub> (R <sub>free</sub> ) <sup>d</sup>	0.23 (0.34)	
a, b, c (Å)	51.2, 109.2, 160.0	Root mean square deviations		
α=β=γ (°)	90	Bond lengths (Å)	0.011	
Unique reflections	11589	Bond angles (°)	1.463	
⟨I/σ(I)⟩ <sup>a, b</sup>	5.34 (1.9)	Average B-factors (Å <sup>2</sup> )		
Completeness (%) <sup>a</sup>	96.4 (95.4)	Protein	23.3	
Redundancy <sup>a, c</sup>	2.2 (2.1)	Solvent	-	
R <sub>sym</sub> <sup>a</sup>	0.29 (0.92)	Ramachandran statistics (%) <sup>e</sup>		
		Favored	82.0	
		Allowed	13.2	
		Outliners	4.8	

<sup>a</sup> Numbers in parentheses refer to the respective highest resolution data shell in the data set.

<sup>b</sup> indicates the average of the intensity divided by its S.D. value.

<sup>c</sup>  $R_{sym} = \frac{\sum_{hkl} \sum_i |I_i - \langle I \rangle|}{\sum_{hkl} \sum_i \langle I \rangle}$ , where  $I_i$  is the  $i$ th measurement and  $\langle I \rangle$  is the weighted mean of all measurements of  $I$ .

<sup>d</sup>  $R_{cryst} = \frac{\sum ||F_o| - |F_c||}{\sum |F_o|}$ , where  $F_o$  and  $F_c$  are the observed and calculated structure factor amplitudes. R<sub>free</sub>, same as R<sub>cryst</sub> for 5% of the data randomly omitted from the refinement.

<sup>e</sup> Ramachandran statistics indicate the fraction of residues in the favored (98%), allowed (>99.8%), and disallowed regions of the Ramachandran diagram, as defined by MolProbity [159].

Comparison of my GephE-GABA<sub>A</sub>R α3 structure with the GephE-GlyR β structure determined earlier reveals that identical residues derived from two gephyrin subdomains (III and IV) engage in direct interaction with similar GlyR β and GABA<sub>A</sub>R α3 residues (Figure 29 and Table 32). In particular, Phe398 of the GlyR β subunit, which is of major importance for the interaction with gephyrin and the corresponding residue Phe397 in GABA<sub>A</sub>R α3 are engaged in hydrophobic interactions with GephE Phe330. Interestingly, the corresponding residues Tyr367 in GABA<sub>A</sub>R α1 and α2 also appear to be strongly conserved aromatic residues highlighted as “a” in Table 32, thus suggesting a similar role for the respective residues. Adjacent to this type-conserved aromatic residue the GephE-GlyR β and GephE-GABA<sub>A</sub>R α3 cocrystal structures display both a hydrogen bond donating residue followed by two hydrophobic residues which tightly fit into the hydrophobic pocket formed by subdomains III and IV of GephE (Ser399, Ile400 and Val401 in GlyR β, and Asn398, Ile399 and Val400 in GABA<sub>A</sub>R α3). Again the corresponding residues are type-conserved in both GABA<sub>A</sub>R α1 and α2 (Table 32 “b”). The ensuing residues, Gly402 in the GlyR β loop and Gly401 in the GABA<sub>A</sub>R α3 loop, both point towards subdomain IV of gephyrin’s E domain, and interestingly the corresponding residue in GABA<sub>A</sub>R α1 is also small (Ala371, Table 32, “c”), whereas GABA<sub>A</sub>R α2 has a significantly bulkier residue at this position (Val371). The GABA<sub>A</sub>R α1, α2 and α3 subunits share a conserved tyrosine positioned eight residues C-terminal of the first conserved aromatic residue (Table 32, “d”), yet the corresponding residue in GlyR β is a proline, thus suggesting that the C-terminal half of the GABA<sub>A</sub>R α1, α2 are recognized in the same way as GABA<sub>A</sub>R α3 which is different from the interaction with the GlyR β subunit.

α1	T	Y	A	P	T	A	T	S	Y	T	P	N	L
α2	A	Y	A	V	A	V	A	V	A	P	N	L	
α3	T	F	N	I	V	G	T	T	Y	P	I	N	L
β	D	F	S	I	V	G	S	L	P	R	D	F	E
		a	b	c	d								

Table 32. **Receptor regions recognized by gephyrin share common features.** Elements a and b are conserved among all receptor subunits, element c, a tyrosine residue is conserved among GABA<sub>A</sub>R subunits but not in the GlyR β subunit. Elements a and b form a hydrophobic motif that occupies an identical binding site on GephE, which mediates similar gephyrin interactions.

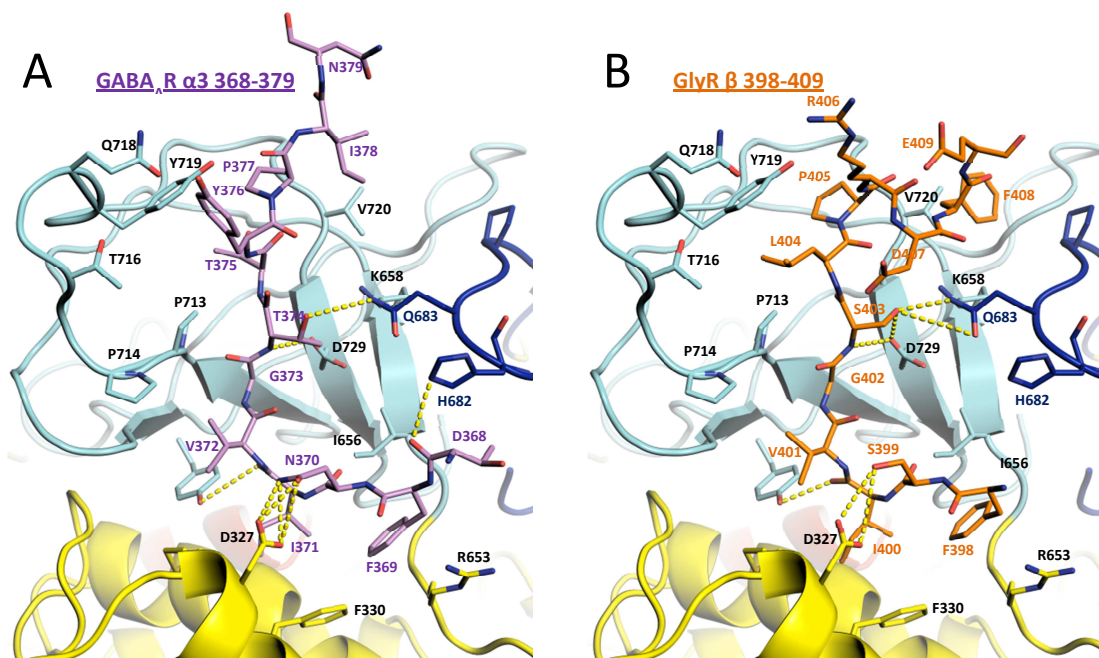


Figure 29. **Gephyrin engages in receptor subunit specific and conserved interactions.** A, Close up view of the GephE-GABA<sub>A</sub>R α3 complex. B, Binding interactions in the GephE-GlyR β loop complex crystal structure solved earlier in our group. GephE is colored according to its subdomain architecture and represented as a ribbon diagram with residues central for the GlyR β loop binding shown as stick model. Receptor residues are also shown in stick representation with GlyR β in orange and GABA<sub>A</sub>R α3 in violet. Notably, the receptor subunit binding motifs engage in similar gephyrin interactions with their N-terminus, while their C-terminus engages in subunit distinct interactions. © 2012 HM Maric and 2006 EY Kim, H Schindelin.

Based on the crystal structures we predicted that not only Phe397 of GABA<sub>A</sub>R α3 but also Tyr367 of GABA<sub>A</sub>R α1 is positioned in an analogous fashion as Phe398 of GlyR β (Table 32 "a"). In line with the over 100-fold reduction in binding strength for GlyR β F398A [55], binding was no longer detectable by ITC for the GABA<sub>A</sub>R α3 F397A and GABA<sub>A</sub>R α1 Y367A variants (Figure 30). In an analogous fashion we proposed a similar role for GABA<sub>A</sub>R α3 Ile399 as compared to GlyR β Ile400 (Table 32 "b") which critically weakened the gephyrin interaction upon alanine mutation. Not surprisingly GABA<sub>A</sub>R α3 Ile399Ala was also significantly impaired in interacting with GephE (Figure 30).

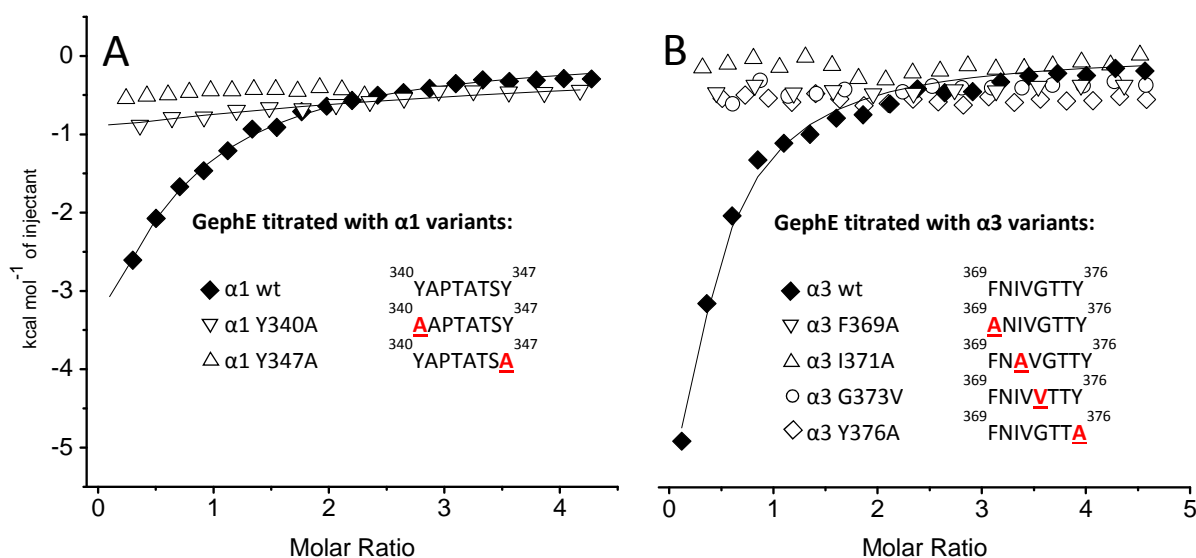


Figure 30. **Identification of GABA<sub>A</sub>R α1 and α3 loop residues critical for gephyrin binding.** Residues that are conserved among GlyR β and GABA<sub>A</sub>R α1, α2 and α3 appear to be critical for GephE complex formation. Overlaid binding isotherms of GephE titrated with (A), different GABA<sub>A</sub>R α1 loop and (B), GABA<sub>A</sub>R α3 loop variants (mutated residues are underlined and marked in red). Binding isotherms are plotted as a function of the molar ratio of receptor loop to GephE. © 2012 HM Maric

Table 33. **Similar receptor residues are critical for GephE binding.** Summary of the GABA<sub>A</sub>R α1-3 and GlyR β affinities for GephE determined by ITC (see Figures 25 and 30). Mutated residues are underlined and marked in red.

Receptor	Sequence	K <sub>d</sub> (μM)	Receptor	Sequence	K <sub>d</sub> (μM)
GlyR β (long)	<sup>398</sup> F <u>A</u> IVGSLP <sup>405</sup>	2.0±0.2	GABA <sub>A</sub> R α1	<sup>340</sup> <u>A</u> APTATSY <sup>347</sup>	n.d.
GABA <sub>A</sub> R α1	<sup>340</sup> YAPTATSY <sup>347</sup>	17±11	GABA <sub>A</sub> R α3	<sup>368</sup> <u>A</u> NIVGTTY <sup>375</sup>	n.d.
GABA <sub>A</sub> R α2	<sup>339</sup> YAVAVANY <sup>346</sup>	n.d.	GlyR β (long)	<sup>398</sup> <u>A</u> SIVGSLP <sup>405</sup>	13±0.1
GABA <sub>A</sub> R α3	<sup>368</sup> FNIV <u>V</u> TTY <sup>375</sup>	n.d.	GABA <sub>A</sub> R α3	<sup>368</sup> FN <u>A</u> VGTTY <sup>375</sup>	n.d.
GABA <sub>A</sub> R α3	<sup>368</sup> FNIVGTTY <sup>375</sup>	5.3±1.5	GlyR β (long)	<sup>398</sup> FS <u>A</u> VGSLP <sup>405</sup>	2.7±0.7
GABA <sub>A</sub> R α1	<sup>340</sup> Y <u>S</u> IATSY <sup>347</sup>	17±8.7	GABA <sub>A</sub> R α1	<sup>340</sup> YAPTAT <u>S</u> A <sup>347</sup>	n.d.
GlyR β (short) <sup>1</sup>	<sup>398</sup> FSIVGSLP <sup>405</sup>	4.9±0.4	GABA <sub>A</sub> R α3	<sup>368</sup> FNIVGTT <u>A</u> <sup>375</sup>	n.d.
GlyR β (long) <sup>2</sup>	<sup>398</sup> FSIVGSLP <sup>405</sup>	0.14±0.1 7.7±0.1			

<sup>1</sup>Residues 398-411 (FSIVGSLPRDFELS)

<sup>2</sup>Residues 378-426 (VGETRCKKVCTSKSDLRSNDFESIVGSLPRDFELSNYDCYKPIEVNGL)

The two crystal structures suggest that moderately conserved key residues within the N-terminal region of both, GABA<sub>A</sub>R and GlyR, interact with critical gephyrin residues. To test this and to expand our findings to the  $\alpha 1$  subunit, I analyzed the effects on GABA<sub>A</sub>R  $\alpha 1/3$  binding of two critical gephyrin point mutants identified earlier [55]. The mutation P713E in gephyrin was shown to completely abolish the tight GlyR  $\beta$  binding, possibly by introducing its bulky and negatively charged side chain into the receptor binding pocket formed by subdomains III, IV and IV' (Figure 29 and Table 32). A less severe change is represented by the gephyrin mutant F330A, which nevertheless significantly weakens GlyR  $\beta$  binding, most likely by diminishing the contribution of the hydrophobic interactions mediated by the hydrophobic core of the GlyR  $\beta$  loop and subdomain III of GephE. The binding of both mutants was analyzed by ITC for the GABA<sub>A</sub>R  $\alpha 1$  and  $\alpha 3$  subunits, and interestingly both impaired binding so strongly that it could no longer be assessed by ITC (Figure 31). The effect of the P713E variant supports the hypothesis that the binding site for the GlyR  $\beta$  subunit overlaps with that of the GABA<sub>A</sub>R  $\alpha 1$  and  $\alpha 3$  subunits in the vicinity of Pro713. The impaired binding of the F330A variant likewise demonstrates overlap of the different binding site in the vicinity of this residue but also argues that interactions with the GABA<sub>A</sub>R  $\alpha 1$  and  $\alpha 3$  subunits is driven by a similar contribution of the hydrophobic core region (Table 32, "a" and "b").

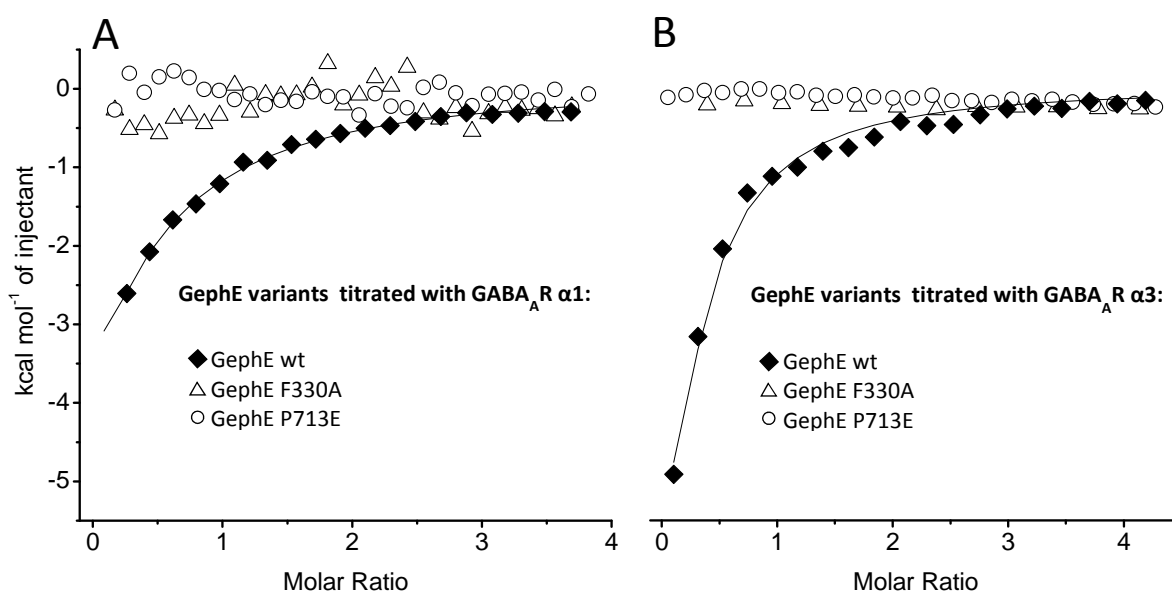


Figure 31. **Identification of GephE residues crucial for GABA<sub>A</sub>R  $\alpha 1$  and  $\alpha 3$  binding.** Gephyrin point mutations critically reduce GABA<sub>A</sub>R  $\alpha 1$  and  $\alpha 3$  affinity in a comparable manner. Overlaid binding isotherms of different GephE variants titrated with A, the  $\alpha 1$ -loop and B, the  $\alpha 3$ -loop. Binding isotherms are plotted as a function of the molar ratio of receptor loop to GephE. © 2012 HM Maric

Table 34. **Identification of key residues in GephE required for GABA<sub>A</sub>R and GlyR binding.** Summary of the GABA<sub>A</sub>R  $\alpha 1$ -3 and GlyR  $\beta$  affinities for different GephE mutation variants as determined by ITC (Figure 31).

Receptor	GephE wt $K_d$ ( $\mu$ M)	GephE F330A $K_d$ ( $\mu$ M)	GephE P713E $K_d$ ( $\mu$ M)
GABA <sub>A</sub> R $\alpha 1$	17 $\pm$ 11	n.d.	n.d.
GABA <sub>A</sub> R $\alpha 3$	5.3 $\pm$ 1.5	n.d.	n.d.
GlyR $\beta$ (long)	0.14 $\pm$ 0.1	9.2 $\pm$ 0.7	n.d.



Puzzled by our finding of a very weak GABA<sub>A</sub>R  $\alpha 2$  affinity for GephE despite the high homology to the GABA<sub>A</sub>R  $\alpha 1$  and  $\alpha 3$  subunits, we carefully compared the identified binding regions, also in light of the GephE-GlyR complex. This analysis focused our attention on Gly374, which points towards subdomain IV of GephE in the GlyR-GephE complex structure and is strictly conserved in GABA<sub>A</sub>R  $\alpha 3$  (Gly373) and type-conserved in GABA<sub>A</sub>R  $\alpha 1$  (Ala344) but not conserved in GABA<sub>A</sub>R  $\alpha 2$ , where it is replaced by a bulkier residue (Val343) (Table 32, element "c"). In line with our suggestion of similar binding modes, we proposed this residue to repel the receptor loop by sterically clashing with subdomain IV of GephE (Figure 29), thus possibly explaining our observation of a rather weak GephE affinity as compared with GABA<sub>A</sub>R  $\alpha 1$  and  $\alpha 3$ .

I replaced the corresponding residue in GABA<sub>A</sub>R  $\alpha 3$  with valine (G373V), and subsequent ITC analysis (Table 33) revealed a significantly reduced affinity. Although I could not reconstitute binding to the level of the GABA<sub>A</sub>R  $\alpha 1$  or  $\alpha 3$  subunit, NAGE of the corresponding GABA<sub>A</sub>R  $\alpha 2$  mutant (V343G) visualizes an increased gephyrin affinity (Figure 32). Taken together this indicates that this residue could at least be partially responsible for the observed weak GephE GABA<sub>A</sub>R  $\alpha 2$  affinity.

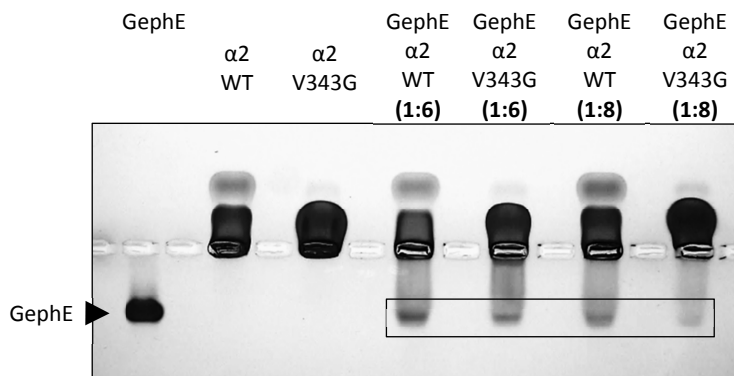


Figure 32. **NAGE verifies an increased GephE affinity for GABA<sub>A</sub>R  $\alpha 2$  V343G.** NAGE of GABAAR  $\alpha 2$  loop variants applied in a 6-fold and 8-fold stoichiometric excess over GephE. Mutation of Val343 to glycine allows less GephE to enter the gel (box), indicating a strengthening of the GephE-GABAAR  $\alpha 2$  loop complex which, at a 1:8 ratio, retains the majority of GephE in the pocket. © 2012 HM Maric

Expanding on the idea of similar binding mechanisms mediated by only moderately conserved residues I hypothesized that different receptor residues mediate similar interactions with gephyrin. To test this assumption I exchanged selected residues within the N-terminal part of the GlyR  $\beta$  and GABA<sub>A</sub>R  $\alpha 1$  motif, which appeared to be involved in the interaction with Phe330 of gephyrin. Compared to GABA<sub>A</sub>R  $\alpha 2/3$ , the GlyR  $\beta$  and the GABA<sub>A</sub>R  $\alpha 1$  subunits show the lowest overall identity in this motif. According to our hypothesis Ala368 and Pro369 of the GABA<sub>A</sub>R  $\alpha 1$  subunit would mediate similar interactions with GephE as do residues Ser399 and Ile400 of the GlyR  $\beta$  subunit which were both shown to be critical contributors to the overall binding strength. I generated an A368S/P369I double mutant of the GABA<sub>A</sub>R  $\alpha 1$  subunit and analyzed its binding by ITC. Although I severely altered the GABA<sub>A</sub>R  $\alpha 1$  core binding site, identified earlier to be crucial for binding, the determined binding parameters were very similar to the wild-type (Table 33), thus lending further support to our hypothesis.

Following my ITC-based mutational analysis I wanted to dissect the relative contributions to the overall binding strength of aromatic residues in the N and C terminal parts of the respective GABA<sub>A</sub>R  $\alpha 1$  and  $\alpha 3$  motifs. The N-terminal region of the GABA<sub>A</sub>R  $\alpha 1$ ,  $\alpha 2$  and  $\alpha 3$  subunits contains either a phenylalanine or tyrosine residue which is homologous to Phe398 of the GlyR  $\beta$  subunit and, based on the GephE-GlyR  $\beta$  complex, would be positioned in close proximity to Phe330 of gephyrin (Figure 29). In contrast, the C-terminal part of the GABA<sub>A</sub>R subunits differs from the GlyR  $\beta$  subunit; a strictly conserved tyrosine residue in the GABA<sub>A</sub>R does not coincide with Phe408 of the GlyR  $\beta$  subunit which was also identified as a critical residue for gephyrin binding (Table 32, 33 and Figure 29).

Given that ITC is not sensitive enough to display any residual binding for the respective mutants I instead used NAGE. As expected, the gel electrophoresis experiments verified a major impact on binding strength for all of the analyzed mutants (Figure 33). In line with my ITC experiments no residual binding could be detected for the F330A variant of GephE when incubated with GABA<sub>A</sub>R  $\alpha 3$ . The Y376A variant of the GABA<sub>A</sub>R  $\alpha 3$  subunit was also significantly impaired, however, it allowed for some residual binding to GephE. The corresponding substitutions in the GABA<sub>A</sub>R  $\alpha 1$  subunit both displayed a weakened receptor binding. A simultaneous substitution of both residues in the GABA<sub>A</sub>R  $\alpha 1$  subunit synergistically weakened the interaction, yet some residual binding could still be detected. Taken together these results underscore the major contribution of the conserved aromatic residues for GABA<sub>A</sub>R  $\alpha 1$  and  $\alpha 3$  but also suggest additional distinct contributions to the binding strength, which are unique to the GABA<sub>A</sub>R  $\alpha 1$  subunit.

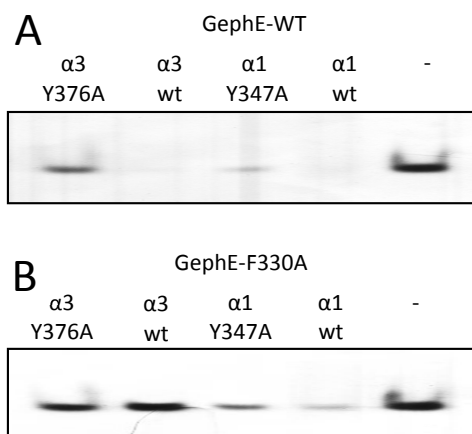
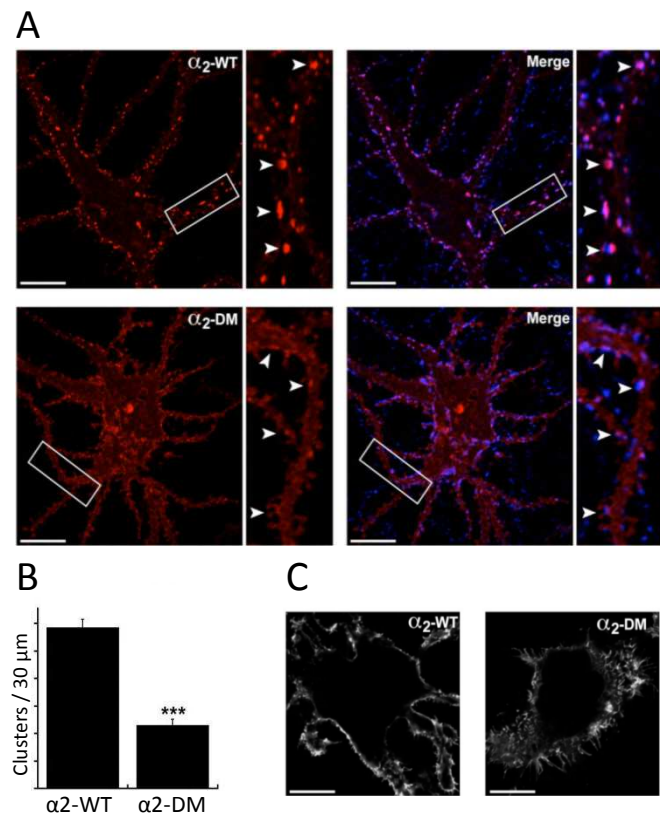


Figure 33. **NAGE reveals a differential contribution of conserved GABA<sub>A</sub>R key residues.** A, NAGE of GephE wt which, when complexed with wt receptor loops, does not enter the gel. Under the same experimental conditions GephE interacting with the altered subunits partially enters the gel indicating a weakening of the complex formation. B, Analogous experiment with the F330A variant of GephE. The presence of the GABA<sub>A</sub>R intracellular loops of the  $\alpha 3$  subunit (wild-type and Y376A variant) does not alter GephE F330A migration towards the anode, indicating a completely abolished complex formation. In contrast the  $\alpha 1$  and  $\alpha 1$  Y347A subunit show residual binding to GephE F330A, partially retaining it in the gel pocket. © 2012 HM Maric

My *in vitro* studies described in this section, identified two conserved aromatic residues in the  $\alpha 1$  and  $\alpha 3$  subunits of GABA<sub>A</sub>Rs and GlyR  $\beta$  subunit as major determinants for the direct and exclusive binding to gephyrin. Following this result, J. Mukherjee in the Moss group tested whether the respective aromatic residues are also crucial for GABA<sub>A</sub>R clustering in hippocampal neurons and hence provide evidence for a gephyrin-mediated clustering mechanism relying on a direct subunit interaction. Therefore GABA<sub>A</sub>R  $\alpha 2$  constructs were generated in which both aromatic residues, Tyr339 and Tyr346 (Table 32 marked red and green, respectively), were exchanged to alanine to abolish the direct gephyrin interaction *in vivo*.

J. Mukherjee analyzed the synaptic accumulation of GABA<sub>A</sub>Rs containing either wild-type  $\alpha 2$  or the respective double mutant subunits using an N-terminal coupled pHluorin reporter ( $^{\text{pH}}\alpha 2$  WT and  $^{\text{pH}}\alpha 2$  DM). Confocal imaging was performed on hippocampal neurons at 21 DIV (days *in vitro*) expressing either  $^{\text{pH}}\alpha 2$  WT or  $^{\text{pH}}\alpha 2$  DM. The cells were lightly fixed with paraformaldehyde and stained with the respective antibodies. Surface staining with a GFP antibody revealed a significant loss of GABA<sub>A</sub>Rs clusters per 30  $\mu\text{m}$  segment ( $11.7 \pm 0.6$  vs.  $4.6 \pm 0.4$ ,  $n = 30$  neurons,  $^{\text{pH}}\alpha 2$  WT and  $^{\text{pH}}\alpha 2$  DM, respectively) (Figure 34A and B). These clusters are primarily synaptic as they are either colocalized or opposed to VIAAT positive puncta. Moreover, cells expressing mutant  $^{\text{pH}}\alpha 2$  subunits are positive for VIAAT puncta, suggesting that they are innervated by inhibitory presynaptic terminals. To control for possible negative effects of mutations on receptor assembly or surface trafficking, the ability of the  $^{\text{pH}}\alpha 2$  WT and  $^{\text{pH}}\alpha 2$  DM subunit to gain access to the plasma membrane on coexpression with the  $\beta 3$  subunit in HEK 293 cells was examined by anti-GFP surface labeling (without permeabilization) (Figure 34C). Indeed, in the presence of the  $\beta 3$  subunit, both  $^{\text{pH}}\alpha 2$  WT and  $^{\text{pH}}\alpha 2$  DM subunits gain access to the surface membrane at similar levels. This process seems specific as he observed minimal surface trafficking, when expressing the  $^{\text{pH}}\alpha 2$  subunit alone.



**Figure 34. Tyrosine-mutations attenuate  $\alpha 2$ -mediated GABA<sub>A</sub>R clustering at postsynaptic sites.** Hippocampal neurons expressing  $^{\text{pH}}\alpha 2$ -WT and  $^{\text{pH}}\alpha 2$ -DM (Tyr339Ala/Tyr346Ala) were lightly fixed ( $\sim 21$  Div), stained with GFP antibody against the extracellular “pHluorin” tag (red) and the presynaptic marker VIAAT (blue). **A**, Single plane confocal images showing the clustering pattern of  $^{\text{pH}}\alpha 2$ -WT (upper panel) and  $^{\text{pH}}\alpha 2$ -DM (lower panel). Note that the ability to form clusters is greatly attenuated for  $^{\text{pH}}\alpha 2$ -DM since both cluster number and intensity are strongly reduced. For each panel, a higher magnification image of the boxed area is shown on the right, with arrows pointing to clusters (scale bar = 15  $\mu\text{m}$ ), showing that clusters are opposed to VIAAT and hence postsynaptic. **B**, Quantification of the average number of clusters formed by  $^{\text{pH}}\alpha 2$ -WT and  $^{\text{pH}}\alpha 2$ -DM at postsynaptic sites along dendrites per 30  $\mu\text{m}$  ( $n=30$  cells each, unpaired t test,  $P<0.001$ ). **C**, HEK 293 cells expressing  $^{\text{pH}}\alpha 2$  and  $^{\text{pH}}\alpha 2$ -DM along with the  $\beta 3$  subunit. Cells were lightly fixed and surface labeled with an anti-GFP antibody against extracellular “pHluorin” tag (red). Confocal images show that both  $^{\text{pH}}\alpha 2$ -WT (left panel) and  $^{\text{pH}}\alpha 2$ -DM (right panel) can access the surface membrane to a similar extent (scale bar = 15  $\mu\text{m}$ ). © 2011 J Mukherjee, K Kretschmannova, G Gouzer, HM Maric, S Ramsden, V Tretter, K Harvey, PA Davies, A Triller, H Schindelin, SJ Moss

Collectively these experiments suggest that both tyrosine residues are critical for regulating the accumulation of GABA<sub>A</sub>R  $\alpha$ 2 subunits at inhibitory postsynaptic sites via a direct interaction with gephyrin. Additionally, the corresponding  $\alpha$ 1 double mutant (Y340A, Y347A) showed a similar effect (data not shown) and taken together it can therefore be inferred that conserved aromatic residues within the intracellular loops of the GABA<sub>A</sub>R and GlyRs are major contributors to the direct gephyrin interaction, which mediates the clustering of these receptors at postsynaptic sites.

3.2.5 Regulation of Gephyrin-Mediated GABA<sub>A</sub>R Clustering

So far, my results suggest that gephyrin mediates the clustering of GABA<sub>A</sub>Rs containing the  $\alpha 1$ ,  $\alpha 2$ ,  $\alpha 3$  and GlyRs containing the  $\beta$  subunit via a universal binding site. Interestingly, Y2H studies, conducted in parallel by the Harvey lab, apparently excluded the GABA<sub>A</sub>R  $\alpha 1$  subunit as a gephyrin interaction partner (Figure 35A). J. Mukherjee hypothesized that phosphorylation of the GABA<sub>A</sub>R fragment in yeast reduces the direct gephyrin interaction and indeed succeeded in demonstrating that the introduction of an acidic residue that mimics phosphorylation of Thr348 attenuates receptor clustering at postsynaptic sites (Figure 35B) in hippocampal neurons. Following this result Sarah Ramsden from the Harvey lab showed that the corresponding alanine mutation indeed reconstitutes a direct gephyrin interaction of this subunit in Y2H assays (Figure 35A). Based on these findings we concluded that Thr348 can be phosphorylated in both, hippocampal neurons derived from mice and in yeast. To verify the suggested reduced affinity of the phospho-mimetic point mutation I quantified the direct interaction strength between gephyrin and the corresponding GABA<sub>A</sub>R  $\alpha 1$  mutants by ITC (Figure 35C). Strikingly, introduction of a phosphomimetic glutamate indeed reduced the overall gephyrin binding strength approximately 10-fold, hence lending further support to the idea that phosphorylation within the GABA<sub>A</sub>R  $\alpha 1$  binding motif reduces GABA<sub>A</sub>R clustering by reducing its direct gephyrin interaction strength.

Notably, the *in vitro* and *in vivo* experiments described in the previous section identified Tyr347 in the  $\alpha 1$  subunit as a major contributor to the respective overall gephyrin binding strength. Introduction of a negative charge at the adjacent residue apparently interferes with the critical hydrophobic interactions mediated by the tyrosine residue which is conserved among the GABA<sub>A</sub>R  $\alpha 1$ ,  $\alpha 2$  and  $\alpha 3$  subunits.

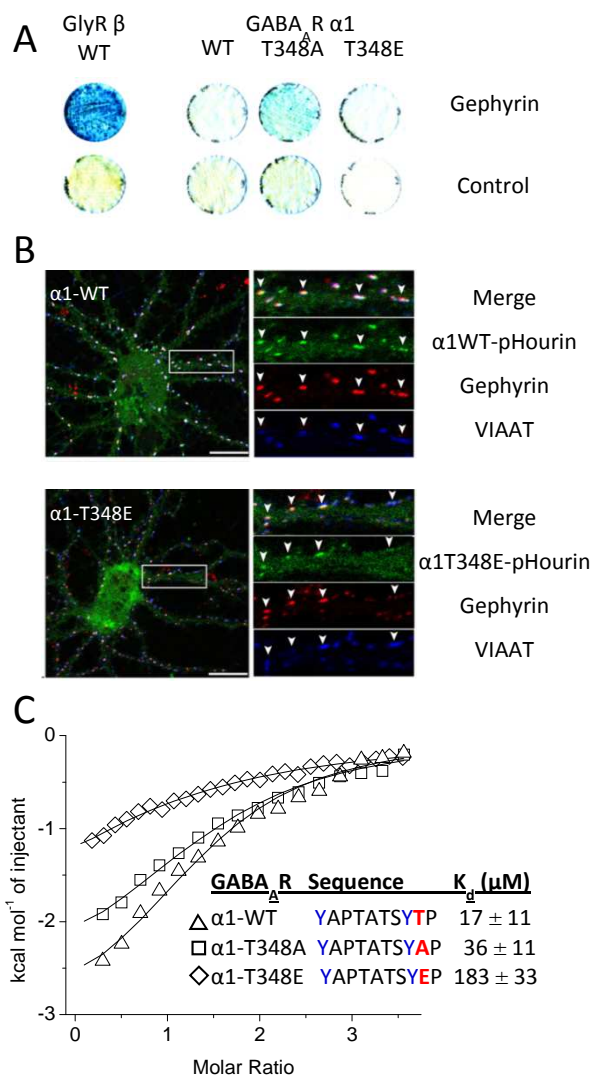


Figure 35. **GABA<sub>A</sub>R  $\alpha 1$  Thr348 regulates receptor clustering by modulating GephE affinity.** A, Y2H experiments conducted by K. Kretschmannova. Only GABA<sub>A</sub>R  $\alpha 1$  Thr348A, but not the wildtype or the phosphomimetic variant interact with gephyrin in Y2H assays. B, J. Mukherjee nucleofected neurons (18-21 DIV) expressing GABA<sub>A</sub>Rs incorporating either WT- $\alpha 1$  or T348E- $\alpha 1$  subunits were fixed, permeabilized, and stained with antibodies against gephyrin (red) and VIAAT (blue). Introduction of glutamate for Thr348 attenuates clustering of GABA<sub>A</sub>Rs in hippocampal neurons. C, ITC-plots of either  $\alpha 1$ -WT,  $\alpha 1$ -T348A and  $\alpha 1$ -T348E. Notably T348E shows a reduced exothermic signal together with an approximately 10-fold reduced gephyrin affinity as compared to the wildtype. Exchange of the threonine by alanine has only a slight effect on both the affinity and the enthalpy. © 2011 J Mukherjee, K Kretschmannova, G Gouzer, HM Maric, S Ramsden, V Tretter, K Harvey, PA Davies, A Triller, H Schindelin, SJ Moss

Finally, my results described here, offer a possible molecular explanation for findings of an earlier functional study [172] that addressed the phosphorylation of GABA<sub>A</sub>R  $\alpha 1$  by the extracellular-signal regulated kinase (ERK), a key effector of the mitogen-activated protein kinase (MAPK) pathway. This signal transduction pathway propagates and amplifies extracellular signals into a biological response. It involves the sequential activation of a small GTPase (Ras), followed by a serine/threonine kinase (Raf), then mitogen-activated ERK-activating kinase (MEK), a dual specificity kinase that subsequently phosphorylates its immediate downstream target, the MAPK [173]. This pathway is involved in the regulation of cell viability and the regulation of synaptic plasticity and memory [174, 175].

C.L. Bell-Horner et al. observed altered GABA-gated currents upon ERK inhibition through pharmacological inhibition of its upstream kinase (MEK) with the inhibitor U0126 (Figure 36). Interestingly the same GABA<sub>A</sub>R  $\alpha 1$  point-mutation (T348A) was introduced [172] as in the work presented here. As expected the removal of the ERK phosphorylation site prevented the U0126-induced enhancement of GABA-gated currents. Based on my own studies I now suggest the MAPK pathway to be a negative modulator of gephyrin-mediated GABA<sub>A</sub>R clustering at postsynaptic sites. Hence my future studies will investigate the effect of U0126 on GABA<sub>A</sub>R clustering in living neurons. Interestingly, all GABA<sub>A</sub>R  $\alpha$  subunits with the exception of the extrasynaptic  $\alpha 5$  subunit harbor an ERK phosphorylation site (P-x-[S/T]-P or [S/T]-P).

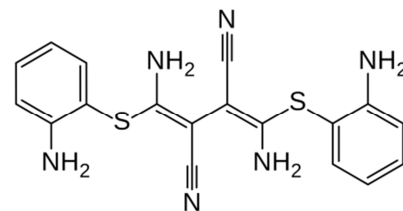


Figure 36. **U0126, a highly potent MEK1 inhibitor ( $IC_{50} = 14$  nM).** MEK inhibition by U0126 is thought to inhibit ERK which phosphorylates Thr348 in the GABA<sub>A</sub>R  $\alpha 1$  subunit. My results demonstrate this phosphorylation weakens the direct interaction with gephyrin, possibly explaining the finding of increased GABA<sub>A</sub>R function upon U0126-induced MEK inhibition. © Public domain

Prompted by this finding I investigated the possibility that earlier large-scale studies already verified phosphorylation within the linear gephyrin binding motifs identified in this work. Strikingly, at least seven known phosphorylation sites have already been verified. Among those, only one was addressed functionally (Table 35), namely the PKC mediated GlyR  $\beta$  phosphorylation which directly interferes with gephyrin binding [65] in a similar fashion as shown in my work for the GABA<sub>A</sub>R  $\alpha 1$  subunit.

Receptor	Sequence
GABA <sub>A</sub> R $\alpha 1$	<sup>339</sup> <span style="border: 1px solid black; padding: 2px;">T<sup>1</sup>Y<sup>2</sup>APTAT</span> <span style="border: 1px solid black; padding: 2px;">SY<sup>3</sup>T<sup>4,5,6</sup></span> PNL <sup>350</sup>
GABA <sub>A</sub> R $\alpha 2$	<sup>338</sup> A <span style="border: 1px solid black; padding: 2px;">YAVAVA</span> <span style="border: 1px solid black; padding: 2px;">NY</span> A PNL <sup>349</sup>
GABA <sub>A</sub> R $\alpha 3$	<sup>369</sup> <span style="border: 1px solid black; padding: 2px;">TFNIVGT</span> <span style="border: 1px solid black; padding: 2px;">TY</span> P INL <sup>380</sup>
GlyR $\beta$	<sup>397</sup> D <span style="border: 1px solid black; padding: 2px;">FSIVGS<sup>7</sup></span> LP R DFE <sup>409</sup>

Table 35. **GABA<sub>A</sub>Rs and GlyRs are phosphorylated within their gephyrin-binding regions.** Critical mediators of the direct interaction are boxed. Residues that were found to be phosphorylated *in vivo* are marked in red and the respective reference given in the footnote: <sup>1</sup>[176]; <sup>2</sup>[177]; <sup>3</sup>[178]; <sup>4</sup>[179]; <sup>5</sup>[180]; <sup>6</sup>[172]; <sup>7</sup>[65].

### 3.3 Development of Bivalent Receptor Peptides that Specifically Target Gephyrin's Receptor-Binding Capacities

So far, biophysical and biochemical studies of gephyrin-receptor interactions, including my own studies described in the previous sections, involved only monomeric receptor-derived peptides and the obtained range of affinities (0.1-20  $\mu$ M) most likely does not mirror the actual binding strength *in vivo*. These binary systems constitute an obvious oversimplification disregarding the possibility of an enhanced affinity due to plurivalent interactions mediated by the complex assembly of the receptors and the multimeric nature of gephyrin. To overcome this shortcoming I have developed dimeric forms of gephyrin-binding, receptor-derived minimum peptides that mimic the multivalent binding sites presented by a pentameric receptor containing at least two gephyrin-binding subunits. In this section I will present:

- The structure-based identification of minimum peptides with optimized gephyrin-binding affinity.
- A quantitative and irreversible one-step peptide dimerization and purification.
- An analysis of bivalent peptide binding specificity via DSC.
- A quantification of the avidity effect via thermofluor and ITC.
- A demonstration of the inhibition of gephyrin's receptor-binding capacities.
- The characterization of a low affinity gephyrin ligand using the dimerization approach.
- A comparison of the total enthalpy change of different gephyrin ligands which reveals a universal receptor binding mechanism.
- The Impact of the E domain architecture on avidity.

### 3.3.1 Identification of a Gephyrin-Binding Minimum Sequence with Maximized Affinity

Crystal structures described in the previous paragraphs verified that residues 398–411 of the GlyR  $\beta$  loop, as well as residues 368–379 of the GABA<sub>A</sub>R  $\alpha 3$  loop, readily occupy a major groove formed by subdomains III and IV of GephE. Subsequent biochemical analyses additionally suggest that GABA<sub>A</sub>R  $\alpha 1$  and  $\alpha 2$  engage in similar interactions despite exhibiting only moderate sequence homology. We defined two hotspots of the receptor-gephyrin interaction, one at the N-terminal end and the other towards the C-terminal end. The N-terminal part is conserved among GlyRs and GABA<sub>A</sub>R and engages in critical interactions with Phe330 and Asp327 of gephyrin, thereby forming the basis of the mutually exclusive receptor binding. In contrast, the C-terminal part shows distinct conservation of critical aromatic residues within GABA<sub>A</sub>R and GlyR subunits and therefore point towards different gephyrin-binding mechanisms.

Based on these findings we hypothesized that the conserved N-terminal part of the receptor-derived peptides should be exchangeable among the different subunits, and in order to decipher the actual binding contribution of each part, I generated chimeric receptor variants (Figure 37A) and analyzed their GephE-binding via ITC (Figure 37B). Taken together, peptides containing the N-terminal part of GlyR  $\beta$  display a maximized affinity towards GephE. *Vice versa*, chimeric GABA<sub>A</sub>R constructs which included the C-terminal part of GlyR  $\beta$ , showed no detectable binding. Specifically, an exchange of three GABA<sub>A</sub>R- $\alpha 3$  residues by type conserved GlyR  $\beta$  residues (D368T; N370S; T374S) already results in a strong amplification of the overall binding strength. Combined, this indicates that the N-terminal region of the receptor-binding motifs is the major determinant of the overall binding strength, and that GlyR  $\beta$  offers the N terminal region with the highest gephyrin affinity. In contrast, the C-terminal part, which shows no sequence conservation between GlyRs and GABA<sub>A</sub>R, adjusts the overall affinity on a smaller scale, yet is still necessary. Quantitatively (Figure 37), the affinity of the seven N-terminal GlyR  $\beta$  residues is

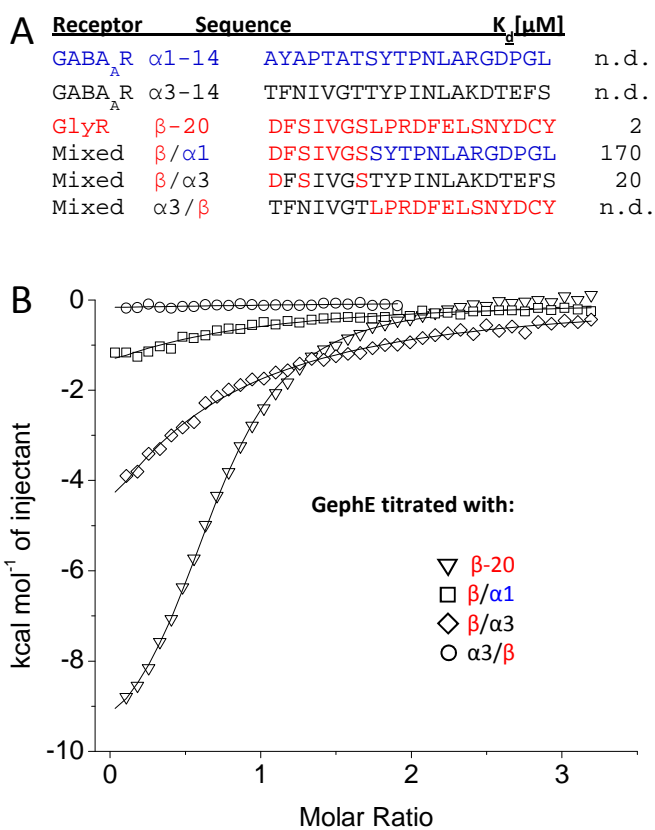


Figure 37. **Seven residues of the GlyR  $\beta$  peptide display a maximized gephyrin affinity.** A, Sequence alignment of the GlyR  $\beta$ , GABA<sub>A</sub>R  $\alpha 1$  and GABA<sub>A</sub>R  $\alpha 3$  derived peptides and their chimeric variants together with their gephyrin affinities as determined via ITC (n.d. = not detectable in ITC). Residues resolved in the crystal structures of GephE in complex with GlyR  $\beta$ -49 and GABA<sub>A</sub>R  $\alpha 3$  are underlined. B, Measured binding enthalpies plotted as a function of the molar ratio of ligand to gephyrin. The N-terminal motif of GlyR  $\beta$  acts as a universal mediator of gephyrin-binding strength in all motifs. Notably, the  $\beta/\alpha 3$  chimeric variant can also be considered as an  $\alpha 3$  mutant with 3 residues exchanged by type-conserved side chains D368T, N370S and T374S. Despite the minor exchanges the affinity of the  $\alpha 3$  peptide is potentiated by several orders of magnitude. © 2012 HM Maric



modified to 1  $\mu\text{M}$  after addition of thirteen GlyR  $\beta$  residues, to 20  $\mu\text{M}$  by addition of thirteen GABA<sub>A</sub>R  $\alpha 3$  residues and to 170  $\mu\text{M}$  when thirteen GABA<sub>A</sub>R  $\alpha 1$  are following (Figure 37). In line with our idea that the N-terminal parts are exchangeable among the different receptor subunits, the chimeric variants mirror the relative binding strengths of their full-length counterparts, albeit potentiated by the introduction of seven GlyR  $\beta$  residues. These findings are also in strong agreement with our earlier studies [55] and results presented in previous paragraphs of this work, which demonstrated that mutations of either gephyrin Pro713 (to glutamate) or Phe330 (to alanine), which are both in close proximity to the N-terminal part of the receptor motif, yielded the most significant weakening of the overall receptor-binding strength.

Next, the length dependence of gephyrin affinity was analyzed with peptide fragments displaying the highest gephyrin affinity, namely GlyR  $\beta$  fragments. Using the same 49 residue GlyR  $\beta$  peptide ( $\beta$ -49) containing residues 378-425, the gephyrin interaction was analyzed extensively with different biophysical methods and, based on a biphasic binding behavior in ITC, two binding sites were proposed with  $K_d$  values in the low nanomolar and low micromolar range [55, 58, 61, 65]. In particular, the high affinity binding site of the elongated GlyR  $\beta$  was described to be in the nanomolar range with values varying between 22-30 nM [61, 65] and 140-400 nM [55, 58] depending on the stoichiometry values which were estimated at 0.28-0.29 [61, 65] and 0.7-1.0 [55, 58], respectively. The low affinity site displayed affinities of 3-6  $\mu\text{M}$  [61, 65] and 16-30  $\mu\text{M}$  [55, 58] with a stoichiometry of 0.6 [61, 65] and 0.6-0.8 [55, 58], respectively. This deviation may be explained by lab-specific systematic differences in protein activity; depending on the purification protocol the discrepancy between active molecules and apparent concentration may vary. A low active fraction of macromolecules in the cell will yield overestimated affinities and underestimated stoichiometry values. In contrast, the discrepancy of a single binding site in the crystal structure versus two binding sites in ITC remains to be explained on the molecular level.

To resolve the apparent discrepancy of a single binding site in the crystal structure and two different binding sites in ITC I analyzed truncated fragments, containing either the 15 residues resolved in the crystal structure ( $\beta$ -15), or a longer fragment that is extended by 5 residues at the C terminus ( $\beta$ -20) (Figure 38). Strikingly, titration of  $\beta$ -15 to GephE, indeed revealed a single binding site displaying a moderate affinity of 5  $\mu$ M. While, the affinity increased slightly to a  $K_d$  of 3  $\mu$ M for the C terminally elongated peptide ( $\beta$ -20), neither the biphasic binding behavior nor the apparently extremely high affinity of  $\sim 0.1$   $\mu$ M for  $\beta$ -49 could be reconstituted (Figure 38 and Table 36).

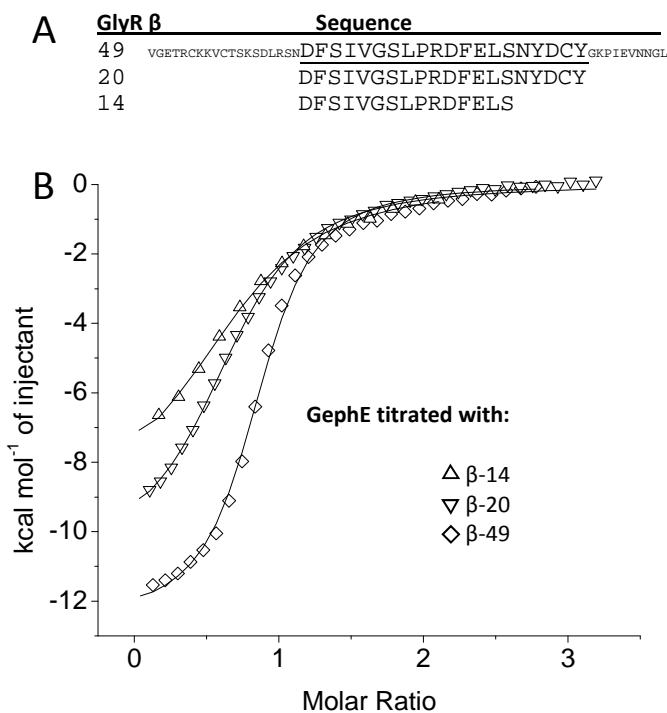


Figure 38. ITC reveals a peptide length dependent GephE affinity of GlyR  $\beta$  derived peptides. A, Sequence alignment of the  $\beta$ -49,  $\beta$ -20 and  $\beta$ -15 peptides together with their gephyrin affinities as determined by ITC. Residues resolved in the crystal structures of GephE in complex with  $\beta$ -49 are underlined. B, Measured binding enthalpies plotted as a function of the molar ratio of ligand to gephyrin. The core motif of GlyR  $\beta$  identified in the crystal structure shows a reduced overall affinity. Titration of both,  $\beta$ -15 and  $\beta$ -20 was fitted using a one binding site model, while titration with  $\beta$ -49 necessitated the use of a two site binding model, yielding two GephE affinities. © 2012 HM Maric

Table 36. Gephyrin E domain binding parameters determined by ITC.

Titrant	Stoichiometry [N]	Affinity [ $\mu$ M]	Enthalpy [kcal/mol]
GlyR $\beta$ -49	0.65 $\pm$ 0.01/0.6 $\pm$ 0.2	0.14 $\pm$ 0.1/7.7 $\pm$ 0.1	-16.1 $\pm$ 1.1/-7.2 $\pm$ 2.3
GlyR $\beta$ -20	0.70 $\pm$ 0.01	2.8 $\pm$ 0.2	-10.8 $\pm$ 0.2
GlyR $\beta$ -15	0.75 $\pm$ 0.02	4.9 $\pm$ 0.4	-8.4 $\pm$ 0.3

To understand this differential binding behavior at the molecular level I determined the crystal structures of GephE in complex with the 15 and the 20 residue fragments. The structures could be refined at 2.0 ( $\beta$ -15) and 2.8 Å ( $\beta$ -20) resolution, and were compared to the earlier structure refined at 2.4 Å ( $\beta$ -49) [55] (Figure 39 and Table 37). The most significant difference, possibly explaining the difference in binding strength, is the absence of electron density for four residues located at the C-terminus of the shortest peptide, despite being present in all peptides. Remarkably, the missing C terminal part of the receptor loop adopts an  $\alpha$ -helical conformation in the elongated fragment which allows GlyR residue Phe 408 to fit into a hydrophobic pocket formed by residues Val727 and Pro685 of gephyrin. Indeed, this C-terminal aromatic residue was shown earlier to be a critical contributor to the overall binding strength [55]. Apparently, the formation of this helix requires additional C terminal residues, not resolved in the crystal-structures and therefore not present in the 15 residue peptide.

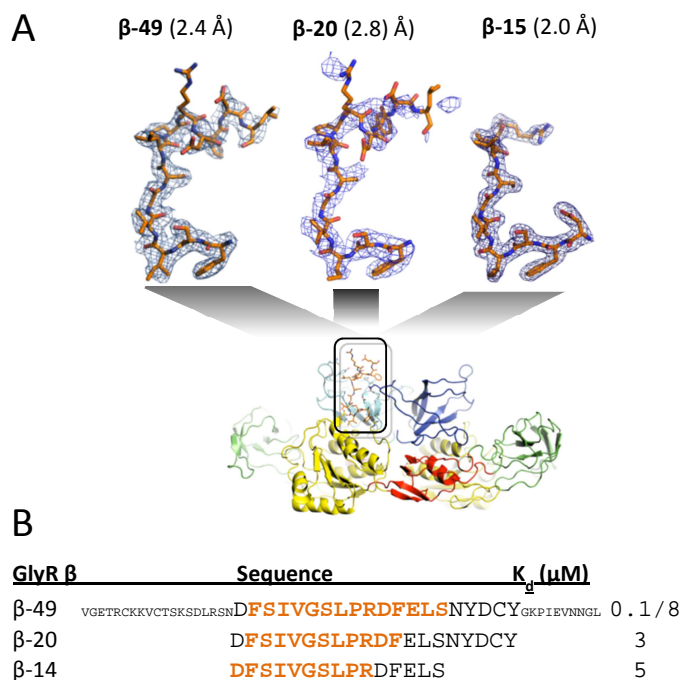


Figure 39. **GephE- $\beta$ -loop cocrystal structures reveal structural rearrangements within the GlyR.** Analyses of crystal structures of different GlyR  $\beta$  derived peptides in complex with GephE. A, Electron density and the assigned stick models of the GephE-GlyR  $\beta$  complex cocrystallized with the 49, 20 or 15 residue fragments. B, Sequence alignment of the peptides with residues resolved in the resulting X-ray structures marked in orange. The 15 residue fragment lacks C terminal residues, which could be resolved with the 49 residue fragment. The 20 residue fragment shows additional electron density as compared to the shorter variant, albeit less well defined as in the 49 residue complex structure. © 2012 HM Maric

This result offers a possible explanation for earlier puzzling findings that changes within the GlyR  $\beta$  motif by both, alanine point mutations and phosphomimetic substitutions, result in monophasic binding curves describing only a single binding site of low micromolar affinity [55, 65]. I propose that alterations among GlyR  $\beta$  key residues disrupts the secondary structure in a similar manner as the truncations investigated here and that both alterations are mirrored by the differential mono- and biphasic binding in ITC and the electron density in the structures. I hypothesize that the N-terminal motif “FSIV” and the C-terminal motif “FELS” together exhibit an avidity-potentiated gephyrin affinity.

Additionally, only the shortest GlyR  $\beta$  fragment has its very N-terminal residue, an aspartate, resolved in the crystal structure, despite being present in all peptides. Interestingly the corresponding residue in GABA<sub>A</sub>R  $\alpha$ 3, a threonine, could also be resolved in the crystal structure and both residues appear to interact in a conserved manner with His682 of gephyrin. The contribution of this very N-terminal interaction was not analyzed, given the low affinity of the respective peptides, and it seems unlikely that this interaction is a major contributor to the overall binding strength.

Table 37. Crystallization, X-ray data collection and refinement tables for the GephE- $\beta$  complexes.

Data collection statistics			
	GephE- $\beta$ -14	GephE- $\beta$ -20	GephE- $\beta$ -49
Wavelength (Å)	1.54178	1.54178	1.10
Resolution (Å) <sup>a</sup>	2.0-40.5 (2.0-2.1)	2.8-32.0	2.4-50.0
Space group	I222	I222	C222 <sub>1</sub>
Cell dimensions			
a, b, c (Å)	87.4, 99.5, 117.4	87.9, 100.2, 113.7	51.3, 123.5, 155.0
$\alpha=\beta=\gamma$ (deg)	90	90	90
Unique reflections	34136	9716	18251
$\langle I/\sigma(I) \rangle$ <sup>a, b</sup>	13.0 (3.3)	6.9 (1.3)	21.5 (2.7)
Completeness (%) <sup>a</sup>	100 (100)	77.6 (82.2)	93.5 (77.0)
Redundancy <sup>a, c</sup>	14.9 (15)	3.3 (3.1)	5.0 (-)
R <sub>sym</sub> <sup>a</sup>	0.19 (1.0)	0.19 (1.14)	0.09 (0.56)
Refinement statistics			
	GephE- $\beta$ -14	GephE- $\beta$ -20	GephE- $\beta$ -49
Resolution (Å)	2.0-40.5	2.8-28.0	2.4-20.0
No. of reflections	33870	9227	17248
No. of protein/solvent atoms	3290/150	3127/-	3298/150
R <sub>cryst</sub> (R <sub>free</sub> ) <sup>d</sup>	0.17 (0.20)	0.22 (0.29)	0.19 (0.27)
Root mean square deviations			
Bond lengths (Å)	0.009	0.016	0.019
Bond angles (°)	1.11	1.79	1.59
Average B-factors (Å <sup>2</sup> )			
Protein	41.6	37.0	40.5
Solvent	42.0	(-)	(-)
Ramachandran statistics(%)			
Favored	99.3	89.2	91.0
Allowed	0.5	7.0	8.6
Outliners	0.2	3.8	0.3
Crystallization conditions			
	GephE- $\beta$ -14	GephE- $\beta$ -20	GephE- $\beta$ -49
Buffer	0.1 M NaAc pH 4.5	0.1 M Cacodylate pH 6.5	0.1 M Tris 7.5-8.5
Additive	0.01 M CoCl <sub>2</sub>	0.2 M MgCl <sub>2</sub>	0.1-0.2 M NaAc
Precipitance	1 M 1,6-Hexanediol	10% PEG 3000	25-30% PEG 4000
GephE- $\beta$ concentration	12-14 mg/ml	12-14 mg/ml	1-2 mg/ml

<sup>a</sup> Numbers in parentheses refer to the respective highest resolution data shell in the data set.

<sup>b</sup> indicates the average of the intensity divided by its S.D. value.

<sup>c</sup>  $R_{sym} = \sum_{hkl} \sum_i |I_i - \langle I \rangle| / \sum_{hkl} \sum_i \langle I \rangle$ , where  $I_i$  is the  $i$ th measurement and  $\langle I \rangle$  is the weighted mean of all measurements of  $I$ .

<sup>d</sup>  $R_{cryst} = \sum ||F_o| - |F_c|| / \sum |F_o|$ , where  $F_o$  and  $F_c$  are the observed and calculated structure factor amplitudes. R<sub>free</sub>, same as R<sub>cryst</sub> for 5% of the data randomly omitted from the refinement.

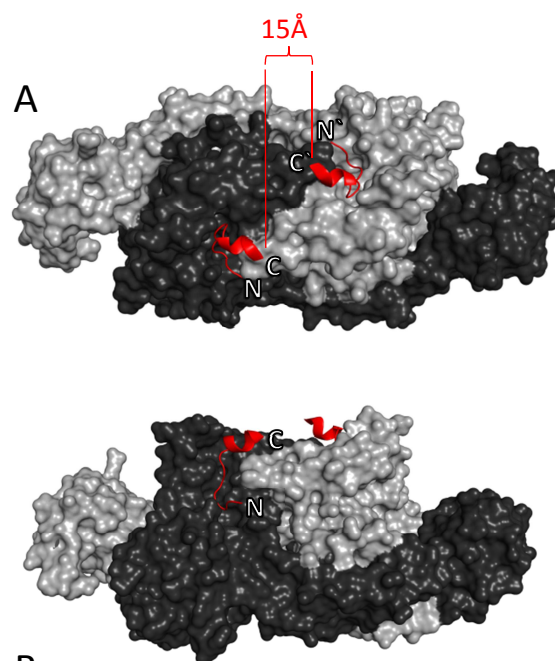
<sup>e</sup> Ramachandran statistics indicate the fraction of residues in the favored (98%), allowed (>99.8%), and disallowed regions of the Ramachandran diagram, as defined by MolProbity [159].

Combined, the crystal structures prove that a short fifteen residue fragment (GlyR  $\beta$  397-411) is sufficient to occupy gephyrin's N terminal core binding site also implicated in GABA<sub>A</sub>R binding which is responsible for the observation of the mutually exclusive binding of the receptors described in the previous chapter. Based on the comparison of three different cocrystal structures of GephE in complex with GlyR  $\beta$  peptides of different length, I suggest that secondary structure elements in the elongated peptides allow for an avidity-based potentiation of gephyrin affinity, and that elongation towards the C-terminus of the  $\beta$ -20 peptide but not N-terminus is necessary for this effect. Based on these results I decided to use the 20 residue peptide for subsequent dimerization approaches. While it does not offer the maximal possible affinity, it is sufficient for crystallization and occupies the largest part of gephyrin's universal receptor binding site. Additionally, it provides a single naturally occurring cysteine residue at its very C terminal part, which enables thiol-based one-step dimerization, as described in the next paragraph.

### 3.3.2 Peptide Dimerization

Bivalent peptides are commonly generated by solid-phase synthesis and subsequent N-terminal dimerization with activated bidentate linkers before they are finally released from the respective resin. Based on the crystal structures described in the previous paragraph I decided to instead link the C-terminal ends of the receptor fragments which, when bound to the GephE dimer, approach each other at a minimum distance of ~15 Å (Figure 40A). In addition, by using the nucleophilicity of the naturally occurring cysteine residue at the very C-terminal end of the peptides (Figure 40B) side group protection or activation as well as the introduction of lysine residues could be omitted.

Different sulfhydryl specific crosslinkers enabled me to dimerize native and unmodified receptor derived peptides via their C-terminally localized cysteine (Table 38). This was accomplished by relying either on a bimolecular nucleophilic substitution (S<sub>N</sub>2) using a bidentate haloalkyl crosslinker as electrophile (Figure 41A), or a Michael-addition that converts reactive maleimide groups to succinimide groups (Figure 41B). Although the succinimides eventually hydrolyze to yield carboxylates, the peptide linkage remains intact and therefore both dimerization strategies can be considered irreversible.



**B**

GlyR  $\beta$  TM3-4:

NNPKRVEAEKARIAKAEQADGKGGNVAKKNTVNGTGTPVH  
ISTLQVGETRCKKVCTSKSDLRSNDFSIVGSLPRDFELSNYDCY  
GKPIEVNNGLGKSQAKNNKPPPAKPVIPATAAKRIDLYAR

Figure 40. **Design of receptor-derived, gephyrin-targeting bivalent peptides.** A, Schematic representations of the GephE-GlyR  $\beta$ -loop complex crystal structure viewed from above and in side-view. The gephyrin E domain dimer is shown in surface representation with the monomers shown in light or dark grey, respectively. The  $\beta$ -loops are shown in cartoon representation in red. B, Sequence of the intracellular loop of the GlyR  $\beta$  subunit. Residues used for subsequent bivalent peptides are underlined, residues resolved in the X-ray structure are marked in red and the naturally occurring cysteine used for dimerization is marked in blue which forms the very C-terminal part of the bivalent peptides. © 2012 HM Maric

Table 38. **Crosslinkers used for the cysteine-specific peptide dimerization.**

Crosslinker	Reactive Group	Structure	Linker Length
Bromomethyl-2,6-dimethyl-pyrazolo 1,2a-pyrazole-1,7-dione (Dibromobimane) (bbBr)	Haloalkyl		6 Å
1,2-Bismaleidoethane (BMOE)	Maleimide		8 Å
1,4-Bismaleidobutane (BMB)	Maleimide		11 Å
1,6-Bismaleidoethane (BMH)	Maleimide		13 Å
1,8-Bismaleidodiethylenglycol (BM(PEG) <sub>2</sub> )	Maleimide		15 Å

A major possible shortcoming of this approach was the inaccurate concentration determination due to the low extinction coefficients of some of the reactants (Bismaleimide  $\epsilon_{302} = 1240 \text{ M}^{-1}\text{cm}^{-1}$ ,  $\beta$ -20  $\epsilon_{280} = 1480 \text{ M}^{-1}\text{cm}^{-1}$ ) which could result in an excess of either the crosslinker or the peptide and hence mono-substitution or residual monomeric peptide, respectively. To overcome this problem I used the VP-ITC as a reaction vessel which allowed for the automated addition of crosslinker in one microliter portions to 1.5 ml of peptide solution. Advantageous for optimizing critical reaction parameters is the real-time control of temperature, stirring speed, incubation time and final stoichiometry (Figure 41). Upon titration of the sulfhydryl-reactive crosslinker into the cysteine-containing peptide, stoichiometric conversion to the bivalent peptide is indicated by the complete abolishment of the heat signature at a final molar ratio of 0.5. Both, the extreme heat signature and the abrupt termination of the exothermic reaction, verify the great driving force for the reactions that both involve the rearrangement of covalent bonds (Figure 41).

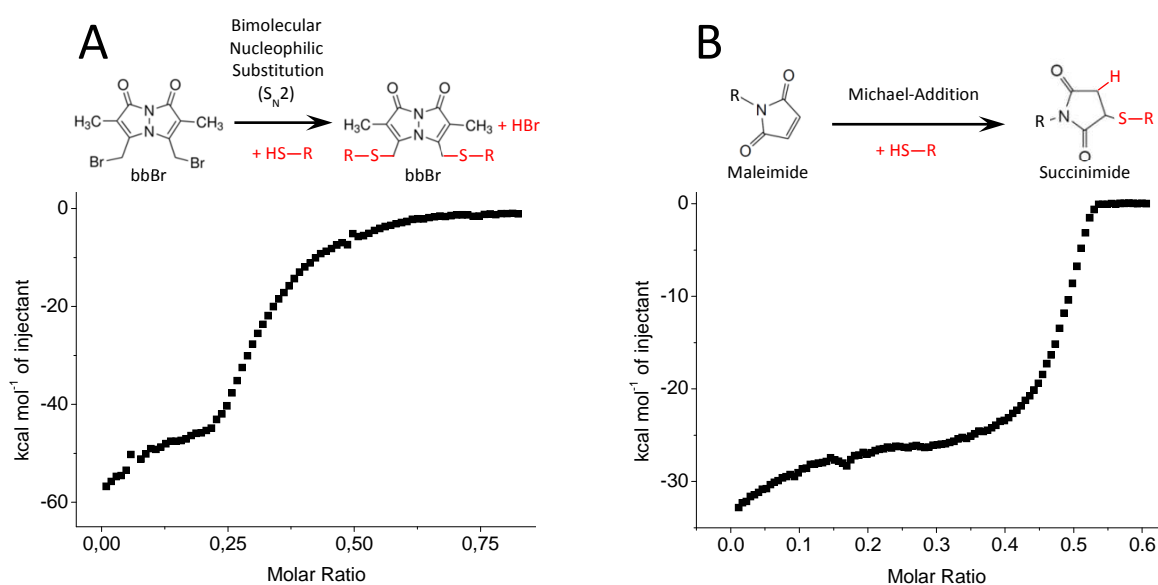


Figure 41. **The VP-ITC allows stoichiometric one-step peptide dimerization.** A, Schematic representation of the conversion of the haloalkyl molecule bbBr which acts as an electrophile towards the bimolecular substitution with thiol-containing peptides indicated as HS-R. bbBr acts as a dimerization hub and allows fluorescence detection of the derived bivalent peptide. The heat signature of the conversion indicates full conversion of all thiols upon a molar stoichiometric excess of bivalent crosslinker of 0.5, indicating that, as expected, two peptides react with one cross linker molecule. B, Schematic representation of the conversion of the maleimide groups within the crosslinkers to succinimide groups by a thiol-specific Michael addition. The heat signature of the reaction verifies a stoichiometric conversion of all monomeric peptides with the maleimides to form succinimide linked dimers. As expected, the endpoint of the conversion is found at 0.5 molar excess of the bivalent crosslinkers over the peptide. © 2012 HM Maric

After crosslinker-mediated dimerization, the solution containing the bivalent peptide was subjected to SEC to estimate reaction efficiency and to separate residual monomeric peptides that may result from partially hydrolyzed [181] bismaleimide crosslinkers (Figure 42). Molecular masses were estimated based on the elution volume of standard proteins under similar experimental conditions. Presumably the peptides exhibit no secondary structure and adopt elongated conformations resulting in systematically overestimated sizes compared to compact folded reference proteins. The lowest yield of dimerized peptides was obtained for the hexyl-linked (approx. 8%), followed by the butyl-linked (approx. 15%) and the ethane-linked maleimide crosslinkers (approx. 30%) (Figure 42A). In contrast, analytical size-exclusion confirmed nearly quantitative dimerization of the peptide in case of the diethyleneglycol-linked maleimide crosslinker (approx. 80%; Figure 42B). Interestingly, the order of the yields mirrors the overall solubility of the respective crosslinkers in water, suggesting that improving the crosslinker solubility by adding either DMSO or DMF to the reaction solution might increase the yield for the alkyl-crosslinkers to be comparable with the highly water soluble PEG-linked-crosslinker (Figure 42B). Nonetheless, analytical SEC permitted the elimination of impurities for all analyzed dimeric peptides and ruled out fragmentation or aggregation processes.

All subsequent experiments with bivalent GlyR  $\beta$  derived peptides were conducted with BMPEG<sub>2</sub>( $\beta$ -20)<sub>2</sub>, and therefore this molecule will be abbreviated with ( $\beta$ -20)<sub>2</sub> in the following paragraphs.

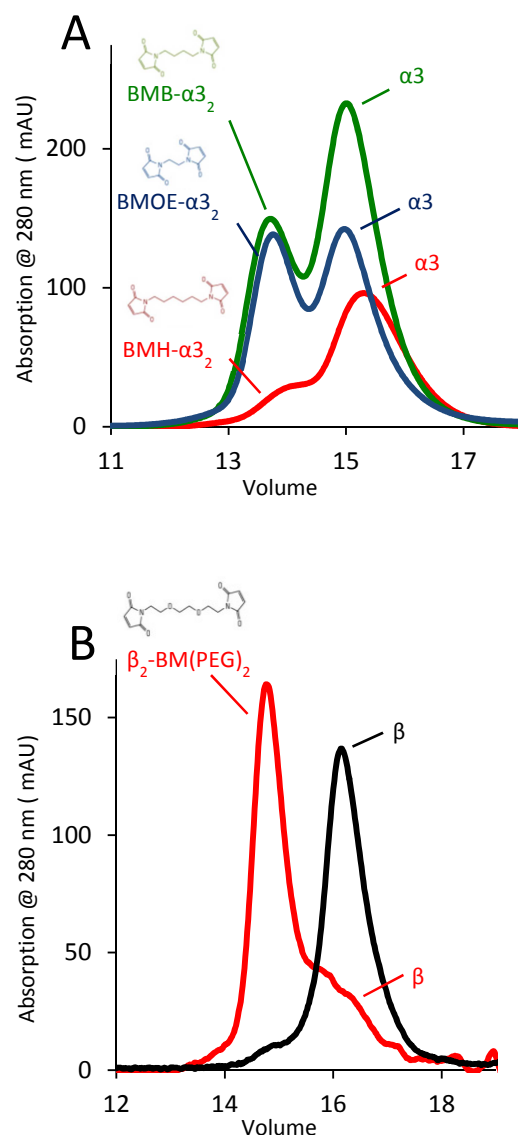


Figure 42. **Analytical SEC of different peptides dimerized with various maleimide crosslinkers.** Elution profiles of peptide-crosslinker mixtures subjected to a Sdx 75 10/300 column. A, Elution profile of the  $\alpha$ 3-20 peptide mixed with 1,6-bismaleidoethane (BMOE, blue), 1,4-bismaleidobutane (BMB, green) or 1,6-bismaleidohexane (BMH, red). Dimerized peptides elute approx. 1 ml earlier due to their doubled size. Alkyl-linked maleimide crosslinkers show a low dimerization yield. The longer the alkyl linker the lower the overall yield of dimerized peptide. B, Sdx-elution profile of the  $\beta$ -20 peptide mixed with 1,8-bismaleidodiethyleneglycol (BM(PEG)<sub>2</sub>, red). The highly water soluble PEG linked maleimide crosslinker allowed stoichiometric conversion of the  $\beta$ -20 peptide to mainly yield the corresponding dimer ( $\beta$ -20)<sub>2</sub>. © 2012 HM Maric

### 3.3.3 Bivalent Peptides Target Gephyrin's Receptor Binding Site with an Unmatched Affinity

Very recently it was demonstrated that binding of the 49 residue GlyR  $\beta$  peptide ( $\beta$ -49) stabilizes gephyrin's E but not G domain as measured by differential scanning calorimetry (DSC) [61]. To test whether binding of a bivalent ligand by trimeric full-length gephyrin results in structural rearrangements and to control for GephE specificity of the bivalent receptor peptide, I analyzed the thermal denaturation of full-length gephyrin (P2 splice variant) in the presence and absence of bivalent peptide by DSC in a similar manner (Figure 43).

In line with a GephE-specific binding, the bivalent peptide yielded a significant stabilization of the E but not the G domain of gephyrin (Figure 43). In contrast to the former study [61], which applied a 10-fold excess of  $\beta$ -49, a ratio of 1:1 was enough for BMPEG<sub>2</sub>( $\beta$ -20)<sub>2</sub>, (abbrev.:  $\beta$ <sub>2</sub>), to yield a significant stabilization of gephyrin's E domain. Specifically, DSC defines a shift from 66 to 68° C for the E domain, while the melting temperature of the G domain remained nearly unaltered at 81° C (Figure 43).

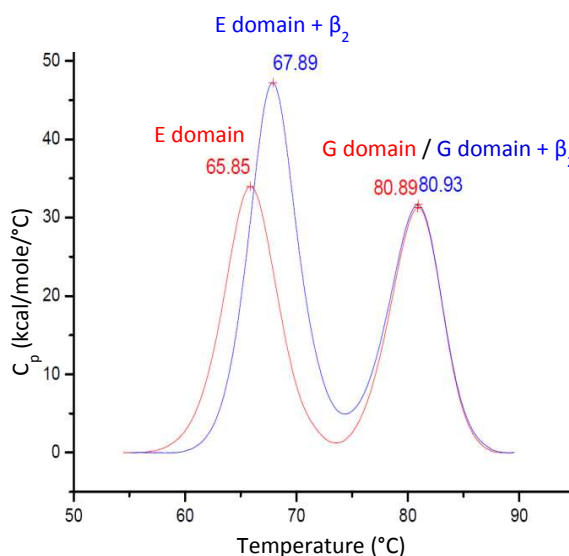
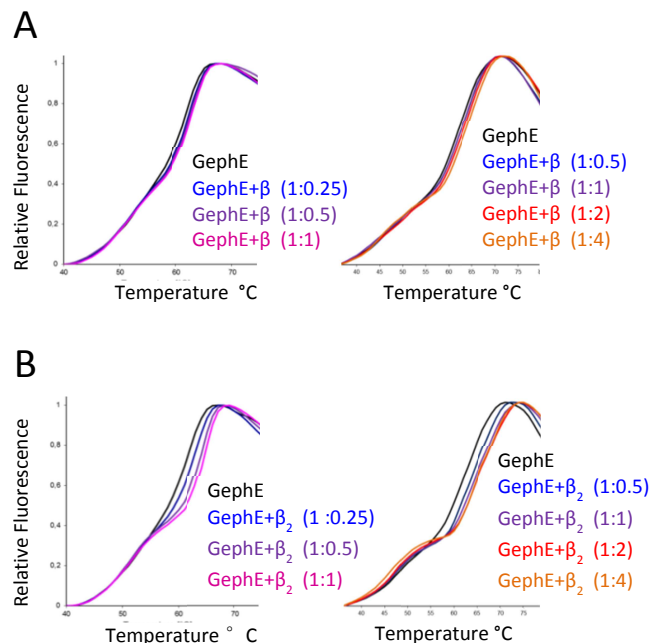


Figure 43. **DSC demonstrates that the dimeric peptides specifically target GephE.** Thermograms of full-length gephyrin in the presence and absence of  $\beta_2$  at a molar ratio of 1:1. While the G domain shows an unaltered melting temperature ( $T_m$ ) with and without the bivalent peptide, the E domain undergoes a significant shift towards a higher  $T_m$  from 66° to 68° C. © 2012 HM Maric



To further explore the stabilizing effect of mono- versus bivalent receptor fragments on GephE I used the thermofluor method, which, similar to DSC, allows to monitor thermal protein unfolding. While thermofluor results in less accurate  $T_m$  determination, it enables the analysis of several different conditions in a single experiment.

To verify a potentiated stabilization of GephE for the bivalent peptide over the monovalent peptide I compared GephE unfolding by thermofluor at different molar ratios of mono- and bivalent ligands. In particular, I used 0.25-, 0.5-, 1-, 2- and 4-fold excesses of the respective ligands over GephE (Figure 44). Thermofluor of the E domain alone confirms the  $T_m$  for the E domain in the full-length protein as determined by DSC (Figure 43), and, in line with the DSC experiments, increasing ligand concentrations raise the melting temperature of GephE. Notably, the bivalent peptide displays a more pronounced shift of the melting temperature. Even more importantly, for the bivalent peptide, the shift reaches its maximum at lower stoichiometric excess. In numbers, thermofluor revealed a 5° C shift for the bivalent peptide which was already reached at a 2-fold excess, while the monovalent peptide exhibited only a moderate 2.5° C shift even at a 4-fold molar excess. Taken together the thermofluor results confirmed the DSC measurements and additionally indicate a stronger affinity for the bivalent over the monovalent peptide to GephE.



**Figure 44. Thermofluor uncovers a potentiated affinity of GephE for the bivalent peptide.** Thermofluor visualizes the thermal unfolding of GephE in the presence of monovalent ( $\beta$ ) and bivalent ( $\beta_2$ ) peptides. Varying ratios of (A) monovalent and (B) bivalent ligands to GephE demonstrate a potentiated stability for the multivalent complex over the GephE complex with the monomeric ligand. In case of the bivalent peptide, not only is the overall shift more distinct, but the shift reaches its maximum of approximately 5° C already at a molar ratio of 1:2. © 2012 HM Maric

Encouraged by the thermofluor results I next performed ITC. As discussed earlier we designed the linker to exactly match the binding site distance in the E domain dimer and hence expected the resulting bivalent peptide to exhibit an avidity-based potentiation of the binding strength. Using ITC, I titrated GephE with the mono- and bivalent peptides under comparable conditions (Figure 45). Remarkably, the sharp transition of the heat signature verifies that dimerization resulted in an at least 10-fold increased E domain affinity. In line with the idea that both binding sites can be occupied by a single bivalent peptide at once, the increase in binding strength is accompanied by an enhanced enthalpic contribution and a reduced stoichiometry (Table 39).

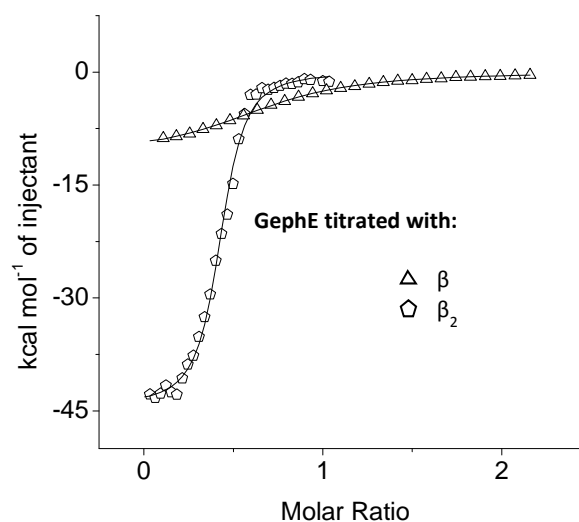


Figure 45. ITC based analysis of multivalent receptor binding to gephyrin. Measured binding enthalpies are plotted as a function of the molar ratio of ligand to gephyrin. Comparison of GephE binding to monovalent ( $\beta$ ) and bivalent ( $\beta_2$ ) peptides. The isothermal binding curves display a 10-fold potentiation of affinity, accompanied by a sharp increase in the molar enthalpy contribution and a reduction of the stoichiometry by two. © 2012 HM Maric

Table 39. Gephyrin E domain binding parameters determined by ITC.

Titant	Gephyrin Stoichiometry [N]	Affinity [ $\mu$ M]	Enthalpy [kcal/mol]
$\beta$ -20	0.70 $\pm$ 0.01	2.83 $\pm$ 0.15	-10.8 $\pm$ 0.2
( $\beta$ -20) <sub>2</sub>	0.40 $\pm$ 0.01	0.29 $\pm$ 0.03	-44.4 $\pm$ 0.5

To test whether the elongated peptide relies on additional binding contributions not covered by the shorter bivalent peptide I performed ITC competition assays (Figure 46). Specifically, I pre-equilibrated gephyrin with the bivalent 20 residue peptide ( $\beta$ -20)<sub>2</sub> at a molar ratio of 1:1 and subsequently used the resulting complex for a titration with the elongated 49 residue peptide. In case of the small bidentate and the elongated monodentate peptides both relying on identical interactions with GephE, they might, depending on the ratio, eventually exchange on the surface of GephE, but since the characteristics of the broken and newly formed interactions would remain similar there would be no measurable heat signature in ITC. Strikingly, the bidentate peptide indeed completely prevents any trace of GephE interaction with the elongated monovalent fragment (Figure 46), thus ruling out that the larger peptide occupies a second binding site on gephyrin. This finding is in line with my structural analyses discussed earlier, which proposed structural rearrangement instead of additional binding sites to result in an apparently enhanced and biphasic binding in ITC.

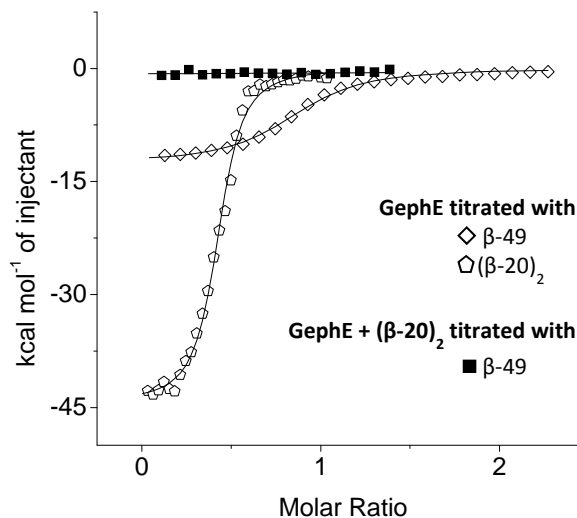


Figure 46. **ITC competition assay between mono- and bivalent gephyrin ligands.** Shown are the binding isotherms of three independent titrations: (i) GephE interacting with the 20 residues bivalent fragment ( $\beta$ -20)<sub>2</sub>, (ii) GephE with an elongated monovalent fragment ( $\beta$ -49), and (iii) a competition experiment between both. The lack of any thermal signature rules out any additional binding contributions in case of the elongated peptide. Hence, the bivalent peptide is sufficient to occupy the entire gephyrin-binding site and thus fully inhibits GephE receptor binding activity. © 2012 HM Maric

Furthermore, we conclude that the bivalent peptide displays the highest possible affinity among all identified fragments that target gephyrin. Due to its short linker it might compete out the naturally occurring receptors in a similar manner and therefore could act as a specific inhibitor on gephyrin's receptor binding activity *in vivo*. Because of its high potency and selectivity we suggest a potential role of this compound as a tool to study synapse formation in neuronal cell culture.

## 3.3.4 Analysis of a Low Affinity Gephyrin Ligand after Dimerization

Based on the results obtained with dimerized peptides derived from the GlyR  $\beta$ -subunit we hypothesized that introduction of similar linkers to other, lower affinity, gephyrin binding receptor subunits might enable their characterization via ITC and X-ray crystallography by potentiating their interaction strength. To test this, we applied the same approach to the minimum motif of GABA<sub>A</sub>R  $\alpha$ 3 which shows no heat signature in ITC when titrated as a monomeric peptide to GephE. Accordingly, I designed a GABA<sub>A</sub>R  $\alpha$ 3 minimum peptide which encompasses residues 364-378, corresponding to the GlyR  $\beta$  fragment. To enable cysteine-mediated dimerization I introduced a cysteine instead of a serine at the very C terminus of the GABA<sub>A</sub>R derived peptides (Table 40, marked in blue). Using linkers of different length, I analyzed their binding via ITC under comparable conditions. As expected, the binding strength was strikingly potentiated, thus allowing analysis of the affinity via ITC which was not possible for the monovalent peptide (Figure 47 and Table 40). As a consequence of dimerization dissociation constants in the low micromolar range could be observed. Specifically, introduction of the 6 Å bbBr linker yielded a potentiation towards  $170 \pm 50 \mu\text{M}$ , while the 18 Å linker BMPEG<sub>2</sub> resulted in an affinity of  $12 \pm 1 \mu\text{M}$ . Interestingly the intermediate length (10 Å) linker BMOE allowed for the highest affinity ( $4 \pm 1 \mu\text{M}$ ). In summary, it can therefore be concluded that the bbBR linker is already too short, while the BM(PEG)<sub>2</sub> linker allows for too much flexibility. As expected, the bivalent minimum peptides (Table 40, III) mirror the relative binding strengths of their monovalent counterparts (Table 40, II) as well as their full-length monovalent counterparts (Table 40, I).

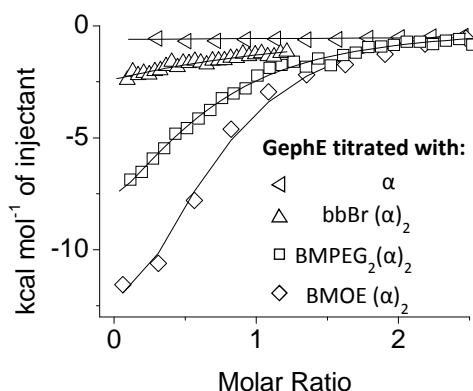


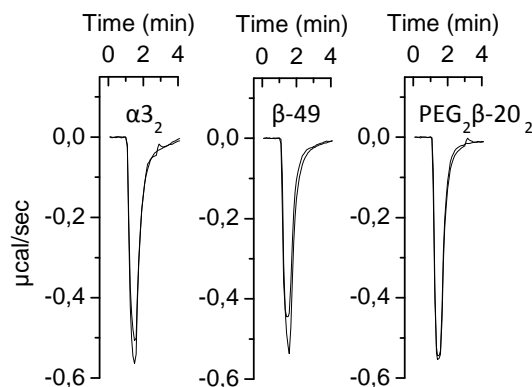
Figure 47. ITC reveals an affinity potentiation for a GABA<sub>A</sub>R derived peptide upon dimerization. ITC based analysis of multivalent receptor binding to gephyrin. Measured binding enthalpies are plotted as a function of the molar ratio of ligand to gephyrin. Comparison of GephE binding to bivalent peptides differing in their linker length. While the monovalent peptide shows no isothermal binding curve (data not shown), dimerization enhances the affinity into the low micromolar range, accompanied by a sharp increase in the molar enthalpy contribution. In particular, the intermediate linker (BMOE) displays an optimized affinity compared to the shorter (bbBr) and longer linker variants (BMPEG<sub>2</sub>). © 2012 HM Maric

Table 40. GephE affinities of receptor derived peptides determined by ITC. (I) Monomeric, full-length GABA<sub>A</sub>R intracellular loops and the elongated GlyR peptide. (II) Monomeric minimum peptides. (III) Bivalent minimum peptides.

Receptor Subtype	Sequence	K <sub>d</sub> [μM]
I β-49	-VGETRCKKVC <sup>T</sup> SKSDLRSNDF <sup>S</sup> IVGSLPRDF <sup>F</sup> ELSNYDCY <sup>G</sup> KPIEVN <sup>N</sup> GL-	0.1±0.1/8±0.1
α1-87	...SVVPEKPKKVKDPLIKKNNTYAPTATSYPN <sup>L</sup> ARGDPGLATI <sup>A</sup> KSATIEP...	17±11
α2-84	...KSVVNDK <sup>K</sup> KEKGSVMIQNNAYAVAVANYAPNLSKDPVLS <sup>T</sup> ISK <sup>S</sup> ATTEP...	n.d.
α3-97	...EAL <sup>E</sup> EMKKKTPAAPT <sup>K</sup> KTST <sup>T</sup> FNIVG <sup>T</sup> TY <sup>P</sup> INLAKDTE <sup>F</sup> STISKAAA <sup>A</sup> PSA...	5±2
II β-20	-----DFSI <sup>V</sup> GSLPRDF <sup>F</sup> ELSNYDCY-----	2.8±0.2
α1-20	-----TYAPTATSYPN <sup>L</sup> ARGDPGL-----	n.d.
α2-20	-----AYAVAVANYAPNLSKDPVLS-----	n.d.
α3-20	-----TFNIVG <sup>T</sup> TY <sup>P</sup> INLAKDTE <sup>F</sup> S-----	n.d.
III BMPEG <sub>2</sub> (β-20) <sub>2</sub>	-----DFSI <sup>V</sup> GSLPRDF <sup>F</sup> ELSNYDCY-----	0.3±0.1
BMPEG <sub>2</sub> (α3-20) <sub>2</sub>	-----TFNIVG <sup>T</sup> TY <sup>P</sup> INLAKDTE <sup>F</sup> C-----	12±1
BMOE(α3-20) <sub>2</sub>	-----TFNIVG <sup>T</sup> TY <sup>P</sup> INLAKDTE <sup>F</sup> C-----	4±1
bbBr(α3-20) <sub>2</sub>	-----TFNIVG <sup>T</sup> TY <sup>P</sup> INLAKDTE <sup>F</sup> C-----	170±50

The ITC experiments presented and cited here involved the titration of gephyrin with different ligands. Comparison of the released enthalpy per gephyrin binding site is therefore not straightforward for the following reasons. First of all, low affinity ligands such as GABA<sub>A</sub>R  $\alpha$ 3 are characterized by so-called “low *c*” titration spectra which yield poorly defined enthalpy values because of a low binding site saturation. Second, the resulting enthalpy values are related to the molar concentration of the ligands, not the involved number of binding sites offered by the macromolecule. Third, depending on concentration accuracy, purity and activity of the ligands, the determined enthalpies can vary systematically among different variants.

To overcome these shortcomings I performed the single injection method (SIM) with the ligands at an eight-fold molar excess over GephE. This allowed me to monitor the maximal possible heat release upon saturation of all gephyrin binding sites, independent of ligand concentration, activity, purity, number of binding sites and even affinity, under the assumption that all gephyrin binding sites are saturated at an 8-fold ligand excess. As expected the comparative single injection titration total enthalpy (cSITE) experiments reveal roughly identical enthalpic contribution for all analyzed ligands (Figure 48). In line with earlier studies [182-184], and discussed detailed in the conclusion, this suggests that the observed difference in affinity, for monomeric *versus* bidentate gephyrin ligands, is solely based on entropy effects resulting from avidity. Therefore, it can be concluded that the GABA<sub>A</sub>R and GlyR derived peptides occupy a common binding site on GephE resulting in comparable van der Waals interactions and H-bridges which are monitored as heat signatures in ITC.



**Figure 48. CSITE reveals similar enthalpic contributions of different GephE ligands.** Comparative single injection titrations of different gephyrin ligands to estimate the absolute binding enthalpy. Overlay of at least two independent experiments for each ligand. Single injection of an 8-fold molar excess of either the GABA<sub>A</sub>R  $\alpha$ 3 derived bivalent peptide (( $\alpha$ 3)<sub>2</sub>), the elongated monovalent GlyR  $\beta$  loop ( $\beta$ -49) and the bivalent GlyR  $\beta$  derived minimum peptide (( $\beta$ -20)<sub>2</sub>) to GephE. Strikingly, the total heat release measured in  $\mu$ cal/sec is nearly identical despite an over 100-fold difference in affinity. © 2012 HM Maric

Encouraged by the ITC assays we asked whether the bivalent peptide now fully covers the receptor-binding site on gephyrin. To address this question and to rule out favorable artificial contributions of the linker I crystallized GephE with the bidentate GlyR  $\beta$  derived peptide (BM(PEG)<sub>2</sub>( $\beta$ -20)<sub>2</sub>). The resulting preliminary 2.9 Å resolution structure verified that the binding site was occupied in the same way (data not shown) as in the monovalent elongated peptide complex described earlier, including formation of the short C-terminal helix. Intriguingly, no electron density could be assigned to the linker, thus indicating a high flexibility of this region despite the otherwise tight binding. In line with my ITC results, which already suggested an optimized  $\alpha$ 3 affinity for the BMOE-linker (10 Å) over the BMPEG<sub>2</sub> (18 Å) and bbBR (8 Å) linkers, it can therefore be inferred that a shorter or less flexible linker has the potential to amplify the  $\beta$  affinity even further by increasing the effective concentration of the interacting parts of the bivalent peptide [183, 185].

### 3.3.5 Bivalent Peptides Reveal Different Modes of Gephyrin's Domain Architecture

Prompted by the increased affinity of the E domain dimer for the bidentate peptides we asked whether full-length gephyrin would show a similar effect. Earlier analyses proposed the complete protein to form a trimer in solution [55, 152], and NAGE analysis additionally proposed higher oligomers such as hexamers [60]. Trimerization was proposed to occur via the G domain at the expense of the E domain dimer interface and, following this idea, titration with a dimerized peptide should not yield a potentiated affinity, unless there is flexibility in the trimeric arrangement allowing at least two E domains to approach each other sufficiently close to allow the bivalent peptide to occupy two binding sites at once.

Strikingly, ITC measurements revealed that full-length gephyrin (FL-Geph) binds to bivalent peptides with a potentiated affinity and additionally reveals distinct features of the multimeric full-length protein receptor peptide complex when compared to the corresponding E domain complex (Figure 49). While FL-Geph and GephE show identical binding parameters for monomeric  $\beta$ -peptides [55], the bivalent peptide, evaluated here, displays a different behavior. Similar to the E domain alone, FL-Geph displays a sharp increase in the enthalpy contribution and affinity for the bivalent over the monovalent peptide (Table 41). Interestingly, the bivalent peptide affinity of FL-Geph is approximately 2-fold lower than GephE, even more importantly, the resulting stoichiometry is significantly larger, indicating that more than one bivalent peptide binds to one gephyrin trimer molecule simultaneously (Table 41).

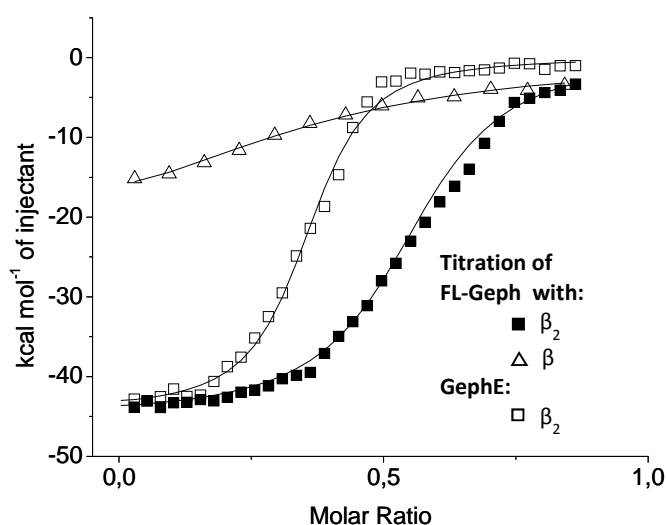


Figure 49. **ITC-based comparison of FL-Geph and GephE binding to bivalent peptides.** Shown are the binding isotherms of three independent titrations: (i) GephE interacting with the 20 residue bivalent fragment ( $\beta_2$ ) described here, (ii) full-length gephyrin titrated with the same bivalent fragment, and (iii) full-length gephyrin titrated with the corresponding monovalent fragment. Full-length gephyrin displays an increased enthalpic contribution and a potentiated affinity when binding the bivalent compared to the monovalent peptide. Notably, the significantly shifted saturation point proposes that a fraction of the bivalent peptides occupies only a single binding site, possibly due to the architecture of the full-length protein. © 2012 HM Maric

Table 41. **Comparison of  $\beta$ -20 and  $(\beta$ -20)<sub>2</sub> binding parameters of GephE and FL-Geph.**

Titratant	GephE [N]	FL-Geph [N]	GephE- $\Delta$ H [kcal/mol]	FL-Geph- $\Delta$ H [kcal/mol]	GephE- $K_d$ [ $\mu$ M]	FL-Geph- $K_d$ [ $\mu$ M]
$\beta$ -20	0.70 $\pm$ 0.01	0.73 $\pm$ 0.01	-11 $\pm$ 1	-11 $\pm$ 1	3 $\pm$ 0.2	3 $\pm$ 0.3
$(\beta$ -20) <sub>2</sub>	0.40 $\pm$ 0.01	0.57 $\pm$ 0.01	-45 $\pm$ 1	-45 $\pm$ 1	0.29 $\pm$ 0.03	0.50 $\pm$ 0.03

One possible scenario would be, that FL-Geph forms a trimer on the basis of the G domain trimerization, but allows two E domains to approach each other close enough to offer a receptor binding interface similar to what we resolved in our X-ray studies of the E domain alone. Following this idea, one third of the offered receptor binding sites would be monovalent, and two thirds would be bivalent. This hypothesis would offer a possible explanation for (i) the reduced stoichiometry and enhanced affinity of FL-Geph for bivalent peptides, which is mediated by the fraction of bivalent receptor binding sites. And additionally it could explain (ii) the increased stoichiometry and lowered affinity of FL-Geph for the bivalent peptides when compared to GephE, mediated by fraction of monovalent peptide binding sites. To understand the different binding behavior of GephE and FL-Geph to bivalent peptides but not monovalent peptides I next examined the possibility of structural rearrangements or a modulation of oligomeric state within FL-Geph upon binding of bivalent peptides. Therefore, I analyzed the resulting multivalent complex via analytical SEC and NAGE (Figure 50).

The size-exclusion method resolves three major gephyrin fractions: (i) A fraction corresponding to oligomers larger than hexamers, (ii) a fraction of roughly the size of a possible hexameric gephyrin, and (iii) the largest fraction corresponding to trimeric gephyrin (Figure 50A). As expected, pre-incubation of gephyrin with the bivalent peptide significantly alters the elution profile despite an only minor overall change in the actual molecular weight (gephyrin monomer: 93 kDa,  $\beta_2$ : 4 kDa). Interestingly, the equilibrium of gephyrin is shifted towards the trimeric gephyrin fraction (Figure 50A). In agreement with the analytical SEC experiments, the multivalent complex also shows a different behavior in NAGE assays (Figure 50B). Only when full-length gephyrin is applied together with the bidentate peptide, an additional band appears which is migrating faster towards the anode. Under the assumption that there is no free gephyrin present this would indicate an altered migration behavior of the gephyrin- $\beta_2$ -complex which could either

be based on an altered charge or architecture. Together, these experiments verify a severe impact of the bidentate peptide on the properties of gephyrin. Especially the SEC experiments propose that either the oligomeric state or the domain arrangement of full-length gephyrin can be modulated by the addition of multivalent high-affinity peptides. Future analysis with more sophisticated biophysical techniques such as atomic force microscopy (AFM), analytical ultracentrifugation (AUC) and small-angle X-ray scattering (SAXS), which have been considered to be beyond the scope of this work, may help to decipher the role of gephyrin's architecture in the multivalent process of receptor clustering.

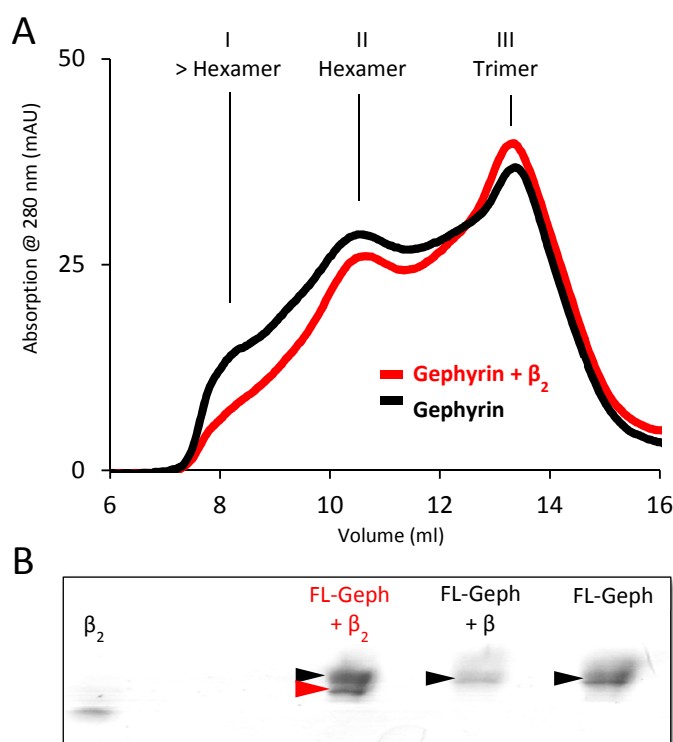


Figure 50. **Bivalent peptides alter gephyrin's hydrodynamic radius.** A, Analytical SEC of gephyrin either alone or in complex with bivalent peptide ( $\beta_2$ ). Despite a slightly increased molecular size of the gephyrin- $\beta_2$  complex, the elution profile displays a shift towards smaller oligomeric states. B, NAGE of either gephyrin alone, in complex with monovalent peptide ( $\beta$ ) or in complex with a bivalent peptide ( $\beta_2$ ). Only in the presence of the bivalent peptide an additional band, which migrates faster towards the anode, is observable. © 2012 HM Maric

### 3.4 Characterization of the Collybistin SH3 GABA<sub>A</sub>R Complex

Collybistin (CB) has been consistently implicated in gephyrin-mediated GABA<sub>A</sub>R clustering and a recent yeast-two-hybrid (Y2H) study found that GABA<sub>A</sub>Rs not only interact with gephyrin but also with the SH3 domain of CB [84], and that this interaction acts synergistically to the GABA<sub>A</sub>R-gephyrin interaction. To decipher the role of CB's SH3 domain in GABA<sub>A</sub>R clustering, on the molecular level, I purified this domain using a construct kindly provided by Dr. Tolga Soykan from the lab of Nils Brose (MPI, Göttingen) and analyzed its suggested GABA<sub>A</sub>R and gephyrin interactions via various biochemical and biophysical methods. Specifically, I present:

- The purification of CB's SH3 domain and the identification of its direct divalent cation binding, which induces major structural rearrangements within this protein.
- The characterization and quantification of the SH3-GABA<sub>A</sub>R  $\alpha 1$ ,  $\alpha 2$  and  $\alpha 3$  binding affinities which suggest a reciprocal receptor subunit preference compared to gephyrin.
- The verification of an overlapping gephyrin and CB receptor binding site and the exclusion of synergistic binding.

#### 3.4.1 Purification of Collybistin's SH3 Domain

The DNA construct provided by T. Soykan corresponds to residues 4-72 of murine CB 1 (CB1) and hence encompasses the complete SH3 domain (residues 8-67) of this protein which is identical to the SH3 domain (residues 8-67) of hPEM-2, the only known human CB isoform.

The protein was expressed in *E. coli* using the pGEX-4T-2 Vector and purified via an N terminal GST-tag. The high expression level and solubility allowed high yields and purity. After *in situ* thrombin cleavage the GST-SH3 mixture was separated via SEC and analyzed by SDS-PAGE. Two separate peaks could be resolved, one containing both the cleaved and un-cleaved GST and GST-SH3, respectively, and the other containing pure SH3 domain (Figure 51).

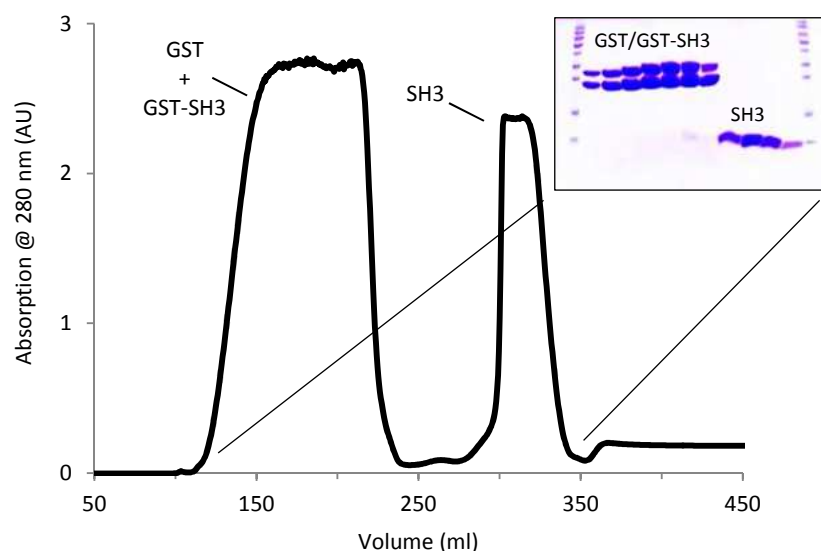


Figure 51. **SEC and SDS-PAGE confirm the homogeneity of CB SH3 (4-72).** Representative elution profile of the CB SH3 domain after affinity chromatography and *in situ* thrombin cleavage. © 2012 HM Maric



### 3.4.2 Divalent Cations Induce Structural Rearrangements within the SH3 Domain

In this section I present the characterization of the SH3 domain (residues 4-72) with respect to its cation-dependent change in hydrodynamic radius.

After purification of the SH3 domain, I aimed to determine its apparent molecular weight via analytical SEC. Remarkably, CB SH3 displays an elution profile that is strongly dependent on divalent cations. Addition of CaCl<sub>2</sub> shifts the elution profile towards higher molecular weights (Figure 52, blue curve). In contrast, addition of the chelating agent EDTA, which complexes bivalent cations, *vice versa* shifts the elution volume towards smaller molecular weights (Figure 52, black curve). Interestingly, addition of ZnCl<sub>2</sub> yielded a non-uniform elution profile, indicating the presence of two SH3 species differing in their respective hydrodynamic radii (Figure 52, red curve). Comparison with reference proteins suggests that the SH3 domain adopts a compact fold and that its elution profile is strongly dependent on additives, promoting either major structural rearrangements or inducing dimerization of CB's SH3 domain. Accordingly, the calculated molecular weights range between 5 and 10 kDa (Table 42).

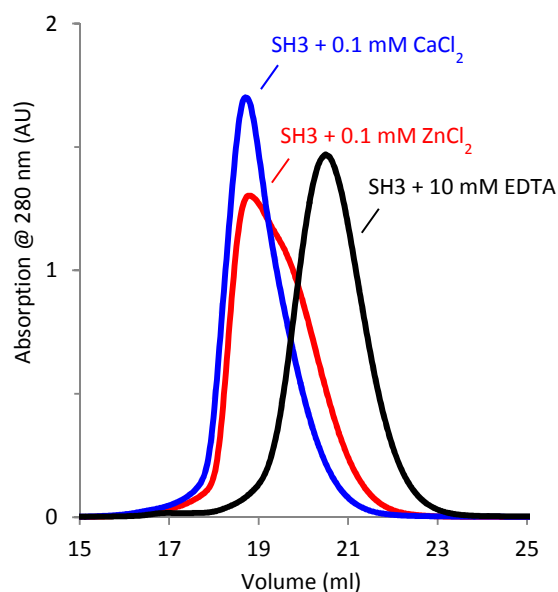


Figure 52. **Analytical SEC of CB SH3 in the presence of bivalent cations or a chelator.** Representative elution profile of CB SH3 in different buffers containing either CaCl<sub>2</sub> (blue), ZnCl<sub>2</sub> (red) or EDTA (black). © 2012 HM Maric

Table 42. **Molecular weights of CB SH3 in SEC in the presence of different additives.**

Additive	Elution Volume Sdx 75 10/300 (ml)	M <sub>w</sub> calculated (kDa)
CaCl <sub>2</sub> (0.1 mM)	19	10
ZnCl <sub>2</sub> (0.1 mM)	19.5	8
EDTA (10 mM)	20.5	5

Encouraged by the analytical SEC experiments that verified a major dependence of CB's SH3 domain hydrodynamic volume on divalent cations, I further investigated the role of these ions. Earlier X-ray crystallographic analysis revealed homologous SH3 domains to form dimers [185-190]. Namely, the C-terminal SH3 domain of the adaptor protein GADS [190] and the Src-type tyrosine kinase (Lck) SH3 domain [189] display a Zinc-induced homo-dimerization as well as additional cation binding sites. To test the possibility of an analogous direct and stoichiometric interaction of specific bivalent cations with CB's SH3 we used ITC as described in the following paragraph.

To eliminate cation contaminations resulting from the expression in *E. coli* and the purification process, the SH3-containing solution was subjected overnight to a 100-fold molar excess of Chelex-100, a water insoluble and recyclable chelating resin. Using EDTA the absence of bivalent cations could be verified in ITC. In contrast to the reference buffer, the chelex-treated buffer showed no heat release upon titration with EDTA (Figure 53 A).

The resulting cation-free SH3 domain was titrated with calcium-, magnesium- and zinc-chloride in ITC experiments. As expected, at least for zinc (Figure 53 B) and magnesium (Figure 53 C) a direct interaction could be verified. Similar to homologous SH3 domains, CB's SH3 domain displays a preference for Zn<sup>2+</sup> ( $K_d = 600 \mu\text{M}$ ) over Ca<sup>2+</sup> ( $K_d = 3 \text{ mM}$ ) (Table 43).

Table 43. Binding parameters of the cation-SH3 interactions determined in ITC.

Cation	$\Delta H$ (kcal/mol)	$-\Delta TS$ (kcal/mol°C)	$K_d$ (mM)
Ca <sup>2+</sup>	n.d.	n.d.	n.d.
Mg <sup>2+</sup>	3 ± 1	-6	3.3 ± 0.8
Zn <sup>2+</sup>	31 ± 1	-35	0.6 ± 0.1

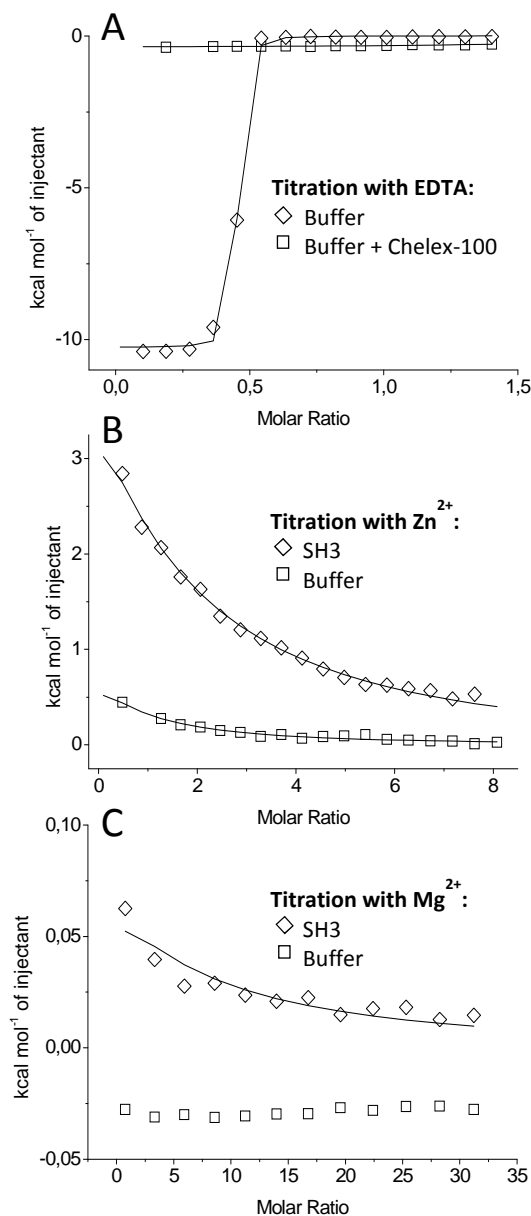


Figure 53. The SH3 domain directly interacts with Zn<sup>2+</sup> and Mg<sup>2+</sup> ions. A, EDTA control titration. The conventional buffer yields a significant heat release upon EDTA titration, indicating a significant amount of free bivalent cationic contaminants. Buffer prepared with Chelex-100 shows no trace of heat release, thus verifying removal of all cations. B, Titration of the SH3 domain with ZnCl<sub>2</sub> reveals an entropy-driven binding interaction. C, Titration with MgCl<sub>2</sub> suggests a very weak direct binding between the cation and the protein. © 2012 HM Maric

Prompted by the ITC results I compared the SH3 domain of CB with homologous SH3 domains which form Zn-induced homodimers. Namely, GADS SH3 and Lck SH3 were characterized earlier via X-ray crystallography and four distinct cation binding sites were identified (Figure 54 A). In particular, zinc, calcium and cadmium could be resolved, critically mediating SH3 dimerization (Figure 54A, marked in yellow) or mediating structural rearrangements (Figure 54 A, marked in red and cyan). Superposition of both structures with CB's SH3 domain structure derived by NMR revealed that the overlapping cation binding sites are moderately conserved among the SH3 domains of Lck, GADS and CB. Based on the superposition (Figure 54, residues engaging in specific cation interactions with their side-chains are marked in cyan, yellow or red) we decided to exchange two residues possibly mediating CB SH3 cation binding, namely CB Asp 33 and Asp 51 with their respective amide homologs (Asn) (Figure 54B, yellow underlined residues). With the moderate Asp/Asn exchange we aimed to impair analogous cation interactions of CB's SH3 domain in a pH-dependent manner without altering the secondary structure.

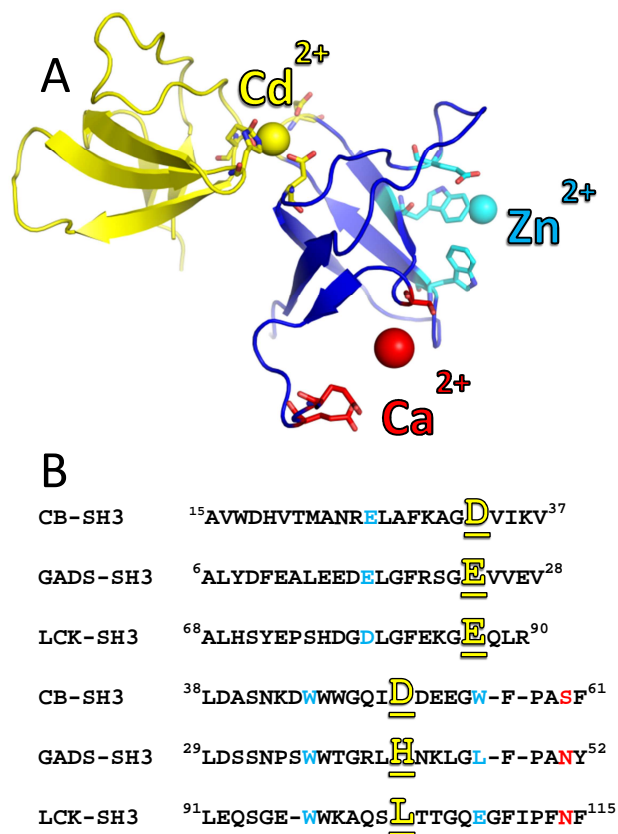


Figure 54. **Structural basis of SH3 bivalent cation binding.** A, Superposition of the crystal structures of GADS-SH3 (PDB-ID: 1OEB) and LCK-SH3 (PDB-ID: 2IIM) and CB SH3 (PDB-ID: 2YSQ). Possible cation interfaces are highlighted in the cartoon representation of CB SH3 (blue) as stick models. GADS exhibits a cadmium and zinc binding site (yellow) that mediates SH3 dimerization. LCK SH3 directly engages in interactions with calcium (red) and zinc (cyan). B, Alignment of the SH3 domains of CB, GADS and LCK. In this work the cadmium and zinc binding aspartate residues were mutated to asparagine (yellow and underlined). © 2012 HM Maric

To elucidate the role of Asp 33 and Asp 51 in the cation-dependent structural rearrangements, we determined the elution profile of the respective D33N/D55N double mutant (DM) in analytical SEC and compared it with the wildtype (WT) in the presence and absence of chelating agents.

Strikingly, the DM displays a significantly reduced hydrodynamic radius resulting in an increased elution volume under all tested conditions (Figure 55). As expected, the WT and the DM protein both show a correlated effect of the chelating agents suggesting that the introduced carboxyl to amide mutations have a moderate effect on cation binding. This finding is in line with the idea that either Asp 33 or 51 or both are directly involved in cation-mediated intra- and/or inter-molecular rearrangement/s. Given that EDTA has a higher preference for magnesium over calcium as compared to EGTA, the pronounced effect of EDTA suggests, in line with ITC results, a major role of magnesium in this process.

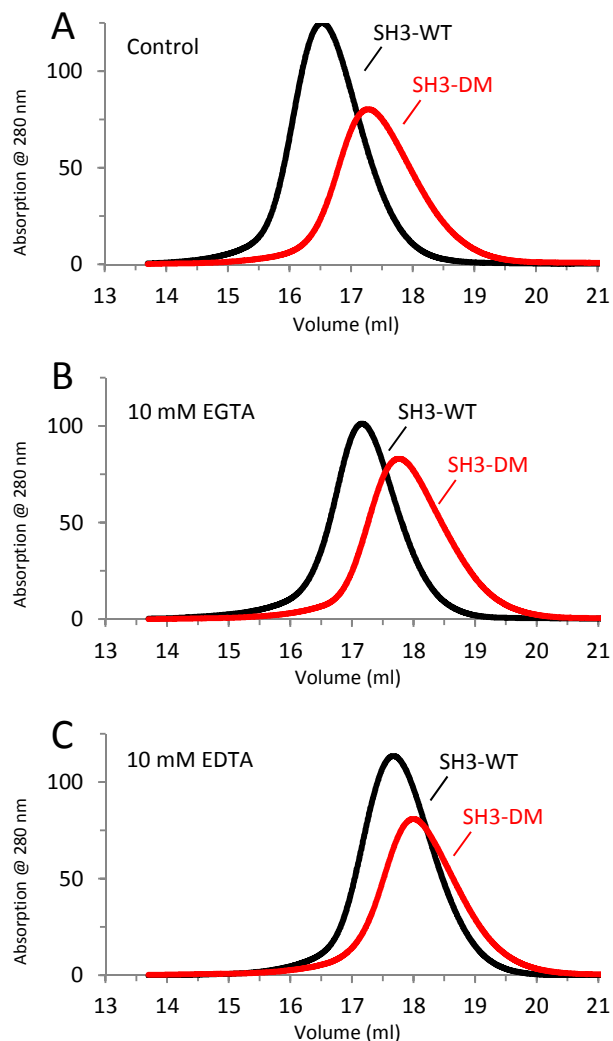


Figure 55. **SEC analysis of cation-SH3 domain interactions.** Superposition of six independent analytical SEC experiments of CB's wildtype SH3 domain (SH3-WT) or the double mutant D33N/D51N (SH3-DM) in (A) SEC-buffer, (B) SEC-buffer with 10 mM EGTA and (C) SEC-buffer with 10 mM EDTA. SH3-DM shows a higher elution volume under all conditions, and additionally displays a correlated effect on the elution profile. © 2012 HM Maric

To decipher whether the altered elution profiles, induced by the presence or absence of bivalent cations, represent a dimer to monomer transition or a conformational change I conducted analytical ultracentrifugation (AUC) experiments of CB's SH3 domain and its double mutant in the presence and absence of CaCl<sub>2</sub> and EDTA. I applied the method of sedimentation velocity, which allows the examination of the hydrodynamic shape (frictional ratio) of proteins as well as an estimation of their oligomeric state by calculation of their apparent molecular weights.

As expected, AUC revealed a difference in the sedimentation behavior of SH3 in dependence of both the bivalent cation-chelating agent EDTA and the introduced mutations. Additionally, in line with the analytical SEC, EDTA mimics the effect of the introduced mutations for all determined parameters. AUC defined a minor difference in the mean sedimentation coefficient for each measured sample. Accordingly, the molecular weights were defined to 8.6 kDa for the WT protein, while the DM protein and the EDTA treated WT protein had a mean molecular weight of 9.7 kDa and 9.8 kDa, respectively (Table 44). The same trend was mirrored by the determined frictional ratios, which visualized a pronounced asymmetrical shape in case of both the EDTA-treated WT and the double-mutated protein (Table 44). Finally, the strongest effect is displayed by the sedimentation coefficient distribution. In contrast to the wildtype protein, the EDTA-treated sample and, in particular, the double mutant protein, shows a very mono-disperse distribution of sedimentation coefficients (Figure 56).

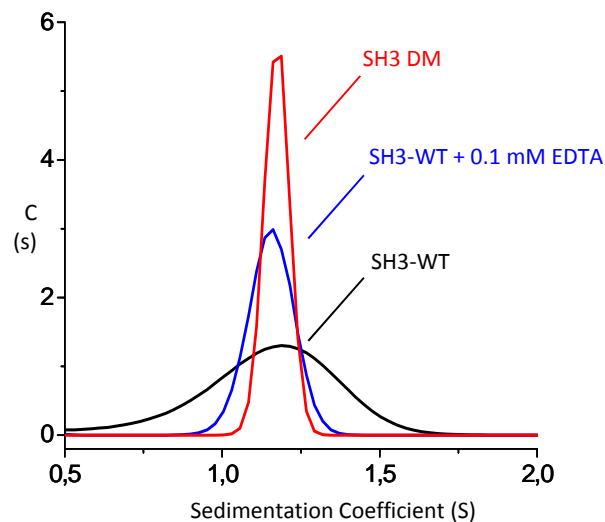


Figure 56. **AUC reveals structural rearrangements within the SH3 domain.** Velocity sedimentation experiment of the SH3 domain in the presence and absence of CaCl<sub>2</sub> or in the presence of EDTA. Note the differences in the distributions of the sedimentation coefficients. © 2012 HM Maric

Table 44. **AUC reveals bivalent cation-dependent rearrangements within the SH3 domain.**

Analyte	rmsd	Molecular weight	Frictional Ratio
SH3-WT	0.007	8.6	1.25
SH3-WT+EDTA	0.006	9.7	1.37
SH3-DM	0.007	9.8	1.36

Based on the analytical SEC and especially the AUC experiments we propose that the SH3 domain does not change its oligomeric state but instead undergoes a conformational change upon directly engaging in interactions with bivalent cations. In detail, AUC describes the double mutant as mono-disperse and elongated, while the wildtype protein is described as more poly-disperse, symmetric and slightly more compact. The role of the cation-binding site and the induced intra-molecular rearrangement remains to be elucidated *in vivo*. Additionally, future *in vitro* studies of the CB SH3 domain-mediated self-masking and the SH3 domain-mediated GABA<sub>A</sub>R  $\alpha$ 2 binding, described in the next section, may provide an appropriate context for further investigations of cation-induced effects. Finally, future crystallization attempts may be facilitated by the mono-dispersity introduced by the described mutations and EDTA, or vice versa by saturation of the cation-binding sites of CB's SH3 domain.

### 3.4.3 Characterization of the Subunit Specific GABA<sub>A</sub>R-SH3 Domain Interaction

Next, I wanted to analyse the GABA<sub>A</sub>R-SH3 domain complex, recently proposed on the basis of Y2H-assays [84].

Therefore, I tested mixtures of CB's SH3 domain and the intracellular loops of GABA<sub>A</sub>R  $\alpha$ 1,  $\alpha$ 2 and  $\alpha$ 3 in NAGE experiments. This technique allows the identification of low affinity interactions. Strikingly, the gel shift assays demonstrate that the GABA<sub>A</sub>R  $\alpha$ 1 and  $\alpha$ 2 loop but not the  $\alpha$ 3 loop readily form a complex with the SH3 domain of CB. While the SH3-GABA<sub>A</sub>R  $\alpha$ 1/2 loop complexes are retained in the pocket, the GABA<sub>A</sub>R  $\alpha$ 3 subunit allows SH3 to enter the gel and migrate towards the anode (Figure 57). This receptor subunit preference is reciprocal to that displayed by gephyrin.

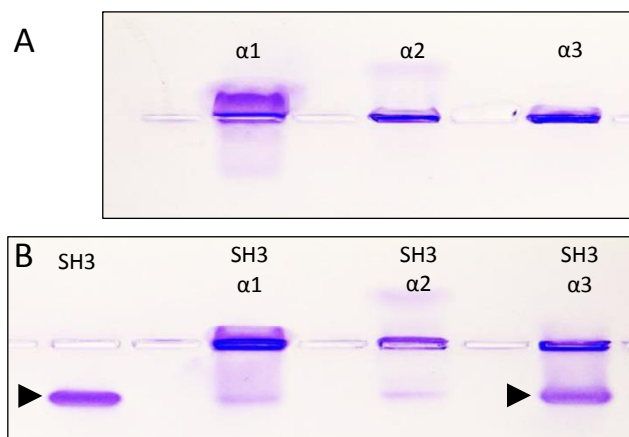


Figure 57. **NAGE of the SH3 domain GABA<sub>A</sub>R  $\alpha$ 1-3 subunit complex.** A, At a pH of 8 only the SH3 domain readily enters the gel towards the anode, while the GABA<sub>A</sub>R intracellular loops slowly migrate towards the cathode. B, The different receptor loops are applied at a 3-fold molar excess over the SH3 domain. The GABA<sub>A</sub>R  $\alpha$ 3 subunit but not the  $\alpha$ 1 and  $\alpha$ 2 subunits allow the SH3 domain to enter the gel and migrate towards the anode. The formation of SH3-GABA<sub>A</sub>R  $\alpha$ 1/2 loop complexes retains the majority of the SH3 domain in the pocket. In contrast, the GABA<sub>A</sub>R  $\alpha$ 3 subunit allows nearly all of the SH3 domain protein (indicated by the right arrow head) to enter the gel. © 2012 HM Maric

To estimate the stoichiometry and stability of the GABA<sub>A</sub>R-SH3 complexes I characterized them by analytical SEC. Specifically, I subjected either the single proteins or equi-molar mixtures of the SH3 domain and the GABA<sub>A</sub>R  $\alpha$ 1,  $\alpha$ 2 and  $\alpha$ 3 loops to a Superdex 10/300 75a column and analyzed the resulting fractions by SDS-PAGE.

Although my NAGE-assay identified an interaction between the SH3 domain and the  $\alpha$ 1-loop, the SEC analysis revealed a low stability of this complex. This results in a slight shoulder (Figure 58B blue arrow head) of the SH3 domain peak towards higher molecular weights as compared to the SH3 domain applied alone to the column (Figure 58A). In line with my NAGE experiments, the  $\alpha$ 3-loop did not alter the elution profile of the SH3 domain (Figure 58D), excluding a possible interaction. Finally, analytical SEC demonstrates a tight SH3- $\alpha$ 2-loop complex, resulting in an extreme 10 ml shift of the SH3 domain towards higher molecular weights and correspondingly lower elution volumes (Figure 58C). The subsequent analysis of the corresponding fractions via SDS-PAGE verified the presence of the SH3 domain and additionally suggests a dissociation of the complex resulting in a molar excess of  $\alpha$ 2-loop in the fractions with the lowest elution volumes (Figure 58C). Taken together the SEC results are in good agreement with NAGE and furthermore define a loose SH3- $\alpha$ 1-loop complex and a tight SH3- $\alpha$ 2-loop complex with an affinity in the micromolar range.

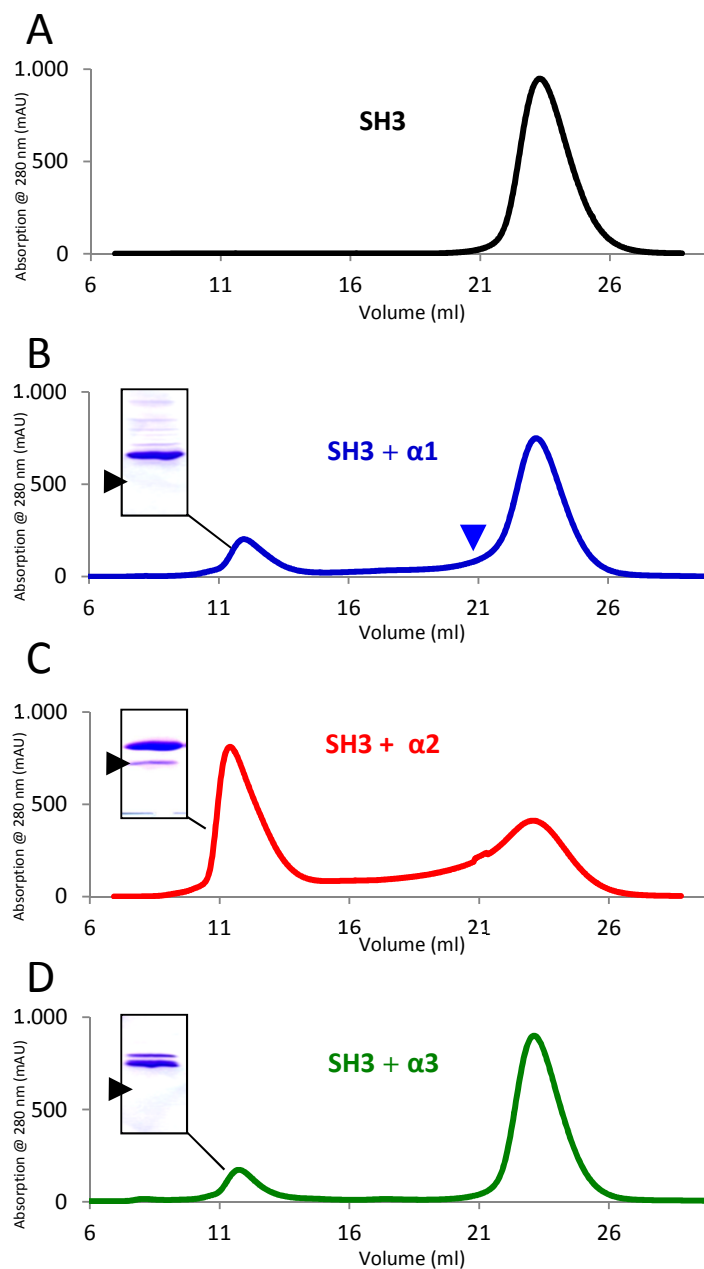


Figure 58. **Analytical SEC reveals the GABA<sub>A</sub>R subunit preference of the SH3 domain.** SEC experiments of (A) the SH3 domain alone (black curve) or as equimolar mixture with (B) the  $\alpha$ 1-loop (blue curve), (C) the  $\alpha$ 2-loop (red curve) and (D) the  $\alpha$ 3-loop (green curve). Only the  $\alpha$ 2-loop significantly alters the elution profile of the SH3 domain. SDS-PAGE (inlets) reveals that only the low elution volume fractions of the  $\alpha$ 2-loop-SH3 run contain the SH3 domain (indicated by arrow heads). © 2012 HM Maric

Encouraged by the analytical SEC experiments, which demonstrated a moderately tight and stoichiometric SH3-GABA<sub>A</sub>R  $\alpha$ 2 interaction, and the NAGE experiments that also suggested a weak SH3-domain-GABA<sub>A</sub>R  $\alpha$ 1 interaction I next quantified the interactions using ITC (Figure 59). In line with the SEC and NAGE experiments, ITC revealed that the  $\alpha$ 2-loop forms a tight ( $K_d = 1 \mu\text{M}$ ) and the  $\alpha$ 1-loop a rather weak complex ( $K_d = 0.5 \text{ mM}$ ) (Table 45). This is surprising, given that the GABA<sub>A</sub>R  $\alpha$ 1-loop harbors several PXXP motifs, while the GABA<sub>A</sub>R  $\alpha$ 2 loop lacks this canonical SH3 binding motif.

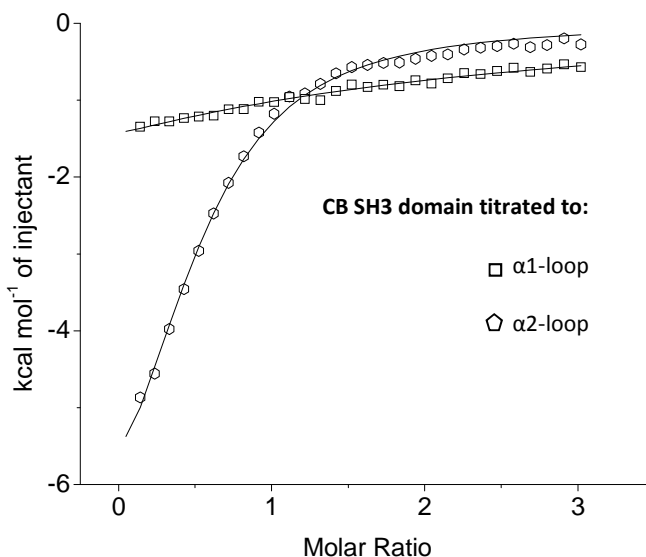


Figure 59. **Quantification of GABA<sub>A</sub>R-SH3 interactions via ITC.** The measured binding enthalpies are plotted as a function of the molar ratio of the SH3 domain to the GABA<sub>A</sub>R  $\alpha$ 1 and  $\alpha$ 2 loops. The binding isotherms display a 100-fold difference in affinity between both loops, and verify the formation of a 1:1 SH3 domain-GABA<sub>A</sub>R  $\alpha$ 2-loop complex. © 2012 HM Maric

Table 45. **Summary of the SH3-GABA<sub>A</sub>R binding parameters as determined by ITC.**

Receptor	Stoichiometry (N)	$K_d$ ( $\mu\text{M}$ )	$\Delta H$ (kcal/mol)	$-T\Delta S$ (kcal/mol)
GABA <sub>A</sub> R $\alpha$ 1 WT	n.d.	500 $\pm$ 400	-3 $\pm$ 0.8	2.1
GABA <sub>A</sub> R $\alpha$ 2 WT	0.62 $\pm$ 0.03	1.3 $\pm$ 0.8	-6.8 $\pm$ 0.4	0.4



Up to date there are 771 SH3 domain structures listed in the PDB, among them an NMR structure of CB's SH3 domain (PDB ID: 2YSQ). Within this set a large number of SH3 domain structures are complexed with ligands containing the canonical PxxP motif. Additionally, there are at least 16 structures that define 12 different modes of SH3-mediated ligand recognition (Table 46). All of these involve a conserved peptide-binding surface on the SH3 domain but deviate substantially from the canonical docking of consensus motif-containing SH3 ligands. Apart from these non-consensus ligands, there are less common atypical ligands that engage in fundamentally different interactions and involve an entirely different surface on the SH3 domain [186 or even tertiary contacts, 191, 192]. Remarkably, comparison of the suggested GABA<sub>A</sub>R  $\alpha$ 2 subunit motif [84] with the structurally resolved canonical and non-canonical SH3 binding motifs (Table 46) reveals no obvious similarities. The unique high affinity of the SH3  $\alpha$ 2-loop complex makes this, presumably atypical, SH3 interaction therefore an interesting target for a detailed structural characterization.

Table 46. **Summary of different SH3 ligand binding modes.** Summary of structurally resolved SH3 consensus and non-consensus ligands as well as GABA<sub>A</sub>R  $\alpha$ 2. The letters N and C shown in parentheses after the name of proteins containing two SH3 domains indicate which SH3 domain is meant. The letter  $\Phi$  refers to hydrophobic residues, x is any amino acid. Underlined sequences interact with conserved xP pockets on the surface of the SH3 domain, while blue residues interact with another conserved area on the SH3 domains, called specificity zone. In case of collybistin SH3 the underlined residues indicate crucial residues, while the shown motif was shown to be sufficient to mediate SH3 binding when inserted in the GABA<sub>A</sub>R  $\alpha$ 1 subunit. Notably, the GABA<sub>A</sub>R motif displays no obvious similarity to common SH3 binding motifs.

SH3 Domain	Ligand	Ligand Motif	PDB Entry
e.g. Src	Class I or II	x $\Phi$ PxxP or xPx $\Phi$ Px	1RLQ, 1SEM
Crk(N)	C3G	<u>PPPALPPK</u> KR	1CKA
abl	p41	<u>APSYSP</u> PPPP	1BBZ
Csk	PEP	<u>PPPLP</u> ERTPESFIV	1JEG
P67phox(C)	P47phox	<u>PQPAV</u> PPRPSADLILNRCSESTKRKLA	1K4U
GADS	HPK1	<u>PPVLP</u> PRKEK	1UTI
GADS	SLP-1	APSID <u>R</u> STKP	1OEB, 1H3H
Nck(N)	CD3 $\epsilon$	PPPVPNP <u>DY</u> EPIR	2JXB, 2JW4
Eps8L1	CD3 $\epsilon$	PPPVPNP <u>DY</u> EPIR	2ROL
$\beta$ PIX	PAK	PPPVIAP <u>R</u> PEHTKS	1ZSG, 2G6F
$\beta$ PIX	AIP4	PS <u>R</u> PPRPSRPPPTP	2P4R
IRTKS	EspF <sub>U</sub>	<u>IPPAP</u> NWPAPTTP	2KXC
Collybistin / hPEM2	GABA <sub>A</sub> R $\alpha$ 2	GSVMIQNN <u>AYAVAVANYA</u>	-

Based on this investigation, Maurizio Amato generated GABA<sub>A</sub>R- $\alpha$ 2 fragments and an SH3 variant to study this interaction in more detail. To narrow down the GABA<sub>A</sub>R  $\alpha$ 2 binding site, the TM3-4  $\alpha$ 2-loop construct (residues 334-420) was shortened to 334-362 and 334-379 residues, respectively. To test whether the SH3 domain mediates receptor binding via its universal peptide-binding site a critical tryptophan residue (Trp45) was exchanged to alanine, a mutation that was shown earlier to impair SH3 substrate binding without disturbing the secondary structure.

### 3.4.4 The SH3 Domain and Gephyrin Share a Reciprocal GABA<sub>A</sub>R Subunit Preference

Comparing the GABA<sub>A</sub>R subunit preference of the SH3 domain described in the previous paragraph with the respective preference of gephyrin described earlier in this work, a striking reciprocal relationship in the respective affinities is obvious (Table 47). Specifically, the  $\alpha 2$  subunit is binding the strongest to the SH3 domain, yet its interaction with gephyrin cannot be detected by ITC. In contrast no  $\alpha 3$ -SH3 domain interaction is detectable, yet  $\alpha 3$  has the tightest interaction with gephyrin. The  $\alpha 1$  subunit has an intermediate affinity in both systems. Due to the reciprocal specificity of gephyrin and CB, the gephyrin-CB complex has the potential to interact with all three mentioned receptor subunits, thus explaining recent video microscopy findings of CB colocalizing with the GABA<sub>A</sub>R  $\alpha 1$ ,  $\alpha 2$  and  $\alpha 3$  subunits [97], and also the observation that gephyrin is strongly colocalizing with the  $\alpha 2$ -subunit [74], although the corresponding affinity of the direct interaction in our *in vitro* assays is very low. Therefore our results indicate that the molecular basis of gephyrin-mediated GABA<sub>A</sub>R and possibly also GlyR clustering lies in the architecture of the CB-gephyrin complex. We propose that the GABA<sub>A</sub>R and GlyR subunit preference depends on details of the CB-gephyrin complex and its spatial and sequential interplay with binding partners such as PI3P, NL2 and the GABA<sub>A</sub>R  $\alpha 2$ -subunit.

As described earlier we identified the residue corresponding to Gly374 of the GlyR  $\beta$  subunit as a critical determinant for the strength of the GABA<sub>A</sub>R-gephyrin complex. This residue is conserved in the GABA<sub>A</sub>R  $\alpha 3$  subunit, replaced by Ala in GABA<sub>A</sub>R  $\alpha 1$  and by Val in GABA<sub>A</sub>R  $\alpha 2$ . Binding studies with the GABA<sub>A</sub>R  $\alpha 3$  (G373V) and GABA<sub>A</sub>R  $\alpha 2$  (V343G) mutants indeed could verify a strengthening of the  $\alpha 2$  interaction and a weakening of the  $\alpha 3$  interaction. As described earlier in this work, we propose this residue to repel the receptor loop by sterically clashing with subdomain IV of GephE, thus possibly explaining our observation of a rather weak GephE affinity of the  $\alpha 2$  subunit compared to the GABA<sub>A</sub>R  $\alpha 1$  and  $\alpha 3$  subunits. These results were presented earlier in this work and are summarized in Table 47 for clarity. A recent study suggested that gephyrin and CB both recognize an identical binding site on the GABA<sub>A</sub>R  $\alpha 2$  subunit. Based on this finding we therefore tested whether the valine/glycine exchange has a similar severe effect on the interaction between the GABA<sub>A</sub>Rs and the SH3 domain. Strikingly, the GABA<sub>A</sub>R  $\alpha 2$  V343G mutant indeed no longer interacts with the SH3 domain of CB (Table 47). This finding is in line with the idea that identical receptor residues mediate critical CB SH3 and GephE interactions, and hence the identified 15 residue motifs mediate distinct targeting processes.

Table 47. **Alignment of the different motifs recognized by gephyrin and presumably CB.** GlyR  $\beta$  Gly374 (boxed and red) points towards subdomain IV of GephE in the GlyR-GephE complex structure. The corresponding residue in the GABA<sub>A</sub>R subunits (boxed and marked in red) is identical in GABA<sub>A</sub>R  $\alpha 3$  (Gly373) and type-conserved in  $\alpha 1$  (Ala344) but different in  $\alpha 2$

Receptor	Gephyrin and CB receptor binding motif	GephE-K <sub>d</sub>	SH3-K <sub>d</sub>
GABA <sub>A</sub> R $\alpha 1$ WT	LIKKNNYAPT <b>A</b> TSYT	17±11	500±400
GABA <sub>A</sub> R $\alpha 2$ WT	VMIQNNAYAVA <b>V</b> ANYA	<b>n.d.</b>	1±1
GABA <sub>A</sub> R $\alpha 3$ WT	AKKTSTTFNIV <b>G</b> TTYT	5±2	<b>n.d.</b>
GlyR $\beta$ WT	NDLRSNDFSI <b>V</b> SLPR	0.1/8	-
GABA <sub>A</sub> R $\alpha 3$ G374V	AKKTSTTFNIV <b>V</b> TTYT	<b>n.d.</b>	-
GABA <sub>A</sub> R $\alpha 2$ V343G	VMIQNNAYAVA <b>G</b> ANYA	-	<b>n.d.</b>

(Val343) marked in blue. (n.d. = no binding detectable; (-) = experiment not yet conducted.

To further explore the possible differential role of the CB-gephyrin complex in GABA<sub>A</sub>R clustering *in vivo* the group of our collaboration partner Steve J. Moss generated mice which express chimeric  $\alpha 1/2$  subunits. Specifically the 15 residues harboring the gephyrin-interacting region, which was extensively characterized in my *in vitro* studies and described in the previous sections, was swapped between both receptor subunits (Table 48). Preliminary results indicate a severe phenotype in mice expressing these chimeric receptors, which is in line with my assumption that these residues encode a differential subunit-specific localization which is mediated by either gephyrin or CB.

Table 48. **Alignment of the large intracellular loops of the GABA<sub>A</sub>R  $\alpha 1$  and  $\alpha 2$  subunits.** The group of Steven J Moss generated mice with swapped gephyrin/CB binding sites ( $\alpha 1/2$  Chim and  $\alpha 2/1$  Chim). GABA<sub>A</sub>R  $\alpha 2$  residues are shown in blue and  $\alpha 1$  residues in black.

GABA <sub>A</sub> R $\alpha 1$ :	NYFTKRGYAWDGKSVVPEKPKKVKDPLIKKNNNTYAPTATSYPNLRGDPGLATIAKSATIEPKVKPETKPEPKKTFNSVSKIDR
GABA <sub>A</sub> R $\alpha 2$ :	NYFTKRGWAWDGKSVVNDKPKKEKGSVMIQNNAYAVAVANYAPNLSKDPVLSTISKSATTPENKKPENKPAEAKKTFNSVSKIDR
$\alpha 1/2$ Chim:	NYFTKRGYAWDGKSVVPEKPKKVKDPMIQNNAYAVAVANYAPNLRGDPGLATIAKSATIEPKVKPETKPEPKKTFNSVSKIDR
$\alpha 2/1$ Chim:	NYFTKRGWAWDGKSVVNDKPKKEKGSLIKNNNTYAPTATSYPNLSKDPVLSTISKSATTPENKKPENKPAEAKKTFNSVSKIDR

3.4.5 GephE and the SH3 Domain Compete for the GABA<sub>A</sub>R  $\alpha$ 2 Subunit

Prompted by the finding that a single point mutation within the GABA<sub>A</sub>R  $\alpha$ 2 loop has an impact on the binding affinity to both, GephE and CB SH3, I wanted to explore the possibility of tripartite complex between the aforementioned proteins and test for synergistic or competitive binding.

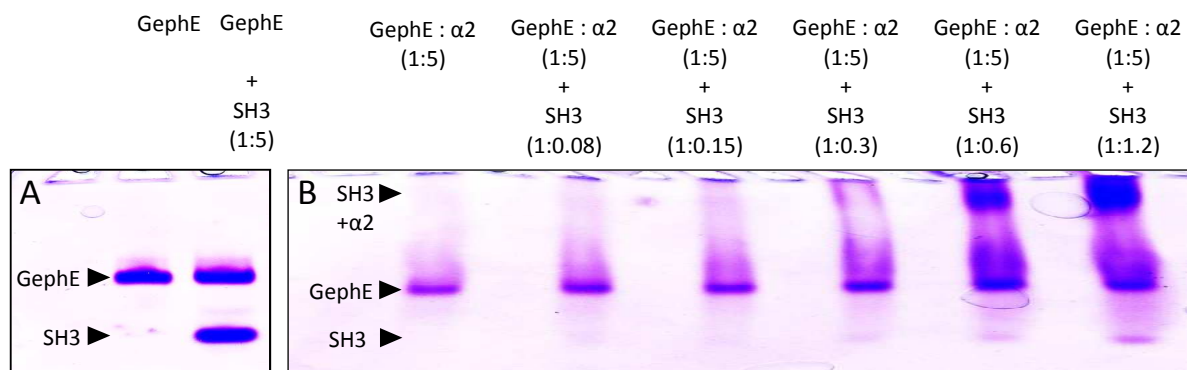
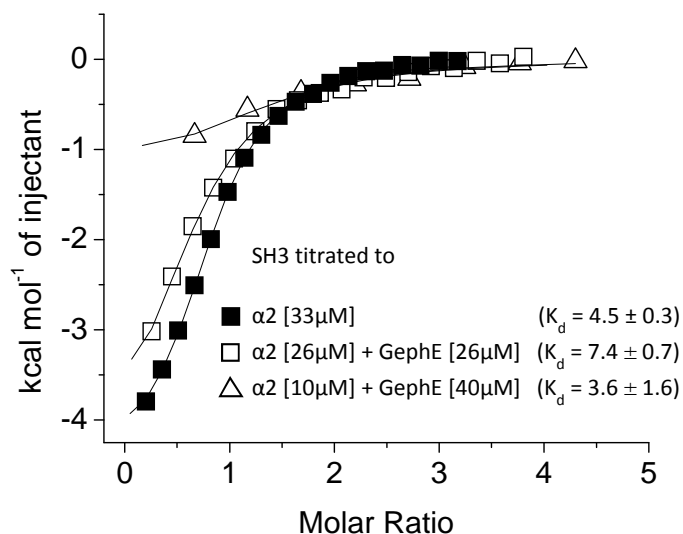


Figure 60. **NAGE visualizes that gephyrin and the SH3 domain compete for the  $\alpha$ 2-loop.** A, The SH3 domain and gephyrin do not interact on NAGE. B, GephE applied at a five-fold molar excess over the GABA<sub>A</sub>R  $\alpha$ 2 subunit is partly kept to the pocket and partly enters the gel towards the anode (lane 1). Addition of increasing amounts of the SH3 domain to the GephE-GABA<sub>A</sub>R  $\alpha$ 2 complex allows more gephyrin to enter the gel and migrate towards the anode (lane 2-6). © 2012 HM Maric

First, I tested whether the SH3 domain of CB and GephE interact using NAGE. While earlier studies [43, 94] suggested that the DH and PH domains of CB directly interact with gephyrin, its SH3 domain does not interact with gephyrin (Figure 60A). NAGE assays described in earlier paragraphs describe the nearly complete saturation of GephE with the GABA<sub>A</sub>R  $\alpha$ 2 subunit upon incubation with an 8-fold excess of the receptor loop. To test for a possible synergistic or competitive binding behavior I generated the gephyrin-GABA<sub>A</sub>R  $\alpha$ 2 complex using a moderate 5-fold molar excess of the receptor loop, resulting in roughly 50% of GephE being complexed and hereby retained in the pocket and 50% entering the gel towards the anode (Figure 60B, lane 1). To this mixture I added increasing amounts of the SH3 domain, which displays a GABA<sub>A</sub>R  $\alpha$ 2 affinity that is several magnitudes larger than the stability of the gephyrin-GABA<sub>A</sub>R  $\alpha$ 2 complex. Strikingly, decreasing amounts of the SH3 domain bind to the GABA<sub>A</sub>R  $\alpha$ 2 loop and therefore cannot enter the gel. Accordingly, gephyrin is competed out, resulting in increasing amounts of gephyrin entering the gel (Figure 60B, lanes 2-6).

### 3.4.6 The GABA<sub>A</sub>R $\alpha$ 2 Subunit Activates Collybistin for Gephyrin Binding

After verification of an overlapping GABA<sub>A</sub>R  $\alpha$ 2-loop binding site of GephE and the SH3 domain of CB I tested whether GephE directly modulates the binding strength of the SH3- $\alpha$ 2-loop-complex. I therefore titrated the  $\alpha$ 2-loop in the presence or absence of GephE with the SH3 domain (Figure 61). As expected, gephyrin had no effect on the interaction between the SH3 domain and the  $\alpha$ 2-loop, irrespective of the molar ratios. While the heat signatures were altered by the differing concentration of the  $\alpha$ 2 subunit, curve fitting with origin revealed that the interaction strength remained unaltered (Figure 61).



**Figure 61. ITC excludes a possible modulation of the SH3- $\alpha$ 2 complex by gephyrin.** Titration of the  $\alpha$ 2-loop with the SH3 domain in the absence of GephE, at a 1:1 ratio of GephE and  $\alpha$ 2 and at a 1:4 ratio of  $\alpha$ 2 and GephE. The thermal profiles are altered by concentration changes. Nevertheless, neither the difference in concentration nor the presence of gephyrin does modulate the affinity of the SH3 domain to the GABA<sub>A</sub>R  $\alpha$ 2 subunit (given in parentheses). © 2012 HM Maric

My earlier results demonstrated that full-length gephyrin displays only a weak  $\alpha$ 2-loop affinity and similarly full-length CB shows only a moderate GABA<sub>A</sub>R  $\alpha$ 2 affinity (Daniela Schneeberger and B. Sander, personal communication). In contrast to these findings, earlier Y2H-studies [84] demonstrated that full-length CB and gephyrin together exhibit a strong GABA<sub>A</sub>R  $\alpha$ 2 affinity. As described in section 1.4.1 structural studies of ASEF, a close homologue of CB, revealed that its N-terminal SH3 domain engages in direct and tight intra-molecular interactions with its PH and its DH domain, thus forming an inactivated complex. Not surprisingly the intra-molecular interaction interface is conserved among ASEF and CB and, even more importantly, gephyrin was shown to indeed associate with CB's PH and DH domain. My own work excluded a possible gephyrin-SH3 domain interaction (Figure 60), and a synergistic binding of the SH3 domain to the GABA<sub>A</sub>R  $\alpha$ 2 subunit in the presence of gephyrin (Figure 61). Therefore it can be concluded that the Y2H-assays, which demonstrated gephyrin to amplify CB's receptor binding [84] uncovered the gephyrin-mediated un-masking of the SH3 domain of CB, rather than the proposed synergistic binding event. Accordingly, I suggest that the free SH3 domain of CB mimics the maximal possible affinity displayed by CB after full activation by PIP<sub>2</sub> and/or gephyrin. On the molecular level this activation would be based on the competition of the intra-molecular SH3 domain-DH/PH domain binding (Section 1.4.1) on the one hand, and the inter-molecular SH3 domain-GABA<sub>A</sub>R  $\alpha$ 2 subunit (Figure 59) as well as the gephyrin-CB PH and DH domain [43, 94] and PH-PIP<sub>2</sub> binding [43, 91] on the other hand.

## 4 Concluding Discussion

Until now, a multitude of neurobiological studies (reviewed in [92, 193-195]) addressed the structural determinants of synaptic transmission, and it was found that excitatory as well as inhibitory neurotransmitter receptors are precisely localized and accumulated by scaffolding proteins which are located beneath the neuronal surface membrane, and that this process is crucial for synaptic function. My thesis presented here aimed to decipher the molecular details of the underlying interactions that accumulate the major mediators of fast synaptic inhibition, namely the GABA<sub>A</sub>Rs and GlyRs, at post- and extrasynaptic sites. Synapses containing the GABA<sub>A</sub>Rs and GlyRs comprise 5–15% of the total synapse number in the human brain, nevertheless, their importance is highlighted in a pleiotropy of studies of human brain disorders such as epilepsy [196, 197], anxiety disorders [198], mood disorders [199], and neurodevelopmental disorders such as autism [200], Fragile X syndrome [201] and schizophrenia [202]. Modulation of GABAergic transmission allows to shift the balance between excitatory and inhibitory activity and accordingly GABA<sub>A</sub>Rs are the principle sites of action for clinically relevant drugs such as anxiolytics, anticonvulsants, and sedative hypnotic agents including benzodiazepines, barbiturates, alcohol, anesthetics and neurosteroids.

## 4.1 Radixin-Mediated GABA<sub>A</sub>R Clustering

Following initial findings by the Kneussel lab, which demonstrated that activated radixin mediates clustering of  $\alpha 5$  subunit containing GABA<sub>A</sub>Rs at extrasynaptic sites [26], I analyzed the respective direct interaction applying various biochemical and biophysical methods to the recombinantly prepared proteins. Combined, my study suggests that subdomain F3 of the FERM domain of radixin indeed engages in a direct interaction with the N-terminal region of the large intracellular loop of the GABA<sub>A</sub>R  $\alpha 5$  subunit which is characterized by a low micromolar affinity ( $K_d = 8 \mu\text{M}$ ). In particular, residues 352 to 364 of the GABA<sub>A</sub>R  $\alpha 5$  subunit form hydrophobic interactions via their side-chains as well as peptide backbone interactions with a universal substrate-binding site within subdomain F3 of the radixin FERM domain. This binding site is formed by an  $\alpha$ -helix that offers a large hydrophobic pocket (residues 273 to 295 marked in blue in Figure 62) and a  $\beta$ -strand that readily engages in peptide backbone interactions (residues 242 to 252 marked in yellow in Figure 62). This binding site on the radixin FERM domain has been implicated in a large variety of different scaffold interactions, and it recognizes moderately conserved motifs. It can therefore be concluded that this interaction is regulated by spatially and temporally controlled inactivation of either radixin, the receptor subunit or the competing ligands. Following this idea, my study underscores the importance of the initial finding that activation of radixin is essential for the clustering process [26].

Additionally, posttranslational modifications within the GABA<sub>A</sub>R  $\alpha 5$  and radixin binding sites, that have been mapped in detail in the context of this thesis, could allow further regulation of this interaction *in vivo*. Notably, the 13 residues minimum motif identified here indeed encompasses a lysine residue that was shown to be ubiquitinated *in vivo* [171](Figure 62), suggesting a new pathway for a negative regulation of extrasynaptic GABA<sub>A</sub>R clustering. Combined biochemical and cell biological studies will have to address the possibility of an ubiquitin-mediated radixin-GABA<sub>A</sub>R  $\alpha 5$  uncoupling and the potentially resulting reduced cluster size and number at extrasynaptic sites.

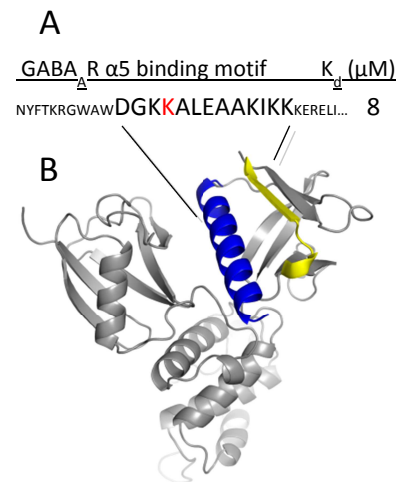


**Figure 62. Structural Basis of radixin-mediated GABA<sub>A</sub>R  $\alpha 5$  clustering.** A, Fine-mapped radixin FERM binding region within the GABA<sub>A</sub>R  $\alpha 5$  subunit. Major contributors to the overall interaction strength are indicated with increased font size. Ubiquitination of the lysine residue (marked in red) within the binding motif offers a possible pathway for negative regulation of extrasynaptic clustering. B, X-ray crystallographic derived structure of radixin FERM solved in this thesis and earlier in cartoon representation and colored grey. The color coded universal binding site is implicated in binding of a variety of only moderately conserved motifs as well as GABA<sub>A</sub>R  $\alpha 5$ . Residues 273-295 colored blue adopt an  $\alpha$ -helical structure, and together with the  $\beta$ -strand formed by residues 242-252 colored yellow they shape a universal ligand binding site within the FERM domain of radixin. © 2012 HM Maric

## 4.2 Gephyrin-Mediated GABA<sub>A</sub>R Clustering

Next, I contributed to a collaborative study with the Moss lab, which explored gephyrin-mediated GABA<sub>A</sub>R clustering at postsynaptic sites and resulted in four recent publications [195, 203-205]. My experiments demonstrate that gephyrin binds to moderately conserved motifs within the large intracellular loops of the GABA<sub>A</sub>R  $\alpha$ 1,  $\alpha$ 2 and  $\alpha$ 3 subunits in a similar manner [204, 205] as found for the GlyR  $\beta$  subunit, which had been characterized earlier in great detail [21, 55]. Gephyrin's subunit preference varies greatly from 0.1  $\mu$ M for the GlyR  $\beta$  subunit, 5  $\mu$ M for the GABA<sub>A</sub>R  $\alpha$ 3 subunits, 17  $\mu$ M for the GABA<sub>A</sub>R  $\alpha$ 1 subunit and approximately 500  $\mu$ M for the GABA<sub>A</sub>R  $\alpha$ 2 subunit. Nevertheless, my binding assays and crystallographic studies revealed that gephyrin mediates all receptor interactions via a universal binding site located in its C-terminal E domain with key residues acting as major contributors to the overall binding strength (Figure 63). Accordingly, the moderately conserved receptor loop residues that engage in direct gephyrin interactions show a correlated contribution to the overall binding strength [203]. In particular, hydrophobic interactions and H-bridges mediated by the seven N-terminal receptor residues within the 15 residues minimum motif act as a major contributor to the overall binding strength (Figure 63). The relevance of these *in vitro* results was confirmed in the Moss lab by means of transfecting primary hippocampal cells with selected point mutated receptor subunits and investigation of their gephyrin colocalization as well as quantification of their synaptic cluster number and size. An exchange of two conserved tyrosine residues (Figure 63, marked in red and green) within the gephyrin-binding motif was sufficient to significantly decrease clustering at postsynaptic sites in case of the GABA<sub>A</sub>R  $\alpha$ 1 and  $\alpha$ 2 subunits [203]. Hence, it can be concluded that gephyrin mediates clustering of GlyRs and GABA<sub>A</sub>Rs via a universal binding site. Notably, the minimum motifs identified here were shown earlier to be phosphorylated *in vivo*, suggesting several novel pathways for negative regulation of fast inhibitory synaptic transmission, which have to be addressed in future studies.

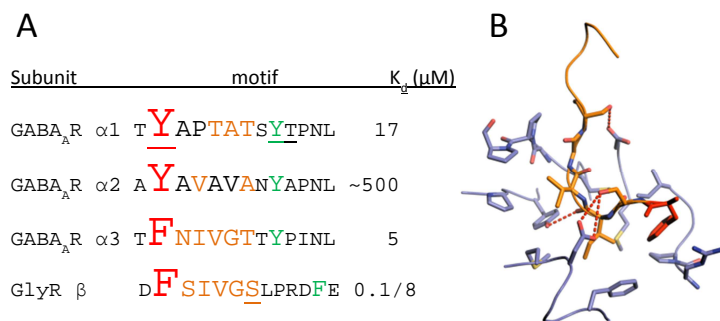


Figure 63. **Structural basis of gephyrin-mediated GABA<sub>A</sub>R clustering.** A, Fine-mapped gephyrin binding motifs within the GlyRs and GABA<sub>A</sub>Rs. Major contributors to the overall interaction strength are indicated with an increased font size and are colored in red, orange and green, while residues that are phosphorylated *in vivo* are underlined. B, Minimum scheme of the receptor gephyrin interaction based on my X-ray crystallographic and binding studies. These studies suggest a major contribution of the N-terminal receptor motif which displays the highest overall conservation among all gephyrin-binding subunits. Representative for all receptor subunits the N-terminal GlyR  $\beta$  peptide is shown as a stick model, colored orange and red. All subunits engage in conserved hydrophobic interactions and H-bridges with gephyrin residues, marked in light blue. © 2012 HM Maric



*In vivo*, gephyrin presumably forms a multivalent scaffold by self-association of its G and E domain, while GABA<sub>A</sub>Rs are assembled from five receptor subunits. Given the multivalent nature of these proteins, I addressed the possibility of avidity in the clustering of inhibitory neurotransmitter receptors. Based on cocrystallization of selected minimum peptides with GephE, I designed bivalent peptides that bind gephyrin with an unmatched high affinity due to avidity potentiation. Notably, I could extend the dimerization approach to low affinity gephyrin ligands, resulting in an extreme potentiation of affinity into the low micromolar range. This approach might enable the future analysis of GABA<sub>A</sub>R subunit  $\beta$ 2 and  $\gamma$ 2, which both contain regions similar to the gephyrin-binding motifs identified in the  $\alpha$ 1-3 subunits analyzed in this thesis (Table 49). Notably the proposed gephyrin-interacting region of GABA<sub>A</sub>R  $\gamma$ 2 contains two residues that were shown earlier to be phosphorylated *in vivo* (Table 49, underlined residues) [179, 180]. In addition, the dimerization might allow the X-ray crystallographic characterization of the low affinity gephyrin-binding GABA<sub>A</sub>R  $\alpha$ 1 and  $\alpha$ 2 subunit that could not be studied in this thesis using the conventional monomeric ligands.

Receptor	Gephyrin binding motif
GlyR $\beta$	<sup>397</sup> <u>D</u> <u>F</u> <u>S</u> <u>I</u> <u>V</u> <u>G</u> <u>S</u> <u>L</u> <u>P</u> <u>R</u> <u>D</u> <u>F</u> <u>E</u> <u>L</u> <sup>410</sup>
GABA <sub>A</sub> R $\gamma$ 2	<sup>379</sup> <u>M</u> <u>F</u> <u>S</u> <u>F</u> <u>K</u> <u>A</u> <u>P</u> <u>T</u> <u>I</u> <u>D</u> <u>I</u> <u>R</u> <u>P</u> <u>R</u> <sup>392</sup>
GABA <sub>A</sub> R $\beta$ 2	<sup>392</sup> <u>D</u> <u>F</u> <u>S</u> <u>L</u> <u>Y</u> <u>T</u> <u>M</u> <u>D</u> <u>P</u> <u>H</u> <u>E</u> <u>N</u> <u>I</u> <u>L</u> <sup>405</sup>
GABA <sub>A</sub> R $\alpha$ 3	<sup>396</sup> <u>T</u> <u>F</u> <u>N</u> <u>I</u> <u>V</u> <u>G</u> <u>T</u> <u>T</u> <u>Y</u> <u>P</u> <u>I</u> <u>N</u> <u>L</u> <u>A</u> <sup>409</sup>
GABA <sub>A</sub> R $\alpha$ 2	<sup>364</sup> <u>A</u> <u>Y</u> <u>A</u> <u>V</u> <u>A</u> <u>V</u> <u>A</u> <u>N</u> <u>Y</u> <u>A</u> <u>P</u> <u>N</u> <u>L</u> <u>S</u> <sup>377</sup>
GABA <sub>A</sub> R $\alpha$ 1	<sup>339</sup> <u>T</u> <u>Y</u> <u>A</u> <u>P</u> <u>T</u> <u>A</u> <u>T</u> <u>S</u> <u>Y</u> <u>T</u> <u>P</u> <u>N</u> <u>L</u> <u>A</u> <sup>351</sup>

Table 49. **Relationship between verified and putative gephyrin-binding GABA<sub>A</sub>R subunits.** Alignment of GABA<sub>A</sub>R subunit sequences, verified to mediate gephyrin binding ( $\alpha$ 1-3), as well as subunits potentially binding to gephyrin ( $\beta$ 2 and  $\gamma$ 2). Residues known to be phosphorylated *in vivo* are underlined. The  $\beta$ 2 and  $\gamma$ 2 motifs show a high similarity to the GlyR  $\beta$  subunit (red) and seem to be distinct from the GABA<sub>A</sub>R  $\alpha$ 1 and  $\alpha$ 2 subunits (blue). Notably, the putative gephyrin-interacting region of GABA<sub>A</sub>R  $\gamma$ 2 contains two residues (underlined) that were shown to be phosphorylated *in vivo*.

### 4.3 Collybistin's Role in GABA<sub>A</sub>R Clustering

During the course of my work, the Harvey group proposed that CB plays a major role in gephyrin-mediated GABA<sub>A</sub>R clustering by amplifying the gephyrin GABA<sub>A</sub>R α2 subunit interaction. My results deny this hypothesis and instead argue in favor of the model suggested by T. Papadopoulos and Tolga Soykan [193]: CB-mediated GABA<sub>A</sub>R clustering relies on CB's self-association, which competes with gephyrin and GABA<sub>A</sub>R α2 binding. Expanding this model, I propose that the free SH3 domain of CB exhibits the maximal possible receptor affinity of CB, while *vice versa* CB missing its N-terminal SH3 domain displays a maximized gephyrin binding strength. My experiments verified that the SH3 domain engages in a direct and tight interaction with the GABA<sub>A</sub>R α2 subunit independent of gephyrin. I conclude that the free SH3 domain used here, mimics full-length CB's α2-loop affinity after gephyrin/PIP<sub>2</sub>-mediated activation. Whether *in vivo* gephyrin/PIP<sub>2</sub> activates CB for receptor binding or, vice versa, GABA<sub>A</sub>R α2 receptors activate CB for gephyrin/PIP<sub>2</sub> binding remains to be elucidated. While this mechanism for GABA<sub>A</sub>R clustering (Figure 64A) differs from the described gephyrin mediated mechanism described earlier in this thesis (Figure 64B), nevertheless, both rely on gephyrin.

My comparison of CB's and gephyrin's receptor subunit preference revealed a reciprocal relationship. GABA<sub>A</sub>R α3 forms a tight gephyrin complex ( $K_d = 5 \mu\text{M}$ ) but does not interact with CB. GABA<sub>A</sub>R α2 binds tightly to CB ( $K_d = 1 \mu\text{M}$ ) but not gephyrin and GABA<sub>A</sub>R α1 displays a moderate binding affinity to both proteins ( $K_d = 20$  and  $400 \mu\text{M}$ ). Selected point mutants as well as competition assays indicate that gephyrin and CB bind to an overlapping site on the receptor subunits. The idea that homologous motifs within the receptor loops mediate receptor targeting differentially is supported by preliminary results from the Moss group which exchanged the gephyrin/CB binding motifs between the GABA<sub>A</sub>R α1 and α2 subunits and found a severe phenotype in transgenic mice which is currently being investigated in detail.

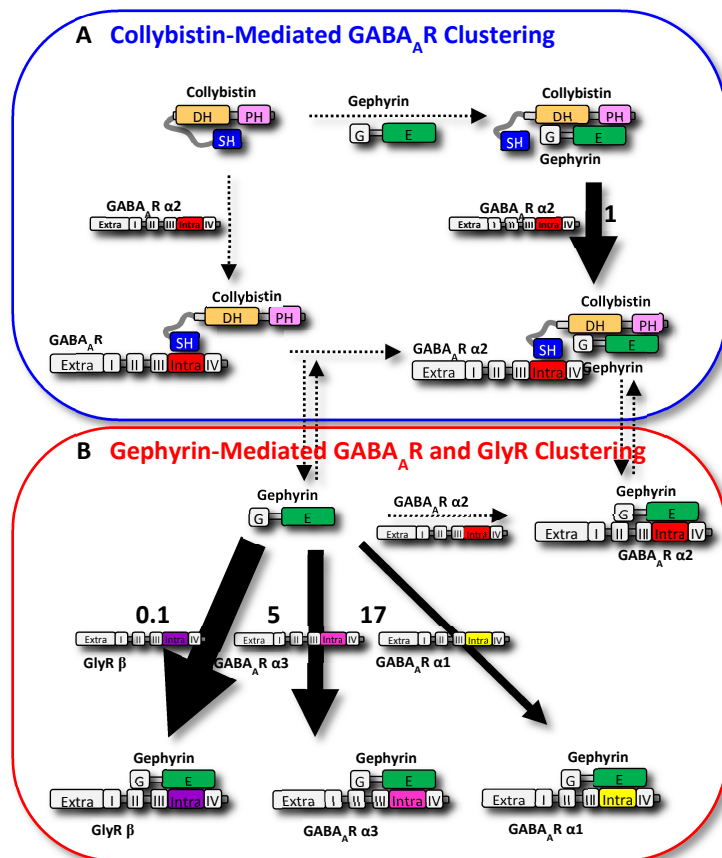


Figure 64. **Minimum scheme of GABA<sub>A</sub>R and GlyR clustering at postsynaptic sites.** My study suggests that (A) CB mediates the clustering of GABA<sub>A</sub>R containing the α2 subunit and (B) that gephyrin directly triggers GlyR clustering and clustering of GABA<sub>A</sub>R containing α1 and α3 subunits. Notably both mechanisms rely on gephyrin which either (A) activates CB or (B) directly mediates receptor clustering via a common binding site. Additionally, the GABA<sub>A</sub>R α1 (excluded in the scheme for clarity) and α2 subunits are involved in both pathways, due to interacting with (A) collybistin and (B) gephyrin. Dotted arrows indicate interactions verified by non-quantitative methods. Interactions quantified in this work are represented by solid arrows with their respective affinity given in [ $\mu\text{M}$ ]. © 2012 HM Maric

## 4.4 Targeting Receptor-Scaffold Interactions

### 4.4.1 Receptor-Scaffold Interaction Share Common Features

Despite the involvement of unrelated protein binding modules, such as PDZs in case of GluRs and SH3, FERM and GephE in case of GABA<sub>A</sub>Rs and GlyRs, the neurotransmitter receptor-scaffold interactions share common key characteristics:

- Short, linear and intrinsically unfolded regions within intracellular receptor domains engage in moderately specific and direct interactions.
- Small interaction surfaces result in medium interaction strengths, typically in the low micromolar range.
- The scaffold proteins recognize moderately conserved motifs and display a wide range of affinities.

These findings are in line with the unique framework of these interactions [206, 207]. Assuming that scaffold proteins form a two dimensional lattice beneath the neuronal membrane and that the targeted receptors enter the membrane before interacting with the scaffold-lattice, it can be concluded that the interactions analyzed here are characterized by a great kinetic advantage, *in vivo*, which is based on a reduced diffusion dimensionality of both binding partners as well as local enrichment effects. Due to limitations of my experimental setup I could not address these mechanisms of affinity-potential. Instead, I analyzed two additional possible determinants of the actual, *in vivo*, receptor-scaffold interaction strength:

- Avidity effects resulting from the oligomerized nature of the protein scaffolds and the oligomeric assembly of the receptors might potentiate the binding strength. This was verified earlier for the PDZ-mediated receptor interactions [208], and I demonstrated the importance of this effect for gephyrin-mediated receptor binding.
- Recent studies revealed the *in vivo* modulation of the direct receptor scaffold interactions analyzed here by phosphorylation, either by PKC in case of the GlyR  $\beta$  subunit [205] or by MAPK in case of the GABA<sub>A</sub>Rs containing the ubiquitously expressed  $\alpha 1$  subunit [65], or alternatively by ubiquitination, as revealed for the  $\alpha 5$  subunit which could modulate its interaction with radixin [171].

#### 4.4.2 Receptor-Scaffold Interactions Are Promising Drug Targets

Notably, the key properties mentioned in the previous section and additional neurobiological findings predestine these protein-protein-interactions to be targeted by effector molecules:

- Synaptically-released neurotransmitters were shown to saturate their receptors [209], therefore it can be inferred that receptor clustering is not only crucial for synaptic function but also for regulating the functional strength of the synapse [101, 210, 211].
- Given that phosphorylation events negatively regulate synaptic inhibition by reducing the gephyrin-receptor affinity, it can be concluded that (i) regulation of the receptor scaffold interaction fulfills a specific role within synaptic transmission, and (ii) that this interaction can be targeted, either by inhibiting the kinases or by interfering with the direct interaction.
- The lack of secondary structure within the peptides and the small interaction surfaces allow the usage of (i) very short minimal fragments [212-215] or (ii) even small molecule inhibitors [216] that mimic these interactions.
- For all scaffold proteins that have been analyzed in the context of this thesis there are corresponding ligands which display a maximized affinity. In case of the radixin FERM domain earlier studies suggested ICAM-2 as a high affinity interactor. In case of the SH3 domain of CB1 I identified a segment within the GABA<sub>A</sub>R  $\alpha$ 2 subunits which is surprisingly devoid of conventional PxxP motifs, and in case of the E domain of gephyrin it is the N-terminal part of the minimum peptide derived from the GlyR  $\beta$  subunit. The resulting affinities in the low micromolar to high nanomolar range provide compound specificity and enable structure based drug design and therefore provide good starting molecules for further development.
- The oligomeric nature of scaffold proteins at postsynaptic sites allows multivalent compounds with optimized linker lengths to provide an artificially high affinity. The major determinant of avidity-based affinity potentiation is the length of the linker [183, 184] and section 4.4.4. In case of the naturally occurring receptors, linker length is determined by their subunit assembly and the overall length of their large intracellular loops. In contrast, the linker length of artificial receptor derived compounds can be optimized towards a maximized avidity to effectively compete, already at low *in vivo* concentrations, with naturally receptors for gephyrin [212-215].

### 4.4.3 Architecture of a Hypothetical Gephyrin Inhibitor

By specifically targeting the receptor binding site formed by the dimer interface of gephyrin's E domain, the bidentate peptide presented here acts as an inhibitor of gephyrin's receptor binding capacity. Further development of this compound may offer the possibility to analyze the effect of uncoupling of the gephyrin receptor interaction in cell culture-based assays. Specifically, I propose the introduction of a TAT-peptide [215] (Figure 64) to the linker to (i) enable its transport across the intact neuronal membrane and to (ii) allow immunofluorescence labeling in the course of video-microscopy studies [212, 215].

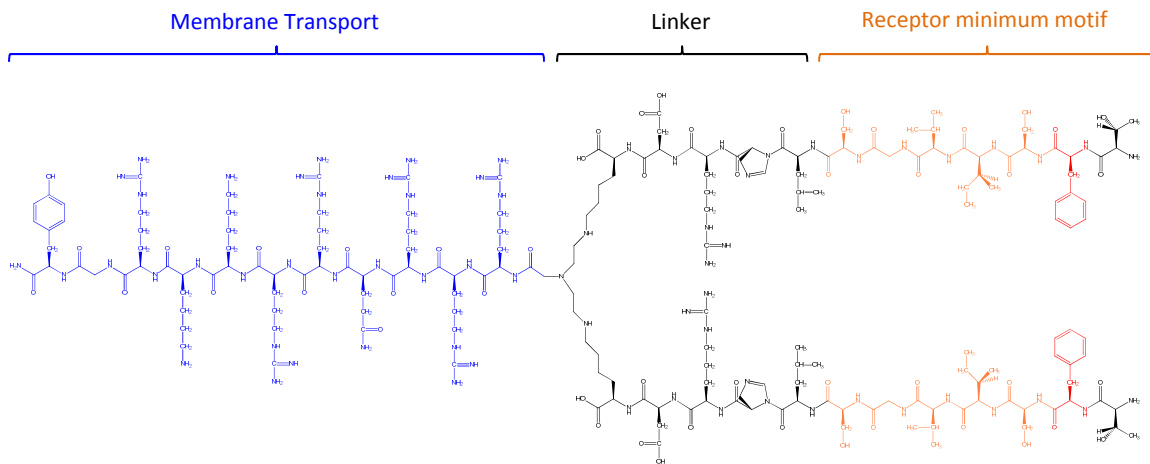


Figure 65. **Structure of a gephyrin-targeting, bivalent and membrane-permeable peptide.** Structure of a hypothetical receptor-derived bidentate peptide that specifically acts on gephyrin's receptor clustering activity. Notably, shortening of the gephyrin binding peptide (marked in orange and red) and the linker (marked in black) as well as introduction of a TAT-peptide (marked in blue) could render the peptide membrane permeable, less prone to degradation and would enable immunofluorescence labeling and therefore imaging studies of the effector molecule. © 2012 HM Maric

Given the central role of gephyrin in the architecture of the inhibitory synapse numerous studies addressed the effect of gephyrin deficiency in either knock-out mice [33, 71, 72] or by application of antisense oligonucleotides [31]. Additionally, the gephyrin protein was targeted by Antibodies [217]. While these studies indeed provided new insights into the function of inhibitory synaptic transmission, they were hampered by (i) the early postnatal death of the knock-out mice, (ii) the complete disruption of the relevant receptor clusters or (iii) the artificially altered protein functions and expression levels. Therefore it seems advantageous for future studies of gephyrin to enable the direct targeting of its receptor clustering function in living neurons. The here described compound would allow the modulation of gephyrin's receptor anchoring function, without altering gephyrin's enzymatic function or its relative abundance.

Finally, in theory such a molecule could be used as lead compound for the development of a novel class of drugs that uncouple the receptor scaffold interaction and thereby modulate synaptic inhibition *in vivo*.

#### 4.4.4 Theory of Avidity-Enhanced Binding

My experiments that involved multivalent interactions shared common features:

- A potentiated affinity.
- Unaltered molar enthalpic signatures per binding site.
- A major impact of linker length on the overall affinity.

Here I shortly describe the theory of free energy of non-covalent and multivalent interactions reviewed in [218] to (i) compare my findings to the theoretical expectation, to (ii) estimate the potential of avidity mediated binding enhancement, and (iii) identify the major determinants of avidity.

In this work I used the dissociation constant  $K_d$  to describe the affinity of protein-protein interactions. Its inverse, the association constant  $K_a$ , is defined as the ratio between the concentration of two binding partners A and B and their respective complex C:

$$A + B \rightarrow C, \quad K_a = \frac{(C_C)_{eq}}{(C_A)_{eq}(C_B)_{eq}}$$

In case of the bivalent peptide-gephyrin-dimer interaction, the second binding event can be described by the intra-molecular binding constant  $K_i$ , where  $C_C$  and  $C_A$  now describe, respectively, the concentrations of the gephyrin-receptor-complexes with one or both binding site occupied by the bivalent ligand.

$$\frac{(C_C)_{eq}}{(C_A)_{eq}} = K_i$$

Notably, their ratio is solely determined by the probability of each conformation and therefore unaffected by the total concentration of the bivalent peptide. This is an important difference to the inter-molecular binding, where the concentration ratio of bound and free receptors depends on the concentration of the ligand. Comparison between  $K_a$  and  $K_i$  results in:

$$K_i = K_a C_{B,eff}$$

A formal derivation [183] shows that the effective concentration  $C_{B,eff}$  is given by the probability density,  $\rho_L(r)$ , of the end-to-end vector  $r$  of the linker, where  $r_0$  is the end-to-end vector when the ligand is bound to the receptor:

$$K_i = K_a \rho_L(r_0)$$

For flexible linkers the values of the effective concentration mainly depend on linker length and the distance of both binding sites. For linkers extending over the minimal necessary binding site distance, the effective concentration of the intra-molecular binding partner is typically found in the mM range [184]. Therefore, tethering the minimum peptides together achieves a similar effect as having the second ligand present at a fixed concentration of roughly 1 mM. Notably, the affinity

potentiation effect, as well as the high relevance of linker length could be verified for the multivalent receptor gephyrin complex in this thesis.

Using ITC I determined the total possible enthalpy release upon gephyrin-binding of bivalent peptides (GABA<sub>A</sub>R α3 and GlyR β derived) and monovalent peptides (GlyR β derived). Despite their widely differing thermal profiles and  $K_d$ 's in conventional titration experiments I verified a roughly identical enthalpic contribution to the overall binding strength. This argues in favor of entropic effects resulting from the multivalent binding of the bidentate peptides:

Neglecting the fact that concentration varies with temperature, the standard binding entropy under constant pressure can be defined as:

$$\Delta S_b^0 = k_B \ln(C^0 K_a) + k_B T^2 \left( \frac{\partial \ln K_a}{\partial T} \right)_P$$

Where  $k_B$  is the Boltzmann's constant,  $T$  the absolute temperature,  $K_a$  the association constant of the binding reaction and  $C^0$  the standard concentration. In contrast, the binding enthalpy has no dependence on concentration:

$$\Delta H_b = k_B T^2 \left( \frac{\partial \ln K_a}{\partial T} \right)_P$$

Thus, changing the arbitrarily selected value of the standard concentration  $C^0$  shifts both the standard free energy and the standard entropy of binding, but does not affect the enthalpy change. Therefore, avidity-potentiated binding strength is solely based on a more favorable entropic contribution to the free energy. This effect relies on the enhanced local concentration of the second binding ligand which is described by an altered effective concentration, where  $V^0$  describes the accessible volume for second binding step when tethered to gephyrin by the introduced linker:

$$\Delta S_i = \Delta S_b^0 + k_B \ln(V^0 \rho_L(r_0))$$

This equation mirrors (i) the here identified affinity-potentiation for bivalent peptides, (ii) the finding that this effect is solely mediated by entropy but not enthalpy and (iii) the importance of the length of linkage between both peptides. In case of the gephyrin-receptor complex this theory suggests that due to the low minimal binding site distance  $r_0 = 15 \text{ \AA}$ , gephyrin offers a great potential for avidity-mediated binding enhancement. Additionally, it suggests that further optimization of linker length and, if possible, flexibility should result in an affinity enhancement for bivalent gephyrin ligands by several magnitudes.

#### 4.4.5 Gephyrin-Mediated GlyR and GABA<sub>A</sub>R binding Is a Multivalent Process

In comparison to GABA<sub>A</sub>R-derived peptides, the GlyR  $\beta$ -derived peptide displays a remarkably high gephyrin affinity, and I found that the high-affinity binding depends critically on the presence of residues C-terminal to the defined minimum motif. My binding assays and X-ray crystallographic studies verified a unique contribution of this C-terminal region to the stability of the  $\alpha$ -helix formed by these residues. This short  $\alpha$ -helical region which is built up by residues 408-411 (Phe, Glu, Leu, Ser) enables Phe408 and Leu410 to engage in critical hydrophobic interactions with gephyrin Val727 and Pro685. While elongated receptor loop fragments of GABA<sub>A</sub>Rs show a similar potentiated affinity towards gephyrin compared to their minimal fragments, the second binding site of GABA<sub>A</sub>Rs could not be defined on the molecular level. Nevertheless, an aromatic residue, conserved among all gephyrin-binding GABA<sub>A</sub>Rs was identified in this region to be essential for the binding event (GABA<sub>A</sub>R  $\alpha$ 1 Tyr347,  $\alpha$ 2 Tyr346,  $\alpha$ 3 Tyr377). Based on these findings I propose that the GlyR and GABA<sub>A</sub>R gephyrin binding interaction relies on two hotspots as major contributors to the overall binding strength. The first hotspot universally mediates binding of all receptor subunits and is formed by conserved hydrophobic residues engaging gephyrin Phe330. The second hotspot is different between GlyRs and GABA<sub>A</sub>Rs and involves distinct receptor binding sites on the gephyrin surface. Following the presence of two independent binding hotspots I assume that already monomeric GlyR and GABA<sub>A</sub>R subunits bind gephyrin with an avidity-potentiated affinity. This hypothesis would explain my finding that the 15 residues GABA<sub>A</sub>R and GlyR peptides show a magnitudes lower gephyrin affinity than their corresponding elongated fragments. The fact that gephyrin binds GABA<sub>A</sub>Rs with an approximately 100-fold lower affinity than GlyRs can be is at least partially based on a weakened contribution of the N-terminal hotspot. My binding assays with chimeric receptor minimum peptides verified a severe reduction of gephyrin binding upon exchange of the N-terminal GlyR hotspot with the corresponding GABA<sub>A</sub>R hotspots. Namely, introduction of seven GABA<sub>A</sub>R  $\alpha$ 1 residues resulted in a 85-fold reduction, whereas introduction of seven GABA<sub>A</sub>R  $\alpha$ 3 residues resulted in a 10-fold reduction. The described theory would provide a molecular explanation for the following previous findings:

- Gephyrin is copurified with GlyRs but not GABA<sub>A</sub>Rs [28] and video-microscopy analyses revealed that GlyRs [65] have enhanced residence times over GABA<sub>A</sub>Rs [205] at the postsynaptic gephyrin scaffold.
- Colocalization of GlyRs and gephyrin is only fully abolished upon alanine mutation of all hydrophobic residues between GlyR 398 to 410 [21].
- Introduction of phosphomimetic acidic or alanine residues into one of the hotspots decreases the overall affinity into the micromolar range and abolishes the biphasic binding behavior observed in ITC studies with 49 residue peptide [55, 65].
- Gephyrin shows no residual heat release upon titration with the elongated monovalent 49 residue GlyR  $\beta$  peptide after pre-equilibration with the bivalent peptides designed here, despite displaying an apparently higher affinity.
- Determination of the maximal possible enthalpic contributions verified that the extreme difference in binding strength between the GABA<sub>A</sub>R  $\alpha$ 3 subunit, the GlyR  $\beta$  subunit and the bivalent peptide is mediated by entropic effects such as avidity.



- Among the different gephyrin mutants only P713E completely abolishes binding to all receptor subunits. I suggest that this unique feature relies on the ability of this mutant to simultaneously target both binding hotspots by introduction of an acidic residue in between both.
- C-terminally truncated GlyR  $\beta$  peptides show a monophasic binding in the micromolar range and X-ray crystallographic analyses identified the disruption of the C terminal helix upon deletion of GlyR residues that do not directly engage in interactions with gephyrin.

Taken together, I assume that naturally occurring GlyRs and GABA<sub>A</sub>Rs display at least two independent avidity effects. Firstly, an avidity-potentiated affinity by simultaneously occupying two hotspots centered around gephyrin Phe330 and, at least in case of GlyRs, gephyrin Val727. The second avidity effect is based on the presence of two GABA<sub>A</sub>R  $\alpha$  subunits or three GlyR  $\beta$  subunits [14] within a single functional pentameric receptor in combination with the oligomeric nature of gephyrin. Remarkably, both avidity-effects rely on gephyrin's architecture:

- Two subunits naturally occupy two gephyrin binding sites and therefore require two gephyrin E domains in close proximity.
- Remarkably, receptor subunit binding occurs at the dimer-interface of gephyrin's E domain and, even more importantly, each hot spot is solely established by a single gephyrin monomer. Therefore, only a dimerized gephyrin E domain offers two binding hotspots. Following this idea, only full length gephyrin that allows all of its constituting E domains to dimerize will offer the maximal possible receptor binding affinity. Under the assumption that the extraordinary strong trimerization interface of the G domain remains intact it can be concluded that only an hexagonal scaffold offers full receptor binding capacity.

Furthermore I conclude that the here described artificial GlyR-derived dimeric minimum peptides relies only on one of the here described avidity effects, since it targets two binding sites but only the N-terminal hotspots within these binding sites. I therefore assume that it will compete out functional GlyRs less efficient than GABA<sub>A</sub>Rs which have an intrinsically lower gephyrin affinity. Hence, targeting of the receptor binding site within gephyrin, may indeed provide a new pathway to interfere with synaptic inhibition *in vivo* without altering receptor function, but should mainly affect GABAergic transmission.

# 5 Tables

## 5.1 Abbreviations

AA	Acrylamide
Amp	Ampicillin
APS	Ammonium peroxydisulfate
BAA	Bisacrylamide
bbBr	Dibromobimane
BSA	Bovine serum albumin
BMB	1,4-Bismaleidobutane
BMH	1,6-Bismaleidoethane
BMOE	1,2-Bismaleidoethane
BM(PEG) <sub>2</sub>	1,8-Bismaleidodiethylenglycol
Cam	Chloramphenicol
CV	Column volume
Da	Dalton
DTT	Dithiothreitol
DNA	Deoxyribonucleic acid
DNase	deoxyribonuclease
<i>E. coli</i>	<i>Escherichia coli</i>
EDTA	Ethylenediaminetetraacetate
h	Hour
IPTG	Isopropyl-β-thiogalactoside
ITC	Isothermal titration calorimetry
LB	Lysogen broth
M	Molar
min	Minute
mL	Milliliter
MPD	2-Methyl-2,4-pentenediol
MR	Molecular Replacement
MWCO	Molecular weight cut off
NAGE	Native agarose gel electrophoresis
nm	Nanometer
nM	Nanomolar
OD	Optical density
PAGE	Polyacrylamide gel electrophoresis
PCR	Polymerase chain reaction
PEG	Polyethyleneglycol
RT	Room temperature
SDS	Sodium dodecyl sulfate
SEC	Size-exclusion chromatography
TEMED	Tetramethylethylenediamine
μL	Microliter
μM	Micromolar
UV	Ultraviolet
WT	Wild type

## 5.2 Aminoacids

Ala/A	Alanine
Arg/R	Arginine
Asn/N	Asparagine
Asp/D	Asparatic acid
Cys/C	Cysteine
Glu/E	Glutamic acid
Gln/Q	Glutamine
Gly/G	Glycine
His/H	Histidine
Ile/I	Isoleucine
Leu/L	Leucine
Lys/K	Lysine
Met/M	Methionine
Phe/F	Phenylalanine
Pro/P	Proline
Ser/S	Serine
Thr/T	Threonine
Trp/W	Tryptophan
Tyr/Y	Tyrosine
Val/V	Valine

## 5.3 Figures

Figure 1. Architecture of Cys-loop pLGICs. ....	12
Figure 2. Subcellular localization of GABA <sub>A</sub> Rs is determined by their subunit composition. ....	13
Figure 3. Minimum-scheme of receptor clustering at the postsynaptic membrane. ....	15
Figure 4. Architecture of gephyrin. ....	16
Figure 5. Structural basis of gephyrin-mediated GlyR anchoring. ....	17
Figure 6. Residues 360-375 mediate clustering of $\alpha$ 2-containing GABA <sub>A</sub> Rs. ....	19
Figure 7. Architecture and structure of Rho GEFs 4 and 9. ....	20
Figure 8. Structural basis of SH3-mediated CB inhibition. ....	21
Figure 9. Architecture of ERM protein family members. ....	23
Figure 10. Comparison of different FERM domain crystal structures. ....	24
Figure 11. Structural basis of the multiple ligand-binding modes of FERM. ....	25
Figure 12. Mapping of the direct FERM GABA <sub>A</sub> R $\alpha$ 5 subunit interaction. ....	26
Figure 13. Scheme of X-ray diffraction. ....	46
Figure 14. SEC and PAGE confirm the homogeneity of radixin FERM and the GABA <sub>A</sub> R $\alpha$ 5 TM3-4. ....	50
Figure 15. Thermofluor defines the optimal pH and ionic strength of the radixin FERM domain. ....	51
Figure 16. Steady-state fluorescence analysis of the FERM domain $\alpha$ 5-loop complex. ....	52
Figure 17. Analytical SEC of the radixin FERM domain GABA <sub>A</sub> R $\alpha$ 5 complex. ....	52
Figure 18. ITC of the radixin FERM domain GABA <sub>A</sub> R $\alpha$ 5 complex. ....	53
Figure 19. FERM domain pull-down with GABA <sub>A</sub> R $\alpha$ 5 derived peptides. ....	54
Figure 20. Structural basis of FERM domain self-masking. ....	56
Figure 21. SEC, SDS-PAGE and anti-His-blot of the trypsinized FERM- $\alpha$ 5-loop complex. ....	57
Figure 22. Comparison of the $\alpha$ 5-loop binding of radixin FERM (1-310) and FERM (1-295). ....	58
Figure 23. Comparison of FERM domain cocrystal structures. ....	60
Figure 24. Comparison of the $\alpha$ 5-loop binding of His-tagged and un-tagged radixin FERM domain. ....	61
Figure 25. ITC reveals gephyrin's receptor subunit preference. ....	64
Figure 26. Minimum peptides are sufficient to mediate a specific gephyrin pull-down. ....	65
Figure 27. ITC competition assays. ....	66
Figure 28. Gephyrin binds different receptors with a universal binding site. ....	67
Figure 29. Gephyrin engages in receptor subunit specific and conserved interactions. ....	68
Figure 30. Identification of GABA <sub>A</sub> R $\alpha$ 1 and $\alpha$ 3 loop residues critical for gephyrin binding. ....	69
Figure 31. Identification of GephE residues crucial for GABA <sub>A</sub> R $\alpha$ 1 and $\alpha$ 3 binding. ....	70
Figure 32. NAGE verifies an increased GephE affinity for GABA <sub>A</sub> R $\alpha$ 2 V343G. ....	71
Figure 33. NAGE reveals a differential contribution of conserved GABA <sub>A</sub> R key residues. ....	72
Figure 34. Tyrosine-mutations attenuate $\alpha$ 2-mediated GABA <sub>A</sub> R clustering at postsynaptic sites. ....	73
Figure 35. GABA <sub>A</sub> R $\alpha$ 1 Thr348 regulates receptor clustering by modulating GephE affinity. ....	75
Figure 36. U0126, a highly potent MEK1 inhibitor (IC <sub>50</sub> = 14 nM). ....	76
Figure 37. Seven residues of the GlyR $\beta$ peptide display a maximized gephyrin affinity. ....	78
Figure 38. ITC reveals a peptide length dependent GephE affinity of GlyR $\beta$ derived peptides. ....	80
Figure 39. GephE- $\beta$ -loop cocrystal structures reveal structural rearrangements within the GlyR. ....	81
Figure 40. Design of receptor-derived, gephyrin-targeting bivalent peptides. ....	83
Figure 41. The VP-ITC allows stoichiometric one-step peptide dimerization. ....	84
Figure 42. Analytical SEC of different peptides dimerized with various maleimide crosslinkers. ....	85
Figure 43. DSC demonstrates that the dimeric peptides specifically target GephE. ....	86

Figure 44. Thermofluor uncovers a potentiated affinity of GephE for the bivalent peptide. ....	87
Figure 45. ITC based analysis of multivalent receptor binding to gephyrin. ....	88
Figure 46. ITC competition assay between mono- and bivalent gephyrin ligands. ....	89
Figure 47. ITC reveals an affinity potentiation for a GABA <sub>A</sub> R derived peptide upon dimerization. ....	90
Figure 48. CSITE reveals similar enthalpic contributions of different GephE ligands. ....	91
Figure 49. ITC-based comparison of FI-Geph and GephE binding to bivalent peptides. ....	92
Figure 50. Bivalent peptides alter gephyrin's hydrodynamic radius. ....	93
Figure 51. SEC and SDS-PAGE confirm the homogeneity of CB SH3 (4-72). ....	94
Figure 52. Analytical SEC of CB SH3 in the presence of bivalent cations or a chelator. ....	95
Figure 53. The SH3 domain directly interacts with Zn <sup>2+</sup> and Mg <sup>2+</sup> ions. ....	96
Figure 54. Structural basis of SH3 bivalent cation binding. ....	97
Figure 55. SEC analysis of cation-SH3 domain interactions. ....	98
Figure 56. AUC reveals structural rearrangements within the SH3 domain. ....	99
Figure 57. NAGE of the SH3 domain GABA <sub>A</sub> R α1-3 subunit complex. ....	100
Figure 58. Analytical SEC reveals the GABA <sub>A</sub> R subunit preference of the SH3 domain. ....	101
Figure 59. Quantification of GABA <sub>A</sub> R-SH3 interactions via ITC. ....	102
Figure 60. NAGE visualizes that gephyrin and the SH3 domain compete for the α2-loop. ....	106
Figure 61. ITC excludes a possible modulation of the SH3-α2 complex by gephyrin. ....	107
Figure 62. Structural Basis of radixin-mediated GABA <sub>A</sub> R α5 clustering. ....	109
Figure 63. Structural basis of gephyrin-mediated GABA <sub>A</sub> R clustering. ....	110
Figure 64. Minimum scheme of GABA <sub>A</sub> R and GlyR clustering at postsynaptic sites. ....	112
Figure 65. Structure of a gephyrin-targeting, bivalent and membrane-permeable peptide. ....	115

## 5.4 Tables

Table 1. Bacterial strains. ....	28
Table 2. Crosslinker. ....	28
Table 3. Enzymes. ....	29
Table 4. Peptides. ....	29
Table 5. Plasmids. ....	30
Table 6. Crystallization screens. ....	32
Table 7. Low molecular weight chemicals. ....	32
Table 8. Media for bacterial culture. ....	33
Table 9. Buffers for bacterial lysis and transformation. ....	34
Table 10. Protein purification buffers. ....	34
Table 11. Protein interaction buffers. ....	34
Table 12. Protein-Gel Solutions. ....	34
Table 12. Instruments. ....	35
Table 13. Consumables. ....	36
Table 13. Kits. ....	36
Table 14. Software and databases. ....	36
Table 15. QuickChange PCR reaction mix. ....	37
Table 16. QuickChange PCR program. ....	38
Table 17. Affinity chromatography. ....	40
Table 18. Thermofluor reaction mix. ....	41
Table 19. DLS parameters. ....	44
Table 20. Parameters for in-house crystal diffraction evaluation. ....	47
Table 21. Molecular weights of the radixin FERM domain and the GABA <sub>A</sub> R $\alpha$ 5 loop. ....	51
Table 22. Molecular weights of the FERM domain, $\alpha$ 5 loop and their complex. ....	53
Table 23. Binding parameters of the radixin FERM domain $\alpha$ 5-loop complex. ....	53
Table 24. Identification of the GABA <sub>A</sub> R $\alpha$ 5 residues crucial for radixin FERM binding. ....	54
Table 25. Comparison of the N terminal TM3-4 sequences of GABA <sub>A</sub> R $\alpha$ 1-6 subunits. ....	55
Table 26. Radixin FERM (1-310) crystallization, X-ray data collection and refinement statistics. ....	56
Table 27. Radixin FERM (1-295) crystallization, X-ray data collection and refinement statistics. ....	59
Table 28. Comparison of ligand motifs binding to an identical binding site in the FERM domain. ....	61
Table 29. GABA <sub>A</sub> R $\alpha$ 1, $\alpha$ 2, $\alpha$ 3 and GlyR $\beta$ loop gephyrin binding site mapping. ....	63
Table 30. Comparison of the identified minimal peptides sufficient for gephyrin binding. ....	66
Table 31. X-ray data collection and refinement statistics of the GephE-GABA <sub>A</sub> R $\alpha$ 3 complex. ....	67
Table 32. Receptor regions recognized by gephyrin share common features. ....	68
Table 33. Similar receptor residues are critical for GephE binding. ....	69
Table 34. Identification of key residues in GephE required for GABA <sub>A</sub> R and GlyR binding. ....	70
Table 35. GABA <sub>A</sub> Rs and GlyRs are phosphorylated within their gephyrin-binding regions. ....	76
Table 36. Gephyrin E domain binding parameters determined by ITC. ....	80
Table 37. Crystallization, X-ray data collection and refinement tables for the GephE- $\beta$ complexes. ....	82
Table 38. Crosslinkers used for the cysteine-specific peptide dimerization. ....	83
Table 39. Gephyrin E domain binding parameters determined by ITC. ....	88
Table 40. GephE affinities of receptor derived peptides determined by ITC. ....	90
Table 41. Comparison of $\beta$ -20 and ( $\beta$ -20) <sub>2</sub> binding parameters of GephE and Fl-Geph. ....	92

Table 42. Molecular weights of CB SH3 in SEC in the presence of different additives. ....	95
Table 43. Binding parameters of the cation-SH3 interactions determined in ITC. ....	96
Table 44. AUC reveals bivalent cation-dependent rearrangements within the SH3 domain. ....	99
Table 45. Summary of the SH3-GABA <sub>A</sub> R binding parameters as determined by ITC. ....	102
Table 46. Summary of different SH3 ligand binding modes. ....	103
Table 47. Alignment of the different motifs recognized by gephyrin and presumably CB. ....	104
Table 48. Alignment of the large intracellular loops of the GABA <sub>A</sub> R $\alpha$ 1 and $\alpha$ 2 subunits. ....	105
Table 49. Relationship between verified and putative gephyrin-binding GABA <sub>A</sub> R subunits. ....	111

## 5.5 Protein Data Bank References

Data files contained in the PDB archive (<ftp://ftp.wwpdb.org>) are free of all copyright restrictions and made fully and freely available for both non-commercial and commercial use. Nevertheless, I attribute the authors of the structural data discussed in this thesis.

PDB-ID	Year of Publication	Authors
1BBZ	1998	Pisabarro, M.T., Serrano, L., Wilmanns, M.
1CKA	1995	Wu, X., Knudsen, B., Feller, S.M., Zheng, J., Sali, A., Cowburn, D., Hanafusa, H., Kuriyan, J.
1GC6	2000	Hamada, K., Shimizu, T., Matsui, T., Tsukita, S., Hakoshima, T.
1GC7	2000	Hamada, K., Shimizu, T., Matsui, T., Tsukita, S., Hakoshima, T.
1H3H	2003	Liu, Q., Berry, D., Nash, P., Pawson, T., Mcglade, C.J., Li, S.S.
1J19	2003	Hamada, K., Shimizu, T., Yonemura, S., Tsukita, S., Tsukita, S., Hakoshima, T.
1JEG	2001	Ghose, R., Shekhtman, A., Goger, M.J., Ji, H., Cowburn, D.
1K4U	2002	Kami, K., Takeya, R., Sumimoto, H., Kohda, D.
1OEB	2003	Harkiolaki, M., Lewitzky, M., Gilbert, R.J.C., Jones, E.Y., Bourette, R.P., Mouchiroud, G., Sondermann, H., Moarefi, I., Feller, S.M.
1RLQ	1994	Feng, S., Chen, J.K., Yu, H., Simon, J.A., Schreiber, S.L.
1SGH	2004	Finnerty, C.M., Chambers, D., Ingraffea, J., Faber, H.R., Karplus, P.A., Bretscher, A.
1SEM	1994	Lim, W.A., Richards, F.M., Fox, R.O.
1UTI	2004	Lewitzky, M., Harkiolaki, M., Domart, M.C., Jones, E., Feller, S.M.
1ZSG	2005	Mott, H.R., Nietlispach, D., Evetts, K.A., Owen, D.
2D11	2006	Terawaki, S., Maesaki, R., Hakoshima, T.
2D2Q	2006	Kitano, K., Yusa, F., Hakoshima, T.
2DFK	2006	Xiang, S., Kim, E.Y., Connelly, J.J., Nassar, N., Kirsch, J., Winking, J., Schwarz, G., Schindelin, H.
2EMS	2008	Takai, Y., Kitano, K., Terawaki, S., Maesaki, R., Hakoshima, T.
2EMT	2007	Takai, Y., Kitano, K., Terawaki, S., Maesaki, R., Hakoshima, T.
2FTS	2006	Kim, E.Y., Schrader, N., Smolinsky, B., Bedet, C., Vannier, C., Schwarz, G., Schindelin, H.
2G6F	2006	Hoelz, A., Janz, J.M., Lawrie, S.D., Corwin, B., Lee, A., Sakmar, T.P.
2IIM	2007	Romir, J., Lilie, H., Egerer-Sieber, C., Bauer, F., Sticht, H., Muller, Y.A.
2JW4	2009	Santiveri, C.M., Borroto, A., Simon, L., Rico, M., Alarcon, B., Jimenez, M.A.
2JXB	2008	Takeuchi, K., Yang, H., Ng, E., Park, S.Y., Sun, Z.Y., Reinherz, E.L., Wagner, G.
2KXC	2010	Aitio, O., Hellman, M., Kazlauskas, A., Vingadassalom, D.F., Leong, J.M., Saksela, K., Permi, P.
2P4R	2007	Janz, J.M., Sakmar, T.P., Min, K.C.
2PZ1	2007	Mitin, N., Betts, L., Yohe, M.E., Der, C.J., Sondak, J., Rossman, K.L.
2ROL	2008	Aitio, O., Hellman, M., Kesti, T., Kleino, I., Samuilova, O., Paakkonen, K., Tossavainen, H., Saksela, K., Permi, P.
2YSQ	unpublished	Qin, X.R., Hayashi, F., Yokoyama, S.
2YVC	2007	Terawaki, S., Kitano, K., Hakoshima, T.
3BIN	2011	Busam, R.D., Thorsell, A.-G., Flores, A., Hammarstrom, M., Persson, C., Obrink, B., Hallberg, B.M.
3IVF	2010	Elliott, P.R., Goult, B.T., Kopp, P.M., Bate, N., Grossmann, J.G., Roberts, G.C.K., Critchley, D.R., Barsukov, I.L.



## 5.6 Literature References

1. Herculano-Houzel, S., *The human brain in numbers: a linearly scaled-up primate brain*. Frontiers in human neuroscience, 2009. **3**: p. 31.
2. Zuber, B., et al., *The mammalian central nervous synaptic cleft contains a high density of periodically organized complexes*. Proceedings of the National Academy of Sciences of the United States of America, 2005. **102**(52): p. 19192-7.
3. Peters A, P.S., Webster HDF, *The Fine Structure of the Nervous System*. Oxford Univ Press, 1991.
4. Olsen, R.W. and W. Sieghart, *GABA A receptors: subtypes provide diversity of function and pharmacology*. Neuropharmacology, 2009. **56**(1): p. 141-8.
5. Betz, H., *Ligand-gated ion channels in the brain: the amino acid receptor superfamily*. Neuron, 1990. **5**(4): p. 383-92.
6. Brejc, K., et al., *Crystal structure of an ACh-binding protein reveals the ligand-binding domain of nicotinic receptors*. Nature, 2001. **411**(6835): p. 269-76.
7. Hilf, R.J. and R. Dutzler, *X-ray structure of a prokaryotic pentameric ligand-gated ion channel*. Nature, 2008. **452**(7185): p. 375-9.
8. Hilf, R.J. and R. Dutzler, *Structure of a potentially open state of a proton-activated pentameric ligand-gated ion channel*. Nature, 2009. **457**(7225): p. 115-8.
9. Bocquet, N., et al., *X-ray structure of a pentameric ligand-gated ion channel in an apparently open conformation*. Nature, 2009. **457**(7225): p. 111-4.
10. Kuhse, J., et al., *Alternative splicing generates two isoforms of the alpha 2 subunit of the inhibitory glycine receptor*. FEBS letters, 1991. **283**(1): p. 73-7.
11. Kuhse, J., et al., *Heterogeneity of the inhibitory glycine receptor*. Annals of the New York Academy of Sciences, 1991. **625**: p. 129-35.
12. Malosio, M.L., et al., *Alternative splicing generates two variants of the alpha 1 subunit of the inhibitory glycine receptor*. The Journal of biological chemistry, 1991. **266**(4): p. 2048-53.
13. Leite, J.F. and M. Cascio, *Structure of ligand-gated ion channels: critical assessment of biochemical data supports novel topology*. Molecular and cellular neurosciences, 2001. **17**(5): p. 777-92.
14. Grudzinska, J., et al., *The beta subunit determines the ligand binding properties of synaptic glycine receptors*. Neuron, 2005. **45**(5): p. 727-39.
15. Sarto-Jackson, I. and W. Sieghart, *Assembly of GABA(A) receptors (Review)*. Mol Membr Biol, 2008. **25**(4): p. 302-10.
16. Whiting, P., R.M. McKernan, and L.L. Iversen, *Another mechanism for creating diversity in gamma-aminobutyrate type A receptors: RNA splicing directs expression of two forms of gamma 2 phosphorylation site*. Proceedings of the National Academy of Sciences of the United States of America, 1990. **87**(24): p. 9966-70.
17. McKinley, D.D., D.J. Lennon, and D.B. Carter, *Cloning, sequence analysis and expression of two forms of mRNA coding for the human beta 2 subunit of the GABAA receptor*. Brain research. Molecular brain research, 1995. **28**(1): p. 175-9.
18. Olsen, R.W. and W. Sieghart, *International Union of Pharmacology. LXX. Subtypes of gamma-aminobutyric acid(A) receptors: classification on the basis of subunit composition, pharmacology, and function. Update*. Pharmacological reviews, 2008. **60**(3): p. 243-60.
19. Meyer, G., et al., *Identification of a gephyrin binding motif on the glycine receptor beta subunit*. Neuron, 1995. **15**(3): p. 563-72.
20. Meier, J., et al., *Fast and reversible trapping of surface glycine receptors by gephyrin*. Nature Neuroscience, 2001. **4**(3): p. 253-60.
21. Kneussel, M., et al., *Hydrophobic interactions mediate binding of the glycine receptor beta-subunit to gephyrin*. Journal of neurochemistry, 1999. **72**(3): p. 1323-6.

22. Perrais, D. and N. Ropert, *Effect of zolpidem on miniature IPSCs and occupancy of postsynaptic GABAA receptors in central synapses*. The Journal of neuroscience : the official journal of the Society for Neuroscience, 1999. **19**(2): p. 578-88.
23. Brunig, I., et al., *Intact sorting, targeting, and clustering of gamma-aminobutyric acid A receptor subtypes in hippocampal neurons in vitro*. The Journal of comparative neurology, 2002. **443**(1): p. 43-55.
24. Crestani, F., et al., *Trace fear conditioning involves hippocampal alpha5 GABA(A) receptors*. Proceedings of the National Academy of Sciences of the United States of America, 2002. **99**(13): p. 8980-5.
25. Serwanski, D.R., et al., *Synaptic and nonsynaptic localization of GABAA receptors containing the alpha5 subunit in the rat brain*. The Journal of comparative neurology, 2006. **499**(3): p. 458-70.
26. Loeblich, S., et al., *Activated radixin is essential for GABAA receptor alpha5 subunit anchoring at the actin cytoskeleton*. The EMBO journal, 2006. **25**(5): p. 987-99.
27. Tretter, V., et al., *The clustering of GABA(A) receptor subtypes at inhibitory synapses is facilitated via the direct binding of receptor alpha 2 subunits to gephyrin*. J Neurosci, 2008. **28**(6): p. 1356-65.
28. Pfeiffer, F., D. Graham, and H. Betz, *Purification by affinity chromatography of the glycine receptor of rat spinal cord*. The Journal of biological chemistry, 1982. **257**(16): p. 9389-93.
29. Dumoulin, A., et al., *Formation of mixed glycine and GABAergic synapses in cultured spinal cord neurons*. The European journal of neuroscience, 2000. **12**(11): p. 3883-92.
30. Prior, P., et al., *Primary structure and alternative splice variants of gephyrin, a putative glycine receptor-tubulin linker protein*. Neuron, 1992. **8**(6): p. 1161-70.
31. Kirsch, J., et al., *Gephyrin antisense oligonucleotides prevent glycine receptor clustering in spinal neurons*. Nature, 1993. **366**(6457): p. 745-8.
32. Stallmeyer, B., et al., *The neurotransmitter receptor-anchoring protein gephyrin reconstitutes molybdenum cofactor biosynthesis in bacteria, plants, and mammalian cells*. Proceedings of the National Academy of Sciences of the United States of America, 1999. **96**(4): p. 1333-8.
33. Feng, G., et al., *Dual requirement for gephyrin in glycine receptor clustering and molybdoenzyme activity*. Science, 1998. **282**(5392): p. 1321-4.
34. Mulhardt, C., et al., *The spastic mouse: aberrant splicing of glycine receptor beta subunit mRNA caused by intronic insertion of L1 element*. Neuron, 1994. **13**(4): p. 1003-15.
35. Ramming, M., H. Betz, and J. Kirsch, *Analysis of the promoter region of the murine gephyrin gene*. FEBS letters, 1997. **405**(2): p. 137-40.
36. Rees, M.I., et al., *Isoform heterogeneity of the human gephyrin gene (GPHN), binding domains to the glycine receptor, and mutation analysis in hyperekplexia*. The Journal of biological chemistry, 2003. **278**(27): p. 24688-96.
37. Kirsch, J., et al., *The 93-kDa glycine receptor-associated protein binds to tubulin*. J Biol Chem, 1991. **266**(33): p. 22242-5.
38. Mammoto, A., et al., *Interactions of drebrin and gephyrin with profilin*. Biochemical and biophysical research communications, 1998. **243**(1): p. 86-9.
39. Giesemann, T., et al., *Complex formation between the postsynaptic scaffolding protein gephyrin, profilin, and Mena: a possible link to the microfilament system*. J Neurosci, 2003. **23**(23): p. 8330-9.
40. Zita, M.M., et al., *Post-phosphorylation prolyl isomerisation of gephyrin represents a mechanism to modulate glycine receptors function*. The EMBO journal, 2007. **26**(7): p. 1761-71.
41. Pouloupoulos, A., et al., *Neuroigin 2 drives postsynaptic assembly at perisomatic inhibitory synapses through gephyrin and collybistin*. Neuron, 2009. **63**(5): p. 628-42.
42. Jedlicka, P., et al., *Increased dentate gyrus excitability in neuroigin-2-deficient mice in vivo*. Cerebral cortex, 2011. **21**(2): p. 357-67.

43. Harvey, K., et al., *The GDP-GTP exchange factor collybistin: an essential determinant of neuronal gephyrin clustering*. The Journal of neuroscience : the official journal of the Society for Neuroscience, 2004. **24**(25): p. 5816-26.
44. Maas, C., et al., *Neuronal cotransport of glycine receptor and the scaffold protein gephyrin*. The Journal of cell biology, 2006. **172**(3): p. 441-51.
45. Fuhrmann, J.C., et al., *Gephyrin interacts with Dynein light chains 1 and 2, components of motor protein complexes*. The Journal of neuroscience : the official journal of the Society for Neuroscience, 2002. **22**(13): p. 5393-402.
46. Wang, H., et al., *GABA(A)-receptor-associated protein links GABA(A) receptors and the cytoskeleton*. Nature, 1999. **397**(6714): p. 69-72.
47. Kneussel, M., et al., *The gamma-aminobutyric acid type A receptor (GABAAR)-associated protein GABARAP interacts with gephyrin but is not involved in receptor anchoring at the synapse*. Proceedings of the National Academy of Sciences of the United States of America, 2000. **97**(15): p. 8594-9.
48. O'Sullivan, G.A., et al., *GABARAP is not essential for GABA receptor targeting to the synapse*. The European journal of neuroscience, 2005. **22**(10): p. 2644-8.
49. Kittler, J.T., et al., *The subcellular distribution of GABARAP and its ability to interact with NSF suggest a role for this protein in the intracellular transport of GABA(A) receptors*. Molecular and cellular neurosciences, 2001. **18**(1): p. 13-25.
50. Bavro, V.N., et al., *Crystal structure of the GABA(A)-receptor-associated protein, GABARAP*. EMBO reports, 2002. **3**(2): p. 183-9.
51. Liu, M.T., et al., *Crystal structure of the gephyrin-related molybdenum cofactor biosynthesis protein MogA from Escherichia coli*. The Journal of biological chemistry, 2000. **275**(3): p. 1814-22.
52. Xiang, S., et al., *The crystal structure of Escherichia coli MoeA and its relationship to the multifunctional protein gephyrin*. Structure, 2001. **9**(4): p. 299-310.
53. Kneussel, M. and H. Betz, *Receptors, gephyrin and gephyrin-associated proteins: novel insights into the assembly of inhibitory postsynaptic membrane specializations*. The Journal of physiology, 2000. **525 Pt 1**: p. 1-9.
54. Sola, M., et al., *Structural basis of dynamic glycine receptor clustering by gephyrin*. The EMBO journal, 2004. **23**(13): p. 2510-9.
55. Kim, E.Y., et al., *Deciphering the structural framework of glycine receptor anchoring by gephyrin*. The EMBO journal, 2006. **25**(6): p. 1385-95.
56. Schwarz, G., et al., *Crystal structures of human gephyrin and plant Cnx1 G domains: comparative analysis and functional implications*. Journal of molecular biology, 2001. **312**(2): p. 405-18.
57. Sola, M., et al., *X-ray crystal structure of the trimeric N-terminal domain of gephyrin*. The Journal of biological chemistry, 2001. **276**(27): p. 25294-301.
58. Schrader, N., et al., *Biochemical characterization of the high affinity binding between the glycine receptor and gephyrin*. The Journal of biological chemistry, 2004. **279**(18): p. 18733-41.
59. Bedet, C., et al., *Regulation of gephyrin assembly and glycine receptor synaptic stability*. The Journal of biological chemistry, 2006. **281**(40): p. 30046-56.
60. Saiyed, T., et al., *Molecular basis of gephyrin clustering at inhibitory synapses: role of G- and E-domain interactions*. The Journal of biological chemistry, 2007. **282**(8): p. 5625-32.
61. Herweg, J. and G. Schwarz, *Splice-specific glycine receptor binding, folding, and phosphorylation of the scaffolding protein gephyrin*. The Journal of biological chemistry, 2012.
62. Meier, J. and R. Grantyn, *A gephyrin-related mechanism restraining glycine receptor anchoring at GABAergic synapses*. The Journal of neuroscience : the official journal of the Society for Neuroscience, 2004. **24**(6): p. 1398-405.

63. Kirsch, J. and H. Betz, *The postsynaptic localization of the glycine receptor-associated protein gephyrin is regulated by the cytoskeleton*. The Journal of neuroscience : the official journal of the Society for Neuroscience, 1995. **15**(6): p. 4148-56.
64. Kirsch, J. and H. Betz, *Glycine-receptor activation is required for receptor clustering in spinal neurons*. Nature, 1998. **392**(6677): p. 717-20.
65. Specht, C.G., et al., *Regulation of glycine receptor diffusion properties and gephyrin interactions by protein kinase C*. The EMBO journal, 2011. **30**(18): p. 3842-53.
66. Levi, S., et al., *Synaptic control of glycine and GABA(A) receptors and gephyrin expression in cultured motoneurons*. The Journal of neuroscience : the official journal of the Society for Neuroscience, 1999. **19**(17): p. 7434-49.
67. Sagne, C., et al., *Cloning of a functional vesicular GABA and glycine transporter by screening of genome databases*. FEBS letters, 1997. **417**(2): p. 177-83.
68. Sassoe-Pognetto, M., et al., *Colocalization of gephyrin and GABAA-receptor subunits in the rat retina*. The Journal of comparative neurology, 1995. **357**(1): p. 1-14.
69. Essrich, C., et al., *Postsynaptic clustering of major GABAA receptor subtypes requires the gamma 2 subunit and gephyrin*. Nature Neuroscience, 1998. **1**(7): p. 563-71.
70. Sassoe-Pognetto, M., et al., *Colocalization of multiple GABA(A) receptor subtypes with gephyrin at postsynaptic sites*. The Journal of comparative neurology, 2000. **420**(4): p. 481-98.
71. Kneussel, M., et al., *Loss of postsynaptic GABA(A) receptor clustering in gephyrin-deficient mice*. The Journal of neuroscience : the official journal of the Society for Neuroscience, 1999. **19**(21): p. 9289-97.
72. Kneussel, M., et al., *Gephyrin-independent clustering of postsynaptic GABA(A) receptor subtypes*. Molecular and cellular neurosciences, 2001. **17**(6): p. 973-82.
73. Levi, S., et al., *Gephyrin is critical for glycine receptor clustering but not for the formation of functional GABAergic synapses in hippocampal neurons*. The Journal of neuroscience : the official journal of the Society for Neuroscience, 2004. **24**(1): p. 207-17.
74. Schweizer, C., et al., *The gamma 2 subunit of GABA(A) receptors is required for maintenance of receptors at mature synapses*. Molecular and cellular neurosciences, 2003. **24**(2): p. 442-50.
75. Kralic, J.E., et al., *Compensatory alteration of inhibitory synaptic circuits in cerebellum and thalamus of gamma-aminobutyric acid type A receptor alpha1 subunit knockout mice*. The Journal of comparative neurology, 2006. **495**(4): p. 408-21.
76. Studer, R., et al., *Alteration of GABAergic synapses and gephyrin clusters in the thalamic reticular nucleus of GABAA receptor alpha3 subunit-null mice*. The European journal of neuroscience, 2006. **24**(5): p. 1307-15.
77. Patrizi, A., et al., *Synapse formation and clustering of neuroligin-2 in the absence of GABAA receptors*. Proceedings of the National Academy of Sciences of the United States of America, 2008. **105**(35): p. 13151-6.
78. Alldred, M.J., et al., *Distinct gamma2 subunit domains mediate clustering and synaptic function of postsynaptic GABAA receptors and gephyrin*. J Neurosci, 2005. **25**(3): p. 594-603.
79. Christie, S.B., et al., *Clustered and non-clustered GABAA receptors in cultured hippocampal neurons*. Molecular and cellular neurosciences, 2006. **31**(1): p. 1-14.
80. Baer, K., et al., *Rescue of gamma2 subunit-deficient mice by transgenic overexpression of the GABAA receptor gamma2S or gamma2L subunit isoforms*. The European journal of neuroscience, 2000. **12**(7): p. 2639-43.
81. Yu, W., et al., *Gephyrin clustering is required for the stability of GABAergic synapses*. Molecular and cellular neurosciences, 2007. **36**(4): p. 484-500.
82. Kasugai, Y., et al., *Quantitative localisation of synaptic and extrasynaptic GABAA receptor subunits on hippocampal pyramidal cells by freeze-fracture replica immunolabelling*. The European journal of neuroscience, 2010. **32**(11): p. 1868-88.
83. Kneussel, M., *Postsynaptic scaffold proteins at non-synaptic sites. The role of postsynaptic scaffold proteins in motor-protein-receptor complexes*. EMBO reports, 2005. **6**(1): p. 22-7.

84. Saiepour, L., et al., *Complex role of collybistin and gephyrin in GABAA receptor clustering*. The Journal of biological chemistry, 2010. **285**(38): p. 29623-31.
85. Wherlock, M. and H. Mellor, *The Rho GTPase family: a Racs to Wrchs story*. Journal of cell science, 2002. **115**(Pt 2): p. 239-40.
86. Reid, T., et al., *Identification and characterization of hPEM-2, a guanine nucleotide exchange factor specific for Cdc42*. The Journal of biological chemistry, 1999. **274**(47): p. 33587-93.
87. Kins, S., H. Betz, and J. Kirsch, *Collybistin, a newly identified brain-specific GEF, induces submembrane clustering of gephyrin*. Nature Neuroscience, 2000. **3**(1): p. 22-9.
88. Grosskreutz, Y., et al., *Identification of a gephyrin-binding motif in the GDP/GTP exchange factor collybistin*. Biological chemistry, 2001. **382**(10): p. 1455-62.
89. Erickson, J.W. and R.A. Cerione, *Multiple roles for Cdc42 in cell regulation*. Current opinion in cell biology, 2001. **13**(2): p. 153-7.
90. Kneussel, M. and H. Betz, *Clustering of inhibitory neurotransmitter receptors at developing postsynaptic sites: the membrane activation model*. Trends in neurosciences, 2000. **23**(9): p. 429-35.
91. Reddy-Alla, S., et al., *PH-domain-driven targeting of collybistin but not Cdc42 activation is required for synaptic gephyrin clustering*. The European journal of neuroscience, 2010. **31**(7): p. 1173-84.
92. Fritschy, J.M., P. Panzanelli, and S.K. Tyagarajan, *Molecular and functional heterogeneity of GABAergic synapses*. Cellular and molecular life sciences : CMLS, 2012.
93. Kavran, J.M., et al., *Specificity and promiscuity in phosphoinositide binding by pleckstrin homology domains*. The Journal of biological chemistry, 1998. **273**(46): p. 30497-508.
94. Xiang, S., et al., *The crystal structure of Cdc42 in complex with collybistin II, a gephyrin-interacting guanine nucleotide exchange factor*. Journal of molecular biology, 2006. **359**(1): p. 35-46.
95. Murayama, K., et al., *Crystal structure of the rac activator, Asef, reveals its autoinhibitory mechanism*. The Journal of biological chemistry, 2007. **282**(7): p. 4238-42.
96. Kalscheuer, V.M., et al., *A balanced chromosomal translocation disrupting ARHGEF9 is associated with epilepsy, anxiety, aggression, and mental retardation*. Human mutation, 2009. **30**(1): p. 61-8.
97. Patrizi, A., et al., *Selective localization of collybistin at a subset of inhibitory synapses in brain circuits*. The Journal of comparative neurology, 2012. **520**(1): p. 130-41.
98. Heller, E.A., et al., *The biochemical anatomy of cortical inhibitory synapses*. PloS one, 2012. **7**(6): p. e39572.
99. Papadopoulos, T., et al., *Impaired GABAergic transmission and altered hippocampal synaptic plasticity in collybistin-deficient mice*. The EMBO journal, 2007. **26**(17): p. 3888-99.
100. Gomeza, J., et al., *Deletion of the mouse glycine transporter 2 results in a hyperekplexia phenotype and postnatal lethality*. Neuron, 2003. **40**(4): p. 797-806.
101. Crestani, F., et al., *Decreased GABAA-receptor clustering results in enhanced anxiety and a bias for threat cues*. Nature Neuroscience, 1999. **2**(9): p. 833-9.
102. Tsukita, S. and Y. Hieda, *A new 82-kD barbed end-capping protein (radixin) localized in the cell-to-cell adherens junction: purification and characterization*. The Journal of cell biology, 1989. **108**(6): p. 2369-82.
103. Kitajiri, S., et al., *Radixin deficiency causes deafness associated with progressive degeneration of cochlear stereocilia*. The Journal of cell biology, 2004. **166**(4): p. 559-70.
104. Zhao, H., et al., *Large membrane domains in hair bundles specify spatially constricted radixin activation*. The Journal of neuroscience : the official journal of the Society for Neuroscience, 2012. **32**(13): p. 4600-9.
105. Khan, S.Y., et al., *Mutations of the RDX gene cause nonsyndromic hearing loss at the DFNB24 locus*. Human mutation, 2007. **28**(5): p. 417-23.
106. He, X.J., et al., *The effect of radixin knockdown on the expression and efflux function of MRP2 in SGC-7901 cells*. European journal of pharmaceutical sciences : official journal of the European Federation for Pharmaceutical Sciences, 2012.

107. Kikuchi, S., et al., *Radixin deficiency causes conjugated hyperbilirubinemia with loss of Mrp2 from bile canalicular membranes*. Nature genetics, 2002. **31**(3): p. 320-5.
108. Serrador, J.M., et al., *Moesin interacts with the cytoplasmic region of intercellular adhesion molecule-3 and is redistributed to the uropod of T lymphocytes during cell polarization*. The Journal of cell biology, 1997. **138**(6): p. 1409-23.
109. Ivetic, A., et al., *The cytoplasmic tail of L-selectin interacts with members of the Ezrin-Radixin-Moesin (ERM) family of proteins: cell activation-dependent binding of Moesin but not Ezrin*. The Journal of biological chemistry, 2002. **277**(3): p. 2321-9.
110. Bono, P., et al., *Layilin, a cell surface hyaluronan receptor, interacts with merlin and radixin*. Experimental cell research, 2005. **308**(1): p. 177-87.
111. Takai, Y., et al., *Crystallographic characterization of the radixin FERM domain bound to the cytoplasmic tails of adhesion molecules CD43 and PSGL-1*. Acta crystallographica. Section F, Structural biology and crystallization communications, 2007. **63**(Pt 1): p. 49-51.
112. Tang, P., et al., *Cytoskeletal protein radixin activates integrin alpha(M)beta(2) by binding to its cytoplasmic tail*. FEBS letters, 2007. **581**(6): p. 1103-8.
113. Terawaki, S., et al., *Crystallographic characterization of the radixin FERM domain bound to the cytoplasmic tail of membrane-type 1 matrix metalloproteinase (MT1-MMP)*. Acta crystallographica. Section F, Structural biology and crystallization communications, 2008. **64**(Pt 10): p. 911-3.
114. Bretscher, A., K. Edwards, and R.G. Fehon, *ERM proteins and merlin: integrators at the cell cortex*. Nature reviews. Molecular cell biology, 2002. **3**(8): p. 586-99.
115. Derouiche, A. and M. Frotscher, *Peripheral astrocyte processes: monitoring by selective immunostaining for the actin-binding ERM proteins*. Glia, 2001. **36**(3): p. 330-41.
116. Mintz, C.D., et al., *ERMs colocalize transiently with L1 during neocortical axon outgrowth*. The Journal of comparative neurology, 2003. **464**(4): p. 438-48.
117. Paglini, G., et al., *Suppression of radixin and moesin alters growth cone morphology, motility, and process formation in primary cultured neurons*. The Journal of cell biology, 1998. **143**(2): p. 443-55.
118. Dickson, T.C., et al., *Functional binding interaction identified between the axonal CAM L1 and members of the ERM family*. The Journal of cell biology, 2002. **157**(7): p. 1105-12.
119. Haas, M.A., J.C. Vickers, and T.C. Dickson, *Binding partners L1 cell adhesion molecule and the ezrin-radixin-moesin (ERM) proteins are involved in development and the regenerative response to injury of hippocampal and cortical neurons*. The European journal of neuroscience, 2004. **20**(6): p. 1436-44.
120. Fehon, R.G., A.I. McClatchey, and A. Bretscher, *Organizing the cell cortex: the role of ERM proteins*. Nature reviews. Molecular cell biology, 2010. **11**(4): p. 276-87.
121. Neisch, A.L. and R.G. Fehon, *Ezrin, Radixin and Moesin: key regulators of membrane-cortex interactions and signaling*. Current opinion in cell biology, 2011. **23**(4): p. 377-82.
122. Castelo, L. and D.G. Jay, *Radixin is involved in lamellipodial stability during nerve growth cone motility*. Molecular biology of the cell, 1999. **10**(5): p. 1511-20.
123. Bretscher, A., R. Gary, and M. Berryman, *Soluble ezrin purified from placenta exists as stable monomers and elongated dimers with masked C-terminal ezrin-radixin-moesin association domains*. Biochemistry, 1995. **34**(51): p. 16830-7.
124. Matsui, T., et al., *Rho-kinase phosphorylates COOH-terminal threonines of ezrin/radixin/moesin (ERM) proteins and regulates their head-to-tail association*. The Journal of cell biology, 1998. **140**(3): p. 647-57.
125. Smith, W.J., et al., *Structure of the active N-terminal domain of Ezrin. Conformational and mobility changes identify keystone interactions*. The Journal of biological chemistry, 2003. **278**(7): p. 4949-56.
126. Hamada, K., et al., *Crystallographic characterization of the membrane-binding domain of radixin*. Acta crystallographica. Section D, Biological crystallography, 2000. **56**(Pt 7): p. 922-3.

127. Edwards, S.D. and N.H. Keep, *The 2.7 Å crystal structure of the activated FERM domain of moesin: an analysis of structural changes on activation*. *Biochemistry*, 2001. **40**(24): p. 7061-8.
128. Elliott, P.R., et al., *The Structure of the talin head reveals a novel extended conformation of the FERM domain*. *Structure*, 2010. **18**(10): p. 1289-99.
129. Shimizu, T., et al., *Structural basis for neurofibromatosis type 2. Crystal structure of the merlin FERM domain*. *The Journal of biological chemistry*, 2002. **277**(12): p. 10332-6.
130. Yogesha, S.D., et al., *Unfurling of the band 4.1, ezrin, radixin, moesin (FERM) domain of the merlin tumor suppressor*. *Protein science : a publication of the Protein Society*, 2011. **20**(12): p. 2113-20.
131. Busam, R.D., et al., *Structural basis of tumor suppressor in lung cancer 1 (TSLC1) binding to differentially expressed in adenocarcinoma of the lung (DAL-1/4.1B)*. *The Journal of biological chemistry*, 2011. **286**(6): p. 4511-6.
132. Hirano, Y., et al., *Structural basis of cargo recognition by the myosin-X MyTH4-FERM domain*. *The EMBO journal*, 2011. **30**(13): p. 2734-47.
133. Ceccarelli, D.F., et al., *Crystal structure of the FERM domain of focal adhesion kinase*. *The Journal of biological chemistry*, 2006. **281**(1): p. 252-9.
134. Nunomura, W., et al., *Structural stabilization of protein 4.1R FERM domain upon binding to apo-calmodulin: novel insights into the biological significance of the calcium-independent binding of calmodulin to protein 4.1R*. *The Biochemical journal*, 2011. **440**(3): p. 367-74.
135. Terawaki, S., K. Kitano, and T. Hakoshima, *Structural basis for type II membrane protein binding by ERM proteins revealed by the radixin-neutral endopeptidase 24.11 (NEP) complex*. *The Journal of biological chemistry*, 2007. **282**(27): p. 19854-62.
136. Mori, T., et al., *Structural basis for CD44 recognition by ERM proteins*. *The Journal of biological chemistry*, 2008. **283**(43): p. 29602-12.
137. Finnerty, C.M., et al., *The EBP50-moesin interaction involves a binding site regulated by direct masking on the FERM domain*. *Journal of cell science*, 2004. **117**(Pt 8): p. 1547-52.
138. Terawaki, S., R. Maesaki, and T. Hakoshima, *Structural basis for NHERF recognition by ERM proteins*. *Structure*, 2006. **14**(4): p. 777-89.
139. Li, Q., et al., *Self-masking in an intact ERM-merlin protein: an active role for the central alpha-helical domain*. *Journal of molecular biology*, 2007. **365**(5): p. 1446-59.
140. Pearson, M.A., et al., *Structure of the ERM protein moesin reveals the FERM domain fold masked by an extended actin binding tail domain*. *Cell*, 2000. **101**(3): p. 259-70.
141. Jayaraman, B. and L.K. Nicholson, *Thermodynamic dissection of the Ezrin FERM/CERMAD interface*. *Biochemistry*, 2007. **46**(43): p. 12174-89.
142. Reczek, D. and A. Bretscher, *The carboxyl-terminal region of EBP50 binds to a site in the amino-terminal domain of ezrin that is masked in the dormant molecule*. *The Journal of biological chemistry*, 1998. **273**(29): p. 18452-8.
143. Magendantz, M., et al., *Interdomain interactions of radixin in vitro*. *The Journal of biological chemistry*, 1995. **270**(43): p. 25324-7.
144. Madsen, C.S., et al., *The Guinea pig as a preclinical model for demonstrating the efficacy and safety of statins*. *The Journal of pharmacology and experimental therapeutics*, 2008. **324**(2): p. 576-86.
145. Kitano, K., F. Yusa, and T. Hakoshima, *Structure of dimerized radixin FERM domain suggests a novel masking motif in C-terminal residues 295-304*. *Acta crystallographica. Section F, Structural biology and crystallization communications*, 2006. **62**(Pt 4): p. 340-5.
146. Fievet, B.T., et al., *Phosphoinositide binding and phosphorylation act sequentially in the activation mechanism of ezrin*. *The Journal of cell biology*, 2004. **164**(5): p. 653-9.
147. Simons, P.C., et al., *C-terminal threonine phosphorylation activates ERM proteins to link the cell's cortical lipid bilayer to the cytoskeleton*. *Biochemical and biophysical research communications*, 1998. **253**(3): p. 561-5.
148. Ishikawa, H., et al., *Structural conversion between open and closed forms of radixin: low-angle shadowing electron microscopy*. *Journal of molecular biology*, 2001. **310**(5): p. 973-8.

149. Hamada, K., et al., *Structural basis of the membrane-targeting and unmasking mechanisms of the radixin FERM domain*. The EMBO journal, 2000. **19**(17): p. 4449-62.
150. Barret, C., et al., *Mutagenesis of the phosphatidylinositol 4,5-bisphosphate (PIP(2)) binding site in the NH(2)-terminal domain of ezrin correlates with its altered cellular distribution*. The Journal of cell biology, 2000. **151**(5): p. 1067-80.
151. Brunig, I., et al., *GABAergic terminals are required for postsynaptic clustering of dystrophin but not of GABA(A) receptors and gephyrin*. The Journal of neuroscience : the official journal of the Society for Neuroscience, 2002. **22**(12): p. 4805-13.
152. Hutcheon, B., J.M. Fritschy, and M.O. Poulter, *Organization of GABA receptor alpha-subunit clustering in the developing rat neocortex and hippocampus*. The European journal of neuroscience, 2004. **19**(9): p. 2475-87.
153. Albrecht, J., A.S. Bender, and M.D. Norenberg, *Potassium-stimulated GABA release is a chloride-dependent but sodium- and calcium-independent process in cultured astrocytes*. Acta neurobiologiae experimentalis, 1998. **58**(3): p. 169-75.
154. Barakat, L. and A. Bordey, *GAT-1 and reversible GABA transport in Bergmann glia in slices*. Journal of neurophysiology, 2002. **88**(3): p. 1407-19.
155. Hardingham, G.E., Y. Fukunaga, and H. Bading, *Extrasynaptic NMDARs oppose synaptic NMDARs by triggering CREB shut-off and cell death pathways*. Nature Neuroscience, 2002. **5**(5): p. 405-14.
156. *The CCP4 suite: programs for protein crystallography*. Acta Crystallogr D Biol Crystallogr, 1994. **50**(Pt 5): p. 760-3.
157. Emsley, P. and K. Cowtan, *Coot: model-building tools for molecular graphics*. Acta crystallographica. Section D, Biological crystallography, 2004. **60**(Pt 12 Pt 1): p. 2126-32.
158. Battye, T.G., et al., *iMOSFLM: a new graphical interface for diffraction-image processing with MOSFLM*. Acta Crystallogr D Biol Crystallogr, 2011. **67**(Pt 4): p. 271-81.
159. Davis, I.W., et al., *MolProbity: all-atom contacts and structure validation for proteins and nucleic acids*. Nucleic acids research, 2007. **35**(Web Server issue): p. W375-83.
160. McCoy, A.J., et al., *Phaser crystallographic software*. Journal of applied crystallography, 2007. **40**(Pt 4): p. 658-674.
161. Adams, P.D., et al., *PHENIX: a comprehensive Python-based system for macromolecular structure solution*. Acta crystallographica. Section D, Biological crystallography, 2010. **66**(Pt 2): p. 213-21.
162. Murshudov, G.N., A.A. Vagin, and E.J. Dodson, *Refinement of macromolecular structures by the maximum-likelihood method*. Acta crystallographica. Section D, Biological crystallography, 1997. **53**(Pt 3): p. 240-55.
163. Evans, P., *Scaling and assessment of data quality*. Acta crystallographica. Section D, Biological crystallography, 2006. **62**(Pt 1): p. 72-82.
164. Kabsch, W., *Xds*. Acta crystallographica. Section D, Biological crystallography, 2010. **66**(Pt 2): p. 125-32.
165. Wang, W. and B.A. Malcolm, *Two-stage PCR protocol allowing introduction of multiple mutations, deletions and insertions using QuikChange Site-Directed Mutagenesis*. BioTechniques, 1999. **26**(4): p. 680-2.
166. Laemmli, U.K., *Cleavage of structural proteins during the assembly of the head of bacteriophage T4*. Nature, 1970. **227**(5259): p. 680-5.
167. Pfeiffer, H. and H. Liebhafsky, *The origins of Beer's law*. Journal of Chemical Education, 1951. **28**: p. 123-125.
168. Matulis, D., et al., *Thermodynamic stability of carbonic anhydrase: measurements of binding affinity and stoichiometry using ThermoFluor*. Biochemistry, 2005. **44**(13): p. 5258-66.
169. Brunger, A.T., *Free R value: cross-validation in crystallography*. Methods in enzymology, 1997. **277**: p. 366-96.
170. Kleywegt, G.J. and T.A. Jones, *Model building and refinement practice*. Methods in enzymology, 1997. **277**: p. 208-30.



171. Denis, N.J., et al., *Tryptic digestion of ubiquitin standards reveals an improved strategy for identifying ubiquitinated proteins by mass spectrometry*. Proteomics, 2007. **7**(6): p. 868-74.
172. Bell-Horner, C.L., et al., *ERK/MAPK pathway regulates GABAA receptors*. Journal of neurobiology, 2006. **66**(13): p. 1467-74.
173. Marshall, C.J., *MAP kinase kinase kinase, MAP kinase kinase and MAP kinase*. Current opinion in genetics & development, 1994. **4**(1): p. 82-9.
174. Thiels, E. and E. Klann, *Extracellular signal-regulated kinase, synaptic plasticity, and memory*. Reviews in the neurosciences, 2001. **12**(4): p. 327-45.
175. Adams, J.P. and J.D. Sweatt, *Molecular psychology: roles for the ERK MAP kinase cascade in memory*. Annual review of pharmacology and toxicology, 2002. **42**: p. 135-63.
176. Hoffert, J.D., et al., *Quantitative phosphoproteomics of vasopressin-sensitive renal cells: regulation of aquaporin-2 phosphorylation at two sites*. Proceedings of the National Academy of Sciences of the United States of America, 2006. **103**(18): p. 7159-64.
177. Ballif, B.A., et al., *Large-scale identification and evolution indexing of tyrosine phosphorylation sites from murine brain*. Journal of proteome research, 2008. **7**(1): p. 311-8.
178. Munton, R.P., et al., *Qualitative and quantitative analyses of protein phosphorylation in naive and stimulated mouse synaptosomal preparations*. Molecular & cellular proteomics : MCP, 2007. **6**(2): p. 283-93.
179. Wisniewski, J.R., et al., *Brain phosphoproteome obtained by a FASP-based method reveals plasma membrane protein topology*. Journal of proteome research, 2010. **9**(6): p. 3280-9.
180. Tweedie-Cullen, R.Y., J.M. Reck, and I.M. Mansuy, *Comprehensive mapping of post-translational modifications on synaptic, nuclear, and histone proteins in the adult mouse brain*. Journal of proteome research, 2009. **8**(11): p. 4966-82.
181. Gregory, J.D., *The Stability of N-Ethylmaleimide and its Reaction with Sulfhydryl Groups*. J. Am. Chem. Soc, 1955. **77**(14): p. 3922-3923.
182. Jencks, W.P., *On the attribution and additivity of binding energies*. Proceedings of the National Academy of Sciences of the United States of America, 1981. **78**(7): p. 4046-50.
183. Zhou, H.X., *The affinity-enhancing roles of flexible linkers in two-domain DNA-binding proteins*. Biochemistry, 2001. **40**(50): p. 15069-73.
184. Zhou, H.X., *Quantitative account of the enhanced affinity of two linked scFvs specific for different epitopes on the same antigen*. Journal of molecular biology, 2003. **329**(1): p. 1-8.
185. Harkioliaki, M., et al., *Structural basis for SH3 domain-mediated high-affinity binding between Mona/Gads and SLP-76*. The EMBO journal, 2003. **22**(11): p. 2571-82.
186. Nishida, M., et al., *Novel recognition mode between Vav and Grb2 SH3 domains*. The EMBO journal, 2001. **20**(12): p. 2995-3007.
187. Delbruck, H., et al., *An Src homology 3-like domain is responsible for dimerization of the repressor protein KorB encoded by the promiscuous IncP plasmid RP4*. The Journal of biological chemistry, 2002. **277**(6): p. 4191-8.
188. Kishan, K.V., et al., *The SH3 domain of Eps8 exists as a novel intertwined dimer*. Nature structural biology, 1997. **4**(9): p. 739-43.
189. Romir, J., et al., *Crystal structure analysis and solution studies of human Lck-SH3; zinc-induced homodimerization competes with the binding of proline-rich motifs*. Journal of molecular biology, 2007. **365**(5): p. 1417-28.
190. Dimasi, N., *Crystal structure of the C-terminal SH3 domain of the adaptor protein GADS in complex with SLP-76 motif peptide reveals a unique SH3-SH3 interaction*. The international journal of biochemistry & cell biology, 2007. **39**(1): p. 109-23.
191. Barnett, P., et al., *The peroxisomal membrane protein Pex13p shows a novel mode of SH3 interaction*. The EMBO journal, 2000. **19**(23): p. 6382-91.
192. Lee, C.H., et al., *Crystal structure of the conserved core of HIV-1 Nef complexed with a Src family SH3 domain*. Cell, 1996. **85**(6): p. 931-42.
193. Papadopoulos, T. and T. Soykan, *The role of collybistin in gephyrin clustering at inhibitory synapses: facts and open questions*. Frontiers in cellular neuroscience, 2011. **5**: p. 11.

194. Tyagarajan, S.K. and J.M. Fritschy, *GABA(A) receptors, gephyrin and homeostatic synaptic plasticity*. The Journal of physiology, 2010. **588**(Pt 1): p. 101-6.
195. Tretter, V., et al., *Gephyrin, the enigmatic organizer at GABAergic synapses*. Frontiers in cellular neuroscience, 2012. **6**: p. 23.
196. Fritschy, J.M., *Epilepsy, E/I Balance and GABA(A) Receptor Plasticity*. Frontiers in molecular neuroscience, 2008. **1**: p. 5.
197. Kang, J.Q., et al., *Slow degradation and aggregation in vitro of mutant GABAA receptor gamma2(Q351X) subunits associated with epilepsy*. The Journal of neuroscience : the official journal of the Society for Neuroscience, 2010. **30**(41): p. 13895-905.
198. Lydiard, R.B., *The role of GABA in anxiety disorders*. The Journal of clinical psychiatry, 2003. **64 Suppl 3**: p. 21-7.
199. Luscher, B., Q. Shen, and N. Sahir, *The GABAergic deficit hypothesis of major depressive disorder*. Molecular psychiatry, 2011. **16**(4): p. 383-406.
200. Pizzarelli, R. and E. Cherubini, *Alterations of GABAergic signaling in autism spectrum disorders*. Neural plasticity, 2011. **2011**: p. 297153.
201. D'Hulst, C., et al., *Decreased expression of the GABAA receptor in fragile X syndrome*. Brain research, 2006. **1121**(1): p. 238-45.
202. Cherlyn, S.Y., et al., *Genetic association studies of glutamate, GABA and related genes in schizophrenia and bipolar disorder: a decade of advance*. Neuroscience and biobehavioral reviews, 2010. **34**(6): p. 958-77.
203. Maric, H.M., et al., *Gephyrin-mediated gamma-aminobutyric acid type A and glycine receptor clustering relies on a common binding site*. The Journal of biological chemistry, 2011. **286**(49): p. 42105-14.
204. Tretter, V., et al., *Molecular basis of the gamma-aminobutyric acid A receptor alpha3 subunit interaction with the clustering protein gephyrin*. The Journal of biological chemistry, 2011. **286**(43): p. 37702-11.
205. Mukherjee, J., et al., *The residence time of GABA(A)Rs at inhibitory synapses is determined by direct binding of the receptor alpha1 subunit to gephyrin*. The Journal of neuroscience : the official journal of the Society for Neuroscience, 2011. **31**(41): p. 14677-87.
206. Adam G, D.M., *Reduction of dimensionality in biological diffusion processes*. In Structural Chemistry and Molecular biology of the cell, 1968: p. 198-215.
207. McCloskey, M.A. and M.M. Poo, *Rates of membrane-associated reactions: reduction of dimensionality revisited*. The Journal of cell biology, 1986. **102**(1): p. 88-96.
208. Chi, C.N., et al., *Deciphering the kinetic binding mechanism of dimeric ligands using a potent plasma-stable dimeric inhibitor of postsynaptic density protein-95 as an example*. The Journal of biological chemistry, 2010. **285**(36): p. 28252-60.
209. Clements, J.D., *Transmitter timecourse in the synaptic cleft: its role in central synaptic function*. Trends in neurosciences, 1996. **19**(5): p. 163-71.
210. Nusser, Z., S. Cull-Candy, and M. Farrant, *Differences in synaptic GABA(A) receptor number underlie variation in GABA mini amplitude*. Neuron, 1997. **19**(3): p. 697-709.
211. Shen, Q., et al., *gamma-Aminobutyric acid-type A receptor deficits cause hypothalamic-pituitary-adrenal axis hyperactivity and antidepressant drug sensitivity reminiscent of melancholic forms of depression*. Biological psychiatry, 2010. **68**(6): p. 512-20.
212. Bach, A., et al., *Modified peptides as potent inhibitors of the postsynaptic density-95/N-methyl-D-aspartate receptor interaction*. Journal of medicinal chemistry, 2008. **51**(20): p. 6450-9.
213. Bach, A., et al., *Design and synthesis of highly potent and plasma-stable dimeric inhibitors of the PSD-95-NMDA receptor interaction*. Angewandte Chemie, 2009. **48**(51): p. 9685-9.
214. Bach, A., et al., *Cell-permeable and plasma-stable peptidomimetic inhibitors of the postsynaptic density-95/N-methyl-D-aspartate receptor interaction*. Journal of medicinal chemistry, 2011. **54**(5): p. 1333-46.

215. Bach, A., et al., *A high-affinity, dimeric inhibitor of PSD-95 bivalently interacts with PDZ1-2 and protects against ischemic brain damage*. Proceedings of the National Academy of Sciences of the United States of America, 2012.
216. Thorsen, T.S., et al., *Identification of a small-molecule inhibitor of the PICK1 PDZ domain that inhibits hippocampal LTP and LTD*. Proceedings of the National Academy of Sciences of the United States of America, 2010. **107**(1): p. 413-8.
217. Varley, Z.K., et al., *Gephyrin regulates GABAergic and glutamatergic synaptic transmission in hippocampal cell cultures*. The Journal of biological chemistry, 2011. **286**(23): p. 20942-51.
218. Zhou, H.X. and M.K. Gilson, *Theory of free energy and entropy in noncovalent binding*. Chemical reviews, 2009. **109**(9): p. 4092-107.

## D Acknowledgements

I thank my collaborators on the radixin project, **Matthias Kneussel** for providing plasmids and sharing unpublished data. Similarly I want to express my gratitude towards our collaborators on the gephyrin project, namely the groups of **Verena Tretter** and **Stephen James Moss** for letting me contribute to their projects, as well as their contribution to my studies and the critical reading of my work. I am especially grateful to **Jayanta Mukherjee** for the great discussions and the resulting intense collaboration. I thank my committee members, **Matthias Kneussel** and **Utz Fischer**, for the discussions in our meetings and their supervision. Finally I acknowledge the members of the **Kisker** and **Schindelin groups**, especially:

**Franz-Xaver Kober:** For your friendship and sharing your brilliant thoughts. I enjoyed our fast-food-runs and intense discussions. Your analytical skills and keen perception are amazing.

**Uwe Dietzel:** For your friendship and nonstop support in scientific and personal issues. I will not forget our late night meetings in lab and our beamline trips. You are an extremely likeable person.

**Carolyn Delto:** For your friendship and help. I thank you for showing me how much fun climbing is. Your perfectionism and love to the detail is amazing.

**Bodo Sander:** I thank you for setting up the Geph-GABA<sub>A</sub>R-collaboration and for our numerous enlightening discussions. Your deep insight in our research field and your endurance in tracking your research goals is impressive.

**Shambahvi Mishram:** For your friendship. I enjoyed our meetings and I am very impressed by your humble, open-minded and strong character.

**Maurizio Amato:** For your friendship, support and motivation - I really enjoyed our time together.

**Daniela Schneeberger:** I thank you for introducing me to the lab and molecular biology.

**Hermann Schindelin:** I hereby want to express my sincere gratitude towards you. You are an extraordinary advisor and I enjoyed your guidance. Thank you for giving me such a great freedom in setting my scientific goals and your support in reaching them.

**Caroline Kisker:** I thank you for your motivating remarks.

**Antje Schäfer:** For your help and your positive attitude. I enjoyed your scientific enthusiasm.

**Petra Hänzelmann:** Your straight-forward advice was very helpful.

**Julia Spegli, Christina Haaslinger and Annica Pschibul:** I enjoyed your support and unclouded scientific enthusiasm.

**Robert Mueller, Christoph Gross, Nicolas Brockmann, Carsten Grassmann and Peter Brenner:** Thanks for staying in touch - it was great to study with you.

**I hereby officially apologize for running in the lab and office corridors.**

Finally, I dedicate this thesis to my family, especially to

**Steffi** and our daughter **Philia**,

for this work would not have been possible without their sacrifices.

## E Own Publications and Congress Contributions

### Research Articles

1. **Maric HM**, Mukherjee J, Tretter V, Moss SJ, Schindelin H.  
*Gephyrin-mediated  $\gamma$ -aminobutyric acid type A and glycine receptor clustering relies on a common binding site.*  
J Biol Chem. 2011 Dec 9; 286(49):42105-14. Epub 2011 Oct 17.
2. Mukherjee J, Kretschmannova K\*, Gouzer G\*, **Maric HM\***, Ramsden S, Tretter V, Harvey K, Davies PA, Triller A, Schindelin H, Moss SJ.  
*The residence time of GABA(A)Rs at inhibitory synapses is determined by direct binding of the receptor  $\alpha$ 1 subunit to gephyrin.*  
J Neurosci. 2011 Oct 12; 31(41):14677-87.  
\*Authors contributed equally.
3. Tretter V, Kerschner B, Milenkovic I, Ramsden SL, Ramerstorfer J, Saiepour L, **Maric HM**, Moss SJ, Schindelin H, Harvey RJ, Sieghart W, Harvey K.  
*Molecular basis of the  $\gamma$ -aminobutyric acid A receptor  $\alpha$ 3 subunit interaction with the clustering protein gephyrin.*  
J Biol Chem. 2011 Oct 28;286(43):37702-11. Epub 2011 Aug 31.
4. **Maric HM** and Schindelin H.  
*Gephyrin-mediated receptor clustering is a multivalent process.*  
Manuscript in preparation.

### Reviews

1. Tretter V, Mukherjee J, **Maric HM**, Schindelin H, Sieghart W, Moss SJ.  
*Gephyrin, the enigmatic organizer at GABAergic synapses.*  
Front Cell Neurosci. 2012; 6:23. Epub 2012 May 15.

## Oral Presentations

Date	Organizer and Meeting Title	Title
2010	RVZ-Graduate Program, Retreat Kloster Schöntal, Germany	“Structural Basis of GABA <sub>A</sub> R Clustering”
2010	SFB 487 – Jour Fixe, Würzburg, Germany	“Structural Basis of GABA <sub>A</sub> R Clustering”
19-20. Oktober 2011	RVZ Graduate Program, 6 <sup>th</sup> international Symposium, Würzburg, Germany	“Molecular Basis of GABA <sub>A</sub> R Clustering”

## Poster Presentations

Date	Organizer and Meeting Title	Author and Title
2009	RVZ-Graduate Program, Retreat Kloster Höchst, Germany	<b>Maric HM</b> and Schindelin H: “GABA <sub>A</sub> R Clustering”
2011	RVZ-Graduate Program, Retreat Kloster Schöntal, Germany	<b>Maric HM</b> , Mukherjee J, Amato M and Schindelin H: “Molecular Basis of Inhibitory Neurotransmitter Receptor Clustering”
28-30. August 2011	SFB-487 – International Symposium, RVZ Würzburg, Germany	<b>Maric HM</b> , Sander B, Delto C, Schneeberger D and Schindelin H: “Gephyrin-Mediated Neurotransmitter Receptor Clustering”

## F Curriculum Vitae

### Personal Information

---

*Name and gender* Hans-Michael Maric, male.  
*Date and Place of birth* February 25, 1981 in Stuttgart, Germany  
*Children:* \*June 04, 2011  
*Languages:* German (native), English (excellent), French (fair)  
*Civil service:* November 2001 to September 2002 at the Gynecological Hospital of Aschaffenburg  
*Contact information:* Lange Str. 4, 63741 Aschaffenburg, Germany  
*Phone:* Office: 0931-31 80 394 / Home: 06021-43 90 550  
*E-mail:* Hans.Maric@virchow-uni-wuerzburg.de

### Education and Awards

---

*July 2008 - present* PhD at the Institute of Structural Biology, Rudolf-Virchow Center for Experimental Biomedicine. Member of the "Sonderforschungsbereich 487, Regulatory Membrane Proteins, C7" and student in the DFG funded Graduate School of Life Sciences, Würzburg, Germany

*July 2012* Career Development Fellowship Award offered by the Graduate School of Life Sciences.

*Mai 2008* Diploma Thesis in Clinical Biochemistry at the Julius-Maximilians-University of Würzburg, "sehr gut".

*October 2002 - Mai 2008* Diploma of Chemistry at the Julius-Maximilians-University of Würzburg, "sehr gut".  
Major Studies: Anorganic-, Physical- and Organic-Chemistry.

*February 2005* Oskar-Karl-Forster Award offered by the Oskar-Karl-Forster foundation, Germany

*June 2001* University entrance qualification (Abitur) at the Friedrich-Dessauer Gymnasium, Aschaffenburg.



## G Affidavit

Affidavit  
(eidesstattliche Erklärung)

I hereby declare that my thesis entitled

“Molecular Basis of the Multivalent  
Glycine and  $\gamma$ -Aminobutyric Acid Type A Receptor Anchoring”

is the result of my own work. I did not receive any help or support from commercial consultants.  
All sources and/or materials applied are listed and specified in the thesis.

Furthermore, I verify that this thesis, has not yet been submitted as part of another examination  
process neither in identical nor in similar form.

Würzburg.....

date

signature